Optimum Design and Control of Hydraulic Systems Driven by Swash Plate Pumps Using Vibration Based Diagnosis

M. MOLHAM HASAN CHIKH AL SOUK

A Thesis in

The Department

Of

Mechanical and Industrial Engineering

Presented in Partial Fulfillment of the Requirements

For the Degree of Doctor of Philosophy in Mechanical Engineering at

Concordia University

Montreal, Quebec, Canada

June 2008

Your file Votre référence
ISBN: 978-0-494-42550-3
Our file Notre référence
ISBN: 978-0-494-42550-3

ABSTRACT

OPTIMUM DESIGN AND CONTROL OF HYDRAULIC SYSTEMS DRIVEN BY SWASH PLATE PUMPS USING VIBRATION BASED DIAGNOSIS

M. MOLHAM HASAN CHIKH AL SOUK, Ph.D.

Concordia University, 2008

Swash plate pumps are widely used to drive hydraulic systems, especially because they offer high specific power. In order to improve their performance and make them more reliable, it is necessary to reduce the flow fluctuations, incorporate a control system that is more responsive, and minimize vibration levels. Furthermore, the flow should be controlled according to load requirements and pipe response at the design level. Moreover, there is a need to monitor the health of the system by analysing its vibration signatures.

A novel port plate design is used with a pair of deep silencing grooves on the edges of delivery and suction ports, which reduces the flow fluctuations and improves the pump output. In addition to the load information, the pipe dynamics are also used as a control input. Hence, pipe instabilities with different boundary conditions are studied, where

simple, accurate and comprehensive expressions to describe the pipe instabilities are produced, solved, and plotted.

In swash plate pumps, the control unit changes the pump output according to the load requirements. The current pump design is equipped with a double negative feedback strategy. The inner loop controls the spool position, and the outer loop controls the swash plate angle. Since this design has a high rise time, it was suggested to equip the pump with a single feedback PD controller. Although this reduced the rise time, it introduced high levels of vibration. The present research proposes a new control strategy with a single feedback PID controller that minimizes vibration levels. Results are obtained experimentally. The control strategy is generalized to control the pump flow according to load requirements and pipe vibration levels. A compensation factor is introduced to moderate the negative impact of the pipe vibrations, and to generate a new set value for the inclination angle.

For timely detection of faults, the application of wavelet analysis to detect different defects is examined. Some defects are produced, such as pipe flutter, pump dynamic instability, and voltage unbalance in the driving electric motor. Continuous wavelet and discrete wavelet analyses are used to analyze the vibration signature by using Debauches' mother wavelet. The data is collected experimentally. The results show that wavelet analysis is very efficient at identifying defects in the pipe or pump. The results are discussed and appropriate conclusions are drawn based on the present research. Suggestions for future extensions of the research are proposed.

This Thesis is dedicated to

My Mother Rowaydah

My Father's Soul Hasan

Syria with love

ACKNOWLEDGEMENT

After more than three years and half, my extensive work comes in this form. This work would not be accomplished without the support of many people. It is the most pleasant task to express my deepest appreciation and gratitude to all of them.

In the beginning, I want to thank my supervisor Dr. Rama B. Bhat for everything he did for me. I am deeply indebted to Dr. Bhat. Without his guidance, common sense, knowledge, and huge efforts, this work would not be accomplished.

I would like to thank Dr. Michael Paidoussis from McGill University and Dr. Ali, S.Twareque from Concordia University, Mathematics and Statistics department for their suggestions. I would like to thank a group of technicians and department secretaries for giving all assistance needed to facilitate this work. I would like to thank Mr. Dainius Juras, Mr. Gilles Huard, and Mr. Robert Oliver. Also, Mr. Jon Horen from DADISP for his continuous assistance. Also, I love to thank some of my best friends for their advice, friendly support, and assistance. Dr. Nabil Nassif, Mr. Surajudeen Adewusi, Dr. Chaher Alzaman, Mr. Raghdan Al Khoury, Mr. Balasubramanian Esakki, Mr. Salem Bashamal, and Mr. Hussam Fares.

Finally, I want to express my sincerest gratitude to my mother Rowaydah for her continuous motivation and emotional support. Also, my brothers Dr. Moutamen, Ameen, Mamoun, Khaldoun, and my sister Randa, and their families. Also, to my fiancé for her emotional support all this time.

TABLE OF CONTENTS

LIST OF FIGURES (LoF)

LIST OF TABLES

NOMENCLATURE

A_{og1}	the instantaneous upper overlapping area of the K^{th} cylinder delivery port with the upper deep groove (port plate with deep triangular grooves)
A_d	area of cylinder delivery port
$A_{de}(t)$	the instantaneous porting area in the delivery stroke
A_{ob}	the instantaneous lower overlapping area of the K^{th} cylinder delivery port with the delivery port (non-grooved port plate)
A_{obg}	area of the lower shallow groove (standard design)
A_{obt}	the instantaneous lower overlapping area of the K^{th} cylinder delivery port with the delivery port (port plate with deep triangular grooves)
A_{og2}	the instantaneous lower overlapping area of the K^{th} cylinder delivery port with the upper deep groove (port plate with deep triangular grooves)
A_{ot}	the instantaneous upper overlapping area of the K^{th} cylinder delivery port with the delivery port (non-grooved port plate)

A_{otg} area of the upper shallow groove (standard design)

A_{ott} the instantaneous upper overlapping area of the K^{th} cylinder delivery port with the delivery port (port plate with deep triangular grooves)

B effective bulk modulus

C_d coefficient of discharge

H height of shallow silencing groove, referred to in Figure 2.16

L_1 length between the top and bottom of the cylinder block, referred to in Figure 2.3

L_2 length, referred to in Figure 2.3

M mass of the fluid of the K^{th} cylinder

P_d cylinder delivery pressure

$P_n(t)$ fluid pressure within the cylinder of the K^{th} piston

P_s cylinder suction pressure

R piston pitch-radius

R_1 radius of the cylinder arrangement at the base of the cylinder block, referred to in Figure 2.3

R_2 radius of the cylinder arrangement at the top of the cylinder block, referred to in Figure 2.3

$S_k(t)$ the K^{th} piston displacement

$V_{ck}(t)$ cylinder instantaneous volume

V_o cylinder clearance volume, referred to in Figure 2.6

$Q_k(t)$ flow rate of the K^{th} cylinder

a_p piston cross-section area

b width of the shallow silencing groove (standard design)

$b_{o1,02}$ instantaneous base of the first and second overlapping areas, referred to in Figures 2.11 and 2.20

c_t a constant contains information about the piston pitch-radius, swivelling angle and cylinder conical angle

$\frac{dP}{dt}$ time-rate change of pressure

$h_{o1,02}$ instantaneous height of the first (upper) and second (lower) overlapping areas, referred to in Figures 2.11 and 2.20

k_1	a constant, contains information regarding the oil density, effective bulk modulus, discharge coefficient, and the pump angular velocity
l_c	total cylinder length, referred to in Figure 2.6
r	port plate radius, referred to in Figure 2.11
y_c	middle angular distance, referred to in Figure 2.11
y_t	the overlapping length, referred to in Figure 2.11
sign	a function takes on value $\mp$ 1 depending upon the sign of the argument
$\dot{S}_k(t)$	the K^{th} piston velocity
$\ddot{S}_k(t)$	the K^{th} piston acceleration
$\dot{V}_{ck}(t)$	time-rate change of instantaneous cylinder volume
α	swash plate angle of inclination
β	cylinder block cone angle
φ	the K^{th} piston angular position
$\varphi_{1,2,3,4,5,6,7}$	angles, referred to in Figures 2.11 and 2.20

ρ	oil density
θ	angle of the shallow silencing groove (standard design)
$\theta_{g1,2}$	the inner angle of the upper and lower triangular grooves, referred to in Figure 2.20 (port plate with deep triangular grooves)
$\theta_{o1,02}$	instantaneous inner angle of the upper and lower overlapping area, referred to in Figures 2.11 and 2.20
ω	angular speed of the pump

LIST OF ACRONYMS

W T: Wavelet Transform

WA: Wavelet Analysis

FT: Fourier Transform

CWT: Continuous Wavelet Transform

DWT: Discrete Wavelet Transform

FFT: Fast Fourier Transform

STFT: Short Time (Term) Fourier Transform

SMS: Safe-Mode Strategy

PID: Proportional Integral Derivative

PD: Proportional Derivative

LVDT: Linear Variable Differential Transducer

CHAPTER ONE

1 INTRODUCTION AND LITERATURE REVIEW

In this chapter, a general introduction to hydraulic systems, pipe dynamics, and wavelets is introduced, followed by an overview of the previous studies on this topic. The thesis objectives are formulated and work focus is outlined.

1.1 Introduction

Hydraulic systems are widely used in many applications such as in petrochemical industries, in nuclear power stations and in the distribution of water, gas and oil. They usually consist of pumps, pipes, valves, support brackets, reservoirs, surge chambers, and a control unit. This study will consider pumps and pipes and study the interaction dynamics between them.

In the present research, a swash plate pump is used. A swash plate pump is a variable displacement pump, which is appropriate for hydraulic systems with variable load demands. It can generate output to fit all loads under all operating conditions. A swash plate pump has excellent advantages that outweigh its disadvantages. Some of these advantages are: their suitability for heavy duty applications, excellent static and dynamic characteristics, convenience of use for mobile and industrial applications, high specific power, the ability to control the pump output by the control unit, low inertia and flexible

power levels. Moreover, it can be used for open and closed hydraulic circuits, and can fit both for mobile and stationary applications. The disadvantages of swash plate pumps are: inflammability, contamination sensitivity and possible fluid leakage.

Pipes in hydraulic networks often have circular cross-sections, and are made from a wide variety of materials. Size choices include their diameter, wall thickness, length, and material. The material can be aluminium, bronze, steel alloys and PVC.

In hydraulic systems, flow-induced vibrations are complicated fluid-structure interaction phenomena that can have disastrous effects. Overlooking these effects may lead to catastrophic breakdown, which, apart from the economic loss, may even claim human lives. For some applications, such as in heat exchangers or in nuclear reactor cooling systems, the flow-induced vibrations of tube banks may cause damage to the installations resulting in the loss of power-generating time.

Reliable, optimum, and effective hydraulic systems can be achieved by understanding the coupling nature of the fluid and the structure and by controlling fluid velocity within certain limits in order to avoid divergence or flutter conditions. In hydraulic systems driven by swash plate pumps, it is possible to control the flow by controlling the swivelling angle of the swash plate.

1.2 Hydraulic System Components

Hydraulic systems convey fluids from one point to another, or can be used for fluid power applications. In both cases, the fluid is the medium used to transmit and control power. In hydraulic systems, the pump converts mechanical power to hydraulic power. The design of the system changes according to the purpose of the system. For example, the design of a power control system is more complicated compared to those used to convey fluids. A hydraulic power control system consists mainly of:

Electric motor or internal combustion engine: the electric motor is used to drive the pump in stationary applications, while the internal combustion engine is used for mobile applications. In both cases, the pump receives its mechanical power from the motor/engine.

Pump: converts mechanical power to hydraulic power. This power is in the form of increased pressure and velocity, manifested in the form of the flow discharge.

Control valves: used to control the magnitude of the hydraulic power and to direct the fluid to the required actuator.

Hydraulic actuators: these reconvert the hydraulic power into mechanical power and perform the desired tasks.

Pipes: these connect the pump outlet to the desired destination, and they convey the fluid to specific locations.

Accessories: some components are used in specific tasks such as tanks, taps, safety units, etc.

1.2.1 Swash Plate Pump

The heart of the hydraulic system is the pump, and the entire system's performance is dependent mainly on the pump performance. For example, a smooth pump operation will enable the system to operate smoothly. Pumps are different in their designs depending on the purpose for which they are used. Gear, vane, radial, and positive displacement pumps are some examples. Some pumps are suitable in certain applications but are likely to fail in others. For heavy-duty applications that require high working pressure (more than 10 MPa.), radial and positive displacement pumps are highly recommended and perform well. The early design of these pumps started with a single cylinder with reciprocating motion. Although they are simple in design (two valves, piston, and housing), performance was rough and it came with a high degree of vibration. In addition, its efficiency and productivity were low.

These disadvantages were overcome by introducing a pump with multiple pistons that work sequentially, where the pump performance and productivity are improved and the flow is smoother.

The swash plate pump has two different designs: the barrel or cylindrical arrangement of the pump cylinders, and a conical arrangement of the cylinders. In the barrel design, the piston axis and the pump driving shaft axis are parallel; while in the conical design, there is an inclination angle (cone angle) between the piston axis and the pump driving shaft axis. The conical arrangement has a specific advantage, because the cone angle reduces the detachment force. This detachment force occurs during the suction stroke and threatens to disconnect the piston from its slipper pad. The cone angle improves the pump

flow rate, by increasing the stroke length, and also enables the pump to run safely at higher speeds.

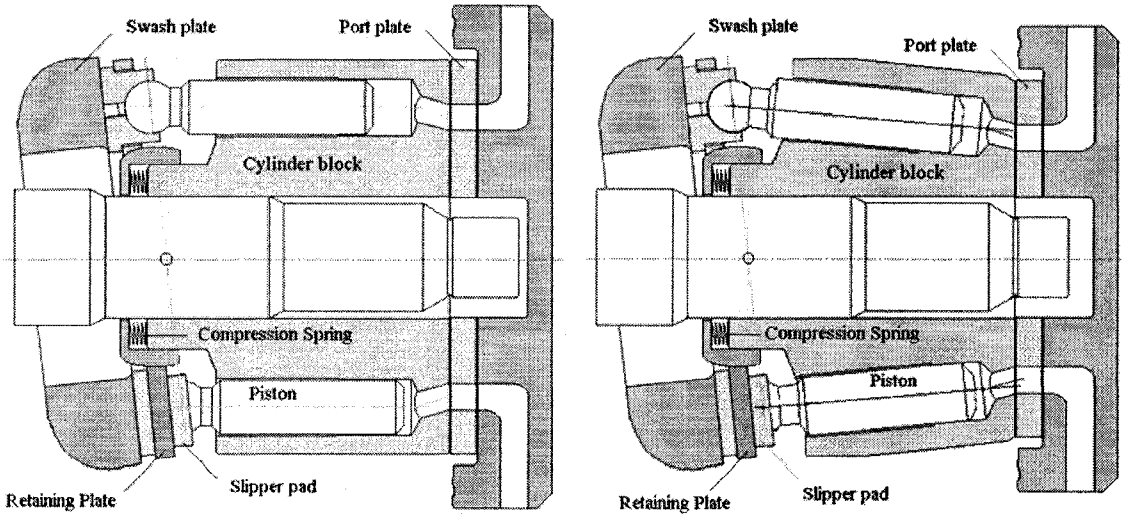

Figure 1.1: Structures of swash plate pump with barrel and conical designs, [35]

1.2.2 **Flow Induced Vibrations**

Catastrophic failure of pipes, especially in power plants, leads to economic loss and could lead to fatalities. Such failure occurs due to different reasons such as: erroneous design, fluid-induced vibration and thermal stress that leads to pipe fatigue, causing damage, and accidents. Several standard codes are available to avoid failure of pipes at the design and manufacturing stages.

A pipe is a flexible system with stiffness and damping, and the fluid motion causes a pipe to vibrate depending on the fluid velocity, pipe material, and pipe dimensions. The fluid flow generates a force creating negative damping which increases the vibration amplitude

instead of damping it (the force is proportional to the fluid velocity and in the same direction). This kind of vibration is called a self-excited vibration. In the self-excited vibration, the pipe vibration disappears when the fluid flow stops.

1.2.3 Wavelet Analysis and Condition Monitoring

Hydraulic systems contain many moving elements such as pumps, motors, fans, and pipes. The continuous operation of the hydraulic system combined with excessive loads would lead to poor performance, and additional noise and vibration. There are certain techniques to verify whether the system is performing satisfactorily, and the most common technique uses the vibration signature. This technique demonstrates certain advantages such as: low cost, non-intrusive, reliable, and easy to use. The vibration signature contains useful information about the health of the piece of equipment, and immediate attention can be brought to the problem in the early stage before it assumes catastrophic proportions. This kind of predictive maintenance is essential in complex hydraulic systems in major installations.

Predictive maintenance: In predictive maintenance, a maintenance activity is scheduled only when a functional defect is detected during the routine monitoring of the mechanical and operational conditions. At the appearance of an unexpected event, the damaged part is located and replaced. The advantages of this approach are:

- The maintenance is carried out at the right time.
- The repairs are small, and hence, the repair time is relatively short.
- The cost of maintenance is generally low.

- Does not require a huge inventory, since the lead time towards impending failure can be used without major breakdowns.

The vibration signature on components with defects has a non-stationary nature. Hence, Fourier transform (frequency domain analysis) is not suitable for this kind of signature. If a Fourier transform is used for the non stationary signals, the expected information from the transient components will be lost.

Wavelet analysis, which analyzes the time variation of frequency contents in the signal, is a suitable tool to analyze the non-stationary signatures.

The advantage of wavelet analysis is its ability to localize information in time and frequency (scale). In wavelet analysis, the signal will be represented in both time and frequency, and both the stationary and the transient components will be localized without losing the transient information. Wavelet analysis demonstrates additional advantages over other methods with time-frequency representations such as short-time Fourier transform (STFT).

STFT is a time-frequency analysis, and it is not a suitable transformation for high frequency signals and those with discontinuities. In STFT, the signal is divided into equal segments and then analyzed. Despite the fact that STFT can represent the given signal in both time and frequency, it has a time-resolution problem; this is due to the equal windows that would not be suitable for some signal frequency contents.

The early application of wavelet analysis began in biomedical research, and it showed promising results and suitability for other fields. It was used to analyze the sound of a

heart by using wavelet analysis, where a comparison between the disturbance of the blood in the cardiovascular problem case and a healthy situation was carried out.

The recorded signals from the hydraulic system and those generated from the heart's sound have a non-stationary nature if a defect is present and contain information that reflects the health of the systems. The continuous monitoring and detecting of the signal evolution can provide clear information about the current condition of a heart, and an early measure can be taken to prevent the system from reaching a failure condition.

1.3 Literature Review

In this section, a comprehensive review is carried out on the swash plate pump, pipe dynamics, and hydraulic systems condition monitoring. This enables us to have a clear idea about the state of art and the relevant background to carry out our study objectives.

1.3.1 Swash Plate Pump Performance

Swash plate pumps have been studied extensively, since they are often used in heavy duty applications in industry. A review of the available literature was carried out in order to identify the studies that would be most helpful in the complete and accurate mathematical modeling of variable displacement axial piston pumps.

Most of the studies can be classified into one of two groups:

1. Research on pump components to understand a specific phenomenon, and

2. Modeling of the entire pump and the control unit for design purposes

In the first group, a significant amount of mathematical developments have taken place thus far. The second category is of more recent interest and most of the newer studies are in this area. This literature review will only discuss the second category.

1.3.1.1 *Effect of Port Plate Configurations on Pump Performance*

Earlier studies have dealt with pump performance, and the effect of the port plate design and configuration on the pump performance. Kaliafetis and Costopoulos [29] investigated the static and dynamic characteristics of a variable displacement pump by implementing a pressure regulator. The proposed mathematical model was validated according to the dynamic operating curves provided by the manufacturer. Edge [17] experimentally studied the benefits of varying a piston's pump port plate timing in reducing pump flow fluctuations and the resulting system noise and vibration. He observed that as the port plate was retracted from neutral position to 15^{o}, the peak-to-peak levels of the delivery pressure ripple signals are reduced by 45%.

In [28], a similar study obtained the same results. The influence of the length of the port plate transitional zones on the flow and pressure fluctuations for a pump with even pistons was investigated. The effect of the number of the pistons in the pump on the flow was studied in [39], where the study was carried out on pumps with even and odd number of cylinders, and they observed that a pump with an even number of cylinders has lower pressure fluctuation levels. In [50-53], Manring conducted an extensive study on swash plate pumps. For example, in [50] a new non-traditional pump design was proposed, with a spring was attached to the pistons; and the corresponding pump performance was

studied and compared with that of the traditional design. In [53], Manring investigated different combinations of the silencing groove designs and simulated the transitional pressure in the grooves, while in [52]; he studied the pump discharge flow fluctuations for seven, eight, and nine cylinders. He concluded that there was no significant difference in actual flow fluctuation characteristics between the different designs and that the use of an even number of cylinders was not a problem in terms of the flow fluctuation.

Another interesting study was carried out by Manring [51], where he compared the pump volumetric efficiency with two port plate designs, a standard port plate with a shallow silencing groove and a non-grooved port plate. He concluded that a pump with a non-grooved port plate has a higher volumetric efficiency and that overshooting is absent. Khalil and Bhat [35] carried out a parametric analysis on the standard port plate design and they introduced a port plate with a configuration that can reduce overshooting. In [11], Chikhalsouk and Bhat studied the impact of utilizing deep grooves in the port plate of a swash plate pump with a conical arrangement for the noise levels. The comparison was conducted between a non-groove design and a port plate with a deep silencing groove design. That study also considered the overlapping areas between the cylinder and the entry and exit of the delivery port and presented some preliminary results.

1.3.1.2 *Effect of Port Plate Design on Pump Efficiency*

In the past 20 years, several studies have addressed pump performance in general, as well as the effect of the port plate design on pump performance and pump efficiency. Some of these have advanced theoretical reasons that support the use of the non-grooved port

plate. For example, in [51], Manring compared the volumetric efficiency of an axial-piston pump for two port plate geometries (with a shallow silencing groove and without a silencing groove) and he observed that using a pump with a non-grooved port plate could increase the pump's volumetric efficiency by 3%. This increase could be achieved by eliminating the volumetric losses that take place due to the uncontrolled fluid expansion in the shallow grooves. A similar study was made by Lin et al [45], where they carried out a numerical investigation on the effect of oil entrapment in swash plate pumps as it related to the control torque acting on the swash plate. That study did not identify any specific advantages for pump efficiency with the use of a non-grooved port plate. Yamaguchi [87] considered the effect of the non-grooved design on pump efficiency. He carried out his study on one single cylinder, and based on a P-V diagram he concluded that the pump with a non-grooved design is more efficient than a pump with the standard design. His work did not show how to design the trapped zones for the given operating conditions.

1.3.1.3 *Pump Control Strategies*

Extensive studies were carried out on swash plate pumps in order to control their operation, where the early models were with a barrel cylinder block formation (conventional design). In [45], Akers and Lin modeled and simulated the pump's performance in order to regulate the pump's pressure. Their arrangement had a combination of a swash plate pump and a single-stage electro hydraulic valve. The pump was subject to a step input on the open loop, and the transient response was observed by applying optimal control theory. They observed an improvement in the system

performance. Kaliftas and Costopoulos [29] modeled and investigated the static and dynamic characteristics of the pump with a pressure regulator. The numerical results were compared with the manufacturer's dynamic operating curves. In [54], Manring and Johnson investigated the effect of certain parameters on the performance of the barrel pump. Recently, another design of a swash plate pump with conical arrangement was presented. Many researchers have studied this type of pump, for example [33, 11, 34, and 35]. The pump's kinematics were modeled and simulated by Khalil et al in [34]. They proposed a single feedback loop to control the pump, and they compared that control strategy with several other control strategies. Their objective was to simplify the control scheme and the associated electronics, which reduces the pump's production cost.

However, pump performance was not investigated in the presence of a delivery side pipe system and the smoothness of the operation was not investigated.

1.3.1.4 *Controlling Pump Performance*

Some techniques were proposed in earlier studies to control the pipe vibration and improve a hydraulic system's performance. For example Omari et al [60] studied the relationship between the dynamics of a centrifugal pump and pipe. They proposed a method to control the excessive pipe vibration by controlling the pump rotational speed with the aid of a neural-network program. In [47], Lin et al introduced an active controller to suppress the pipe vibration under divergence conditions. They added dual spring-damper systems on both sides of the pipe to reduce the levels of pipe vibration. Steve et al [79] studied the effect of the ground motion on pipelines under earthquake

excitations of high magnitude and they proposed some design aspects that can help to protect pipelines under severe earthquake excitations (greater than 7.9 on the Richter scale).

1.3.2 **Pipe Dynamics**

Studies of pipe dynamics received some attention towards the end of the 1800's. It started with an experimental approach by Aitken (1898), where the focus was on the progressive motion of elastic pipes. Serious trials to understand the vibration of pipes and their general dynamic behaviour began in the 1930s. Over the last 70 years, flow-induced vibration of pipes has been the subject of considerable and systematic research. The first study was carried by Bourrieres in 1939. He formulated the equation of motion for a pipe conveying fluid. He also examined the fluid velocity at which a pipe loses stability. Another serious study was carried out by Ashely and Haviland (1950). The objective of that study was to explain and analyze the vibrations in the Trans-Arabian pipelines. The first studies to consider boundary conditions were carried out by Housner (1952) and Niordson (1953). Housner considered the simply supported conditions, while Niordson was interested in the behaviour of the cantilevers. They were able to obtain a good understanding of pipe stability.

In the last 40 years, more interest has been directed towards the flow-induced vibration of pipes. The trend to design better heat exchangers led to studying the vibration problems, where [7, 58, 64, and 66] studied and analyzed the vibration in the heat exchanger, which in turn led to more work in the field of flow-induced vibration.

Misra et al [57] studied the dynamic behaviour of simply supported and cantilever pipes and they concluded that with the increase of the velocity of fluid inside a pipe, the frequencies of oscillations were reduced. When the velocity reaches a critical value, the pipe loses stability by static divergence (buckling) if both ends are supported, or by flutter if one end is free to move.

Paidoussis [64] defined the mathematical expression for the flutter as characterized by a pair of eigenvalues crossing from the negative side of the real part of the eigenvalue axis to the positive real part as a result of the increase in fluid velocity.

1.3.3 **Wavelet Analysis and Hydraulic Systems Condition Monitoring**

1.3.3.1 ***Wavelet Transform and other Signal Transforms***

Fourier Transform (FT) is localized in the frequency domain and accordingly they are not suitable for signals that change with time, are non-stationary or are transient. In order to evaluate the non-stationary or transient signals, the Joint Time-Frequency Analysis (JTFA), which is used to obtain information on the way the frequency contents of signals evolve with time, was developed. Short-Time Fourier Transformation (STFT) and Wavelet Transform (WT) are examples of JTFT. This representation is important and interesting because the signal can be regenerated. However, STFT would produce a poor resolution of time-frequency. The properties and characteristics of different wavelet bases are well-illustrated in the literature. For example, many researchers have started investigating the properties of wavelet functions, such as Newland (1993), Misiti (1998), Torrence and Compo (1998) and Burrus (1998).

WT has a unique multi-resolution effectiveness, and consequently is recognized as a powerful analysis tool in different fields. The success of using WT in signal de-noising, signal discontinuity detection and in image processing has attracted researchers to examine the applicability of WT in the analysis of vibration signals. Mathoudakis and Aretakis (1997) implemented WT on vibration signals of gas turbines for fault diagnosis. The advantage of WT is its ability to give frequency information directly, where it gives dimensionless scale and space information. Different researchers have tried to provide a mathematical expression to express wavelet scales in terms of the frequency, such as Newland (1994), Dorize (1992) and Jubran et al (1998). However, none of them have presented an exact expression that matches the frequencies and scales. Therefore, it is well accepted practice in WT to compare signals on certain level to obtain the change in the amplitude and the location of this change.

1.3.3.2 *Wavelet Transform and Diagnosis of Hydraulic System Components*

Wang, [86] analyzed the steady-state performance of an induction motor connected to unbalanced three-line voltage. He also formulated and discussed the motor's operating characteristics under voltage unbalance, and paid extra attention to the angle of the complex voltage unbalance factor.

A statistical analysis has been performed on electric power by using wavelet analysis in order to identify the quality of supplied electric power by Chandrasekaran and Kopparapu [42]. Goa et al [21] investigated the use of wavelet analysis for real-time health diagnosis of a hydraulic pump, where they obtained on-line signal measurements. They identified

the type of the pump based on the patterns and the amplitudes of the wavelet coefficients thus obtained.

Some researchers used wavelet transform to experimentally detect damages in hydraulic components, since it is an ideal tool for extracting signal features. This is true especially when the hydraulic network vibration has an impulsive nature that is created because of components' interactions (for example, [1, 9, and 27]).

1.3.3.3 *Flutter*

Staszewski and Cooper [78] considered the flutter phenomena in aircraft and identified damping during flight tests. The flutter test data was evaluated by using a time-scale domain method. The flutter was produced by exciting the structure by impulsive force, and the corresponding response was recorded and analyzed. A similar study was conducted by NASA [55]. The study used wavelet transform to reduce uncertainty levels in stability estimates, and provided valuable data for analysis of excitation mechanisms and stability boundary prediction. Paidoussis studied stability in pipes conveying fluids [64]. His study examined the conditions at which a pipe loses its dynamic (flutter) and static stability (divergence). Tucker et al [82] used wavelet analysis to detect a crack in a pipeline. They generated an ultrasonic wave, and then analyzed the wave signature by using continuous wavelet. Then they compared the results with the analyzed signature of a healthy pipe. They found that wavelet analysis is useful in detecting local damages in pipelines.

1.4 Objectives

Although the individual components of the hydraulic system have been studied, in terms of coupling between the system components, it is important to study the hydraulic system as a whole. In the present thesis the main objective is to study the complete hydraulic system from the point view of improving pump performance, controlling the performance of the pump, along with the pipe dynamics, pipe divergence and flutter phenomena due to the pump dynamics, fault detection in the system during operation by vibration signature analysis. The individual sub-objectives are detailed below.

1.4.1 Effect of Port Plate Configurations on Pump Performance

A new configuration for the port plate is proposed in order to smooth the flow and reduce flow induced vibrations, which would make the control action much more effective. In particular, two port plate geometries are compared to show that alteration in the port plate design can cause a difference in a pump's dynamic operation and improve its operation smoothness. This enhancement eliminates pressure overshooting and reduces the pump flow fluctuations. Thus, the improvement of operation smoothness leads to reducing the vibrations that are transmitted to the attached pipes.

1.4.2 Control Strategies

In the present study, a new control strategy is introduced to control the pump with a conical arrangement. This strategy has a single feedback PID controller. The expected advantages are: simple design, improved performance by making it more responsive to the load requirements, and the smoothness of its operation, which reduces the vibration levels and increases its service life.

Another new control strategy is proposed to control the pump with a conical arrangement to control the load as well as pipe vibrations. This strategy has a single feedback PID controller, and the pump flow rate is determined based on two factors: the load requirement, and the pipe vibration amplitude. The objective of this study is to improve the entire system performance, controlling the pump flow in the presence of the undesired disturbances to prevent pipe vibration and fatigue and to improve the safety of the entire hydraulic system.

1.4.3 **Studying the Vibration Dynamics and Pipe Stability**

Analysis of flutter and divergence phenomena is carried out to better understand the flow-induced vibration that is produced by variable displacement pumps in pipes. Furthermore, these phenomena will influence the dynamics of the entire system.

1.4.4 **Wavelet Analysis in Detecting System Defects**

After introducing the optimum designs for a pump and pipes, and controlling the pump flow rate according to the load requirements and the pipe vibration levels, vibration condition monitoring and analysis are carried out. Several predetermined defects are introduced in the hydraulic system components, and then the vibration signatures are recorded from the pump and another section (the pipe, for example). Different approaches are used to analyze the signals, such as Wavelet Transform, Waterfall diagram, and FFT. Finally, the results of the analyses are used to arrive at the correct control action.

1.5 Thesis Outline

The thesis is divided into seven chapters.

In the first chapter, a survey of the previous work and the thesis objectives are provided. The first chapter starts with a general introduction to the hydraulic system components, and several types of pumps, and different kinds of control strategies used with variable displacement pumps are presented. A brief overview of the general concepts of flow-induced vibrations and pipe dynamics is also discussed, and the thesis objectives are outlined.

The second chapter includes the general description of the swash plate pump with conical arrangement, the principle of its operation, piston kinematics, port plate designs, and the cylinder fluid control volume and its time rate of change. The pump performance measures are defined in general. A comprehensive study of the current design of the port plates is obtained. Then, new expressions for the porting areas, considering the overlapping between the cylinder opening and the port plate endings, are derived and simulated. Hence, new porting area expressions are solved for pump performance. A new design for a port plate is introduced and the corresponding pump performance is investigated. Finally, the pump output is numerically compared with that of the proposed port plate (deep silencing grooves) and without silencing grooves.

The pipe dynamics and the fluid-induced vibrations are discussed in the third chapter. This chapter explains the relationship between the fluid flow and the pipe vibrations, and a classification of the different kinds of fluid-induced vibrations is given. The equations of motion are also given. The pipe stability is determined for different boundary

conditions and with several approaches. Finally, the complex Argand diagrams are plotted for simply supported, fixed-fixed, and cantilever pipes.

Experimental studies are carried out in order to validate the control strategies and to detect any defects in the hydraulic system. The experimental setup and its methodology are discussed in chapter four. Also, the components of the different sub-units of the hydraulic and control units are presented.

Chapter five deals with the control of the pump flow rate, ensuring optimum performance. The different control strategies of the swash plate pump are discussed showing the advantages and the disadvantages of every strategy. The current strategies are: with double negative feedback (the inner loop with the PID controller controls the spool position, while the outer loop with PD controller controls the swash plate swivelling angle), and with negative single feedback (with PD controller). A new single PID controller is proposed, simulated, and compared with the current strategies showing all of the advantages. Also, the same control strategy is used to control the pump output according to the load demands and pipe vibration levels. The results are obtained numerically, and different external disturbances are introduced to validate the control strategy.

In chapter six the vibration signatures from the pipe are used to monitor the hydraulic systems. The importance of the information included in vibration signatures is discussed, especially how it indicates the health of the machines. The different types of the signal transforms and their suitability for the different kinds of signals are discussed. Also, wavelet transforms' properties, types, and suitability are presented. Finally, different predetermined defects in the hydraulic system are created and the signals are studied by

wavelet transform to examine the appropriateness of wavelet transform in identifying the defects. The results are presented and discussed.

Finally, chapter seven contains a summary, conclusions, and recommendations for future work.

CHAPTER TWO

2 IMPROVING PUMP PERFORMANCE WITH A BETTER PORT PLATE DESIGN

2.1 Introduction

The previous chapter provided a general introduction to hydraulic systems, along with a review of the relevant literature, and outlined the objectives of this thesis.

In general, pumps are used in hydraulic circuits to pressurize a fluid and to convert mechanical power into hydraulic power. Because of their capacity for high specific power, great efficiency and reliability, swash plate pumps are widely used in industry. One of the objectives of this work is to investigate a novel design of the port plate in a swash plate pump, using a pair of deep triangular silencing grooves to improve pump performance with minimal fluid flow fluctuations and increase in the cylinder pressure, without any overshooting. Furthermore, the impact of the new port plate design on a swash plate pump's power is investigated.

2.2 Pump Components

Among the different kinds of pumps, swash plate pumps have a simple construction and are good for heavy-duty industrial applications. The pump can have either variable or constant displacement. Figure 2.1 shows the general components of a swash plate pump with a cylindrical arrangement.

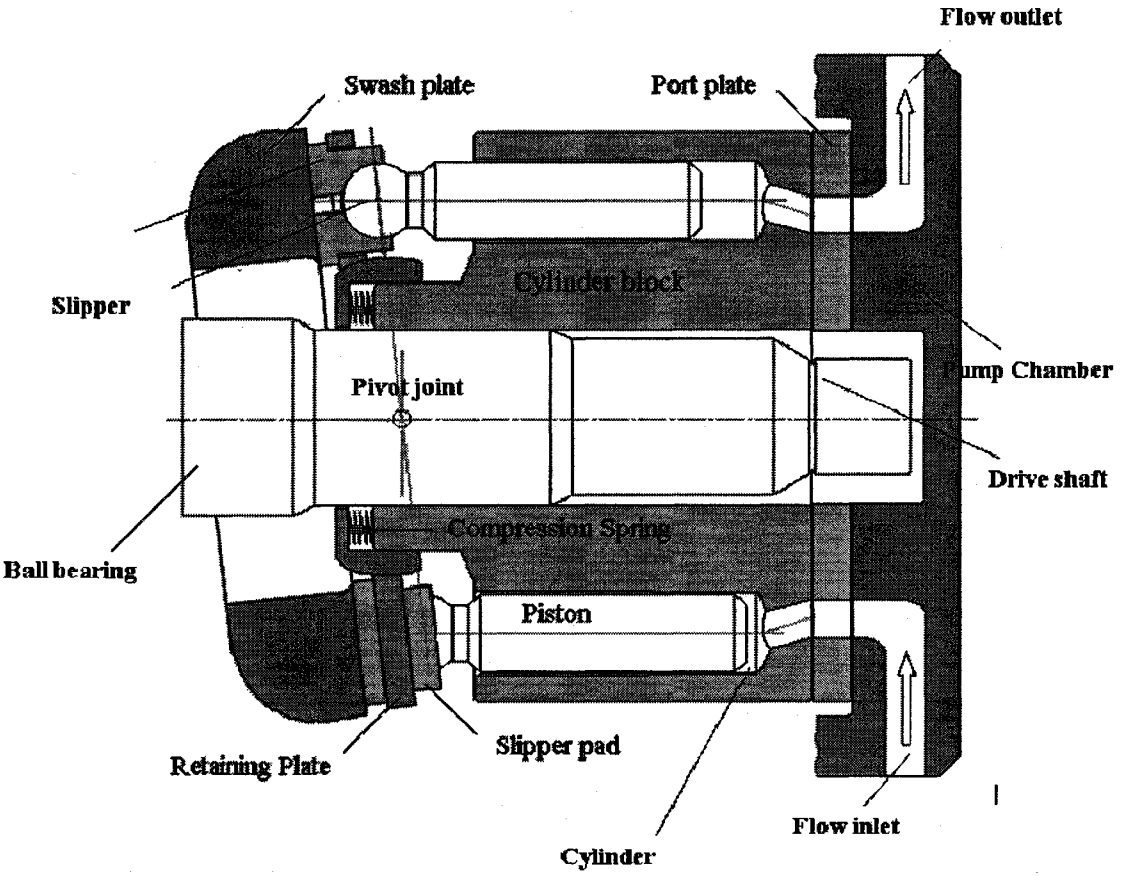

Figure 2.1: General components of a swash plate pump with a cylindrical arrangement

The pump is operated by an electric motor for stationary applications, or by an internal combustion engine for mobile applications. The pump is connected to the mechanical power source through a shaft, which passes through the swash plate in a ball bearing. The pump has a finite number of pistons nested in a common cylindrical block (in a circular array). The pump studied in this thesis has 9 cylinders, with each cylinder separated from the next with a phase difference of 40^{o}. The pistons are rigidly connected to the swash plate through ball-and socket joints and a slipper pad, while the block is kept firm against a port plate by a spring. The slippers are maintained in acceptable contact with the swash plate by a spring. The cylinder block is rotating with a constant angular speed while the port plate is stationary. In one operating cycle, each cylinder periodically passes over the port plate suction and delivery ports. In a suction stroke, the piston is retracted and fluid is sucked into the cylinder under the suction pressure and it will be completely filled with the fluid at the top dead center (T.D.C). Afterwards, the piston starts its delivery stroke, the cylinder moves over the delivery port and the piston advances in the cylinder -- pushing the fluid out of the cylinder.

2.3 Swash Plate Pump Operating Principle

The pump operation can be described by the operation of one of its cylindrical piston pairs. Two strokes are needed for the cylinder/piston pair to complete one operating cycle. These are the suction stroke and the delivery stroke, where the cylinder intakes hydraulic fluid from the pump reservoir during the suction stroke and delivers the pressurized fluid to the pump outlet in the delivery stroke. The beginning of the suction stroke is at the bottom dead center, B.D.C., and it ends at the top dead center, T.D.C., where the delivery stroke starts. This operation is repeated for each cylinder/piston pair. In the beginning of the suction stroke, the cylinder has just ended its delivery stroke and it has the minimum fluid. The cylinder block rotates, and the cylinder/piston pair moves away from B.D.C. and a suction pressure is developed as a result of the piston retraction. The cylinder's suction pressure forces more fluid to fill the cylinder and the cylinder is filled with the hydraulic fluid at the end of the suction stroke, when the cylinder is at the T.D.C. However, there must be regions where the cylinder is isolated from both the suction and delivery port plate slots. These regions are known as transitional zones. At the beginning of the delivery stroke, the cylinder leaves the T.D.C. toward the delivery slot; and the piston pressurizes the fluid and increases its pressure. It is a reasonable assumption to consider the cylinder pressure is equal to the delivery pressure in the delivery slot. The pressure drops to the suction pressure in the B.D.C., where another operating cycle starts.

2.4 Swash Plate Pump Designs

The early design of swash plate pumps did not have a control unit, and they had a completely cylindrical shape (the two sides of the cylinder block are identical). In this design, the piston reciprocating axis and the pump drive axis are parallel (illustrated in Figure 2.1). An improved design for the swash plate pump was introduced with the cylinders in a conical arrangement. Figure 2.2 shows the forces acting on the piston in the suction stroke for a circular swash plate pump and for a pump with a conical arrangement. During the suction stroke, the conical arrangement reduces the detachment force that tries to detach the piston from the slipper pad or the slipper pads away from the swash plate, which allows the pump to operate at higher speeds, and thereby enhances the pump specific power, and increases the piston stroke.

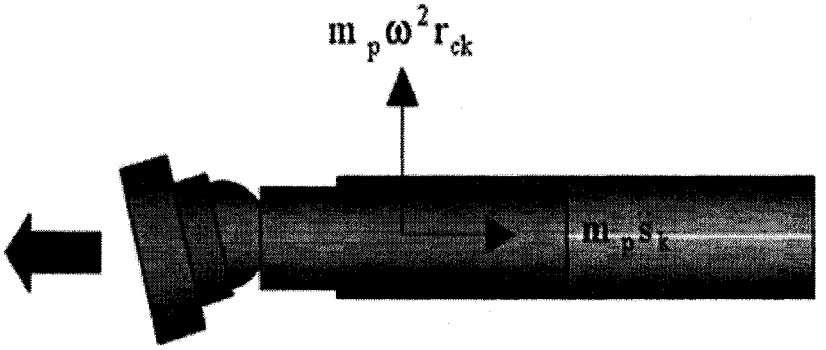

a- In a circular cylinder block

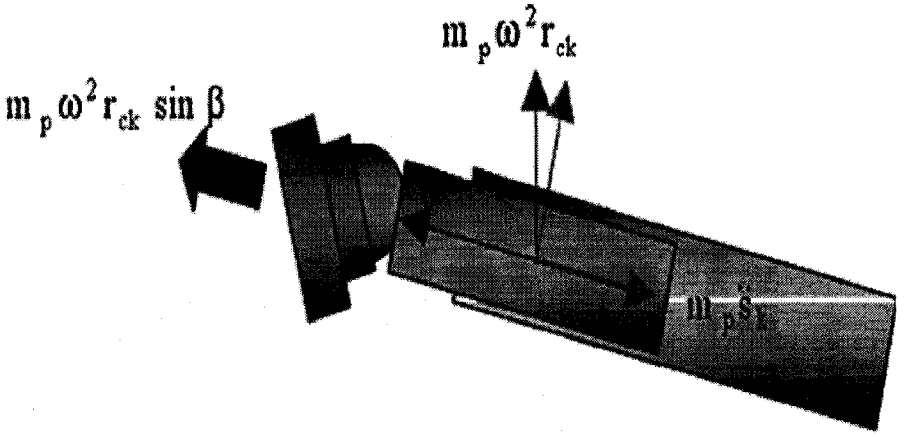

b- In a conical cylinder block

Figure 2.2: Line of action of a piston during suction stroke, [35]

2.5 Piston Kinematics

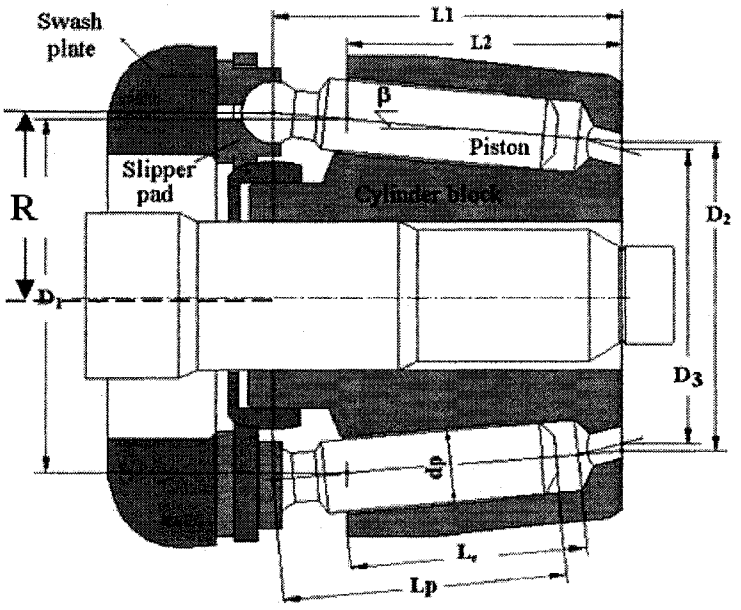

Figure 2.3: General dimensions of a swash plate axial piston pump with a conical cylinder block

In order to model the pump performance, the piston's kinematics must be considered. A swash plate pump has a complex design and simplified expressions for the piston kinematics will be derived. The K^{th} piston displacement is determined according to the swash plate inclination angle. The piston displacement is obtained with respect to fixed coordinates, by choosing a proper arrangement that includes the relationship between the inclination angle, the piston angular position and a key dimension that describes the motion of the piston at any given time. The K^{th} piston moves on the surface of the swash plate forming the piston pitch circle, which is the key dimension.

From Figure 1, the piston displacement can be expressed as

$$S_k(t) = -c_t.cos(\varphi) \tag{2.1}$$

where $\varphi = \omega.t$, and ω is the angular velocity of the pump shaft. Further,

$$c_t = \frac{R.tan\,(\alpha)}{cos\,(\beta)} \tag{2.2}$$

$$R = 0.5D_1 + [L_1 - L_2].tan\,(\beta) \tag{2.3}$$

The piston velocity and acceleration are given by differentiating Eq. (2.1), as

$$\dot{S}_k(t) = c_t.\omega.sin\,(\varphi) \tag{2.4}$$

$$\ddot{S}_k(t) = c_t.\omega^2.cos\,(\varphi) \tag{2.5}$$

The piston displacement, velocity and acceleration derived in Eqs. (2.1) – (2.5) were compared with known expressions derived by using frame transformation (introduced by Khalil and Bhat [35]), given by

$$S_k(t) = -\left(\frac{R_2.cos\varphi.tan\alpha + L_1}{cos\beta - cos\varphi.sin\beta.tan\alpha} - \frac{L_1}{cos\beta}\right) \tag{2.6}$$

$$\dot{S}_k(t) = \frac{\omega.sin\varphi.tan\alpha(L_1.sin\beta + cos\beta.R_2)}{(cos\beta - cos\varphi.sin\beta.tan\alpha)^2} \tag{2.7}$$

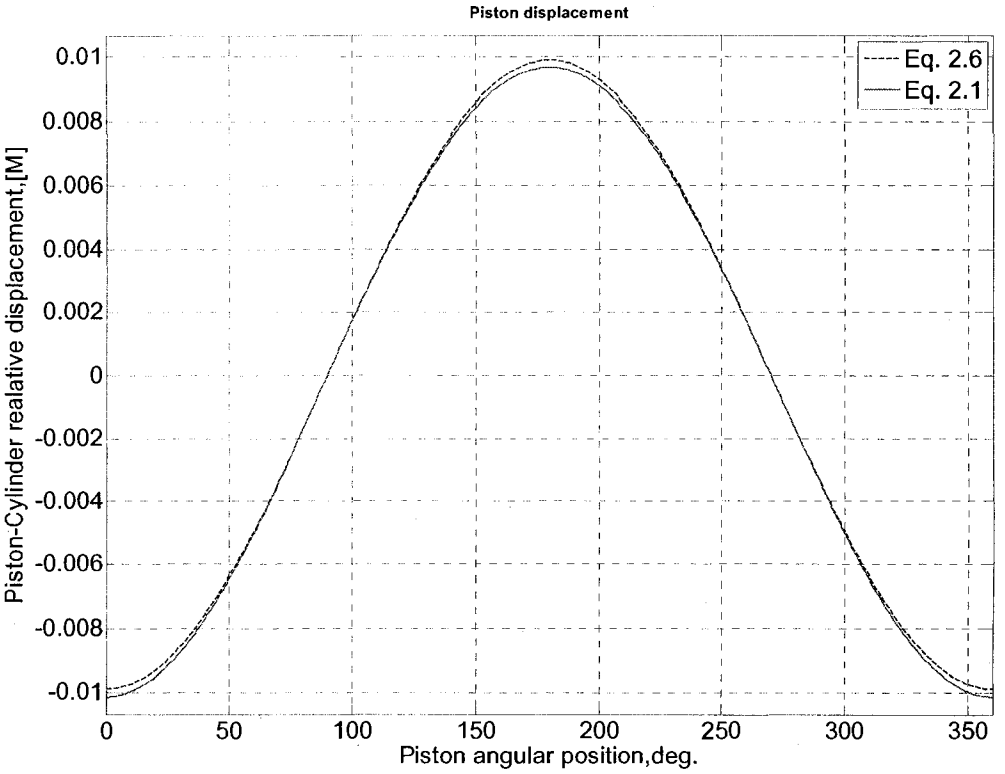

Figure 2.4 : Piston displacement

Figure 2.4 illustrates the piston displacement with both approaches, and it is obvious that the results agree closely. The dashed line represents Eq. (2.1) and the solid line represents Eq. (2.6) (from [35]). For the sake of simplicity, Eqs. (2.1), (2.4) and (2.5) will be used to express piston kinematics.

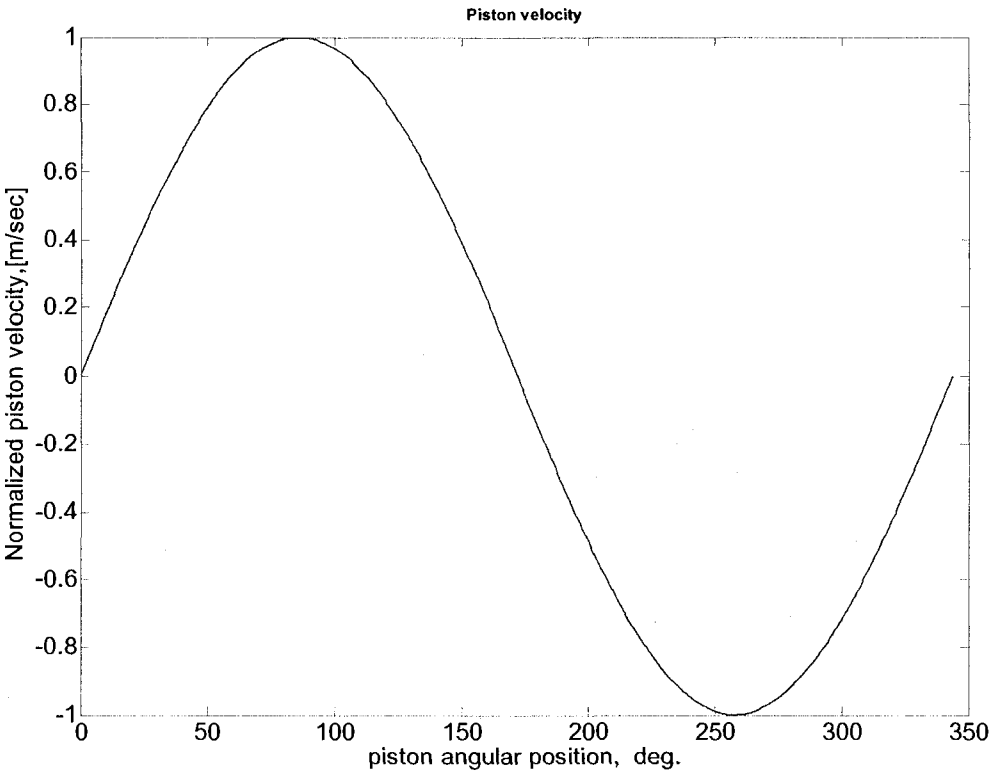

Figure 2.5: Piston velocity

Figure 2.5 shows the harmonic nature of the piston velocity. The velocity piston maximum occurs at the middle of the strokes, where the piston angular positions are 90° and 270°, respectively.

2.6 Instantaneous Cylinder Volume and Time Rate of Change

Hydraulic fluid is the medium that is used in pumps to convert mechanical power into hydraulic power in the form of a high-pressure fluid. Fluid pressure rise time rate is associated with different parameters such as the cylinder control volume and its rate of change.

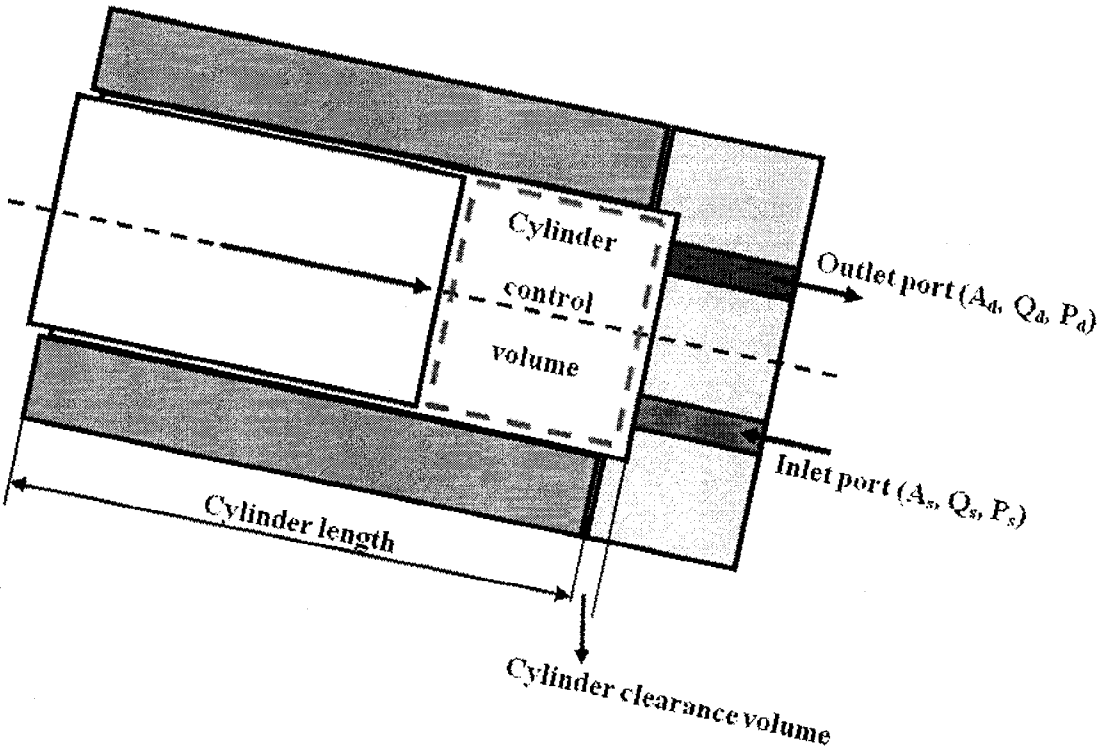

Figure 2.6: Cylinder parameters

The instantaneous cylinder volume is dependent upon the piston cross sectional area, the relative piston displacement in the cylinder, and the piston control length; and it is given as

$$V_{ck}(t) = a_p.\left(\frac{l_c}{2} - S_k(t)\right) + V_o \tag{2.8}$$

By differentiating Eq. (2.8), the volume time rate change is obtained as

$$\dot{V}_{ck}(t) = -a_p.\omega.c_t.sin\varphi \tag{2.9}$$

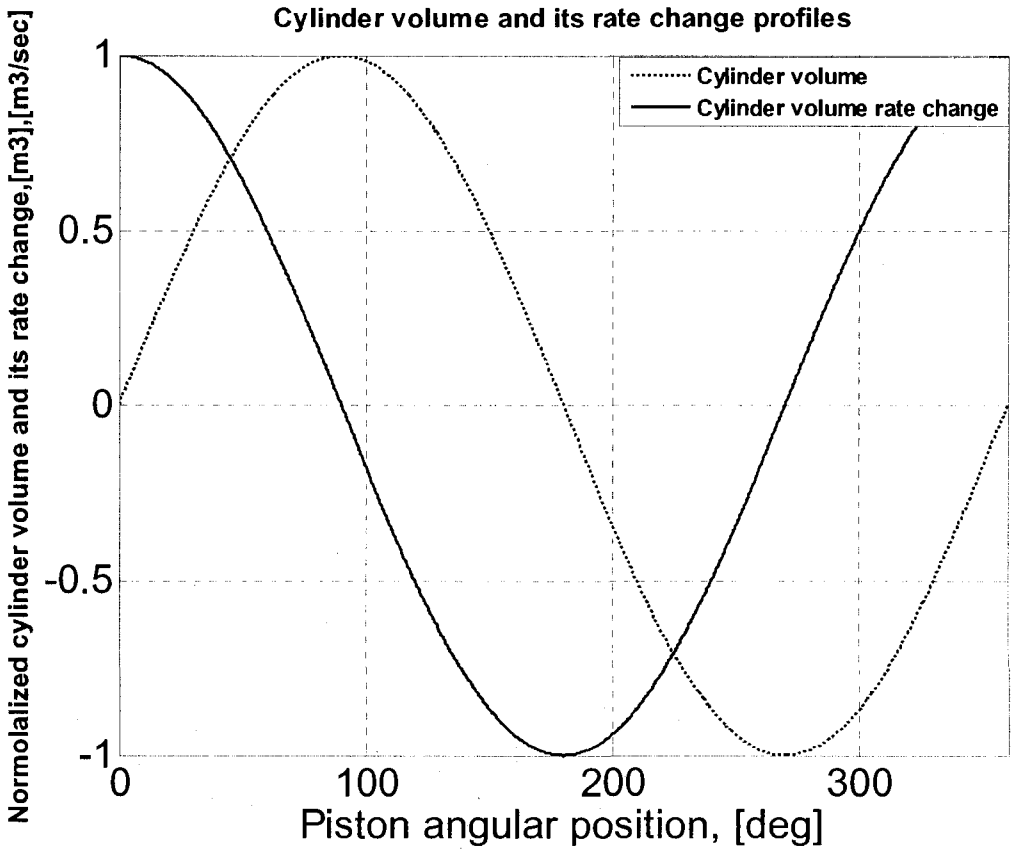

Figure 2.7: Cylinder control volume and the cylinder volume change rate with respect to piston angular position

Figure 2.7 shows the cylinder control volume and volume change rate as a function of the cylinder position. The maximum fluid volume happens when the piston starts its delivery stroke at the T.D.C. The maximum volume change rate, like the piston velocity, occurs when the piston angular positions are 90^{o} and 270^{o}.

2.7 Pump Performance

Swash plate pumps use hydraulic fluid to control and transfer power by converting mechanical power into hydraulic power, where the fluid is the means that produces this conversion. The cylinder pressure and the pump flow rate are the major parameters in this process. To evaluate the overall pump performance, requires two measures: cylinder pressure and the total pump flow rate. The pressure that exists inside the hydraulic cylinder should vary between the suction and delivery pressures. The cylinder flow rate is determined in relation to the delivery pressure value and the communicating area between the cylinder and the pump discharge chamber. In the delivery port, the pressure is equal to the delivery pressure. The recommended cylinder pressure must be developed and increased gradually to match the delivery pressure. This increase in the pressure should not exceed the delivery pressure, in order to prevent pressure overshooting. In the suction stroke the same process occurs, but in the reverse order, and the pressure should drop from delivery to suction pressure. The fluid flow takes place from the pump tank to the cylinder under a vacuum pressure.

In order to obtain the pump performance parameters, cylinder pressure and its respective volumetric flow rate, it is necessary to study the parameters that have an effect on the pump, such as pump kinematics, hydraulic fluid volume and its respective change rate and porting area change.

2.7.1 The Cylinder Pressure and the Pump Flow Rate

The governing equations for the cylinder pressure and its respective flow rate will be derived by considering that the pump is ideal, it does not exhibit any internal leak, and the fluid is incompressible.

The mass of fluid inside each cylinder varies with time. The mass can be given at any time as

$$M = \rho . V_{ck}(t) \tag{2.10}$$

The mass time rate change can be expressed as

$$\frac{dM}{dt} = \rho . \frac{dV_{ck}(t)}{dt} + V_{ck}(t) . \frac{d\rho}{dt} \tag{2.11}$$

The fluid mass does not experience any leak or compressibility, and hence the fluid mass time rate change can be expressed as

$$\frac{dM}{dt} = \rho . Q_k(t) \tag{2.12}$$

Also, the fluid bulk, which is a material property characterizing the compressibility of the fluid, can be presented as

$$B = \frac{dP}{d\rho/\rho} \tag{2.13}$$

Substituting Eq. (2.10) and Eq. (2.12) into Eq. (2.11) gives:

$$\frac{dM}{dt} = \rho . Q_k(t) = \rho . \frac{dV_{ck}(t)}{dt} + V_{ck}(t) . \frac{d\rho}{dt} \tag{2.14}$$

By simplifying the previous equation and substituting the equivalent formula of the fluid bulk into it, the pressure time rate change as a function of cylinder volumetric flow rate, bulk modulus, the cylinder fluid instant volume and time rate change of instantaneous cylinder volume is obtained as

$$\frac{dP}{dt} = \frac{B}{V_{ck}} [Q_k(t) - \frac{dV_{ck}(t)}{dt}] \tag{2.15}$$

And, by applying the cylinder volumetric flow rate, cylinder volume and volume rate change, the final form of the pressure time change rate can then be given as

$$\frac{dP}{dt} = \frac{B}{a_p . \left(\frac{l_c}{2} + c_t . cos\varphi\right) + V_o} [Q_k(t) - a_p . \dot{S_k}(t)] \tag{2.16}$$

where the flow rate can be expressed either as:

$$Q_k(t) = A_{de}(t) . \dot{S_k}(t) \tag{2.17}$$

or by using the Bernoulli expression,

$$Q_k(t) = sign\left(\sqrt{P_n - P_s}\right) . A_{de}(t) . C_d . \sqrt{\frac{2}{\rho}} \left(\sqrt{P_n - P_s}\right) \tag{2.18}$$

Furthermore,

$$V_{ck}(t) = a_p . \left(\frac{l_c}{2} + c_t . cos\varphi\right) + V_o$$

$$\dot{S_k}(t) = c_t . \omega . sin\varphi$$

$$\dot{V}_{ck}(t) = -a_p.\omega.c_t.sin\varphi$$

Eq. (2.16) does not have an identical solution, and in order to obtain the pressure within a single cylinder in one complete revolution, a piece-wise method will be used. For this purpose, knowledge of the configurations of the port plate is fundamental in obtaining the cylinder pressure and its flow rate and the total pump flow rate.

2.7.2 **Port Plate**

The port plate constrains the fluid passage into or out of the pump cylinders. It connects the cylinder port with the pump hydraulic reservoir at the suction port and with the pump discharge chamber at the delivery port. The port plate design must ensure a complete isolation between the cylinder and the discharge chamber and the reservoir. A pump's performance is determined by the characteristics of its port plate's design. All port plates have the same structure and vary only in the design of the ends of the grooves. They consist of two kidney ports, where the first port connects the cylinder delivery port to the pump delivery chamber and is named the delivery port and the second port connects the cylinder port to the reservoir and is called the suction port. The cylinder has two strokes, completed in one rotation of the pump shaft. The two strokes are the delivery stroke, or when the cylinder moves from the port plate T.D.C. and ends at the B.D.C., and the suction stroke, that happens when the cylinder moves from the B.D.C. to the T.D.C. The port plate is classified according to the presence of silencing grooves, the shape of the groove (shallow triangular or shallow rectangular) and the length of the transitional zones (the zone that does not allow any fluid suction or discharge into or out the cylinder). In the current design, the port plate is classified into these three types:

1- Without silencing groove.

2- With a triangular shallow silencing groove.

3- With a rectangular shallow silencing groove.

2.8 Effect of Port Plate Design on Pump Performance

The design of a swash plate pump for optimum performance needs to be completely reexamined. There are many key parts that should be redesigned from a functional point of view. Some of these would affect the pump dynamics and increase vibration levels; and others will help to improve the pump performance without changing the pump dynamics. Pressure overshooting and pump flow rate fluctuations are real problems for a swash plate pump, where pressure overshooting happens due to a sudden communication between the cylinder opening and port plate delivery slot (for the non-groove port plate); and the uncontrolled fluid expansion in the grooves leads to the pump flow fluctuations. The design of the port plate can help to reduce/eliminate pressure overshooting and the fluid flow fluctuations.

2.8.1 Port Plate without Silencing Grooves

2.8.1.1 *Approximate Expressions*

Earlier studies did not take into consideration the overlapping that occurs between the cylinder mouth and the delivery and suction ports. Hence, the results do not show the exact behaviour of cylinder pressure and flow rate profiles. In the earlier studies, the governing equations for the cylinder pressure and its respective flow rate for the delivery stroke are as follows:

In the delivery port only

The delivery area rate is equal to that of the area of the cylinder opening, while the pressure within the cylinder should equal the delivery pressure. The cylinder flow rate in the delivery slot is proportional to the area of the delivery slot (the cylinder opening is machined to match the port plate slots) and the piston velocity relative to the cylinder. Therefore, we may write

$$A_{de}(t) = A_d = \pi . r_d^2$$

$$Q_k(t) = \dot{S}_k(t) . A_d$$

$$P_n(t) = P_d$$

In the remainder of the port plate

The cylinder is completely closed off in the two transitional zones and in the T.D.C. and B.D.C. Hence, the cylinder does not discharge in these zones (absence of delivery areas), and the pressure can be approximated to be equal to the cylinder suction pressure. Therefore, the cylinder pressure, the delivery area, and the cylinder delivery flow rate may be written as;

$$A_{de}(t) = 0$$

$$Q_k(t) = 0$$

$$P_n(t) = P_s$$

The simulation results for the cylinder pressure and its flow rate are shown in Figure 2.8 2.8 and 2.9.

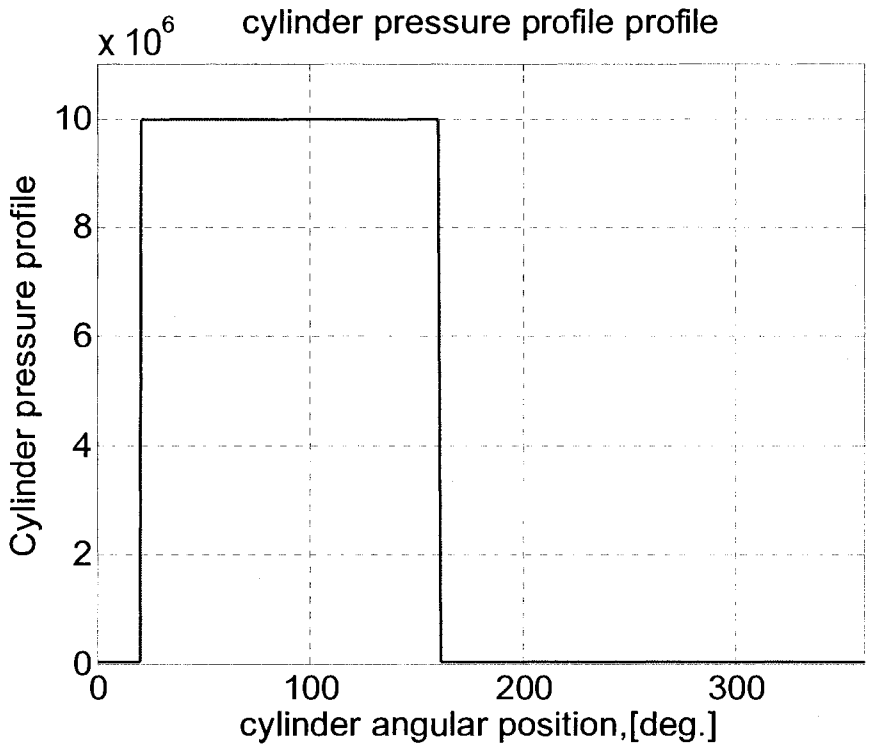

Figure 2.8: Cylinder pressure profile (port plate without grooved design)

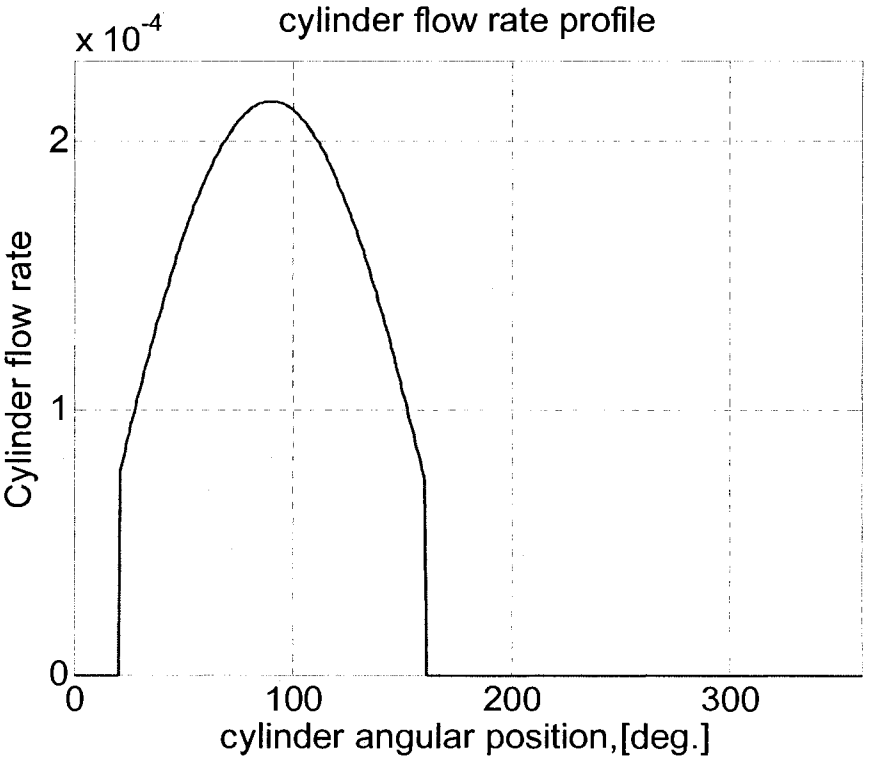

Figure 2.9: Cylinder flow rate profile (port plate without grooved design)

Figures 2.8 and 2.9 illustrate the cylinder pressure and flow rate profile for a pump that has a non-grooved port plate and the modeling does not consider the overlapping. From Figure 2.8, the pressure alternates between two values of the pressure (delivery and suction), with a sharp jump. Also, the cylinder discharge flow rate increases suddenly at the beginning of the delivery port and cuts off suddenly at the end of the delivery port. These results do not simulate real pump performance. In order to ensure early communication between the cylinder and the load, silencing grooves are machined on both ends of the ports. Manufacturers usually prefer to have an early communication that would lead to a reversal flow from the pump discharge chamber into the cylinder rather than allowing for fluid cavitation. The port plate with shallow silencing groove will be discussed later. But first, we will study the exact expressions of the port plate without silencing grooves and how the pump performance profiles will be different from those considered in Figures. 2.8 and 2.9.

2.8.1.2 *Exact Expressions (considering overlapping areas)*

As observed in the previous approach (no overlapping areas), the results do not really show the exact pump performance. In order to generate more reliable results, more accurate modeling of the instantaneous motion of the cylinder opening over the port plate, including the overlapping zones, needs to be considered. In these areas, the transition from suction pressure to delivery pressure takes place and vice versa, and an accurate modeling of the variations of the cylinder mouth opening with the port plate grooves would predict the overshooting phenomenon more realistically.

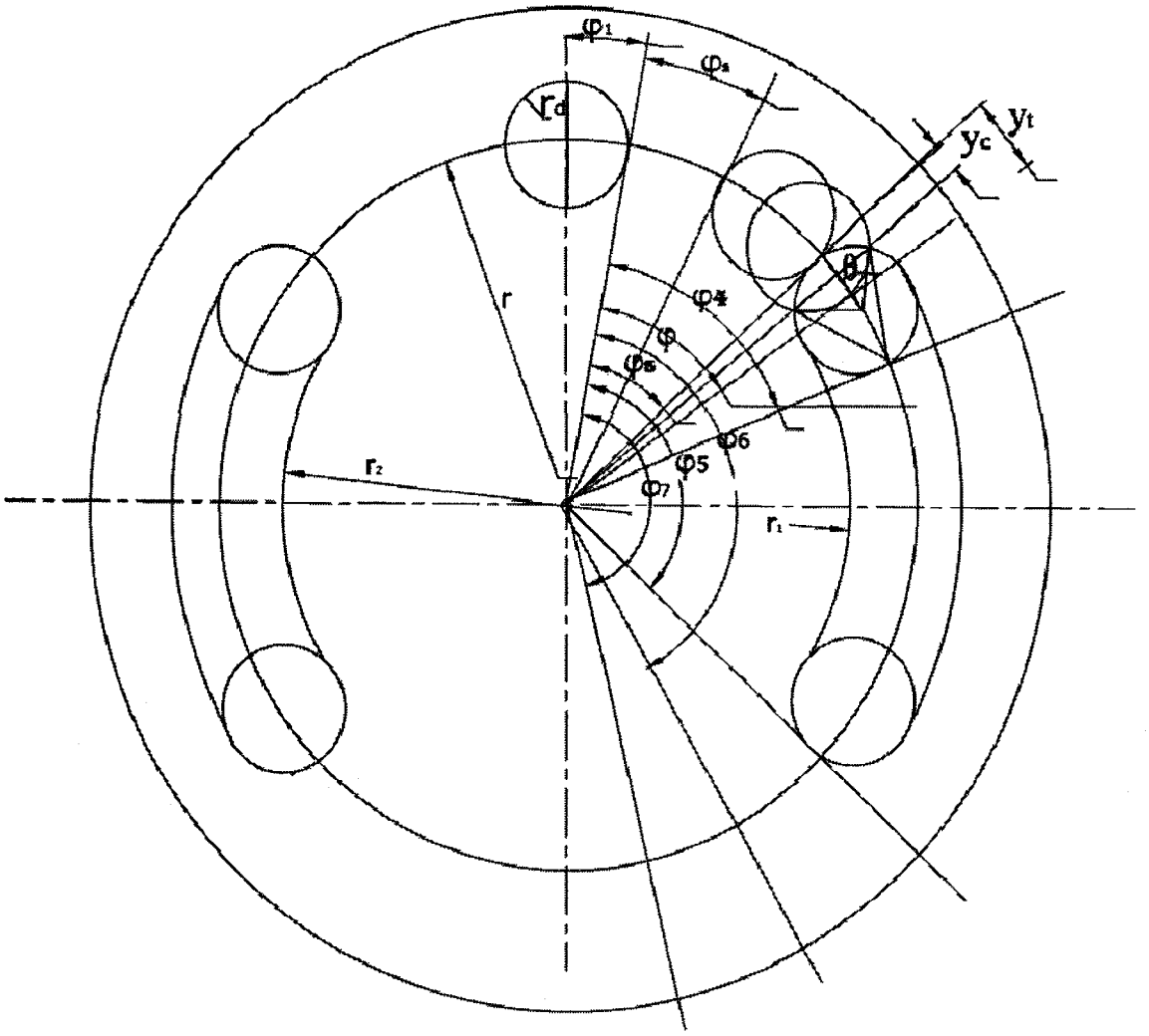

Figure 2.10: General configuration of a port plate with a non-grooved design

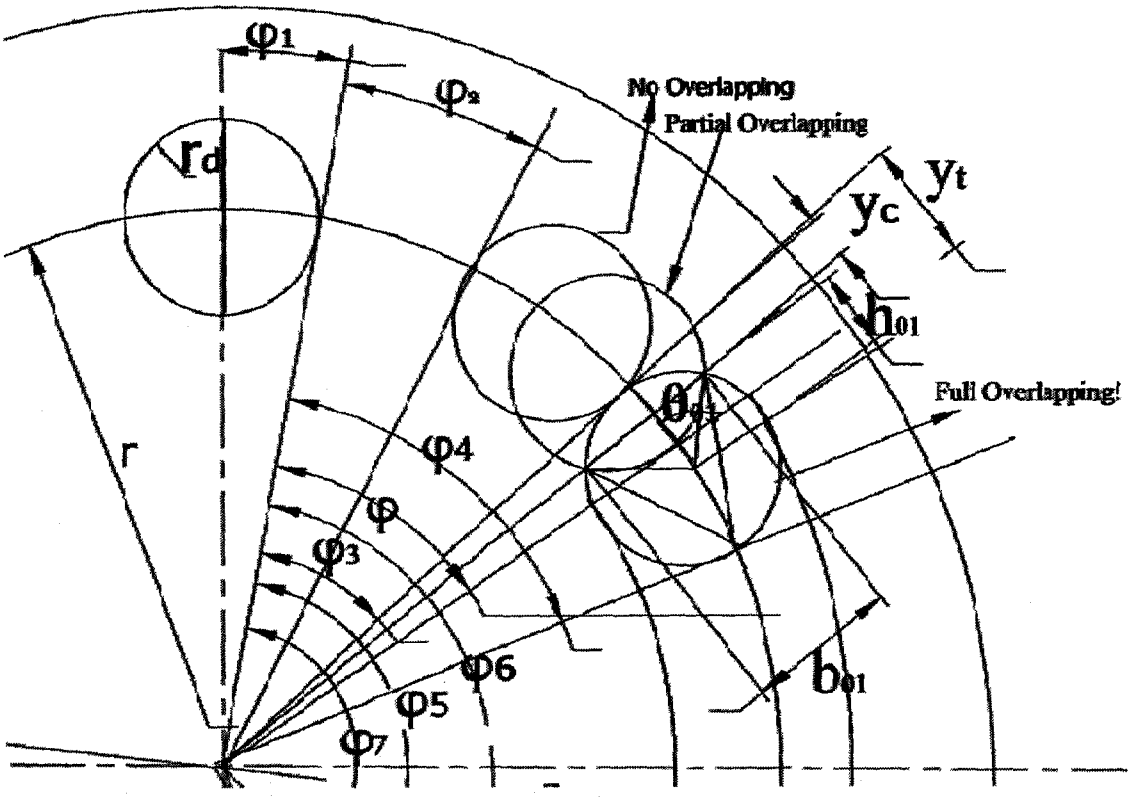

Figure 2.11: Main dimensions of the overlapping area for a non-grooved design in the entry area

2.8.1.2.1 Porting Area Profile

Figure 2.10 shows the general configuration of a port plate with no silencing groove. The plate is divided into four transitional zones (on both sides of the dead centers), the delivery and suction ports and four overlapping areas (located at the entrance and exit of the ports).

In order to calculate the porting area of the different zones, the port plate geometry should be considered in piecewise fashion. The porting area starts at the first overlapping zone and ends at the end of the second overlapping zone.

In the transitional zone:

Here, there is no communication between the cylinder and the load. The importance of this zone is to grant the cylinder enough time to build up the pressure. Its length is an important aspect in the design of the port plate. A short zone will not allow the pressure inside the cylinder to reach the required value and there will be flow reversal to the cylinder (according to the load requirement), and a long zone will lead to an increase in pressure and probably attaining high values that would lead to cavitation.

The porting area in this zone can be expressed as

$$A_{de}(t) = 0$$

In the entry overlapping zone:

The actual flow takes place when the cylinder port starts to communicate with the load via the entry overlapping zone. The flow increases proportionally to the cylinder porting area and the cylinder angular velocity, and reaches a steady value in the delivery port.

The porting area in the overlapping zone increases in nonlinear fashion, where it equals zero at φ_3 and becomes equal to the area of the cylinder opening at the end of the zone, or φ_4. The center of the cylinder opening moves in a circular orbit (coincides on the radius of the port plate), and there is a certain angular length for every zone on the port plate. The porting areas are expressed in terms of these angular lengths. The first term

that is needed to model the porting area of the entry overlapping zone is defined by the overlapping angular length.

From Figures 2.10, and 2.11, the overlapping angular length is denoted as y_t and can be expressed as:

$$y_t = r.(\varphi - \varphi_3)$$

where y_t is the overlapping length, r is the port plate radius, φ is the cylinder angular position at that instant, and φ_3 is the angle at which the overlapping zone starts.

Hence, the middle angular distance can be given as:

$$y_c = 0.5\, y_t = 0.5\, r.(\varphi - \varphi_3)$$

The entry side of the delivery port increases with the advance of the cylinder/piston pair towards the delivery slot. From Figure 2.11, the porting area can be visualized simplified as two crescents and two triangles; and the crescents become a full circle at the end of the overlapping zone. The porting area of the entry overlapping zone may be written as:

$$A_{de} = A_{ot} = 2.[r_d^2.\theta_{01} - h_{01}.b_{01}]$$

where

$$h_{01} = r_d - y_c = r_d - 0.5\, r.(\varphi - \varphi_3),$$

$$b_{01} = r_d.\sin\theta_{01}$$

$$\theta_{01} = cos^{-1}(\frac{r_d - 0.5\, r.(\varphi - \varphi_3)}{r_d})$$

In the delivery port

In this zone, the cylinder opening matches the delivery slot; and hence, the porting area is equal to the cylinder delivery port.

$$A_{de} = \pi . r_d^2$$

In the exit overlapping zone:

Here, the porting area decreases with the advancement towards the B.D.C. The porting area in the exit overlapping zone is derived in a similar fashion as on the entry side, and the porting area in the second overlapping area can be expressed as:

$$A_{de} = A_{ob} = 2.[r_d^2.\theta_{02} - b_{02}.h_{02}]$$

where

$$\theta_{02} = cos^{-1}\left(\frac{r_d - 0.5(\varphi_6 - \varphi)}{r_d}\right)$$

$$h_{02} = (r_d - 0.5(\varphi_6 - \varphi))$$

$$b_{02} = r_d . sin\,\theta_{02}$$

As the porting area becomes smaller, the flow decreases gradually in this zone.

In the second transitional zone:

When the pair leaves the exit overlapping zone, there will be no communication between the cylinder and the pump discharge chamber. Therefore, the porting area may be written as:

$$A_{de} = 0$$

2.8.1.2.2 Cylinder Pressure and Pump Flow Rate Profiles:

As shown in the previous section, the delivery section on the port plate can be divided into five different zones. These different zones have different values for the pressure and cylinder flow rate. The previous porting areas are used to obtain the pressure and flow analysis for a single piston-bore within the pump. The values in the different zones are:

In the first transitional zone, φ_1 to φ_3:

In this zone, the pressure can be approximated to be equal to the suction pressure. The cylinder is isolated from both the suction and delivery ports. Therefore, the governing equations that can express the porting area, cylinder pressure, and the cylinder flow rate may be written as

$A_{de}(t)=0$

$Q_k(t) = 0$

$P_n(t) = P_s$

The first overlapping zone, φ_3 to φ_4:

In this zone, the cylinder is moving from the first transitional zone into the discharge port. The cylinder delivery port starts to match the delivery port, opening gradually at φ_3, and the discharge area increases to become equal to the cylinder delivery port at φ_4. The angular length of this zone is fixed and is equal to the diameter of the cylinder port. The pressure increases as a result of the motion of the piston inside the cylinder, pressurizing the fluid. The flow rate depends on two factors: the pressure difference and the porting area, and as the pressure increases the flow rate increases (if there is a porting area). The

pressure increase is proportional to the porting area, cylinder volume, piston velocity, and the discharge coefficient. The mathematical expressions are:

$$A_{de}(t) = A_{ot} = 2[r_d^2 . \theta_{o1} - b_{o1} . h_{o1}]$$

$$Q_k(t) = sign(\sqrt{P_n - P_s}) . A_{ot} . C_d . \sqrt{\frac{2}{\rho}} (\sqrt{P_n - P_s})$$

$$P_n(t) = P_s + \left(\frac{A_{ot} . B . \dot{S}_k(t)}{\omega . V_{ck}(t)} . (\varphi - \varphi_3) \right)$$

where

$$h_{o1} = r_d - 0.5(r . (\varphi - \varphi_3))$$

$$\theta_{o1} = cos^{-1} \frac{h_{o1}}{r_d}$$

$$b_{o1} = h_{o1} . sin\, \theta_{o1}$$

The zone of delivery flow, φ_4 to φ_5:

Here, the cylinder is in full communication with the load via the delivery port. The cylinder port matches the accurate porting geometry of the valve plate. The pressure is equal to the delivery pressure and the flow rate is proportional to the porting area and the piston velocity. We may write

$$A_{de}(t) = A_d = \pi . r_d^2$$

$$Q_k(t) = sign(\sqrt{P_n - P_s}) . A_d . C_d . \sqrt{\frac{2}{\rho}} (\sqrt{P_n - P_s})$$

$$P_n(t) = P_d$$

The second overlapping zone, φ_5 to φ_6:

As the piston chamber moves toward the second transitional zone near the bottom dead center, the actual flow passage is gradually cut off due to the terminating port-geometry of the valve plate in this region. The pressure is supposed to drop from the delivery pressure to the suction pressure at the total close off of the cylinder. The flow rate should also gradually cut off and does not discharge at the end of the second overlapping zone. The porting area, cylinder pressure, and the cylinder flow rate are

$$A_{de}(t) = A_{ob} = 2[r_d^2 . \theta_{o2} - b_{o2} . h_{o2}]$$

$$Q_k(t) = sign\left(\sqrt{P_n - P_s}\right) . A_{ob} . C_d . \sqrt{\frac{2}{\rho}} \left(\sqrt{P_n - P_s}\right)$$

$$P_n(t) = P_d - \left(\frac{A_{ob} . B . \dot{S}_k(t)}{\omega . V_{ck}(t)} . (\varphi - \varphi_5) \right)$$

where

$$h_{o2} = r_d - 0.5\left(r . (\varphi_6 - \varphi)\right)$$

$$\theta_{o2} = cos^{-1} \frac{h_{o2}}{r_d}$$

$$b_{o2} = h_{o2} . sin\, \theta_{o2}$$

The second transitional zone, φ_6 to $\pi + \varphi_1$:

In this zone, the piston bore is completely closed off, and there is no fluid flow into or out of the cylinder. The cylinder pressure is assumed to be equal to the suction pressure. The characteristics of this zone are expressed as

$$A_{de}(t) = 0$$

$$Q_k(t) = 0$$

$$P_n(t) = P_s$$

Numerical Simulation

The K^{th} cylinder delivery area at any given angular position is computed from the above expressions. The value of the area, in addition to the corresponding cylinder instantaneous volume and the piston velocity were used to determine the cylinder pressure and its respective flow rate for each angular position of the K^{th} cylinder.

The delivery area, cylinder pressure and cylinder discharge versus the angle φ for any pump running speed are plotted in Figures 2.12, 2.13 and 2.14, respectively. A simulation run was carried out for a 9-piston pump of geometric volume 40 cc/rev, running at a constant speed of 1800 rpm; with the hydraulic fluid ISO 46 and a bulk modulus of 1.3X 10^9 Pa. The various configurations of the port plate are shown in Figure 2.10. The length of the first transitional zone is proportional to 18^o and the second to 162^o. The cylinder pressure profile and the pump total flow rate are illustrated in Figures 2.13 and 2.14, respectively.

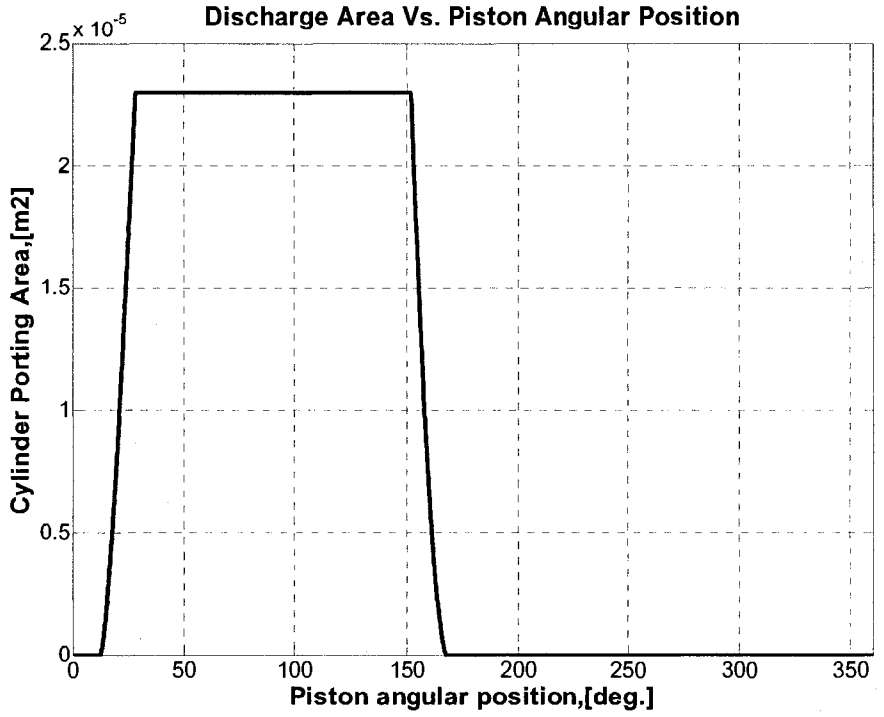

Figure 2.12: The porting area of the K^{th} cylinder in the delivery stroke

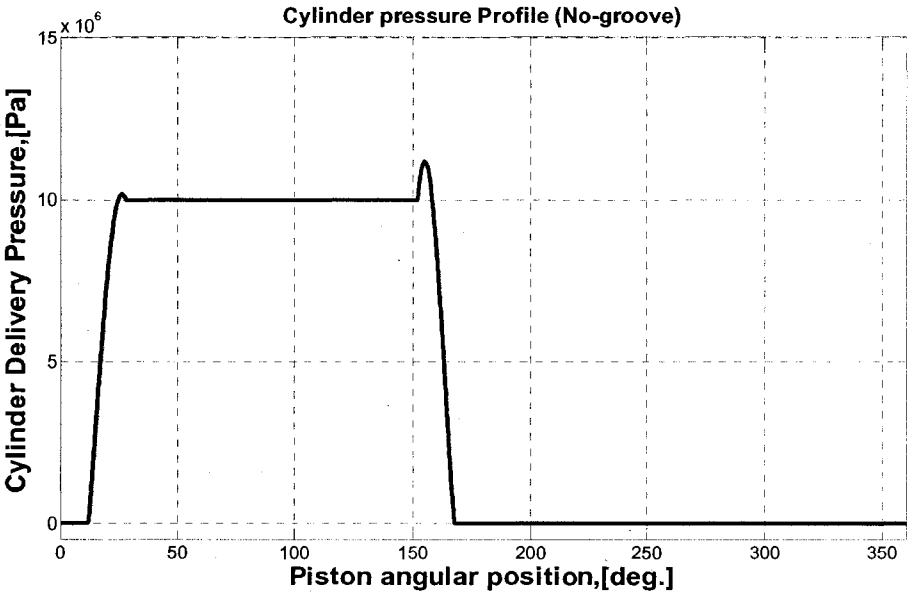

Figure 2.13: Cylinder pressure profile (Non-grooved port plate)

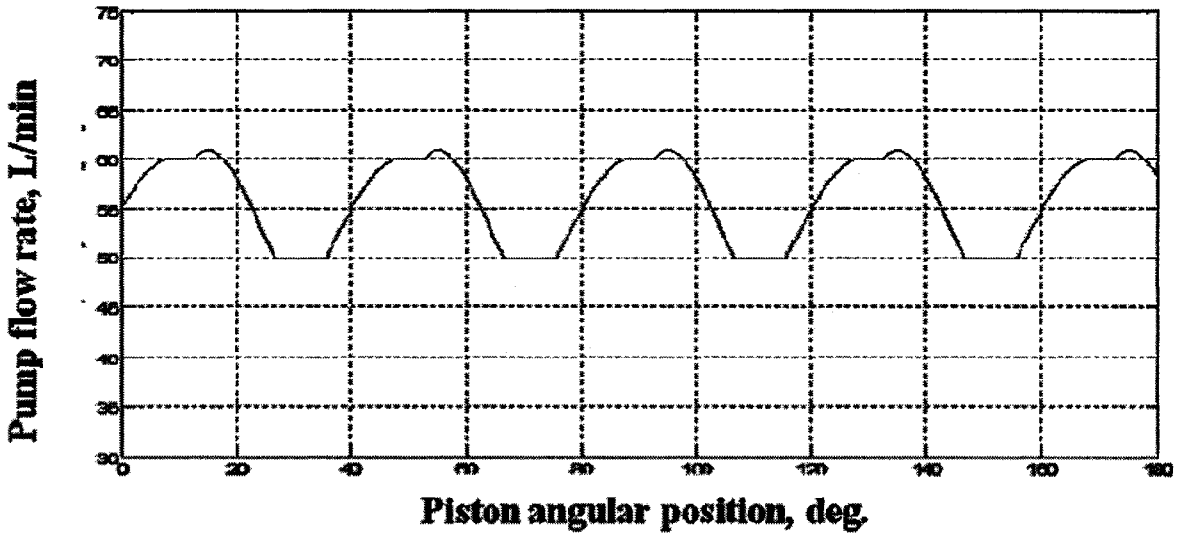

Figure 2.14: Pump volumetric flow rate profile (Non-grooved port plate)

Figure 2.12 shows the cylinder porting area profile during the delivery stroke. In the transitional zones, there is no communication between the cylinder port and the pump discharge chamber (the porting area is zero). Afterwards, in the first overlapping zone, the porting area increases nonlinearly and then it remains constant in the delivery port. The porting area starts to decline in the second overlapping zone and becomes zero at the beginning of the second transitional zone. Figures 2.13 and 2.14 show the cylinder pressure and the pump flow rate profiles, respectively. The pressure profile shows two cases of overshooting at the edges of the delivery port. The first pressure overshooting is produced by the sudden contact of the pressure in the pump discharge chamber and the high pressure that is generated by the cylinder. The second case of overshooting occurs due to the sudden closure of the delivery port near the B.D.C. The cylinder flow rate profile resembles the cylinder pressure profile.

2.8.2 **Standard Design**

The current generation of pumps are equipped with port plates that have shallow end silencing grooves, referred to hereafter as standard design port plates. The shape of the end grooves can be triangular or rectangular, and the grooves are machined on both sides of each port plate slot, as shown in Figure 2.15. The objective of these grooves is to have earlier gradual communication between the cylinder and the slots, see Figure 2.16. However, this design causes spikes in the groove ends and does not allow enough time for the pressure to build up. Also, it leads to a drop in the pump volumetric efficiency [51. The grooves are considered as orifices and the Bernoulli principle is used to model pump performance.

Manring [51] studied this type of port plate and found that this design has some disadvantages. He supported his analysis by comparing this design with a non-grooved design. His work will be replicated in this part of the current study before introducing the new port plate design. In [51], there was no consideration for overlapping, and hence, it is not included in the present analysis. As mentioned in the previous chapter, the plate should be divided into sections to characterize the pressure and volumetric flow rate. The general configuration of the standard port plate design is shown in Figure 2.15, while Figure 2.16 shows the side section of the standard port plate.

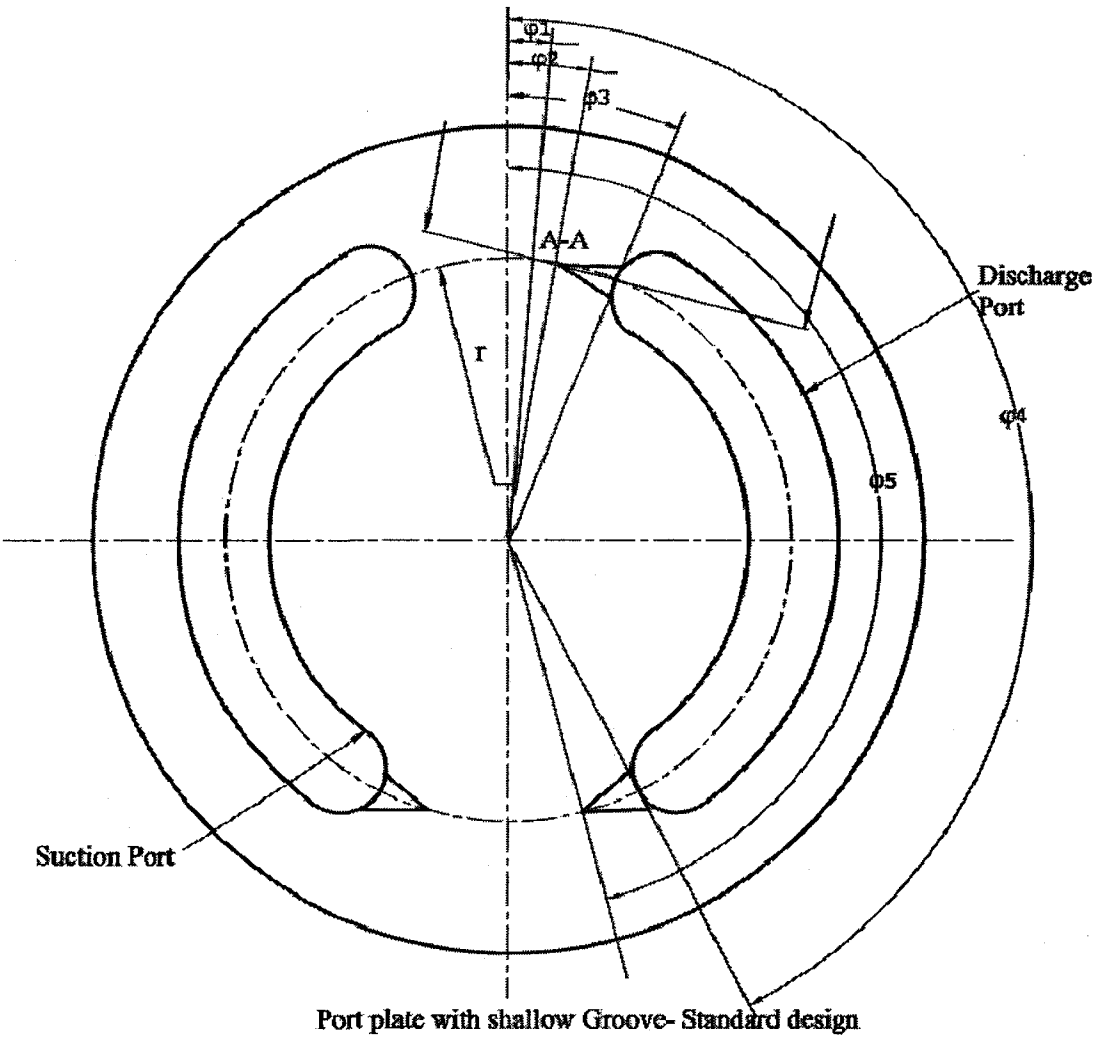

Figure 2.15: General configurations of the standard design of shallow triangular grooved port plate

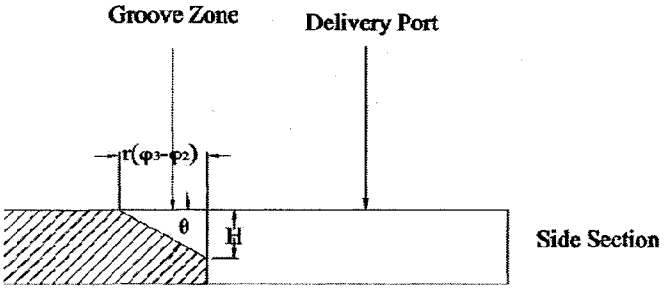

Figure 2.16: Side section of the standard design of a shallow triangular groove.

2.8.2.1 *Pressure and Pump Flow Rate Profiles*

For the standard port plate, the port plate regions may be characterized by the following:

1) The first transitional zone: $\varphi_1 \leq \varphi \leq \varphi_2$

$$A_{de}(t) = 0$$

$$Q_k(t) = 0$$

$$P_n(t) = P_s$$

2) The upper groove zone: $\varphi_2 \leq \varphi \leq \varphi_3$

The delivery area, A_{de}, which is the area of the triangular silencing groove opening into the discharge port, can be given as:

$$A_{de}(t) = A_{otg} = 0.5.\tan\theta\,.\,b.\,r.\,(\varphi_3 - \varphi_2)$$

$$Q_k(t) = A_{otg}.\,C_d.\sqrt{\frac{2}{\rho}}\left(\sqrt{P_d - P_s} - k_1.\frac{A_{otg}}{V_{ck}(t)}.(\varphi - \varphi_2)\right)$$

$$P_n(t) = P_d - \left(\sqrt{P_d - P_s} - k_1.\frac{A_{otg}}{V_{ck}(t)}.(\varphi - \varphi_2)\right)^2$$

where

$$k_1 = \frac{B.\,C_d.\sqrt{\frac{2}{\rho}}}{2.\omega}$$

3) The delivery port zone: $\varphi_3 \leq \varphi \leq \varphi_4$

$$A_{de}(t) = A_d = \pi.\,r_d^2$$

$$Q_k(t) = \dot{S}_k(t).A_d$$

$$P_n(t) = P_d$$

4) The lower groove zone: $\varphi_4 \leq \varphi \leq \varphi_5$

$$A_{de}(t) = A_{obg} = 0.5.\tan\theta.b.r.(\varphi_5 - \varphi_4)$$

$$Q_k(t) = A_{obg}.C_d.\sqrt{\frac{2}{\rho}}\left(\sqrt{P_d - P_s} - k_1.\frac{A_{obg}}{V_{ck}(t)}.(\varphi - \varphi_4)\right)$$

$$P_n(t) = P_s + (\sqrt{P_d - P_s} - k_1.\frac{A_{obg}}{V_{ck}(t)}.(\varphi - \varphi_4))^2$$

5) The second transitional zone: $\varphi_5 \leq \varphi \leq \pi + \varphi_1$

$$A_{de}(t) = 0$$

$$Q_k(t) = 0$$

$$P_n(t) = P_s$$

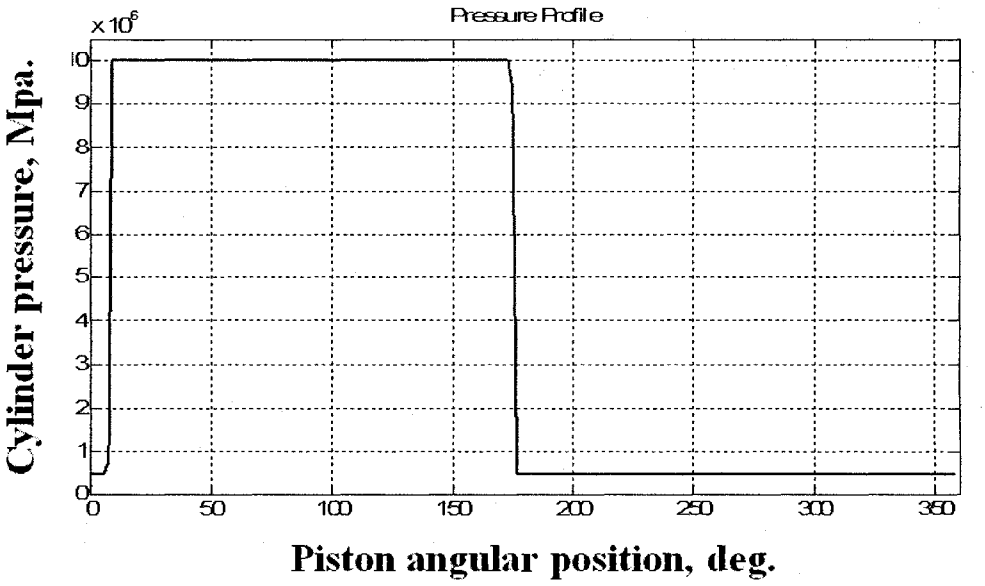

Figure 2.17: Pressure profile for a standard-design pump, without considering the overlapping area

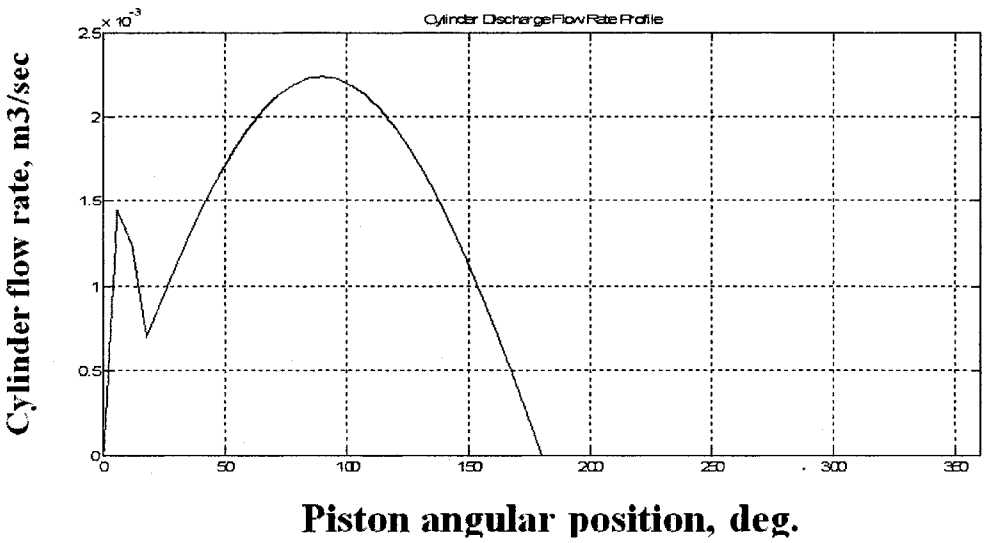

Figure 2.18: Flow profile for a standard-design pump, without considering the overlapping area

Figures 2.17 and 2.18 show the cylinder pressure and the cylinder flow rate [51]. The grooves generate spikes that result from the uncontrolled expansion of fluid which occurs through the grooves at the beginning and end of the delivery stroke. In Figure 2.18, it was assumed that a delivery slot utilizes a single groove in the beginning of the communication with the cylinder. Figure 2.18 shows only one spike.

2.8.3 **The Proposed Design**

The standard design produces undesirable pump performance. The cylinder pressure exhibits overshooting, and the corresponding pump flow rate has a considerable flow fluctuation. In order to reduce the fluctuations, a pair of deep silencing grooves at the ends of the delivery port are introduced.

The grooves will:

1- Allow the cylinder to enter and leave the port plate groove in a gradual fashion.

2- Improve the pump volumetric efficiency, whereas a volumetric flow leak occurs though the shallow grooves [51].

3- The triangular shape of the groove helps to develop the transitional pressure without overshooting.

4- Reduce the pump flow rate fluctuations.

5- Provide a longer time for the pressure to change between the required pressure values.

2.8.3.1 ***Porting Area Profile***

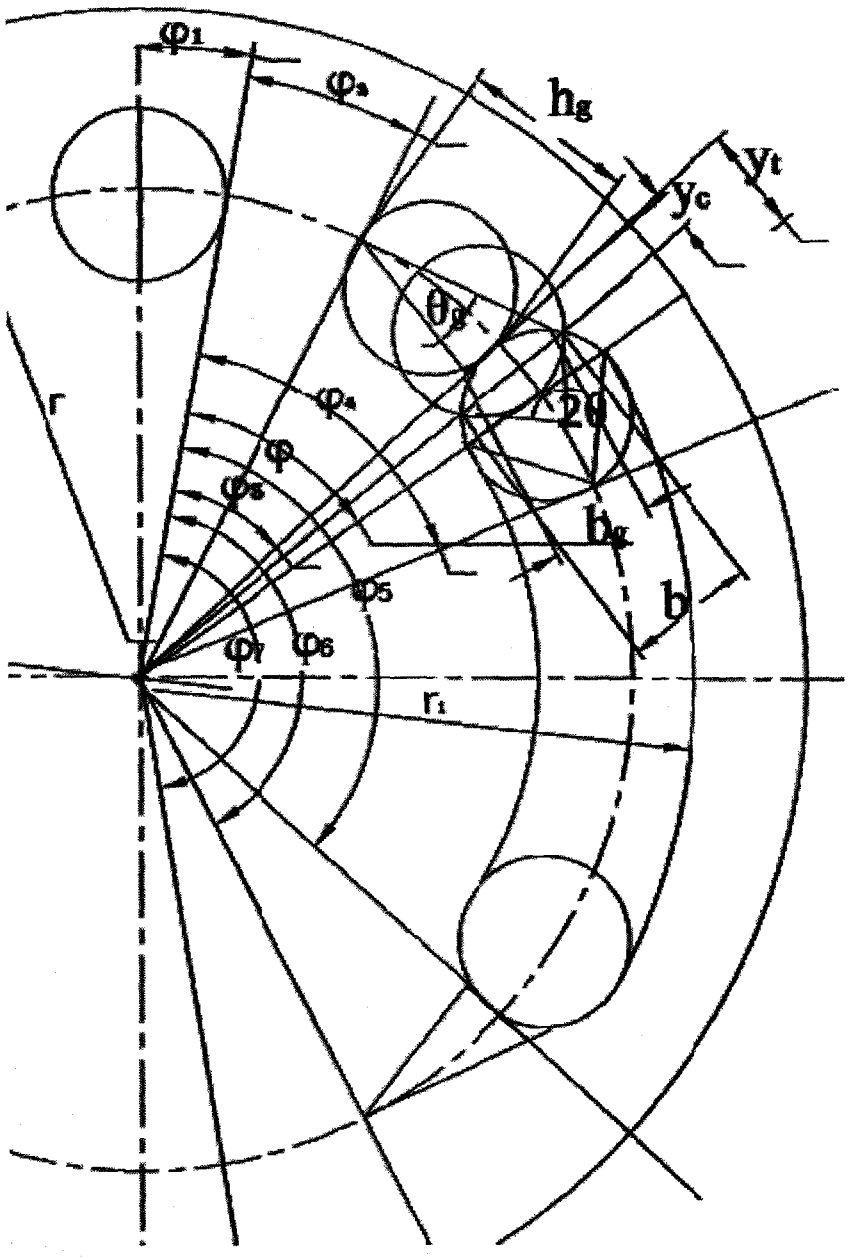

Figure 2.19: General configurations of port plate with deep triangular groove design

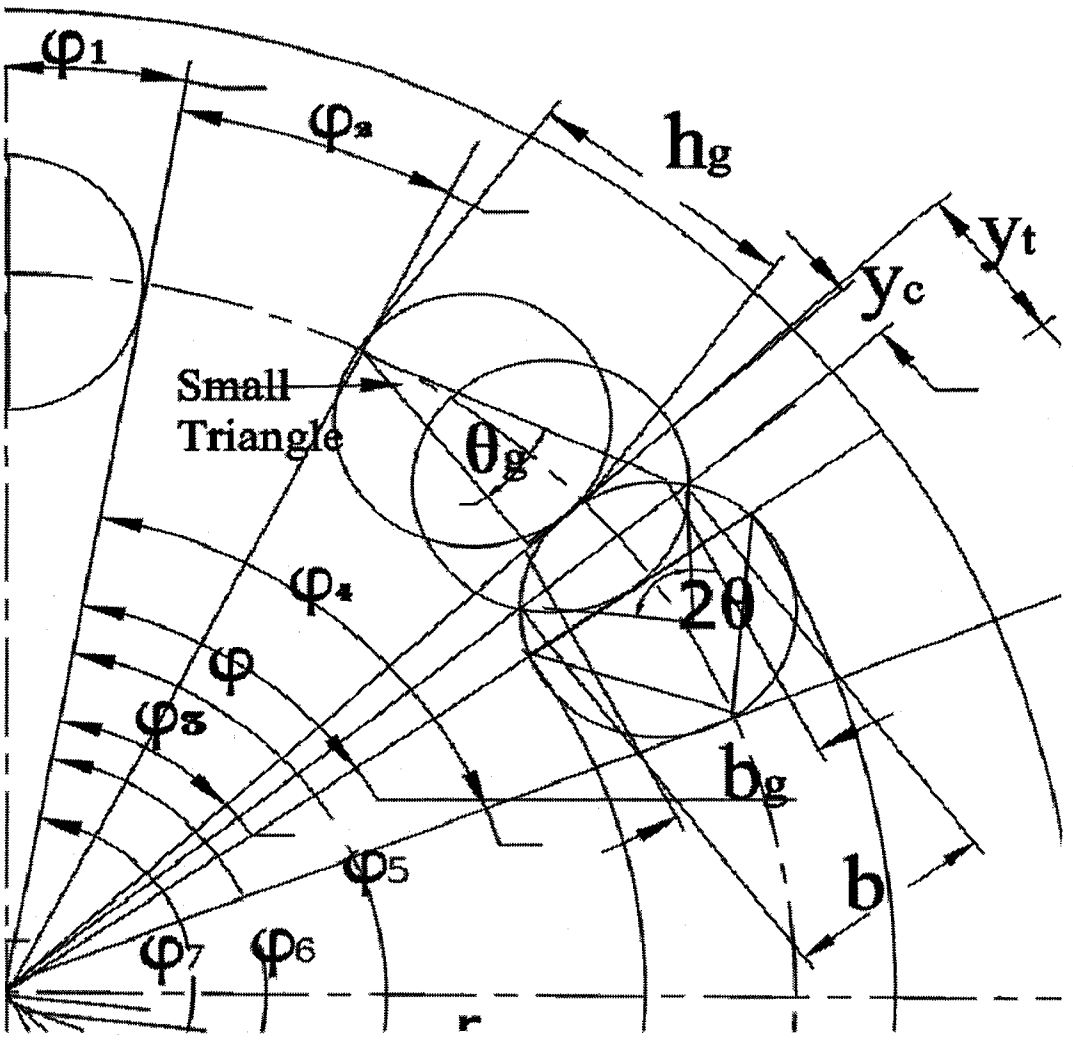

Figure 2.20: Main dimensions of the overlapping area for a port plate with a deep triangular groove design

Figures 2.19 and 2.20 show the port plate general configurations and the overlapping area on the entry side of the delivery slot, respectively. The right half of the port plate represents the cylinder delivery stroke trajectory. That half is divided into seven different

zones: two transitional zones, two overlapping zones, two grooves and the delivery port zone. It can be seen that:

1) When the cylinder port is in the first transitional zone ($\varphi_1$to φ_2), there is no delivery area.
2) When the cylinder port is in the first groove zone ($\varphi_2$to φ_3), the delivery area is dependent on the silencing groove's dimensions.
3) When the cylinder port is in the first overlapping zone ($\varphi_3$to φ_4), the delivery area is a common area between the delivery port and the groove, and there is an instantaneous delivery area, according to the piston angular position. The delivery area in this sector is the sum of two areas, which are covered with part of the groove and part of the delivery port at the same time.
4) When the cylinder port is in the delivery port ($\varphi_4$to φ_5), the delivery area is equal to the area of cylinder delivery port.
5) When the cylinder port is in the second overlapping zone ($\varphi_5$to φ_6), the delivery area is the sum of two areas, which are covered with part of the groove and part of the delivery port at the same time.
6) When the cylinder port is in the exit groove zone ($\varphi_6$to φ_7), the delivery area is dependent on the silencing groove's dimensions only.
7) When the cylinder port is in the second transitional zone (φ_7 to $\pi + \varphi_1$), there is no delivery area.

Referring to Figure 2.19 and Figure 2.20, the porting area varies according to the angular position of the K^{th} cylinder, and it has a maximum value in the sector φ_4 to φ_5 . The cylinder starts to communicate with the pump discharge chamber earlier, at φ_2.

The mathematical expressions for the porting (delivery) area are:

1. The first transitional zone, φ_1 to φ_2:

   The cylinder is isolated from both the delivery and suction slots.

   The delivery area is $A_{de} = 0$.

2. The upper groove zone, φ_2 to φ_3:

The delivery area A_{de} is proportional to the groove area and dependent on the cylinder angular position.

$$A_{de} = A_{og1} = \tan\frac{\theta_{g1}}{2}.(r.(\varphi - \varphi_2))^2$$

3. The upper overlapping zone , φ_3 to φ_4 :

The delivery area is defined as

$$A_{de} = A_{ott} = 2.\left[r_d^2.\cos^{-1}(\theta_{o1}) - (r_d - 0.5\,r.(\varphi - \varphi_3)).(r_d.\sin\theta_{o1})\right] +$$

$$\left[\tan\frac{\theta_{g1}}{2}.(r.(\varphi_3 - \varphi_2))^2 - \tan\frac{\theta_{g1}}{2}.(r.(\varphi - \varphi_3))^2\right]$$

where

$$\theta_{o1} = \left(\frac{r_d - 0.5\,r.(\varphi - \varphi_3)}{r_d}\right)$$

4. The delivery port zone, $\varphi_4$to φ_5:

$$A_{de} = A_d = \pi . r_d^2$$

5. The lower overlapping zone, $\varphi_5$to φ_6:

The delivery area is given as

$$A_{de} = A_{obt} = 2.\left[r_d^2.\cos^{-1}(\theta_{o2}) - \left(r_d - 0.5\ r.(\varphi_6 - \varphi)\right).(r_d.\sin\theta_{o2})\right] +$$

$$\left[\tan\frac{\theta_{g2}}{2}.\left(r.(\varphi_7 - \varphi_6)\right)^2 - \tan\frac{\theta_{g2}}{2}.(r.(\varphi_7 - \varphi))^2\right]$$

where

$$\theta_{o2} = \left(\frac{r_d - 0.5\ r.(\varphi_6 - \varphi)}{r_d}\right)$$

6. The lower groove zone, φ_6 to φ_7:

The delivery area A_{de} is proportional to the groove area and dependent on the cylinder angular position.

$$A_{de} = A_{og2} = \tan\frac{\theta_{g2}}{2}.(r.(\varphi - \varphi_7))^2$$

7. The second transitional zone, $\varphi_7$to B. D. C.

The delivery area A_{de}=0;

2.8.3.2 *The Cylinder Pressure and Pump Flow Rate Profiles:*

Seven different zones for the delivery stroke are considered in the pressure and flow analysis for a single piston-bore within a pump with a port plate with a triangular silencing groove. They are:

1- The first transitional zone, φ_1 to φ_2 :

The pressure can be approximated to be the suction pressure. The delivery area A_{de} is proportional to the groove area and dependent upon the cylinder angular position.

There is no discharge or intake flow in this zone and the piston moves forward to pressurize the fluid. The characteristics of this region may be expressed as

$A_{de}(t)=0$

$Q_k(t) = 0$

$P_n(t) = P_s$

2- The first overlapping zone in the groove part , $\varphi_2 to\ \varphi_3$:

In this zone, the cylinder is moving from the first transitional zone into the discharge port over the groove and the discharge area is proportional to the area of the groove and angular position of the cylinder with respect to the groove. The flow characteristics in this region are given by

$$A_{de}(t)=A_{og1} = tan\frac{\theta_{g1}}{2}.(r.(\varphi - \varphi_2))^2$$

$$Q_k(t) = sign\left(\sqrt{P_n - P_s}\right).A_{og1}.C_d.\sqrt{\frac{2}{\rho}}\left(\sqrt{P_n - P_s}\right)$$

$$P_n(t) = P_s + \left(\frac{A_{og1}.B.\dot{S}_k(t)}{\omega.V_{ck}(t)}.(\varphi - \varphi_2)\right)$$

When the cylinder port leaves the groove at φ_3 to go towards the delivery port, there is another common overlapping area. This area is a combination of two areas, the overlapping in the groove portion and the delivery port area. This zone ends at φ_4. Its characteristics are:

$$A_{de}(t) = A_{ott} = 2.\left[r_d^2.cos^{-1}(\theta_{o1}) - \left(r_d - 0.5\,r.(\varphi - \varphi_3)\right).(r_d.\sin\theta_{o1})\right] + \left[\tan\frac{\theta_g}{2}.\left(r.(\varphi_3 - \varphi_2)\right)^2 - \tan\frac{\theta_g}{2}.(r.(\varphi - \varphi_3))^2\right]$$

$$Q_k(t) = sign\left(\sqrt{P_n - P_s}\right).A_{ott}.C_d.\sqrt{\frac{2}{\rho}}\left(\sqrt{P_n - P_s}\right)$$

$$P_n = P_d - \left(\frac{A_{ott}.B.\dot{S}_k(t)}{\omega.V_{ck}(t)}.(\varphi_4 - \varphi)\right)$$

where

$$\theta_{o1} = \left(\frac{r_d - 0.5\,r.(\varphi - \varphi_3)}{r_d}\right)$$

3- The zone of delivery port, φ_4 to φ_5 :

The cylinder has full communication with the load via the delivery slot. The cylinder port matches the accurate porting geometry of the port plate. The characteristics of this zone are:

$$A_{de}(t) = A_d = \pi.r_d^2$$

$$Q_k(t) = sign\left(\sqrt{P_n - P_s}\right).A_d.C_d.\sqrt{\frac{2}{\rho}}\left(\sqrt{P_n - P_s}\right)$$

$$P_n(t) = P_d$$

4- The second overlapping zone, φ_5 to φ_6 :

As the cylinder moves toward the second transitional zone of the port plate near the bottom dead center, the actual flow passage is gradually cut off due to the terminating port-geometry of the port plate in this region. This area is a combination of two areas, as in the entry overlapping area. The flow characteristic quantities are given by

$$A_{de}(t)=A_{obt} = 2.\left[r_d^2.cos^{-1}(\theta_{o2}) - \left(r_d - 0.5\,r.(\varphi_6 - \varphi)\right).(r_d.sin\,\theta_{o2})\right] +$$

$$\left[tan\frac{\theta_g}{2}.\left(r.(\varphi_7 - \varphi_6)\right)^2 - tan\frac{\theta_g}{2}.(r.(\varphi_7 - \varphi))^2\right]$$

$$Q_k(t) = sign\left(\sqrt{P_n - P_s}\right).A_{obt}.C_d.\sqrt{\frac{2}{\rho}}\left(\sqrt{P_n - P_s}\right)$$

$$P_n(t) = P_d - \left(\frac{A_{obt}.B.\dot{S}_k(t)}{\omega.V_{ck}(t)}.(\varphi - \varphi_5)\right)$$

where

$$\theta_{o2} = \left(\frac{r_d - 0.5\,r.(\varphi_6 - \varphi)}{r_d}\right)$$

5- The exit groove zone, φ_6 to φ_7 :

The area is reduced as the cylinder approaches φ_7. The overlapping area is dependent on the dimensions of the triangular groove and the angular location of the cylinder at time t, where the delivery area A_{de} is proportional to the groove area and dependent on the cylinder angular position as well. The flow characteristic expressions are

$$A_{de}(t)=A_{og2} = tan\frac{\theta_{g2}}{2}.(r.(\varphi_7 - \varphi))^2$$

$$Q_k(t) = sign(\sqrt{P_n - P_s}).A_{og2}.C_d.\sqrt{\frac{2}{\rho}}(\sqrt{P_n - P_s})$$

$$P_n(t) = P_d - \left(\frac{A_{og2}.B.\dot{S}_k(t)}{\omega.V_{ck}(t)}.(\varphi - \varphi_6)\right)$$

6- The second transitional zone, φ_7 to $\pi + \varphi_1$:

The cylinder is completely closed off, and there is no fluid flow into or out of the cylinder. The cylinder pressure can be approximated to be equal to the suction pressure. The zone characteristics are:

$A_{de}(t)=0$

$Q_k(t) = 0$

$P_n(t) = P_s$

Numerical Simulation:

A MATLAB simulation program is used to calculate and plot the K^{th} cylinder delivery area at any given angular position. The areas, in addition to the corresponding cylinder instantaneous volume and the piston velocity, were used to determine the cylinder pressure and its respective flow rate for each angular position of the K^{th} cylinder. The

delivery area, cylinder pressure and pump discharge flow rate versus the angle φ were simulated and are illustrated in Figures 2.21, 2.22, and 2.23, respectively.

A simulation run was carried out for a 9-piston pump of geometric volume 40 cc/rev running at a constant speed of 1800 rpm; with the hydraulic fluid ISO 46 and bulk modulus $1.3X10^9$ Pa. The various configurations of this port plate with triangular groove design are shown in Figure 2.19. The length of the first transitional zone is proportional to $8^\circ$and the length of the second is proportional to 172°. Also, the inner angle of the groove is 60°.

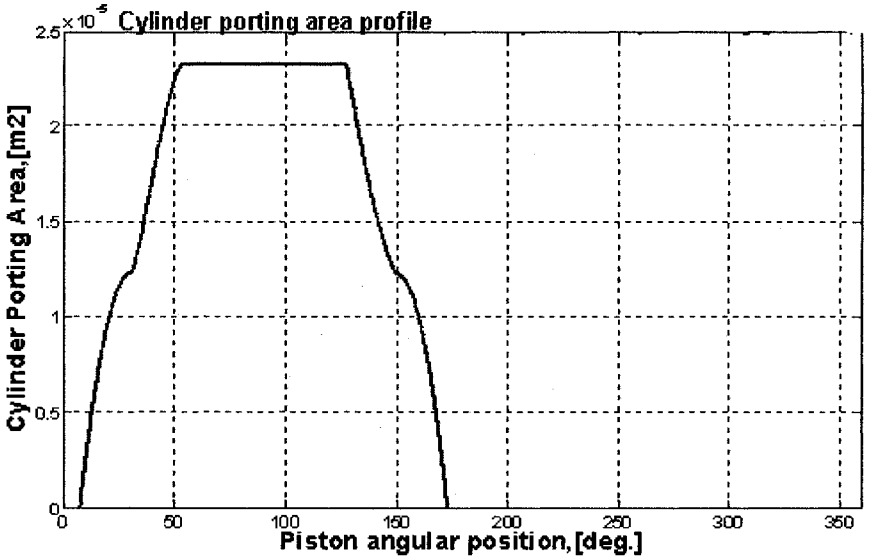

Figure 2.21: The discharge area of the K^{th} cylinder in the delivery stroke

Figure 2.21 shows the cylinder delivery area through a port plate with deep triangular grooves. The inner angle of the triangle is 60°, and its length is equal to the diameter of the cylinder discharge port. The lengths of the first and second transitional zones are 8° and 172°, respectively.

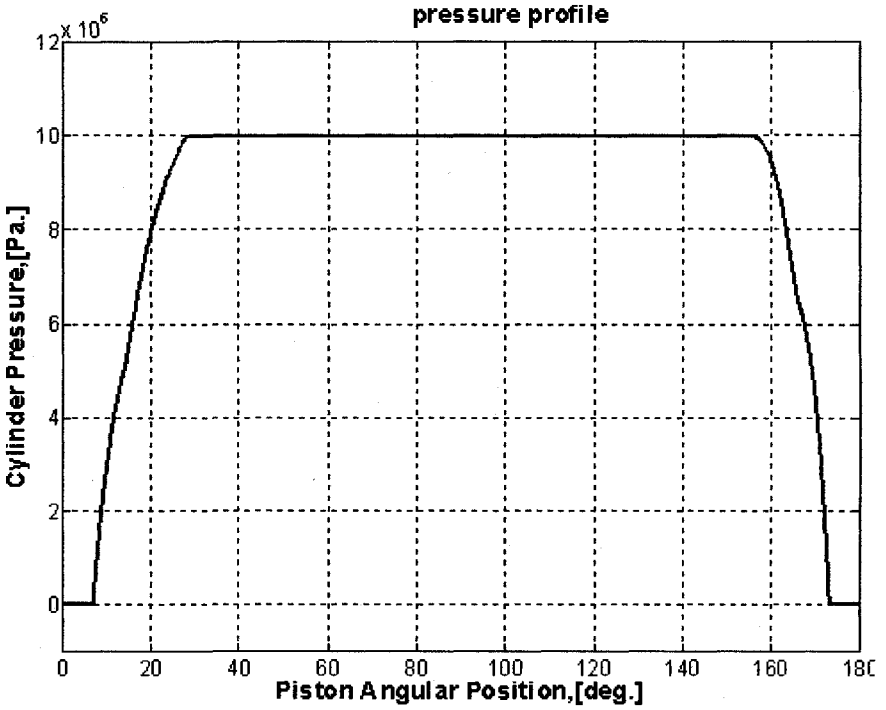

Figure 2.22: Cylinder pressure profile

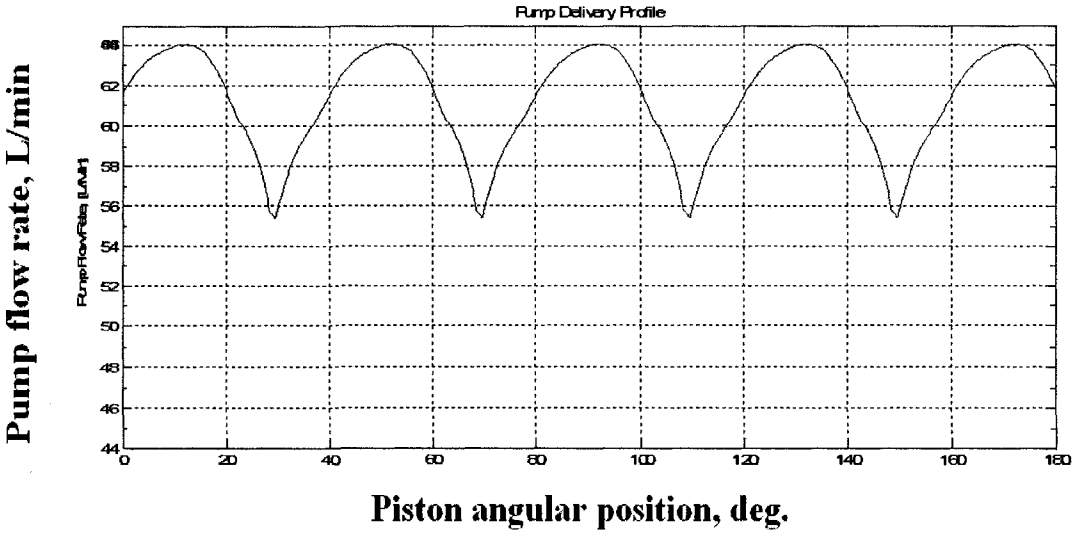

Figure 2.23: Pump flow rate profile

Figures 2.22 and 2.23 show the cylinder pressure and the pump flow rate profiles. In the first transitional zone, the cylinder is totally isolated from both the suction and the delivery ports, and the pressure is the same as the cylinder suction pressure. As the cylinder moves from φ_1 to φ_2, the piston moves forward in its cylinder, and the fluid pressure increases with the decrease in the fluid volume. The pressure rise is dependent on the piston velocity, the fluid bulk modulus and the cylinder volume. This rise continues till the cylinder communicates with the pump discharge chamber at φ_2. The communication starts with a very small porting area, and this helps to build a light contact between the fluid (that has a relatively high pressure) and the load. As the cylinder moves toward φ_3, the pressure continues to build up more and more with the decrease in the cylinder volume. The piston is still pushing the fluid and ejecting it. At φ_4, the cylinder pressure and the load have the same value and the fluid moves from

the cylinder to the pump discharge chamber with the piston movement. This motion continues till φ_5. At φ_5, the porting geometry starts to decrease and the pressure decreases till it becomes equal to P_s at φ_7. The silencing groove ends next to the B.D.C. At the B.D.C., the cylinder ends the delivery stroke and starts its suction stroke. The pump flow rate was obtained using the Bernoulli principle. The smooth pressure transition leads to a pump flow rate with minimum fluctuations, which is illustrated in Figure 2.23. The pump flow rate is the sum of the individual cylinder flows, and the length of the transitional zone is important to characterize the pump flow rate and it can shed more light on the expected flow rate behaviour.

2.9 Harmonic Analysis of the Pump Flow Rate

From Figures 2.14 and 2.23 it can be observed that the pump flow rate has periodic fluctuations superimposed upon the mean value of the flow rate. This is because all of the cylinders are evenly separated and each cylinder has the same operation as the previous and the next cylinders, but with phase differences. The periodicity in the cylinders' flow rate enables us to express the pump flow rate in the form of a Fourier series. The mathematical expression of the periodic pump flow rate may be written as:

$$Q_{FT}(\varphi) = A_o + \sum_{n=1}^{\infty} [A_n Cos(n\varphi) + B_n Sin(n\varphi)]$$

where:

$$A_o = \frac{1}{T}\int_0^T Q(\varphi)d\varphi$$

$$A_n = \frac{2}{T}\int_0^T Q(\varphi)Cos(\varphi)d\varphi$$

$$B_n = \frac{2}{T}\int_0^T Q(\varphi)Sin(\varphi)d\varphi$$

$Q_{FT}(\varphi)$: general Fourier series

φ: pump shaft angle

n: number of terms

The swash plate pump has 9 cylinders, and hence, there are 9 different phase angles, δ_k. These angles can be given as

$$\delta_k = \frac{(k-1)2\pi}{9}$$

Thus, we have

$\delta_1 = 0$

$\delta_2 = \frac{2\pi}{9}, \quad or\ 40\ deg.$

$\delta_3 = \frac{4\pi}{9}, \quad or\ 80\ deg.$

$\delta_4 = \frac{6\pi}{9}, \quad or\ 120\ deg.$

$\delta_5 = \frac{8\pi}{9}, \quad or\ 160\ deg.$

$\delta_6 = \frac{10\pi}{9}, \quad or\ 200\ deg.$

$\delta_7 = \frac{12\pi}{9}, \quad or\ 240\ deg.$

$$\delta_8 = \frac{14\pi}{9}, \qquad or\ 280\ deg.$$

$$\delta_9 = \frac{16\pi}{9}, \qquad or\ 320\ deg.$$

$Q_{FT}(\varphi)$ can be expressed with respect to the individual cylinder flow rate, as

$$Q_{FT}(\varphi)_k = A_{o_k} + \sum_{n=1}^{\infty} [A_n Cos(n.\varphi - n.\delta_k) + B_n Sin(n.\varphi - n.\delta_k)]$$

The Fourier series can be represented in a time domain as

$$Q_{FT}(t)_k = A_{o_k} + \sum_{n=1}^{\infty} [A_n Cos(n.\omega t/9) + B_n Sin(n.\omega t/9)]$$

where

$\varphi = \omega t$

ω : the pump running speed

k: the index for the number of the cylinders of the pump

MATLAB based software was developed to compute the series coefficients and plot the Fourier series representation for the pump flow rate in one period. The simulation results of the pump flow rate with the harmonic analysis are presented in Figure 2.24. The simulation is carried out for a pump equipped with the proposed port plate and for one complete revolution of the pump shaft, using only 10 terms. It can be seen that the pump flow rate fluctuates about a mean value (0.001 M^3/Sec.), and there are nine peaks (equal to the number of cylinders). The result for one single cylinder is shown in Figure 2.25.

The Fourier series coefficients are shown in Figure 2.26. It is obvious that the first coefficient is the dominant one.

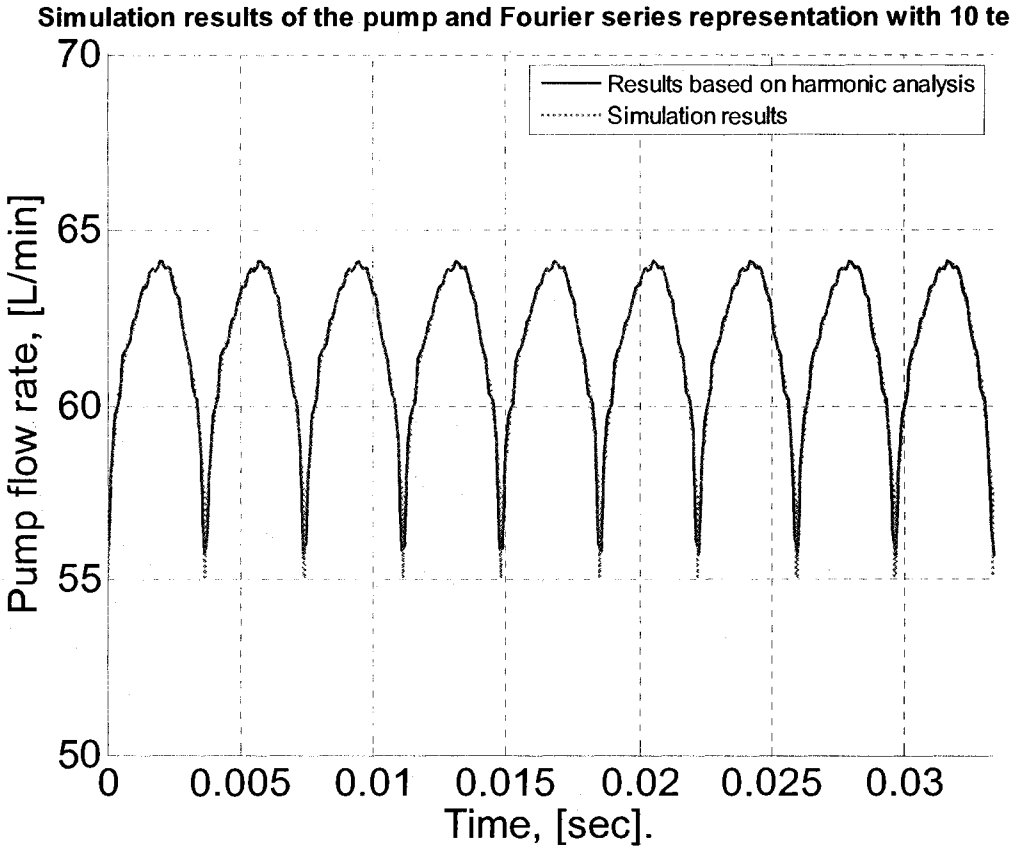

Figure 2.24: The Fourier series representation for the pump flow rate over one period

(With the proposed port plate)

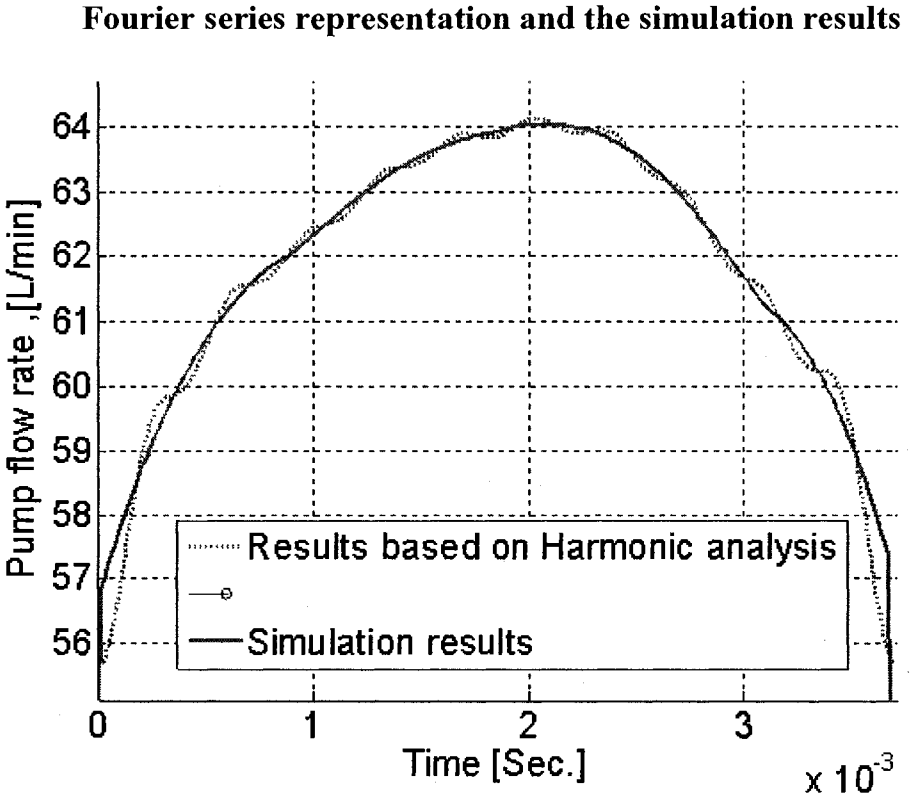

Figure 2.25: The Fourier series representation for the k^{th} cylinder flow rate in 1 period

(With the proposed port plate)

(..... Results based on harmonic analysis, -- simulation results)

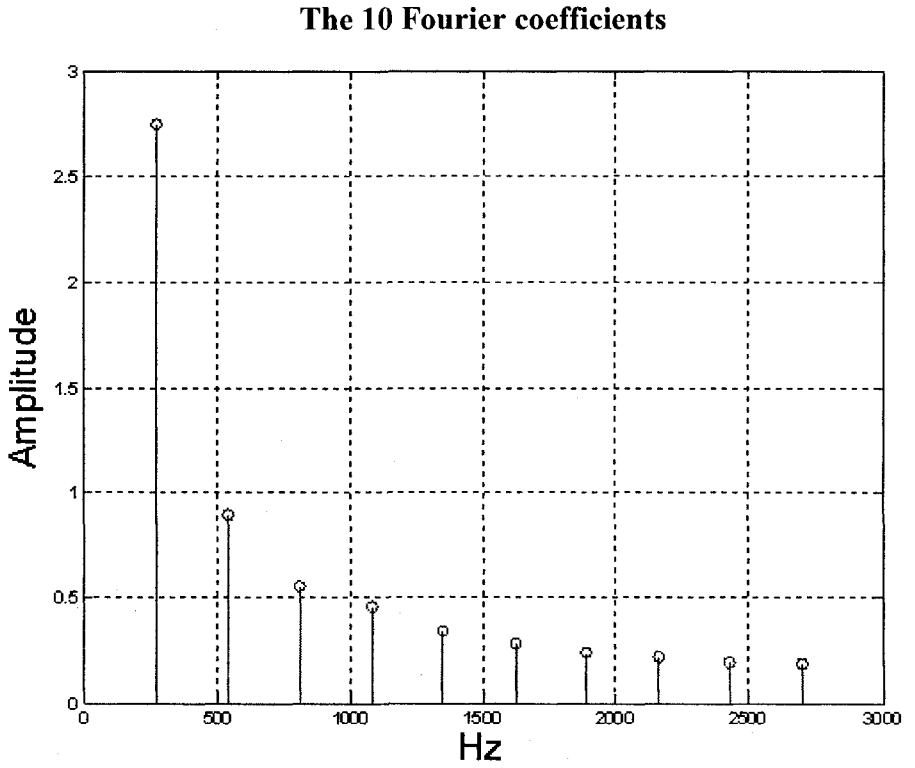

Figure 2.26: The 10 Fourier series coefficients

2.10 Pump Work and Power

A pump converts mechanical power to hydraulic power; the hydraulic power is in the form of pressurized fluid flow at the pump outlet. Therefore, the characteristics of the fluid are determined by the fluid pressure and its flow rate, and both are required to compute the pump power. To compute the power, a path of the fluid stream is indicated to trace the hydraulic power. In this analysis, the path will be determined between two points: the starting point (at the cylinder discharge port plane), and the ending point (on

the plane of the port plate, i.e. on the side of the pump discharge chamber). The stream experiences a hydraulic force that can be given as

$$F_{hyd}(t) = (P_n(t) - P_s).A_{st}(t) \tag{2.19}$$

where $F_{hyd}(t)$ is the hydraulic force exerted on the stream line, $P_n(t)$ is the pressure within the Kth cylinder, $A_{st}(t)$ is the instantaneous cross-section of the stream line that leaves the Kth cylinder to the port plate, and P_S is the suction pressure (set to be equal to the pump suction pressure [51]). The hydraulic work, which is the work done by the hydraulic force, can be defined as

$$w_{hyd}(t) = F_{hyd}(t).ds \tag{2.20}$$

where is w_{hyd} is the pump hydraulic work and *ds* is the instantaneous displacement of the fluid stream.

The hydraulic power of the Kth single cylinder can be given as

$$P_{outk}(t) = \frac{dw_{hyd}}{dt} = (P_n(t) - P_s).Q_k(t) \tag{2.21}$$

where $P_{outk}(t)$ is the Kth cylinder hydraulic power, $w_{hyd}(t)$ is the Kth cylinder hydraulic work, $Q_k(t)$ is the Kth cylinder flow rate.

Hence, the total power of the pump can be given as

$$P_{out}(t) = \frac{K}{2\pi}\int_0^{\pi}(P_n(t) - P_s).Q_k(t).d\varphi \tag{2.22}$$

Eq. (2.22) represents the total power of the pump, where $Q_k(t)$ and $P_n(t)$ have instantaneous values with respect to the cylinder angular position, φ. In order to calculate (2.22), values of the K^{th} cylinder pressure and its flow rate must be determined for every sector of the delivery half of the port plate.

2.10.1 Without Silencing Grooves

The governing equations derived in 2.8.1.2.2 are used to determine the pump power. The cylinder discharges in three zones (the two overlapping zones and the delivery port) and the pump power can be deduced for the pump without silencing grooves as follows:

In the first overlapping zone, the angular length of this zone is determined by φ_3 and φ_4.

The pump power is the sum of the pump cylinder flow, at any time while some of the cylinders are discharging. The total instantaneous pump power in the first overlapping zone can be expressed as

$$p_{out1n} = \frac{K}{2\pi}\int_{\varphi_3}^{\varphi_4}\left(P_s + \left(\frac{A_{ot}.B.\dot{S}_k(t)}{\omega.V_{ck}(t)}.(\varphi-\varphi_3)\right) - P_s\right).A_{ot}.c_t.\omega.sin\,(\varphi).d\varphi$$

$$p_{out1n} = \frac{K}{2\pi}\frac{{A_{ot}}^2.\omega.B.{c_t}^2}{4.V_{ck}(t)}\left\{(\varphi_3-\varphi_4)[(\varphi_3-\varphi_4)-sin(2\varphi_4)] - \frac{(cos(2\varphi_4)-cos\,(2\varphi_3))}{2}\right\} \quad (2.23)$$

Similarly, in the delivery port that is limited by φ_4 and φ_5, the instantaneous pump power in the delivery zone is expressed as

$$p_{out2n} = \frac{K}{2\pi}(P_d - P_s).c_t.\omega.A_d.[cos(\varphi_4) - cos\ (\varphi_5)] \tag{2.24}$$

Finally, the total instantaneous pump power in the second overlapping zone has the following form

$$p_{out3n} = \frac{K}{2\pi}\frac{{A_{ob}}^2.\omega.B.{c_t}^2}{4.V_{ck}(t)}\left\{(\varphi_6 - \varphi_5)[(\varphi_6 - \varphi_5) + sin(2\varphi_5)] + \frac{(cos(2\varphi_6) - cos\ (2\varphi_5))}{2}\right\} \tag{2.25}$$

Hence, the pump power is the sum of the instantaneous pump power of the three zones, and can be expressed as

$$p_{outn} = p_{out1n} + p_{out2n} + p_{out3n} \tag{2.26}$$

where

p_{out1n}: The pump power in the first overlapping area

p_{out2n}: The pump power in delivery port

p_{out3n}: The pump power in the second overlapping area

The numerical results are present in Figure 2.27, where they are compared with the proposed design.

2.10.2 **With Deep Triangular Silencing Grooves**

Another advantage of utilizing deep grooves on the port plate can be observed from the pump output. As in the non-grooved port plate case, the pump power can be computed by considering the different zones of the delivery half of the port plate.

With the changes in the pressure and pump flow rate profiles associated with this design; the pump power is expected to be different. The pump power will be divided into three parts: the first overlapping area (in the groove and the entry side of the delivery port), the delivery port, and in the second overlapping area (on the exit side of the delivery port and the exit groove).

In the first overlapping zone the instantaneous pump power can be expressed as

$$p_{out1t} = \frac{K}{2\pi}\frac{{A_{ot}}^2.\omega.B.{c_t}^2}{4.V_{ck}(t)}\left\{(\varphi_2 - \varphi_4)[(\varphi_2 - \varphi_4) - sin(2\varphi_4)] - \frac{(cos(2\varphi_4) - cos\,(2\varphi_2))}{2}\right\} \quad (2.27)$$

In the delivery port, the instantaneous pump power in the delivery slot is given as

$$p_{out2t} = \frac{K}{2\pi}(P_d - P_s).c_t.\omega.A_d.[cos(\varphi_4) - cos\,(\varphi_5)] \quad (2.28)$$

And, in the second overlapping zone, the contribution of this area on the exit side of the delivery port to the instantaneous pump power has the form

(2.29)

(2 7– (2 5))2

The total instantaneous pump power is thus

(2.30)

In order to evaluate the pump power associated with each design, Eqs. (2.26) and (2.30) are solved numerically. The results are shown in

Figure 2.27.

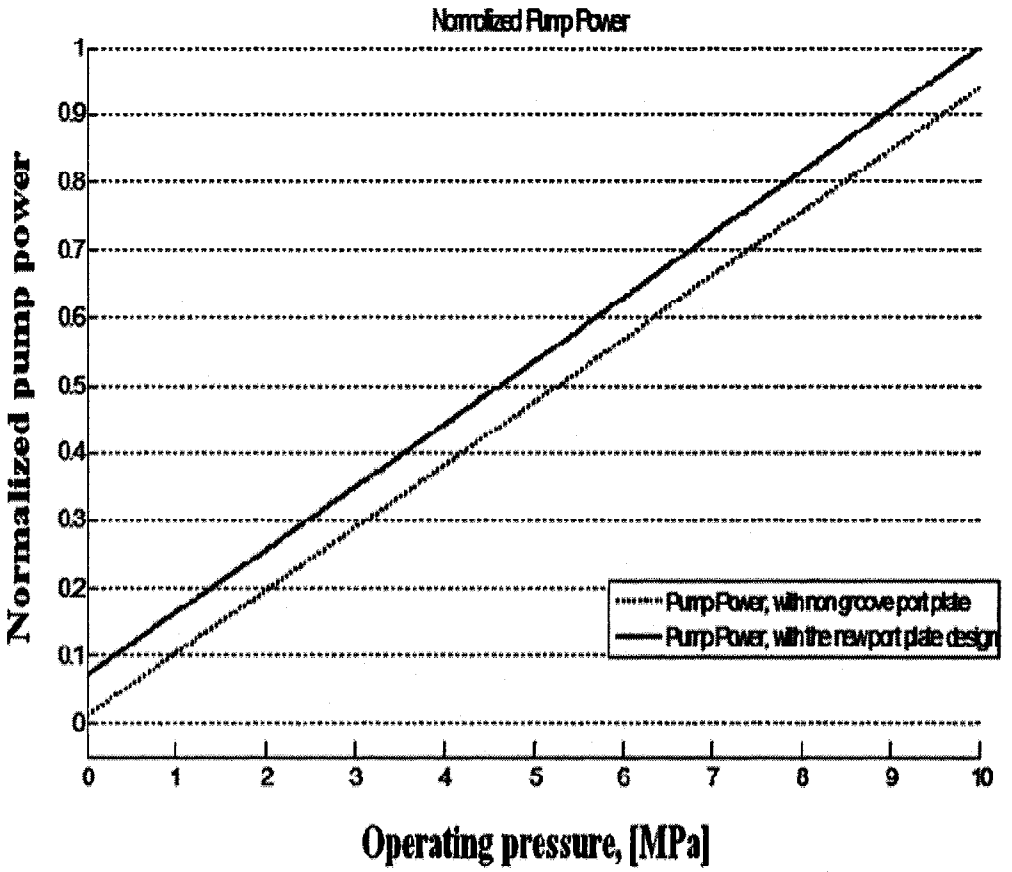

Figure 2.27: Comparison of the normalized pump power of both port plate designs

Figure 2.27 shows the normalized pump power of two different port plate designs, non-grooved (dotted line) and with a pair of deep silencing grooves (the solid line). From the figure, it can be noted that using a port plate with deep silencing grooves can improve the pump power by about 4%. This significant improvement is due to the pump porting area with the new design incorporating the two grooves.

2.11 Conclusions

Pump performances with different port plate designs were analyzed and presented. The designs were port plates without silencing a groove, with a shallow silencing groove, and with the proposed port plate design that incorporates a pair of triangular deep grooves. The pump performance was studied first for the two current designs (non-grooved and a shallow groove) without considering the overlapping, which showed that the non-grooved port plate exhibited better pump characteristics; and by considering the overlapping between the cylinder discharge port and the port plate, where the pump showed undesirable behaviour. The results showed that the proposed port plate with triangular deep silencing grooves helped in transiting the pressure between the two cylinder pressure values smoothly, and the extra length of the overlapping helped in the early opening close to the T.D.C and at the later cut-off next to the B.D.C. From the results, it can be said that this design can improve the pump performance and the fluid will have minimum fluctuations.

In particular, the study compared the pump power of two different port plate designs, one that had trapped volume zones (a port plate without grooves) and the proposed design with a pair of deep silencing grooves. It was found that using port plates with deep

silencing grooves generates more power in comparison with the port plates with trapped volume This study shows that the new design could improve a pump's power, and improve pump performance with a smooth pressure rise and less fluid flow fluctuation.

In the next chapter, the fluid-induced vibrations will be discussed. Also, the dynamics of pipes conveying fluid, including the critical velocities at which pipes lose their static and dynamic stabilities, will be determined. In addition, the response of simply supported pipes will be modeled and simulated by considering the pulsating nature of the fluid discharged from the swash plate pumps.

CHAPTER THREE

3 PIPE DYNAMICS AND VIBRATION

3.1 Introduction

In the previous chapter, a comprehensive modeling was carried out to investigate the effect of the modified port plate design on pump performance and on the overall flow rate. The results were compared with the current port plates design, and they showed considerable enhancements in both the pump performance and output. Pressure overshooting was eliminated in the proposed port plate and the fluid fluctuations also decreased.

In this chapter, the dynamics of the pipes conveying fluids will be discussed, along with a brief introduction about the relationship between the fluid flow and pipe vibration. The focus will be on the static and dynamic instabilities, which are known as divergence and flutter, respectively.

3.2 Self-Excited and Flow-Induced Vibrations

The fluid flow in pipes is the major source of pipe vibration, known as self-excited vibration, or flow-induced vibration. Self-excited vibration is a free vibration (no external forces) with negative damping value. The negative damping generates a damping force that is proportional to the velocity of the vibration and acts in the same direction,

boosting the vibration. There is a key difference between self-excited and forced vibration, in that the magnitude of the vibration is dependent on the fluid flow (the scope of this thesis) and it stops in the absence of the flow, while in forced vibration, the exciting force is independent of the vibration response.

3.3 Relationship between Pipe Vibration and Fluid Velocity

There are various explanations as to why the fluid forces the pipe to vibrate when it runs through it, and how the pipe vibration levels increase with increasing fluid velocity.

The simplest explanation is that the pipe bows out under its own weight and that of the fluid and the fluid has momentum. This momentum changes its direction while flowing through the bent pipe.

There are other factors that cause the pipe to vibrate such as:

1- Pump overshooting

2- Acoustic waves: the acoustic energy has different sources, and will be transmitted to the pipes through the fluid. The waves exert axial forces on the pipes, and if the diameter of the pipes or their direction changes, these waves cause the pipes to oscillate.

3.4 Theoretical Analysis

In this section, the governing equations for a pipe with fluid flow will be derived following the approach in [64]. The pipe can be considered as a one-dimensional

Timchenko beam, shown in Figure 3.1. The divergence and flutter expressions for the pipe with specific boundary conditions will be studied in particular.

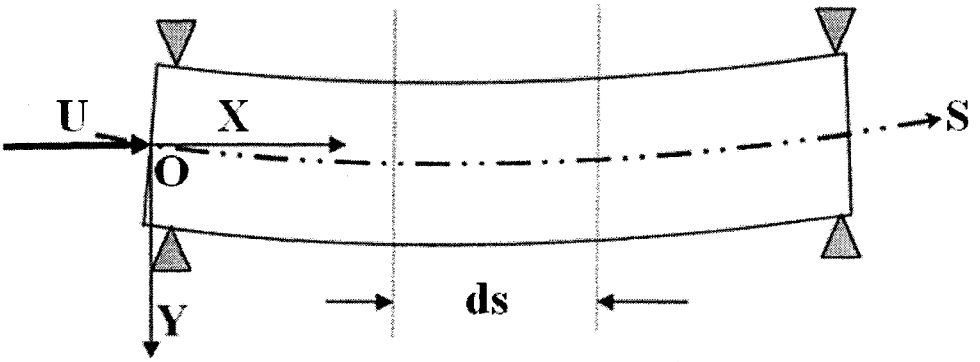

Figure 3.1: A simply supported pipe conveying fluid with a velocity u

Figure 3.1 shows a segment of simply supported fluid-filled pipe with length L(m), flexure rigidity EI (Nm^2), Young's modulus E (N/m^2), moment of inertia I (m^4), mass of the pipe per unit length m_p(Kg/m), mass per unit length of the fluid inside the pipe m_f(Kg/m), and pipe inner cross sectional area A (m^2). The flowing area equals the pipe inner cross sectional area, A (m^2).

The pipe under its own weight and the weight of the fluid will experience bending (has curvature). Hence, the fluid path does not coincide with the x axis (illustrated in Figure 3.1); and runs along the bent pipe, which is denoted as S.

The following assumptions are used in the derivation:

- The fluid is incompressible
- The fluid velocity is constant, u
- The pipe material is homogeneous
- The pipe is uniform

- The pipe has only lateral deflection, $w(x,t)$
- The pipe deflection is small
- The ratio of the pipe diameter to its length is also small (slender pipe)
- The fluid travels as a flexible rod through the pipe. This assumption is required in order to derive the fluid transverse acceleration

3.4.1 Forces and Moments Acting on the Pipe Element and the Forces Acting On the Fluid Element

By considering an element of the pipe with the fluid inside, the forces and moments acting on the pipe element and the forces acting on the fluid element are illustrated in Figure 3.2 and Figure 3.3.

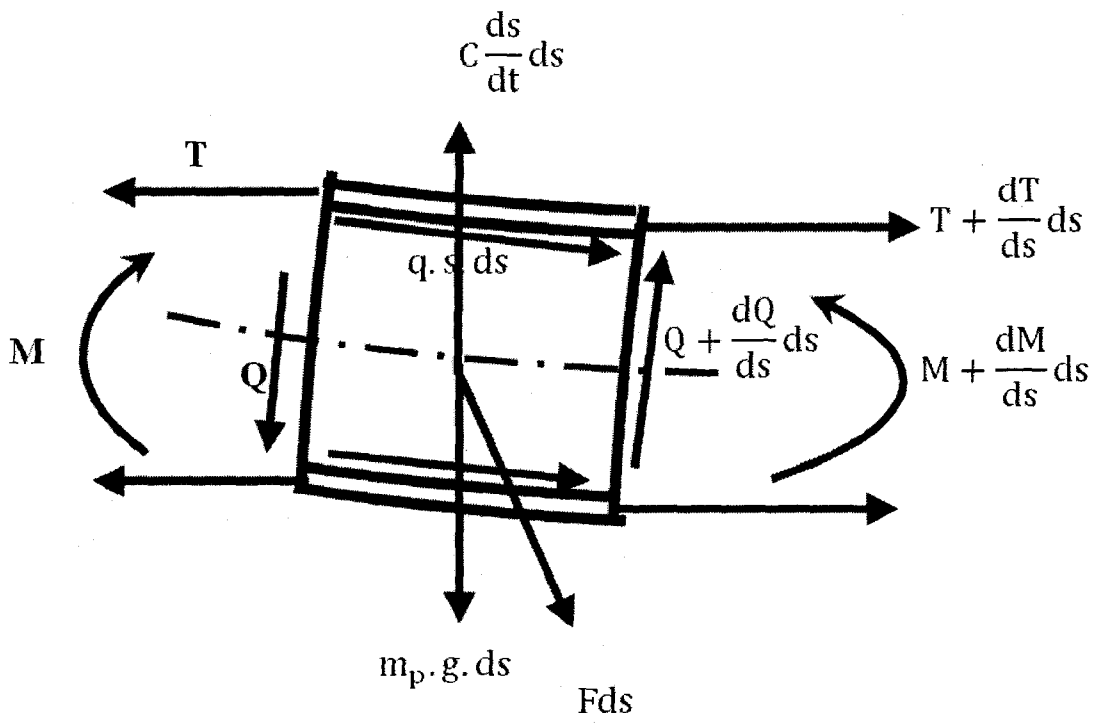

Figure 3.2: Forces and moments acting on the pipe element

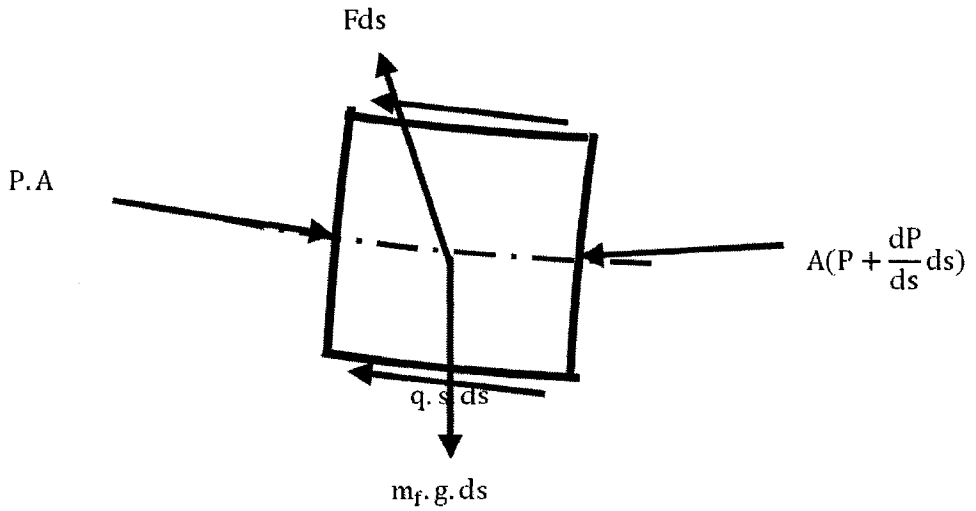

Figure 3.3: Forces acting on the fluid element

Considering the entry side of the pipe as the origin of the coordinates, the fluid velocity, u, is along the curvilinear coordinate, S.

The pipe element is under the following forces and moments:

- Longitudinal tension force, with resultant $-\frac{dT}{ds}ds$
- Gravity force due to the mass of the pipe element, which equals $m_p.g.ds$
- Bending moment, with resultant $-\frac{dM}{ds}ds$
- Transverse shear force, which is equivalent to $-\frac{dQ}{ds}ds$
- Damping force, which is created due to the friction between the pipe and fluid, and is equal to $C.\frac{dS}{dt}ds$
- Pipe-fluid reaction force, Fds, which is perpendicular to the upper surface of the fluid element
- Pipe-fluid wall shear forces, $q.S.ds$, have the same direction as the pipe, however, in the reverse direction to that encountered for the fluid element.

Most of these forces have a coupling effect on the fluid, and can be summarized as follows:

- Pipe-fluid transverse shear force, $q.S.ds$
- Pipe-fluid reaction force, Fds
- Gravity force due to the mass of the fluid element, or $m_f.g.ds$
- One additional force is created, which is the pressure loss on the fluid element. The pressure drops due to fluid-pipe wall friction, and it can be expressed as $-A\frac{dP}{ds}ds$

3.4.2 Pipe and Fluid Transverse Accelerations

In the previous section, we defined the forces acting on the pipe and fluid elements, where the mass per unit length for the pipe and fluid elements are known. The accelerations of the pipe and the fluid are required in order to obtain the equations of motion.

3.4.2.1 *Pipe Transverse Acceleration*

In Figure 3.1, there are two components for the pipe position vector, which are $\vec{i}$ and $\vec{j}$. The reference point for the vector is "O". Hence, the position vector of the pipe can be written as

$$r_p(t) = x.\vec{i} + y.\vec{j} \tag{3.1}$$

The velocity is the rate of change of the position vector with time. Hence, the pipe velocity can be obtained by differentiating Eq. (3.1) , as follows:

$$V_p(t) = \dot{x}.\vec{i} + \dot{y}.\vec{j} \tag{3.2}$$

The pipe is assumed to have vibration in the Y-direction only. Hence, $\dot{x} = 0$, and the fluid velocity can be expressed as:

$$V_p(t) = \dot{y}.\vec{j} \tag{3.3}$$

Differentiating Eq. (3.3), the pipe transverse acceleration is expressed as:

$$a_p(t) = \ddot{y}.\vec{j} \tag{3.4}$$

3.4.2.2 *The Fluid Transverse Acceleration*

Since the fluid is moving through the pipe, the fluid transverse acceleration is obtained in the following manner. The center of the fluid element moves with respect to the pipe element, and hence, its velocity is given as

$$V_f(t) = V_p(t) + u.\tau \tag{3.5}$$

where $V_f(t)$ is the velocity of the center of the fluid elements, $V_p(t)$ is the velocity of the center of the pipe element, u is the fluid velocity, and τ is tangent (to the pipe) vector. The tangent vector is needed to describe the motion of the fluid element along the

curvature. Figure 3.4 shows the relationship between the fluid velocity and the tangent vector.

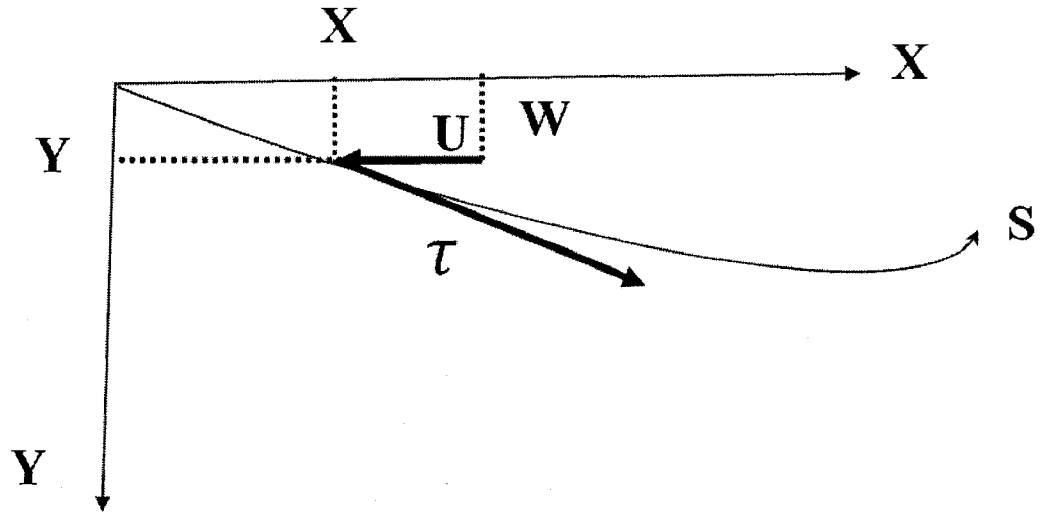

Figure 3.4: Fluid element velocity

The tangent vector can be represented as

$$\tau = \frac{dx}{dS}.\vec{\imath} + \frac{dy}{dS}.\vec{\jmath} \tag{3.6}$$

Assuming the curvilinear radius to be very small, we can approximate

$S \approx x \quad and \quad y \approx w$

And then, from the previous assumptions, Eq. (3.5) can be reproduced as follows

$$V_f(t) = u.\vec{\imath} + (u.\frac{dw}{dx} + \frac{dw}{dt})\vec{\jmath} \tag{3.7}$$

In order to obtain the fluid transverse acceleration, Eq. (3.7) must be differentiated, which gives

$$a_f(t) = \dot{u}.\vec{\imath} + w(u.\frac{d}{dx} + \frac{d}{dt})^2 \vec{\jmath} \tag{3.8}$$

Eq. (3.8) can represent the two components of the fluid transverse acceleration. Only the acceleration projection on the y axis is needed. The form of this component is

$$a_{fj}(t) = \frac{d^2w}{dt^2} + u^2\frac{d^2w}{dx^2} + 2u\frac{dw}{dxdt} \tag{3.9}$$

The force acting on the fluid element and the forces acting on the pipe element and moment can help to couple the pipe and the fluid into one equation of motion as follows:

- The fluid element

$$\sum F_{fx} = m_f \,.\, a_{fx} \tag{3.10}$$

$$-A\frac{dP}{dx} - q.S + m_f.g + F.\frac{dw}{dx} = m_f.\frac{du}{dt} \tag{3.11}$$

$$\sum F_{fy} = m_f \,.\, a_{fy} \tag{3.12}$$

$$-F - A\frac{d}{dx}\left(P\frac{dw}{dx}\right) - q.S.\frac{dw}{dx} = m_f.[w(u.\frac{d}{dx} + \frac{d}{dt})^2] \tag{3.13}$$

- The pipe element

$$\sum F_{px} = 0 \tag{3.14}$$

$$\frac{dT}{dx} + q.S + m_p.g - F.\frac{dw}{dx} = 0 \tag{3.15}$$

$$\sum F_{py} = m_p \,.\, a_{py} \tag{3.16}$$

$$\frac{dQ}{dx} + F + \frac{d}{ds}\left(T\frac{dw}{dx}\right) + q.S.\frac{dw}{dx} - C\frac{dw}{dt} = m_f.[w(u.\frac{d}{dx} + \frac{d}{dt})^2] \tag{3.17}$$

where

$$Q = \frac{dM}{dx} = -EI\frac{d^3w}{dx^3} \tag{3.18}$$

By substituting Eqs. (3.11), (3.13), (3.15), and (3.18) into (3.17), and rearranging, the final form of the equation of motion for a pipe filled with fluid can be expressed as

$$EI\frac{d^4w}{dx^4} + m_f.u^2\frac{d^2w}{dx^2} + 2m_f.u\frac{d^2w}{dxdt} + (m_f + m_p)\frac{d^2w}{dt^2} = 0 \tag{3.19}$$

where w is the lateral deflection, x is the axial coordinate, and t is the time.

Eq. (3.19) is a fourth-order differential equation with respect to the space, x, and a second-order differential equation with respect to time. In order to solve it, we need four boundary conditions and two initial conditions.

Eq. (3.19) includes four terms, which represent forces:

- $EI\frac{d^4w}{dx^4}$: is the flexural restoring force for the pipe (beam)

- $m_{f.}u^2\frac{d^2w}{dx^2}$: is associated with the centrifugal force, where this term can be written as $m_{f.}u^2/R_l$,

where $\frac{d^2w}{dx^2} \sim \frac{1}{R_l}$, R_l is the local radius of the pipe curvature.

- $2m_{f.}u\frac{dw}{dxdt}$ is associated with the Coriolis force. This force can be explained as follows:

  $$\frac{d^2w}{dxdt} = \frac{d\Theta}{dt} = \Omega$$

  where Ω is the fluid local angular velocity.

  The fluid flow along $\vec{\imath}$ with velocity equals u, while section of the fluid is rotates with Ω along $\vec{\jmath}$ with the opposite direction. Hence, Coriolis can be expressed as $-2\Omega\vec{j}\,X u\vec{\imath}$

- $(m_f + m_p)\frac{d^2w}{dt^2}$: are the inertia forces of the fluid and the pipe.

3.5 Stability of the Pipe Conveying Fluid

In the previous section, the governing equation for a pipe conveying fluid and the related forces were defined. In this section, we will present the different techniques used to solve this equation, which does not have a straightforward solution. Two different approaches are presented in this section. The first was suggested by Blevins [7], and the second was introduced by Paidoussis [64]. The first approach is quite simple, but it is not accurate; it gives the critical velocity and the fundamental frequency without introducing the type of

instability. The second approach gives the regions and type of instability (static or dynamic), however, it is very difficult in terms of computation.

3.5.1 **Approximate Solution**

In this section, Eq. (3.19) will be solved to obtain the critical velocity and the fundamental frequency with some approximations. Eq. (3.19) has four terms, the first and the fourth terms are independent of the fluid flow; while the second and third terms are dependent upon the flow.

Blevins [7] suggested solving the equation according to Timchenko's beam, a pure beam with no consideration of the flow. The solution is done by expanding it in terms of the mode shape of the beam's vibration.

For a simply supported beam, the boundary conditions are

$$w(0,t) = w(L,t) = 0 \tag{3.20}$$

$$\frac{d^2w}{dx^2}(0,t) = \frac{d^2w}{dx^2}(L,t) = 0 \tag{3.21}$$

The mode shapes of a simply supported beam have a sinusoidal form, and can be expressed as

$$w(x) = sin\frac{n\pi x}{L} \tag{3.22}$$

where n is an integer (n=1,2,3,..)

The solution of the equation of motion for a simply supported pipe conveying fluid (including the mode shape and its corresponding natural frequency) can be re-written as

$$w_j(x,t) = \sum_{n=1,3,5} a_n \sin\frac{n\pi x}{L} \sin\omega_j t + \sum_{n=2,4,6} a_n \sin\frac{n\pi x}{L} \cos\omega_j t \qquad (3.23)$$

where ω_j is the natural frequency of the j vibration mode (j=1,2,3..).

After substituting Eq. (3.23) in Eq. (3.19), various observations can be made. For example, terms that have $\cos\frac{n\pi x}{L}$ will be produced due to the third term, which represents the Coriolis force. The terms can be expanded using Fourier series and then by expanding them over the entire span of the beam ($0 \leq x \leq L$).

After expansion, the terms will be the grouped as coefficients of the $\cos\omega_j t$ or $\sin\omega_j t$ terms. Blevins [7] organized these terms in the form of stiffness and mass matrices, which can be expressed as:

$$\left|[K] - \omega_j{}^2(m_f + m_p)[I]\right|\{a\} = 0 \qquad (3.24)$$

where $[K]$ is the stiffness matrix, $[I]$ is the identity matrix, and $\{a\}$ is a single column vector with N rows, representing the independent constants.

For a continuous system, there are an infinite number of mode shapes (and natural frequencies). However, we usually consider only the first few frequencies.

The natural frequencies are obtained by solving the characteristic equation for Eq. (3.24), which can be produced by solving the equation for the non-trivial solution (the determinant equals zero).

The solution of Eq. (3.24) for the first two natural frequencies can be expressed as

$$\left[1-(\frac{u}{u_c})^2-(\frac{\omega_j}{\omega_N})^2\right]\left[16-4(\frac{u}{u_c})^2-(\frac{\omega_j}{\omega_N})^2\right]-\frac{256}{9\pi^2}(\frac{u}{u_c})^2\left(\frac{\omega_j}{\omega_N}\right)\frac{(m_f)}{(m_f+m_p)}=0 \quad (3.25)$$

where ω_j is the natural frequency of the j vibration mode, u is the fluid velocity, u_c is the critical fluid flow velocity, and ω_N is the natural frequency for the pipe filled with fluid that has zero flow velocity.

Solving Eq. (3.25) is quite complex. However, we can solve it for the fundamental natural frequency with the following approximate solution

$$\omega=\omega_N\sqrt{\left[1-(\frac{u}{u_c})^2\right]} \quad (3.26)$$

From Eq. (3.19) , the critical velocity can be obtained by setting t=0; while the natural frequency for a simply supported pipe filled with fluid that has zero fluid flow velocity can be produced by setting u=0. These expressions are given in Eq.(3.27) and Eq. (3.28), respectively.

$$u_c=\frac{\pi}{L}\sqrt{\frac{EI}{m_f}} \quad (3.27)$$

$$\omega_N=\frac{\pi^2}{L^2}\sqrt{\frac{EI}{(m_f+m_p)}} \quad (3.28)$$

From Eq. (3.27) and Eq. (3.28), it can be seen that the critical velocity and the natural frequency for a simply supported pipe filled with zero fluid-flow velocity are dependent on pipe and fluid properties and pipe dimensions.

Also from Eq. (3.26), it is obvious that the increasing the fluid velocity decreases the pipe's natural frequency.

3.5.1.1 *Calculating the Fundamental Frequency for the Case Study*

The fundamental natural frequencies of the pipe for the different flow rates of the swash plate pump are calculated. The pipe material is steel with the following dimensions and specifications:

Length (m)	Inner radius (m)	outer radius (m)	Young's Modulus (GPa)	Density (Kg./m^3)
3.5	0.011	0.0127	200	8000

- The fluid (ISO46) density equals 980 (Kg./m^3)
- The fluid flow area can be given as

  $A = \pi r^2_{\text{inner}} = 3.8\,e-4$, [m^2]

- The moment of inertia for the pipe

  $I = \frac{\pi}{4}(r^4_{outter} - r^4_{inner}) = 8.9327e-9$, [m^4]

- Hence, the flexural rigidity of the pipe

  $EI = 1786$, [N.m^2]

- From Eq. (3.27), the critical flow velocity is 93.58 [m/sec.]
- Also, from Eq. (3.28), natural frequency of the pipe filled with fluid (zero flow velocity) equals [65.5915 rad. /sec.] or 10.4392 Hz.

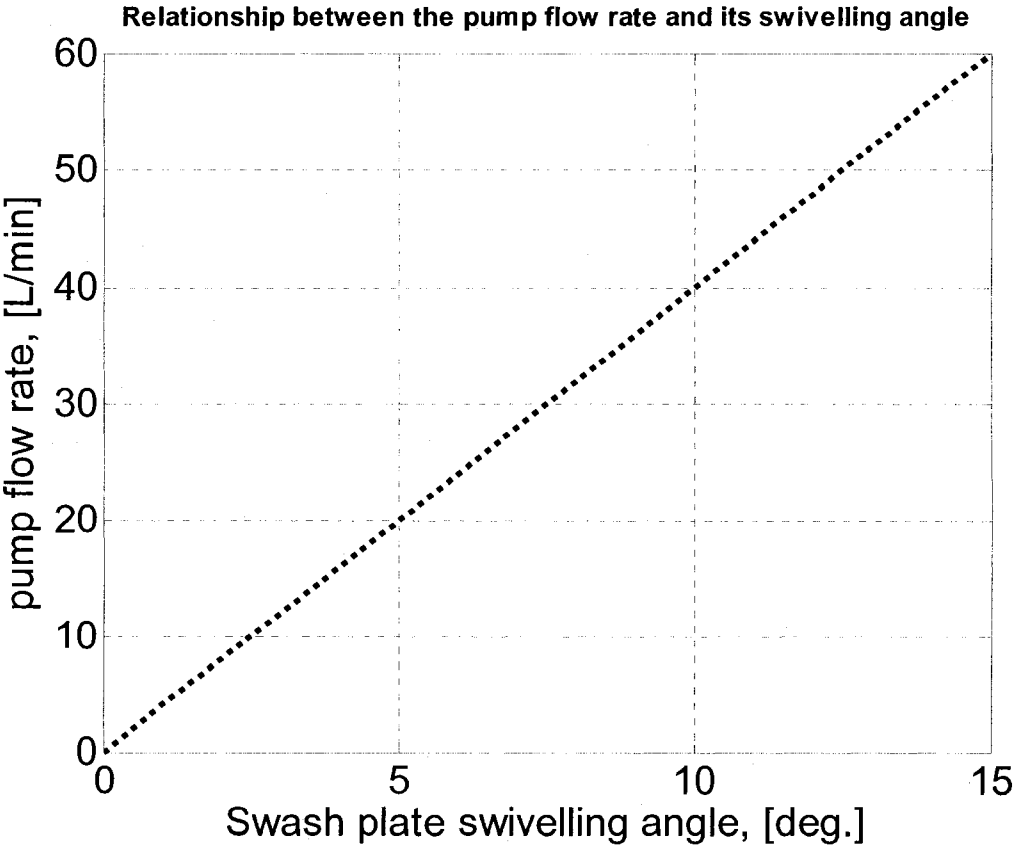

Figure 3.5: Relationship between the pump flow rate and the swash plate swiveling angle

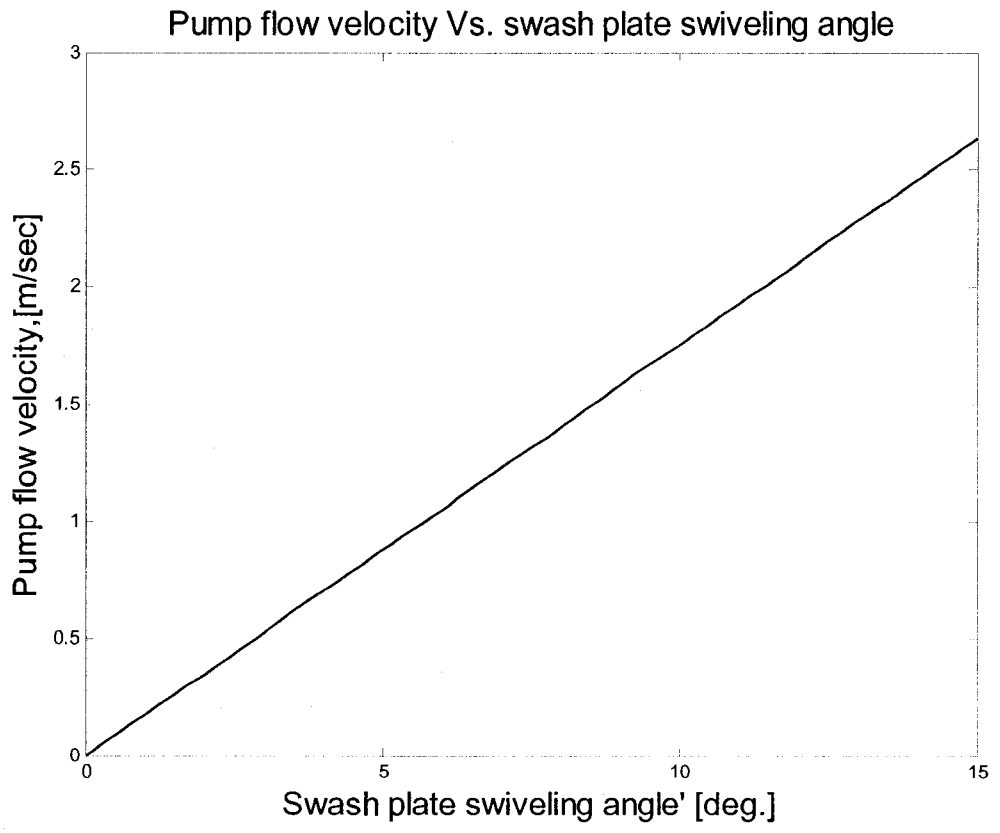

Figure 3.6: Relationship between the fluid flow velocity and the swash plate swiveling angle

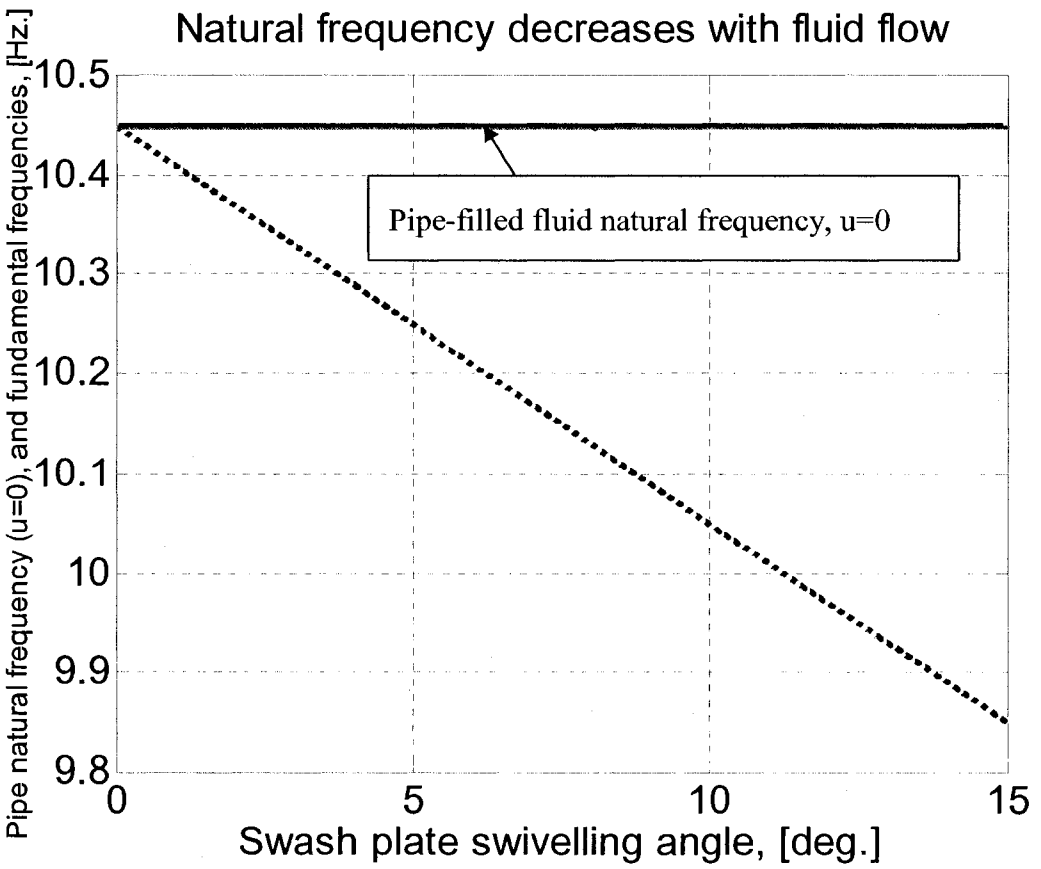

Figure 3.7: Fluid frequencies with different swash plate swiveling angles

Figure 3.5, Figure 3.6, and Figure 3.7 show the change of the pump flow rate, pump fluid flow velocity, and the natural frequencies, respectively.

The pump flow rate increases from zero at no inclination for the swash plate, to 0.001 M^3/Sec. with the maximum swiveling angle (15°). The fluid flow velocity has the same attribute, where it has the maximum flow velocity (2.67 m/sec) at the maximum swiveling angle. The pipe's natural frequency shows an opposite trend, where the maximum frequency (10.45 Hz.) occurs when the fluid is stagnant, u=0. The natural frequency drops 6.7% when the fluid flow velocity is at its maximum.

3.5.2 **Exact Solution**

In the previous section, the critical fluid flow velocity and the natural frequency were obtained approximately. It was assumed that the pipe loses its stability when the fluid flows with a velocity greater than the critical velocity, and this type of instability is dependent on the boundary conditions. For example, when the pipe is simply supported there is a divergence, and for a cantilever there is flutter.

Following the approach of Paidoussis [64], flutter and divergence of simply supported pipes are presented as follows:

Using the nondimensional form of parameters of the dynamic model as

$$X=\frac{x}{L},\ W=\frac{w}{L},\ T=\frac{t}{a},\ U=L.u\sqrt{\frac{m_f}{EI}},\ \text{and}\ \beta=\frac{m_f}{m_f+m_p}$$

Equation (3.19), can be written in the nondimenssional form as

$$\frac{d^4W}{dX^4}+U^2\frac{d^2W}{dX^2}+2\sqrt{\beta}U\frac{d^2W}{dXdT}+\frac{d^2W}{dT^2}=0 \qquad (3.29)$$

where β is the mass ratio, which varies from 0 to 1.

when:

- $\beta = 0$, no fluid runs in the pipe
- $\beta \approx 1$, this implies that the fluid is extremely heavy compared to the pipe

From Eq. (3.29), it can be noticed that the system stability is dependent upon two parameters: the nondimenssional flow velocity and the mass ratio.

In the next section, the static and dynamic stabilities will be discussed for the most practical applications, such as simply supported pipes, fixed-fixed pipes, and cantilever pipes. Also, the evolution of the system stability will be tracked as the fluid velocity increases, and the complex Argand plane diagram will be plotted.

3.5.2.1 *Stability in the Simply Supported Pipe Conveying Fluid*

We will start the analysis by defining the static stability, and then we will study the dynamic stability.

3.5.2.1.1 Divergence

The critical velocities at which the pipe will buckle can be obtained by solving Eq. (3.29) statically (T=0), where the pipe deflection, W, is independent of time, we have

$$\frac{d^4W}{dX^4} + U^2\frac{d^2W}{dX^2} = 0 \tag{3.30}$$

Let

$$W(X) = Ae^{px}$$

Substituting this solution into Eq. (3.30) results in

$$p^4 + U^2p^2 = 0$$

The four roots are: $p_{1,2=0}$ and $p_{3,4=\mp iU}$

The pipe deflection, can be written as

$$W(X) = \sum_{k=1}^{4} A_k e^{p_k X} \tag{3.31}$$

where A_k is a constant and is determined from the boundary condition.

Eq. (3.31) can also be expressed as

$$W(X) = A_1 + A_2X + A_3\,cos(UX) + A_4sin\,(UX) \tag{3.32}$$

The four boundary conditions for a simply supported pipe are:

- The deflection W=0, at X=0 and X=1
- The bending moment = EI$\frac{d^2W}{dX^2}$ =0, at X=0 and X=1

Eq. (3.32) will have four solutions, the same as the number of boundary conditions

$$\frac{d^2W}{dX^2}(X) = -A_3.U^2\cos(UX) - A_4.\ U^2\sin(UX) \tag{3.33}$$

By substituting the four boundary conditions, we can get

$X = 0 \leftrightarrow A_1 + A_3 = 0$

$X = 0 \leftrightarrow -A_3.U^2 = 0$

$X = 1 \leftrightarrow A_1 + A_2 + A_3.\cos(U) + A_4.\sin\,(U)=0$

$X = 1 \leftrightarrow -A_3.U^2\cos(U) - A_4\,.U^2\sin(U) = 0$

For nontrivial solution, setting the determinant of the coefficients to zero gives

$$D = \begin{vmatrix} 1 & 0 & 1 & 0 \\ 0 & 0 & -U^2 & 0 \\ 1 & 1 & \cos(U) & \sin(U) \\ 0 & 0 & -U^2\cos(U) & -U^2\sin(U) \end{vmatrix} = 0 \tag{3.34}$$

The frequency equation can be written as

$$sin(U)=0 \tag{3.35}$$

Hence, $U = \pi, 2\pi, 3\pi, \ldots., n\pi$

Solving for the dimensional values, $U = L.u\sqrt{\frac{m_f}{EI}}$, and the divergence corresponds to the lowest value for $U = \pi$. The divergence velocity can be expressed as

Since the lowest root, U , equals π , the divergence velocity for the simply supported case can be expressed as

$$u = \frac{\pi}{L}\sqrt{\frac{EI}{m_f}} \tag{3.36}$$

Eqs. (3.27) and (3.36) are identical.

3.5.2.1.2 Flutter

In order to obtain the dynamic instability velocity, the flutter velocity, Eq. (3.29) must be solved. Eq. (3.29) is a differential equation with two variables, X (fourth order), and T (second order). The coupling between the time and space in the second term complicates the solution, and hence, we cannot solve it by separating the two variables. Certain techniques presented by Paidoussis [64] will be used in this analysis.

Assume the solution of the ordinary differential equation in the form

$$W(X,T) = \sum_{k=1}^{4} A_k e^{ip_k X} . e^{iwT} \tag{3.37}$$

By differentiating the different terms of Eq. (3.29) with respect to T and X, we may get

$$p^4 - U^2p^2 - 2\sqrt{\beta}U\omega p - \omega^2 = 0 \tag{3.38}$$

Eq. (3.38) has four roots (p_1, p_2, p_3, $and\ p_4$), and they are dependent on the nondimensional fluid velocity, mass ratio, and nondimensional angular frequency. The general solution can be written as

$$W(X,T) = A_{1e^{p_1X}} + A_2.e^{p_2X} + A_3.e^{p_3X} + A_4.e^{p_4X} \tag{3.39}$$

Using the four boundary conditions

$X = 0 \leftrightarrow A_1 + A_2 + A_3 + A_4 = 0$

$X = 0 \leftrightarrow A_1p_1^2 + A_2p_2^2 + A_3p_3^2 + A_4p_4^2 = 0$

$X = 1 \leftrightarrow A_1e^{p1} + A_2e^{p2} + A_3e^{p3} + A_4e^{p4}=0$

$X = 1 \leftrightarrow A_1p_1^2e^{p1} + A_2p_2^2e^{p2} + A_3p_3^2e^{p3} + A_4p_4^2e^{p4} = 0$

Rearranging the previous equations and formulating the determinant of the coefficients, as in the previous section, we get

$$D = \begin{vmatrix} 1 & 1 & 1 & 1 \\ p_1^2 & p_2^2 & p_3^2 & p_4^2 \\ e^{p1} & e^{p2} & e^{p3} & e^{p4} \\ p_1^2e^{p1} & p_2^2e^{p2} & p_3^2e^{p3} & p_4^2e^{p4} \end{vmatrix} = 0$$

The closed form solution to this determinant to obtain the flutter speed $\boldsymbol{u}$ is difficult. Discretizing this continuous system problem into finite lumped masses, the governing equation for our problem using Galerkin's method becomes [64]

$$\begin{bmatrix}\ddot{q}_1\\ \ddot{q}_2\end{bmatrix}+2\sqrt{\beta}U\begin{bmatrix}b_{11} & b_{12}\\ b_{21} & b_{22}\end{bmatrix}\begin{bmatrix}\dot{q}_1\\ \dot{q}_2\end{bmatrix}+\begin{bmatrix}\lambda_1^4-U^2c_{11} & U^2c_{12}\\ U^2c_{21} & \lambda_2^4-U^2c_{22}\end{bmatrix}\begin{bmatrix}q_1\\ q_2\end{bmatrix}=0 \qquad (3.40)$$

Eq. (3.40) represents a two-mode Galerkin approximation of a pipe conveying fluid. The matrices have (r) columns and (s) rows. Hence, the coefficients b_{rs}, c_{rs} can be determined by the end support conditions, explained in detail by Paidoussis [64]. We start with the simply supported case where $b_{rr}=0$, $b_{rs}=-b_{sr}$ and $c_{rs}=0$. Thus, Eq. (3.40) becomes

$$\begin{bmatrix}\ddot{q}_1\\ \ddot{q}_2\end{bmatrix}+2\sqrt{\beta}U\begin{bmatrix}0 & b_{12}\\ b_{21} & 0\end{bmatrix}\begin{bmatrix}\dot{q}_1\\ \dot{q}_2\end{bmatrix}+\begin{bmatrix}\lambda_1^4-U^2c_{11} & 0\\ 0 & \lambda_2^4-U^2c_{22}\end{bmatrix}\begin{bmatrix}q_1\\ q_2\end{bmatrix}=0 \qquad (3.41)$$

where $\{q_i\}$ is a vector in the generalized coordinates.

Eq. (3.41) can be written in the standard form of a multi degree of freedoms. Hence, we can write the mass, damping, and stiffness matrices as follows:

$$M=\begin{bmatrix}1 & 0\\ 0 & 1\end{bmatrix}$$

$$C=2\sqrt{\beta}U\begin{bmatrix}0 & b_{12}\\ b_{21} & 0\end{bmatrix}$$

$$K=\begin{bmatrix}\lambda_1^4-U^2c_{11} & 0\\ 0 & \lambda_2^4-U^2c_{22}\end{bmatrix}$$

The coefficients b_{rs} and c_{rs} are obtained from Paidoussis [64], and they have the following forms

$$b_{rs}=\frac{\lambda_s\lambda_r}{\lambda_s^4-\lambda_r^4}[-(-1)^{s+r}(\lambda_s^2+\lambda_r^2)]$$

$$b_{rr}=b_{ss}=0$$

$$c_{rs} = 0$$

$$c_{rr} = -\lambda_r^2$$

where λ_s is the eigenvalue for the (s) mode, and λ_r is the eigenvalue for the (r) mode.

Rearranging Eq. (3.41) using new matrices, we get

$$[A]\{\dot{P}(T)\} + [B]\{P(T)\} = 0 \tag{3.42}$$

where

$$[A] = \begin{bmatrix} [0] & [M] \\ [M] & [C] \end{bmatrix}$$

$$[B] = \begin{bmatrix} -[M] & [0] \\ [0] & [K] \end{bmatrix}$$

$$\{P(T)\} = \begin{Bmatrix} \dot{q}_i(T) \\ q_i(T) \end{Bmatrix}$$

$$\{\dot{P}(T)\} = \begin{Bmatrix} \ddot{q}_i(T) \\ \dot{q}_i(T) \end{Bmatrix}$$

Multiplying Eq. (3.42) by $[A]^{-1}$, it becomes

$$[I]\{\dot{P}(T)\} + [A]^{-1}[B]\{P(T)\} = 0 \tag{3.43}$$

where $[A]$ is a unity matrix.

Assuming the solution Eq. (3.42) in the form

$$P(T) = \bar{P}e^{\lambda T}$$

$$\dot{P}(T) = \bar{P}\lambda e^{\lambda T} = \lambda P(T)$$

Rearranging Eq. (3.43), we may write

$$(\lambda[I] - D])\{P(T)\} = 0 \tag{3.44}$$

where $[A]^{-1}[B] = -[D]$

For the nontrivial solution,

$$|\lambda[I] - [D]]| = 0 \tag{3.45}$$

A new MATLAB program was developed to numerically solve the eigenvalue problem shown in Eq. (3.45). Solving Eq. (3.45) with the aid of the program enables us to map the evolution of the system stability, and to determine the nondimensional fluid velocities at which the pipe loses its static and dynamic stabilities.

The program starts with entering the pipe dimensions and specification and the fluid properties such as the fluid density, pipe density, pipe length, inner and outer diameters, and pipe material (Young's Modulus). The program computes the pipe moment of inertia, flow area, pipe mass per unit length, fluid mass per unit length, and mass ratio. The flow chart of the program is illustrated in Figure 3.8.

The program functions using the following steps:

1 Assumes the velocity equals zero, and the matrices (A, B, C, D, M, and K) will be computed.

2 Computes (3.45)

3 Separates the eigenvalues into real and imaginary parts

4 Expresses the eigenvalue components as frequency components as follows

$$Re(\omega) = Im(\lambda)$$

$$Im(\omega) = -Re(\lambda)$$

5 Plots three figures, which are:

- Non-dimensionless frequency representation (Imaginary Vs. Real)
- Imaginary Vs. nondimensional fluid velocity
- Real Vs. nondimensional fluid velocity

6 Evaluates the real component of the frequency. For negative values, the program indicates the presence of divergence.

7 Compares the imaginary part to the real part (damping ratio), and if it is negative, it exits the program and prints FLUTTER

8 If there is neither divergence nor flutter, the velocity is increased, and the same procedure will be repeated.

9 The locus of stability will be obtained

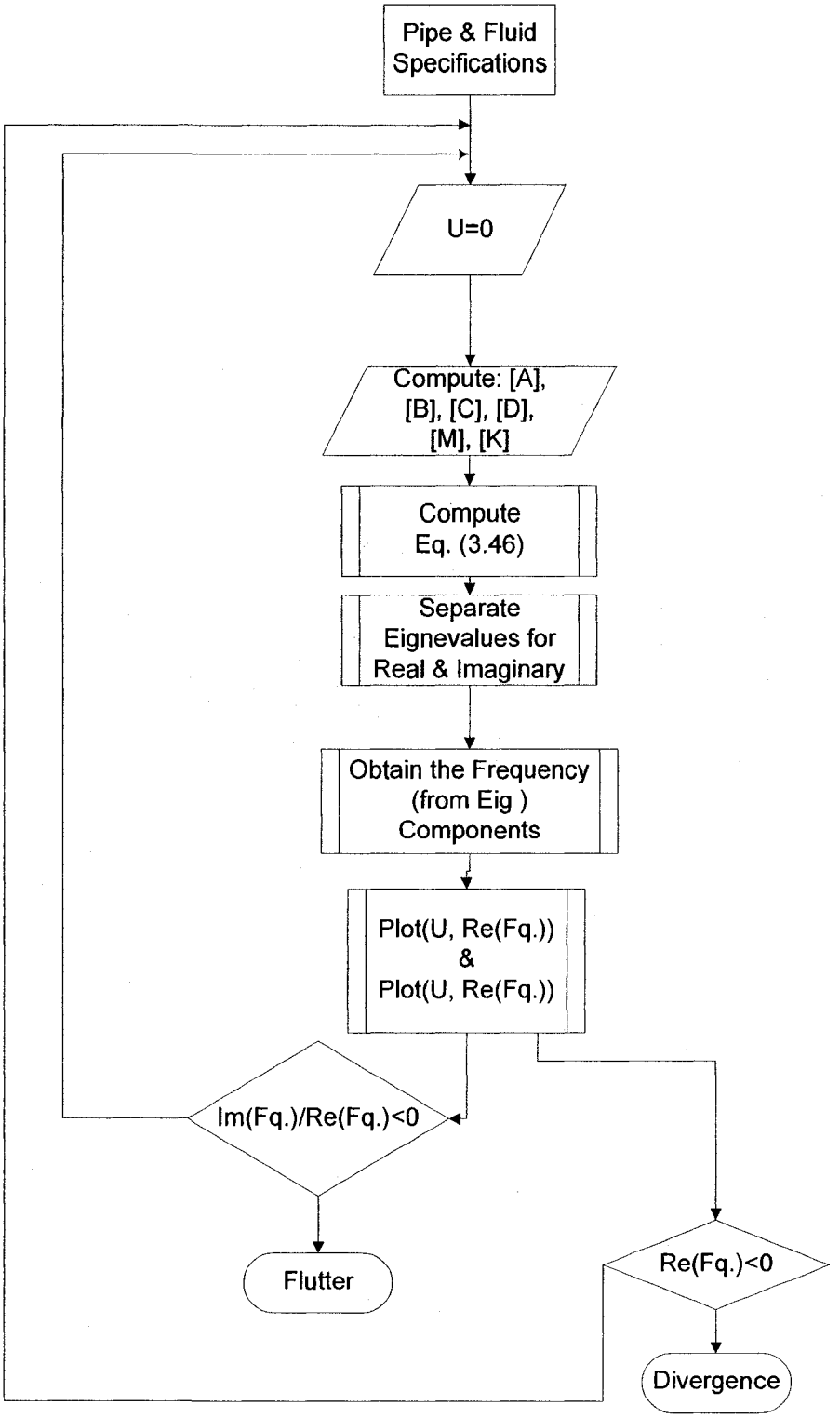

Figure 3.8: Flow chart for computing and plotting the stability of a simply supported pipe

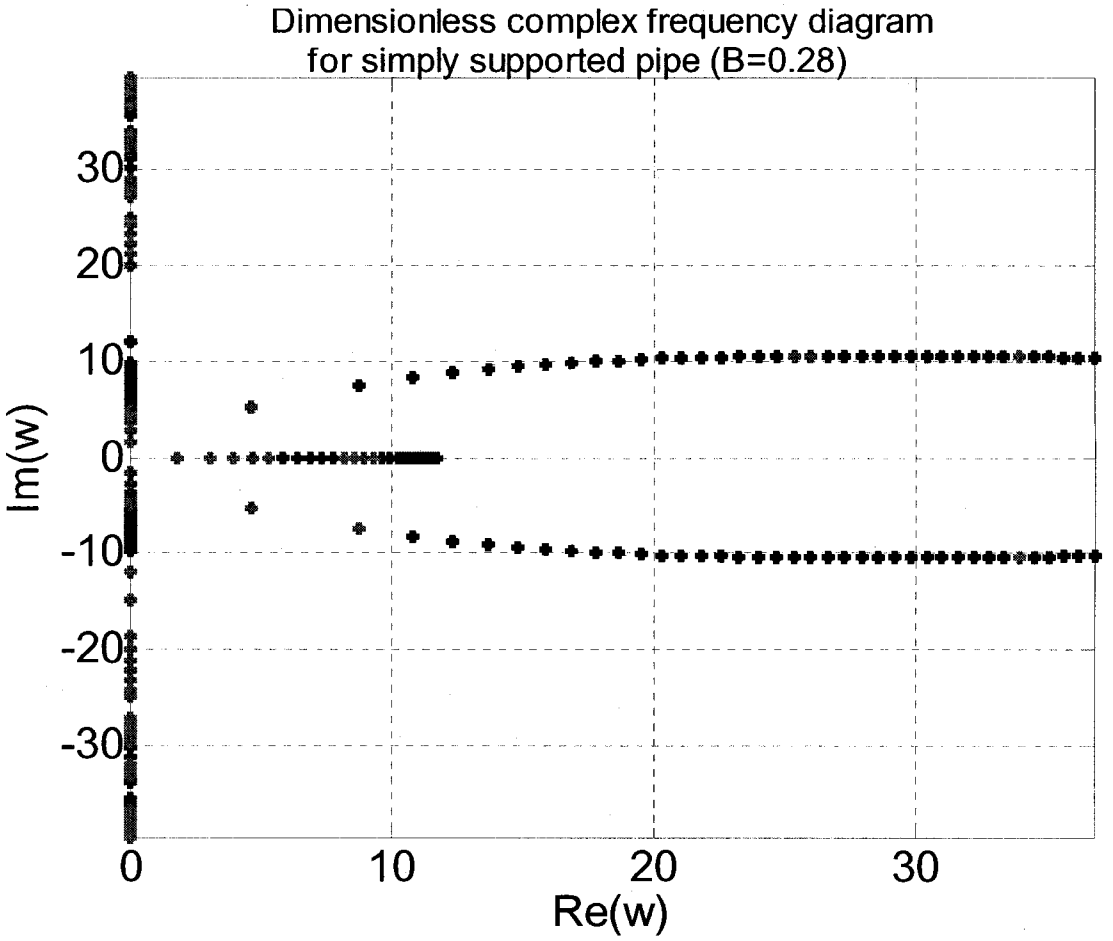

Figure 3.9: Complex Argand plane representation for a simply supported pipe with mass ratio (0.28)

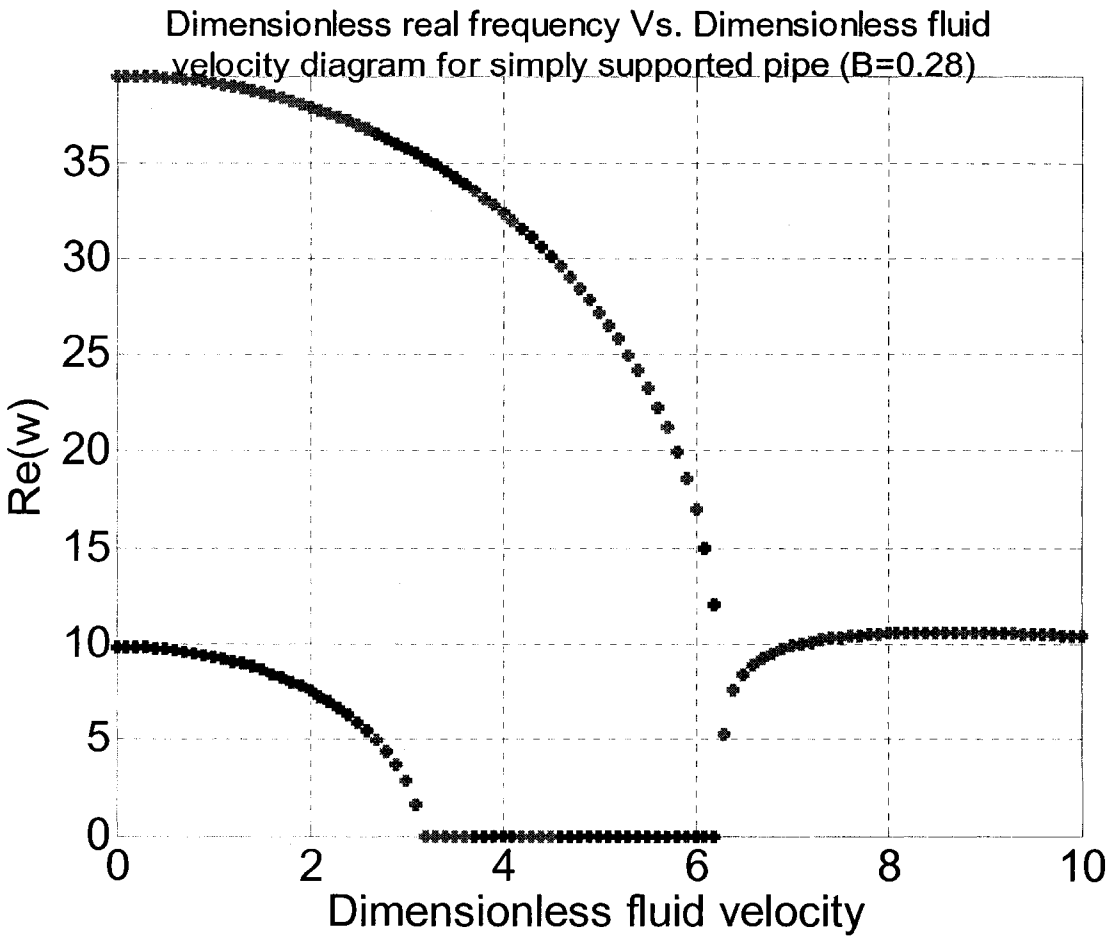

Figure 3.10: Dimensionless real frequency as a function of the dimensionless fluid velocity for a simply supported pipe with mass ratio (0.28)

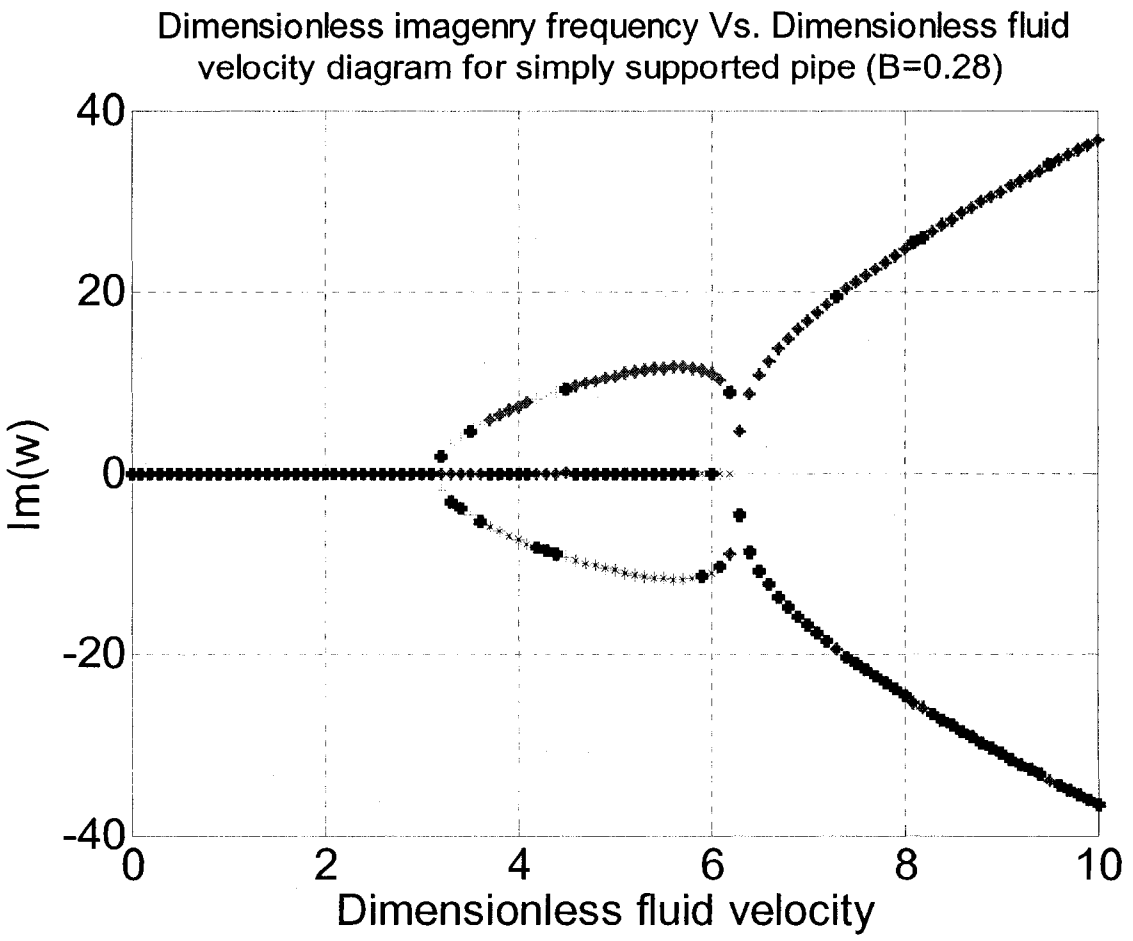

Figure 3.11: Dimensionless imaginary frequency as a function of the dimensionless fluid velocity for a simply supported pipe with mass ratio (0.28)

Figure 3.9, Figure 3.10, and Figure 3.11 show the evolution of the system stability for a simply supported pipe with increasing nondimensional velocity. Figure 3.9 shows the different values of the frequency with the change of the fluid velocity. The results of Figure 3.9 can be more descriptive in Figure 3.10 and Figure 3.11. In Figure 3.10, it can be seen that the pipe with this boundary condition (simply supported) develops divergence at two occasions (we have two modes); the first divergence occurs at U=3.14)

for the first mode and the second divergence of the second mode occurs at U=6.28. These results agree with what we calculated in 3.5.2.1.1, which are simple and predictable.

Figure 3.11 shows the divergence and flutter velocities. The loci of the two modes intersects with the fluid velocity axis at U=3.14 and U=6.28, representing the divergence velocities for the two modes. The two modes couple at U=6.7, representing the onset of flutter. Hence, the pipe buckles at low fluid flow velocity U=3.14 and starts its flutter at U=6.7.

3.5.2.2 *Stability in Fixed-Fixed Pipe Conveying Fluid*

The stability of a pipe changes with the change of its boundary conditions. The pipe behaviour for simply supported and fixed-fixed pipes is almost similar, with some modifications that will be discussed in the next section, where there will be a brief presentation about divergence and flutter. We will take into consideration the effect of the new boundary conditions on the system stability.

3.5.2.2.1 Divergence

The boundary conditions for the fixed-fixed pipes are:

- Deflection on the ends: $W = 0$
- Slope on the ends: $W' = 0$

Using the four boundary conditions, and subtitling in Eq.(3.30), we may obtain the determinant of the constants as

$$D = \begin{vmatrix} 1 & 0 & 1 & 0 \\ 0 & 1 & 0 & U \\ 1 & 1 & \cos(U) & \sin(U) \\ 0 & 1 & -U\sin(U) & U\cos(U) \end{vmatrix} = 0 \tag{3.46}$$

Solving Eq. (3.46) for the nontrivial solution, we can obtain the frequency equation as

$$U.\sin(U) + 2\cos(U) - 2 = 0 \tag{3.47}$$

The roots of Eq. (3.47) represent the values of the divergence velocities for a fixed-fixed pipe. These values can be written as

$$U = \pi m + \frac{\pi}{2}$$

where m=1,2,3,...

For the lowest value for U=4.73, we may obtain the dimensional divergence fluid velocity (according to Eq. (3.48)) as

$$u = \frac{4.73}{L}\sqrt{\frac{EI}{m_f}} \tag{3.48}$$

3.5.2.2.2 Flutter

Solving for the flutter velocity (as in the simply supported case), the determinant of the coefficients can be written as

$$\begin{vmatrix} 1 & 1 & 1 & 1 \\ p_1 & p_2 & p_3 & p_4 \\ e^{p1} & e^{p2} & e^{p3} & e^{p4} \\ p_1 e^{p1} & p_2 e^{p2} & p_3 e^{p3} & p_4 e^{p4} \end{vmatrix} = 0 \tag{3.49}$$

As discussed in the simply supported case, it is necessary to solve Eq. (3.40) in a similar fashion as in the simply supported case. The new coefficients (b_{rr}, b_{rs}, and c_{rs}) can be given as

$$c_{rs} = \frac{\lambda_s \lambda_r}{\lambda_s^4 - \lambda_r^4}[-(-1)^{s+r}(\lambda_s^2 + \lambda_r^2)]$$

$$c_{rr} = c_{ss} = 0$$

$$b_{rs} = \frac{2\lambda_s^2 \lambda_r^2}{\lambda_s^4 - \lambda_r^4}[\{1 + (-1)^{s+r}\}(\sigma_s \lambda_s - \sigma_r \lambda_r)]$$

$$b_{rr} = b_{ss} = 0$$

Substituting these coefficients in Eqs. (3.40), (3.42), and (3.45), we obtain the following results

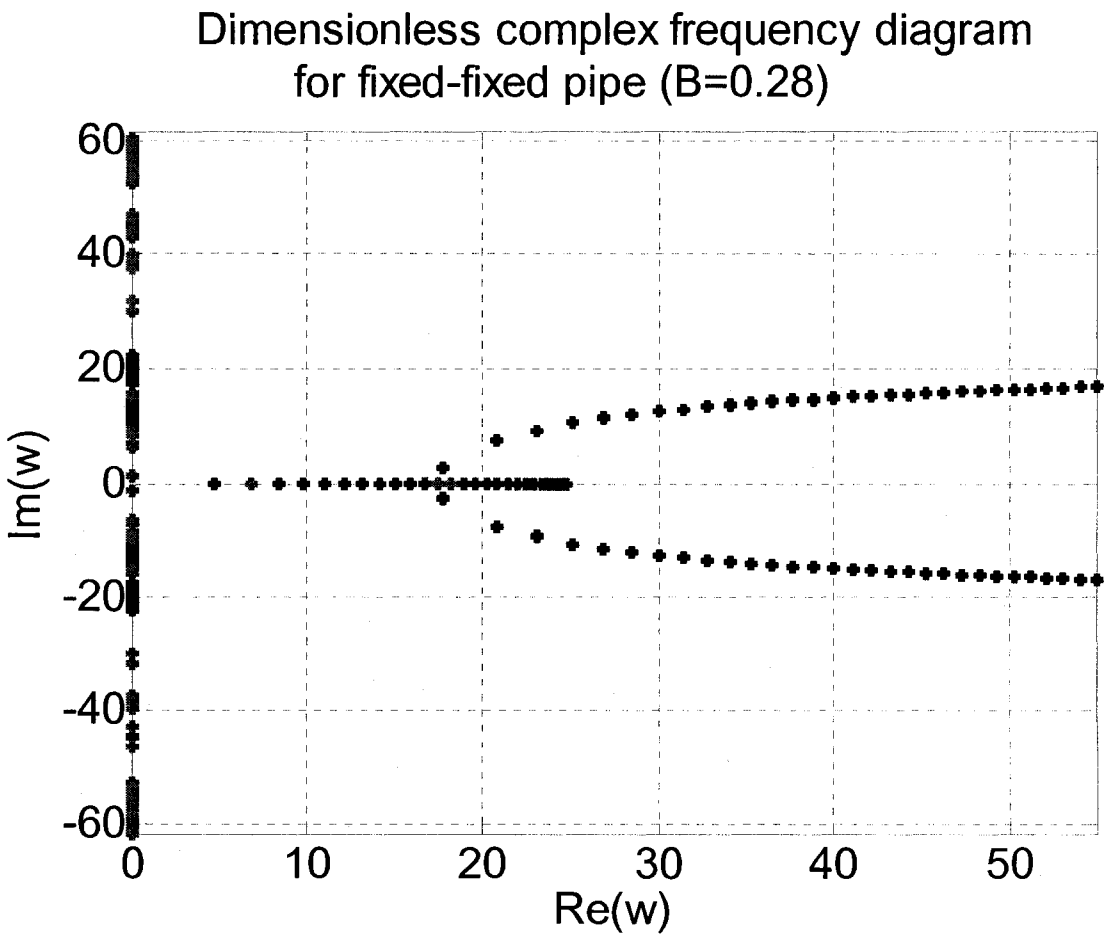

Figure 3.12: Complex Argand plane representation for a fixed-fixed pipe with mass ratio (0.28)

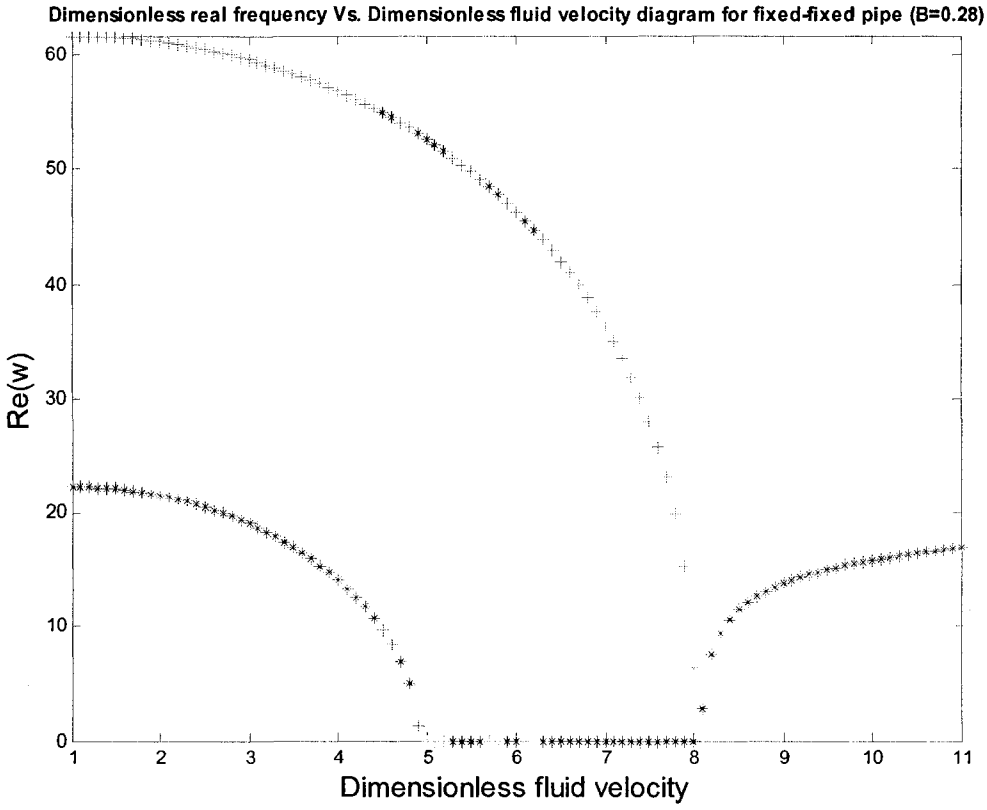

Figure 3.13: Dimensionless real frequency as a function of dimensionless fluid velocity for a fixed-fixed pipe with mass ratio (0.28)

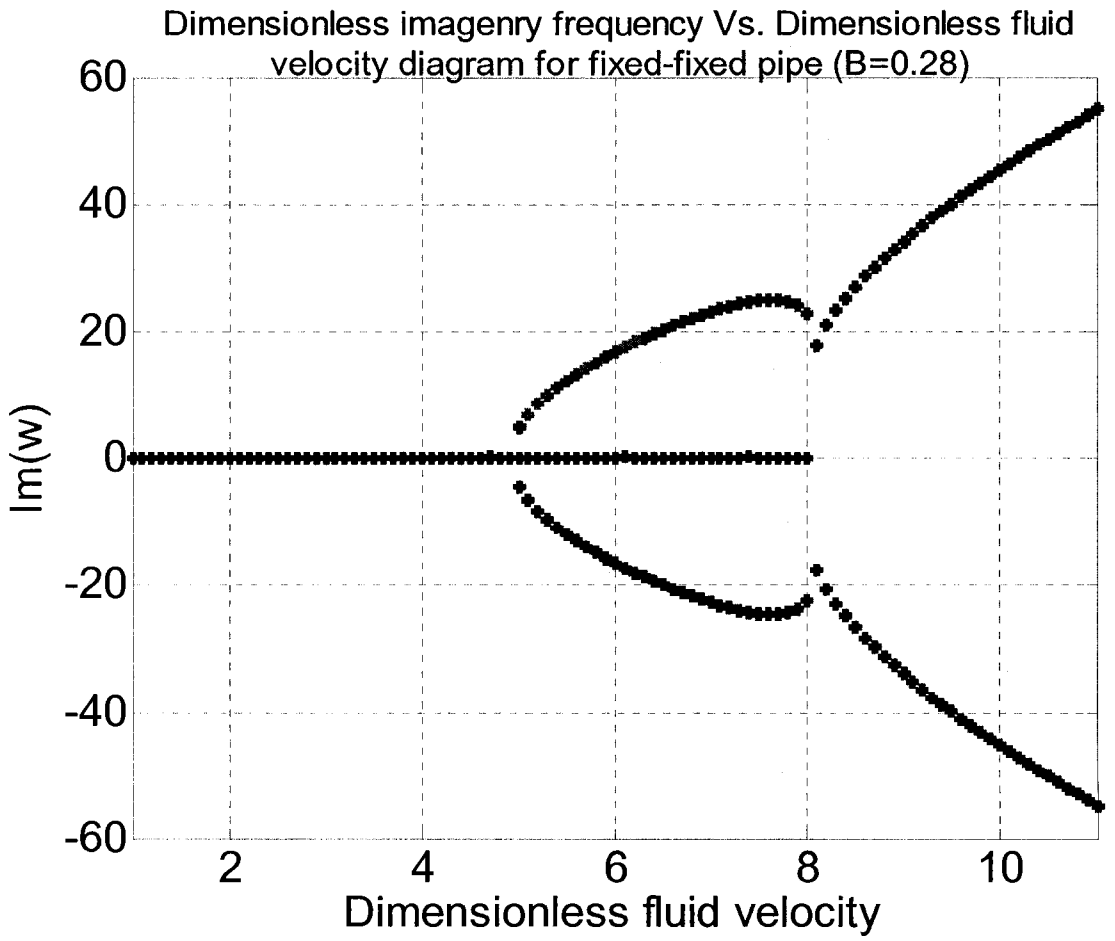

Figure 3.14: Dimensionless imaginary frequency as a function of dimensionless fluid velocity for a fixed-fixed pipe with mass ratio (0.28)

Comparing fixed–fixed pipes with simply supported pipes, we can see that the pipe stability improves. Figure 3.12, Figure 3.13, and Figure 3.14 illustrate the stability evolution for a fixed-fixed pipe. From Figure 3.13 it can be seen that the pipe will develop divergence for the first mode at U= 4.73, while the second divergence happens at U=7.78. As in the previous section, the flutter is recognized when the two modes intersect, and this occurs at U=8.

A comparison of the stability conditions are given in a tabular form below

	Simply supported pipe	Fixed-fixed pipe
	Nondimensional fluid velocity	
First mode divergence	3.14	4.73
First mode divergence	6.28	7.8
Flutter	6.7	8

Table 3-1: Comparison between the simply supported and fixed-fixed pipes (stability)

3.5.2.3 *Stability in Cantilever Pipe Conveying Fluid*

Cantilever pipes have only dynamic instability, i.e. there is no divergence with cantilever pipes.

3.5.2.3.1 Divergence

The free end of the pipe disables the pipe to have a divergence, which is a buckling pressure.

3.5.2.3.2 Flutter

As in the two previous cases, simply supported and fixed-fixed pipes, the new coefficients are determined following a similar approach.

The boundary conditions for a cantilever pipe are:

- $W(0) = W'(0) = 0$
- $W''(1) = W'''(1) = 0$

The corresponding coefficients are:

$$b_{sr} = \frac{4}{(\frac{\lambda_s}{\lambda_r})^2 + (-1)^{r+s}}$$

$$b_{rr} = b_{ss} = 2$$

$$c_{rs} = \frac{2(\sigma_s\lambda_s - \sigma_r\lambda_r)}{(-1)^{s+r} - (\frac{\lambda_s}{\lambda_r})^2}$$

$$c_{rr} = \sigma_r\lambda_r(2 - \sigma_s\lambda_s)$$

The numerical solutions for Eqs (3.40), (3.42), and (3.45) with these coefficients are illustrated in Figure 3.15 and Figure 3.16.

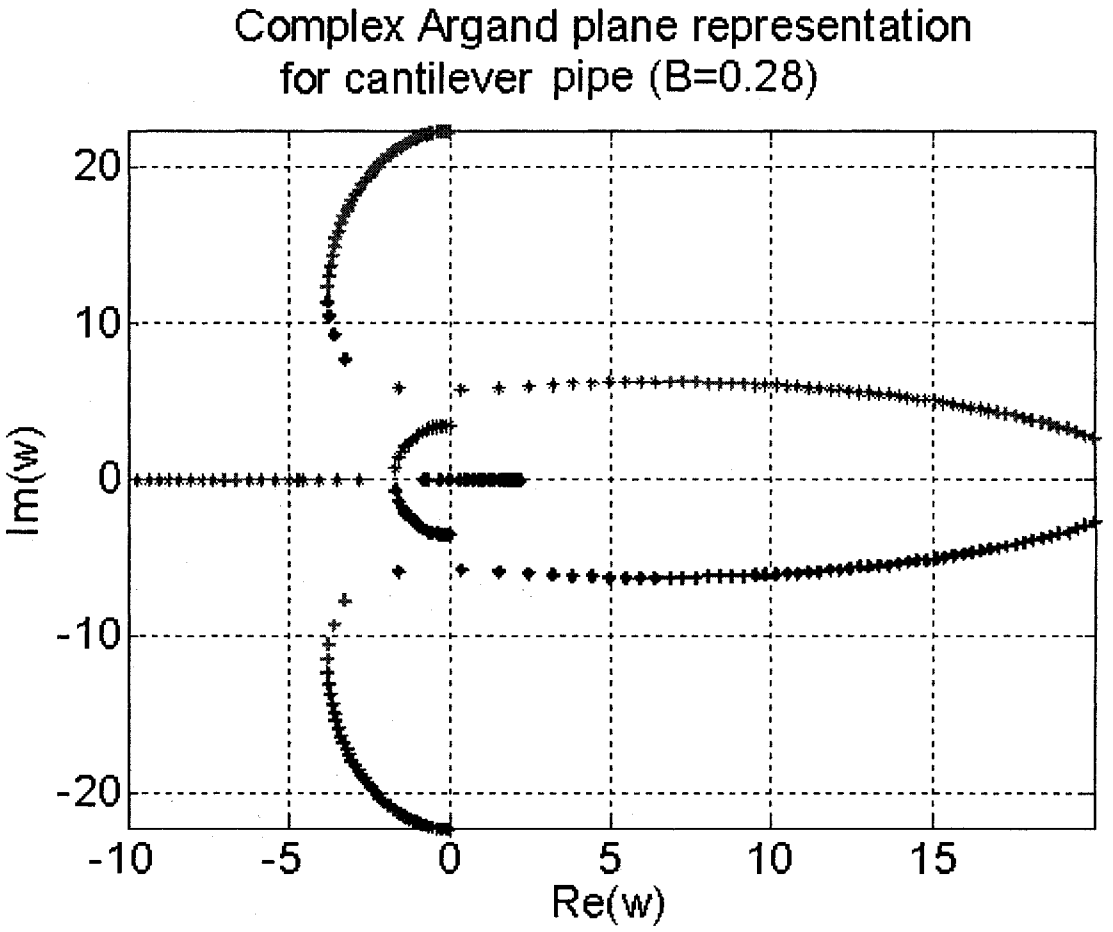

Figure 3.15: Complex Argand plane representation for a cantilever pipe with mass ratio (0.28)

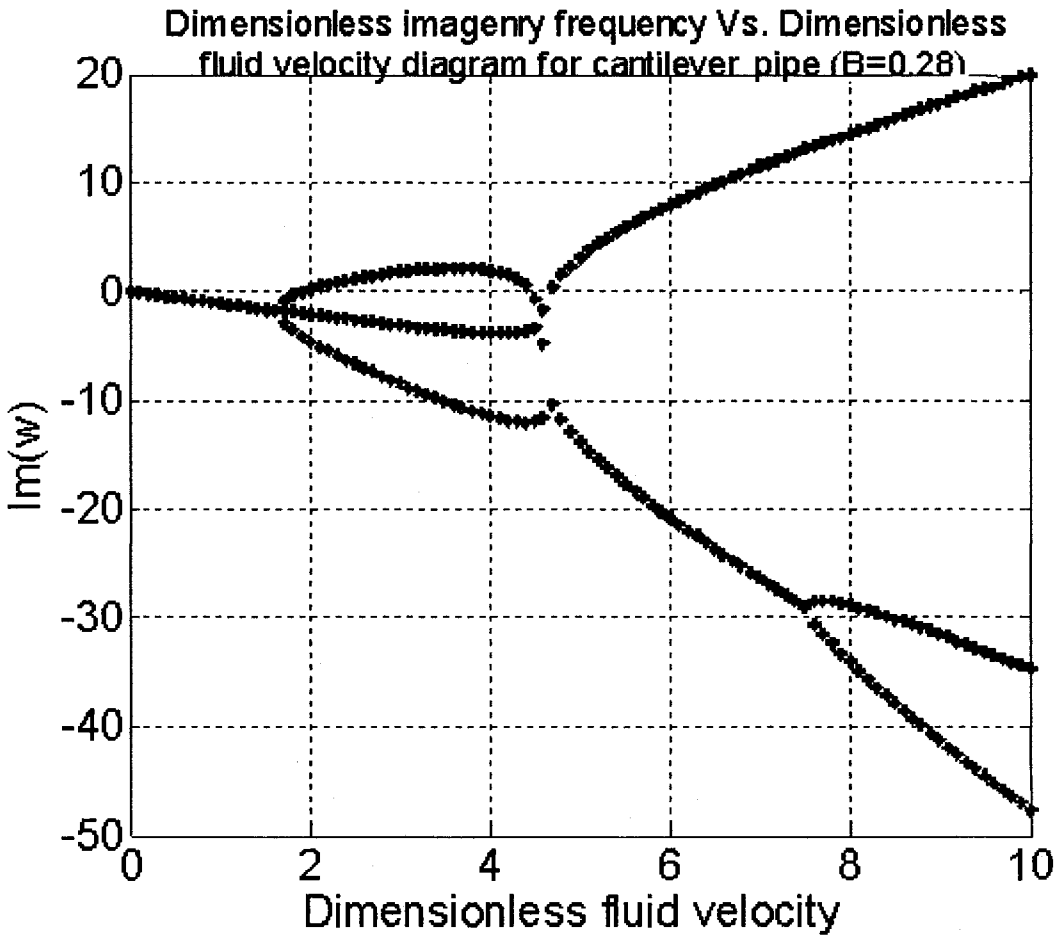

Figure 3.16: Dimensionless real frequency as a function of dimensionless fluid velocity for a cantilever pipe with mass ratio (0.28)

Figure 3.16 shows the loci of the first two modes for a cantilever pipe at different velocities. The first mode merges with the second mode at a low velocity (U=4.8), which means that the pipe loses its dynamic stability at this low velocity.

3.6 Investigation of the Response of a Simply Supported Pipe with a Swash Plate Pump

In the previous sections, the fluid was considered with a mean value (without fluctuations), and the pipe stability was studied accordingly, which is an ideal assumption. However, in practical applications and in our study, the fluid flow has fluctuations, with increases or decreases according to the pump design. The fluid flow fluctuations affect the performance of the hydraulic system, and the vibration levels increase with the increase in the flow fluctuations. Considering fluid fluctuations as a periodic process in the form of a Fourier series with 10 terms, the fluid velocity can be expressed as

$$U = N.\frac{1}{A}\sum_{k}^{9} Q_k(\varphi) = N.\frac{1}{A}(A_{o_k} + \sum_{n=1}^{10}[A_n Cos(n.\omega t) + B_n Sin(n.\omega t)]) \qquad (3.50)$$

or

$$U = N.\frac{1}{A}\sum_{k}^{9} Q_k(\varphi) = N.\frac{1}{A}(A_{o_k} + \sum_{n=1}^{10}[A_n Cos(n.\omega t/9)])$$

where

A: is the fluid flow area (pipe inner area)

$Q_k(\varphi)$: is the k^{th} cylinder flow rate

N: is the nondimensional coefficient (for this study, N=0.4364)

A_n: is the n^{th} Fourier coefficient

In order to investigate the response of the simply supported pipe with the swash plate pump case studied here, fluid flow fluctuations must be considered.

Substituting Eq. (3.51) in Eq. (3.29), the equation of motion for a pipe filled with a pulsating fluid can be obtained, as follows

$$\frac{d^4W}{dX^4} + (N.\frac{1}{A}(A_{o_k} + \sum_{n=1}^{10}[A_n Cos(n.\omega t/9)]))^2 \frac{d^2W}{dX^2} + 2\sqrt{\beta}N.\frac{1}{A}(A_{o_k} + \sum_{n=1}^{10}[A_n Cos(n.\omega t/9)])\frac{d^2W}{dXdT} + \frac{d^2W}{dT^2} = 0 \quad (3.51)$$

for simplicity, we will assume that

$$L = (N.\frac{1}{A}(A_{o_k} + \sum_{n=1}^{10}[A_n Cos(n.\omega t/9)]))^2$$

$$\emptyset = 2\sqrt{\beta}N.\frac{1}{A}(A_{o_k} + \sum_{n=1}^{10}[A_n Cos(n.\omega t/9)])$$

Eq. (3.51) can be rewritten as

$$\frac{d^4W}{dX^4} + L\frac{d^2W}{dX^2} + \emptyset\frac{d^2W}{dXdT} + \frac{d^2W}{dT^2} = 0 \quad (3.52)$$

In order to obtain the response of the simply supported pipe, a suitable solution for Eq. (3.52) must be found.

Galerkin proposed a solution by superimposing the modes of the pipe according to its boundary conditions. Accordingly, we may write the equation by considering the different differentiation of the terms, which are

$$W(X,T) = \sum_{n=1} r_n(T).Sin(n\pi X)$$

$$W''''(X,T) = \sum_{n=1} r_n(T).(n\pi)^4 Sin(n\pi X)$$

$$W''(X,T) = -\sum_{n=1} r_n(T).(n\pi)^2 Sin(n\pi X)$$

$$W'(X,T) = \sum_{n=1} \dot{r_n}(T).(n\pi)Cos(n\pi X)$$

$$\ddot{W}(X,T) = \sum_{n=1} \ddot{r_n}(T).Sin(n\pi X)$$

where

$sin(n\pi X)$: is the nth normal mode, and $r_n(T)$ is the nth generalized coordinates

Substituting these terms in Eq. (3.52), and using the orthogonal property of the mode shape, we obtain

$$\ddot{r_s} + \emptyset(\sum_{\substack{n=1 \\ n\neq s}} Cos(n\pi X).Sin(s\pi X))\,\dot{r_s} + [(s\pi)^4 - L(s\pi)^2]r_s = 0 \qquad (3.53)$$

The solution of Eq. (3.53) can be carried out for n modes --the solution varies according to the combinations of the modes, because of the sensitivity of the second term. Solving the equation for the first mode, the second term vanishes. Hence, the solution can be expressed as

$$\ddot{r_1} + [(\pi)^4 - L(\pi)^2]r_1 = 0 \tag{3.54}$$

and for the second mode (s=1, n=2 or s=2, n=1), we may obtain the two equations as

$$\ddot{r_1} - \frac{8}{3}\emptyset\, \dot{r_2} + [(\pi)^4 - L(\pi)^2]r_1 = 0 \tag{3.55}$$

$$\ddot{r_2} + \frac{8}{3}\emptyset\, \dot{r_1} + [(2\pi)^4 - L(2\pi)^2]r_2 = 0$$

For further analysis, Eq. (3.54) is simulated and the following parameters are considered:

- For the pipe: L=3.5, Din=2.3 cm, E= 200 Gpa, I= $8.9327e-9$ m^4, and β=0.28
- For the fluid: A1=2.7489, A2=0.8928, A3=0.5541, A4=0.4565, A5=0.3412, A6=0.2837, A7=0.2422, A8=0.2197, A9=0.1959, A10=0.1907, and A0=60.

The equation is numerically integrated using the fourth order Runge-Kutta scheme, and the sampling time is selected to be very small, t=1 mSec., while the initial conditions are: initial velocity is equal to zero and the initial displacement is equal to 0.05 m. The results of the three cases are illustrated in Figure 3.17.

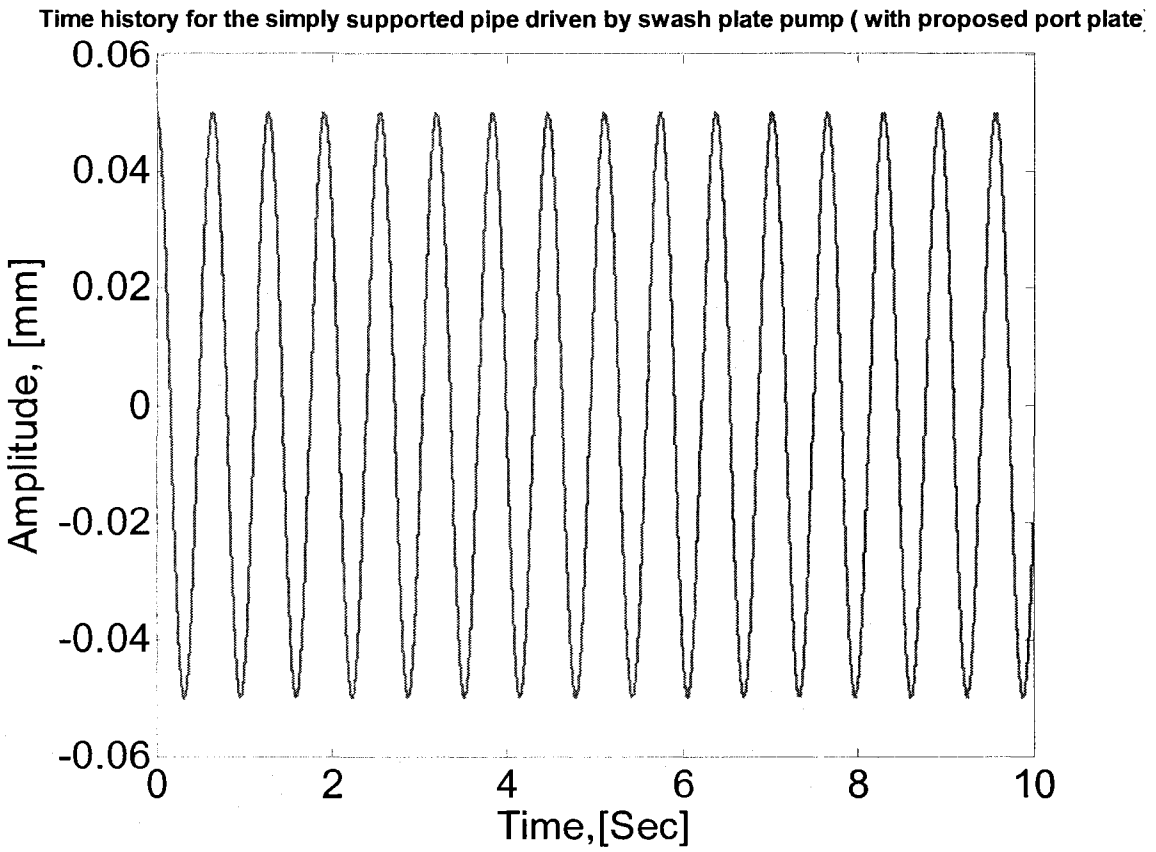

Figure 3.17: Time history for a simply supported pipe driven by a swash plate pump (with the proposed port plate)

3.7 Conclusions

This chapter dealt with pipe dynamics and fluid flow induced vibrations. It started with the definition of the fluid-flow induced vibrations, and then their different types were listed and discussed. Also, the causes of the vibration in pipes due to fluid flow were discussed according to momentum and boundary layer theories. The equation of motion for a fluid filled pipe was derived, where we analyzed the forces on the fluid element (free body) and the forces and moments on the pipe element.

The equation of motion has two variables, which are time and space. The coupling between time and space in Coriolis terms did make its solution difficult. Hence, we solved it for divergence and flutter with different approaches. First, we approximately solved the equation of motion of a simply supported pipe for the critical velocity, which buckles the pipe; and then we found the natural frequency as a function of the fluid velocity and pipe specifications. We found that the lowest critical velocity for this case equals 3.14.

Then we tried to obtain the exact solution for the equation of motion, and were able to find the divergence velocities, which are identical to the instability velocity with the approximated approach, for the simply supported and fixed-fixed conditions. Solving for flutter velocities, however, was a complex process. In order to overcome this problem, the system was discritized according to Galerkin's approach. General coordinates were set and eigenvalue problems were established. According to Galerkin's approach, we obtained square matrices (their dimensions equal to the required mode shape) and the coefficients of the matrices were determined according to the boundary conditions.

The complex Argand planes were plotted for every case; and the loci of the imaginary and real parts of the nondimensional frequency were also plotted.

According to the previous approaches, it was found that:

1 From the approximated solution, the frequency decreases by increasing the fluid velocity till it reaches a velocity (the critical velocity) at which the pipe stiffness vanishes and the pipe buckles.

2 From the exact solution, the divergence is only dependent on fluid velocity and the boundary conditions.

3 The divergence has different values for a simply supported pipe (U=3.14) and a fixed-fixed (U=4.73). There is no divergence for a cantilever pipe.

4 The flutter has the same trend as the divergence. The cantilever pipe experiences flutter at U=4.8; while for the simply supported and fixed-fixed pipes, they develop flutter at fluid velocities of 6.7 and 8, respectively.

5 The pipe response is affected by the fluid velocity profile, and with higher levels of flow fluctuations, the pipe vibrates with higher levels of vibrations. These can be reduced by reconsidering the design of the port plate (with deep silencing grooves). The proper design of the port plate produces a smoother operation for the pump and for all of the hydraulic system components.

Comprehensive theoretical investigations were carried out on the pump and the pipe-filled fluid, detailed in the last two chapters. In the next chapter, the experimental investigations will be discussed. This will include the description of the facilities of the setup, the testing methodology, and the test steps.

4 EXPERIMENTAL INVESTIGATIONS

4.1 Introduction

In chapters two and three, we modeled the pump static characteristics with the new port plate design and studied the pipe stability. Experiments were then conducted to verify some control strategies, to validate the analytical predictions of the dynamic behavior and also to study some health monitoring strategies. Before discussing these strategies, the experimental set up is described here in order to contextualize the discussions on the control strategies covered in the next chapter.

In this chapter, the experimental facility, testing methodology, test steps, and the schematic representation will be discussed. At the end of the chapter, a conclusion and discussion will be presented.

4.2 Experimental Facility

Figure 4.2 shows the scheme of the experimental facility.

The facility mainly consists of:

1. The hydraulic unit
2. The control unit
3. The test instrument unit
4. The data acquisition, conditioning, and recording unit
5. A Flow loop

Figure 4.1 illustrates the schematic representation of the experimental facilities, which are described in detail in this chapter.

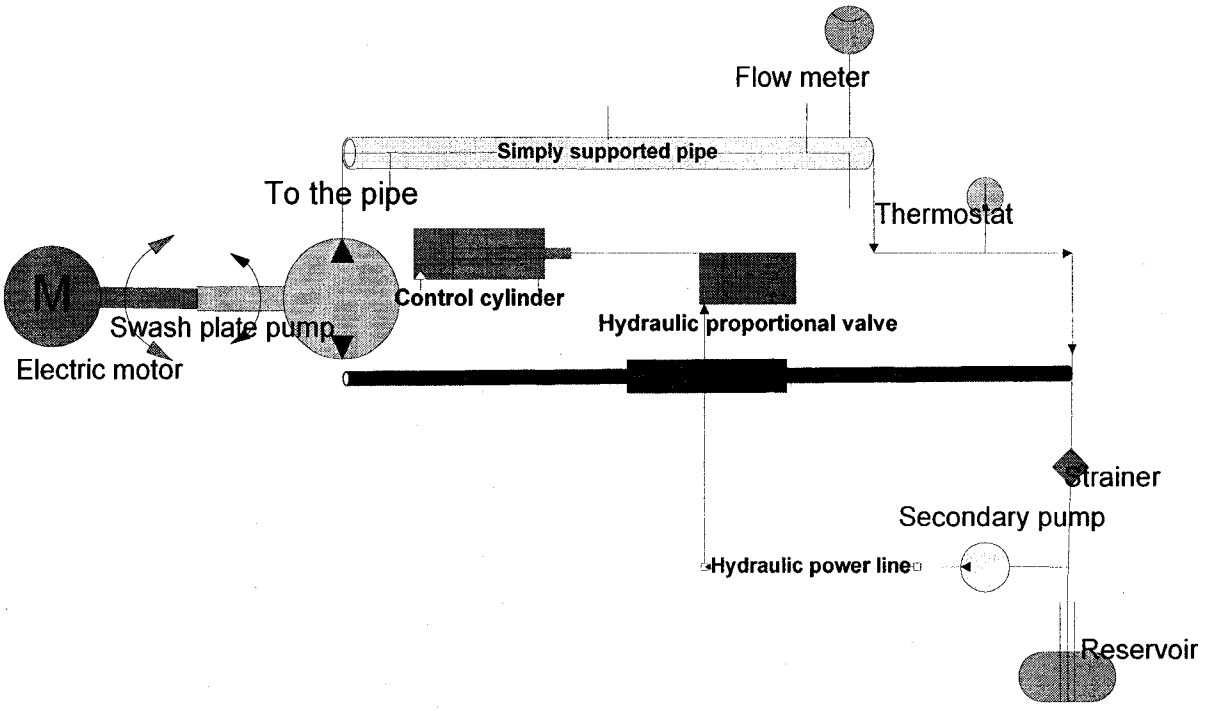

Figure 4.1: The schematic representation of the pump-pipe model

4.2.1 The Hydraulic Unit

The hydraulic unit consists of five major parts: a swash plate pump, the secondary pump, a load disturbance unit, oil conditioner, and accessories.

The Swash Plate Pump Arrangement:

The arrangement has the pump (1) driven by a 10 H.P. electric motor (2). The pump changes its swivelling angle by means of a control cylinder (3) mechanically attached to the swash plate. The proportional valve (4) receives a control signal from the controller to generate the control pressure in the hydraulic lines connected to the control cylinder pushing it. Three transducers are used to feed the control unit by the hydraulic system inputs, and these transducers provide the load pressure, swash plate inclination angle, and the spool position. The Arithmetic unit computes the inclination angle according to the load.

The Secondary Pump Unit:

A separate hydraulic unit is used to create the control pressure (up to 15 MPa.). This pressure is needed to push the control cylinder (3) through the hydraulic proportional valve (4). The secondary pump (9) is driven by an electric motor (8), which intakes the hydraulic fluid from the tank (10). In order to maintain the quality of the oil, two mesh strainers are installed. The first mesh (11) is installed on the pump's incoming line, and the second mesh (12) on the by-pass line. The dial gauge displays the value of the delivered pressure (13). An accumulator (14) is equipped to control the pressure and keep it constant under the different operating conditions, and a relief valve (15) is installed to

relieve the excess pressure. An electrical switch is used to operate the pump (17), which is integrated with safety (unloading) valve (16).

Load Disturbance Unit:

In order to simulate different operating conditions, a load disturbance unit is added. It has a two-way loading valve (18) that links or cuts off the pump delivery line (31) to the reservoir (10). It also contains a throttle valve (19) to manually tune the loading pressure, and the pressure value is shown on a dial gauge (20). A relief valve (22) is installed to maintain the desired pressure.

Oil Conditioning Unit:

Oil contamination and overheating are major problems in hydraulic systems. Certain steps should be taken to keep the oil within its functional specifications. For example, a mesh (23) traps the oil contaminations, and an oil cooler (24) is installed to lower the temperature of the oil so that it remains less than 60 C^{o}, as recommended. To isolate this unit, two valves are installed (25 and 26). A thermometer (27) is used to measure the oil temperature.

Accessories:

An oil breather (28) is installed to eliminate air from the hydraulic system, and cut-off valves (30-33) are added to isolate the swash plate and the secondary pumps and the rest of the hydraulic circuit from the reservoir, eliminating the need to drain the oil tank. A simply supported steel pipe conveys the hydraulic fluid. The specifications of the pipe were introduced in the previous chapter.

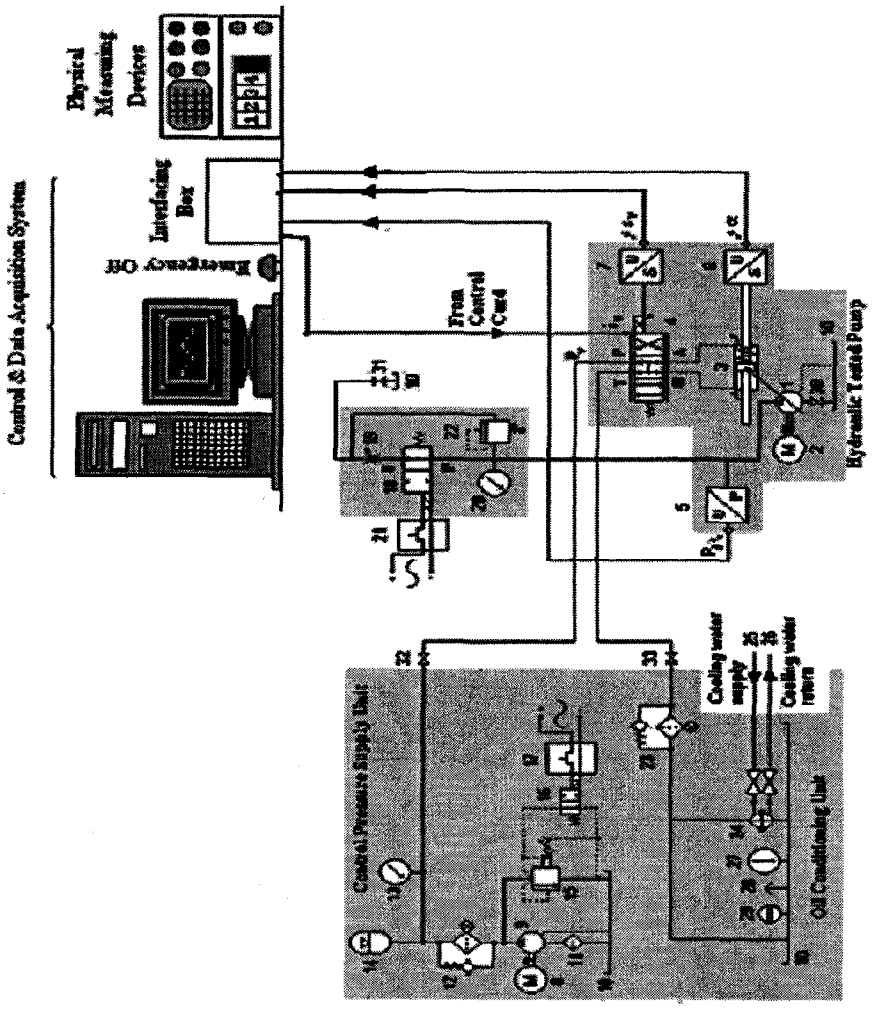

Figure 4.2: Experiment setup scheme, including the hydraulic and control parts (with the data acquisition unit)

4.2.2 **The Control Unit**

In order to parameterize, build, and test the proposed control schemes and strategies, real time control software is constructed based on SIMULINK 7-1 R. Figure 4.3 shows the contents of the control unit. This consists of a computer connected to an I/O card. The I/O

card converts the measured values (voltage values that can be read through the multi-meter) to numerical input and then feeds that to the computer. The computer, with the aid of SIMULINK, generates the required voltage according to the controller's input. The output card reconverts the output of the computer to a voltage and then feeds it to the controller.

The hardware of the control units includes the following components: An arithmetic logic unit and the PID swash plate controller. These components are built on a green card. The arithmetic unit receives a signal from the pressure transducer and then calculates the required swash plate swivelling angle in the form of voltage. These values are limited by the maximum pump power, pressure, and the flow rate. The control unit is powered by two 12 DC-volt units. Computers process only the analog values, and for this reason LABVIEW software is used to convert the digital signals that are received via the I/O card to analog signals.

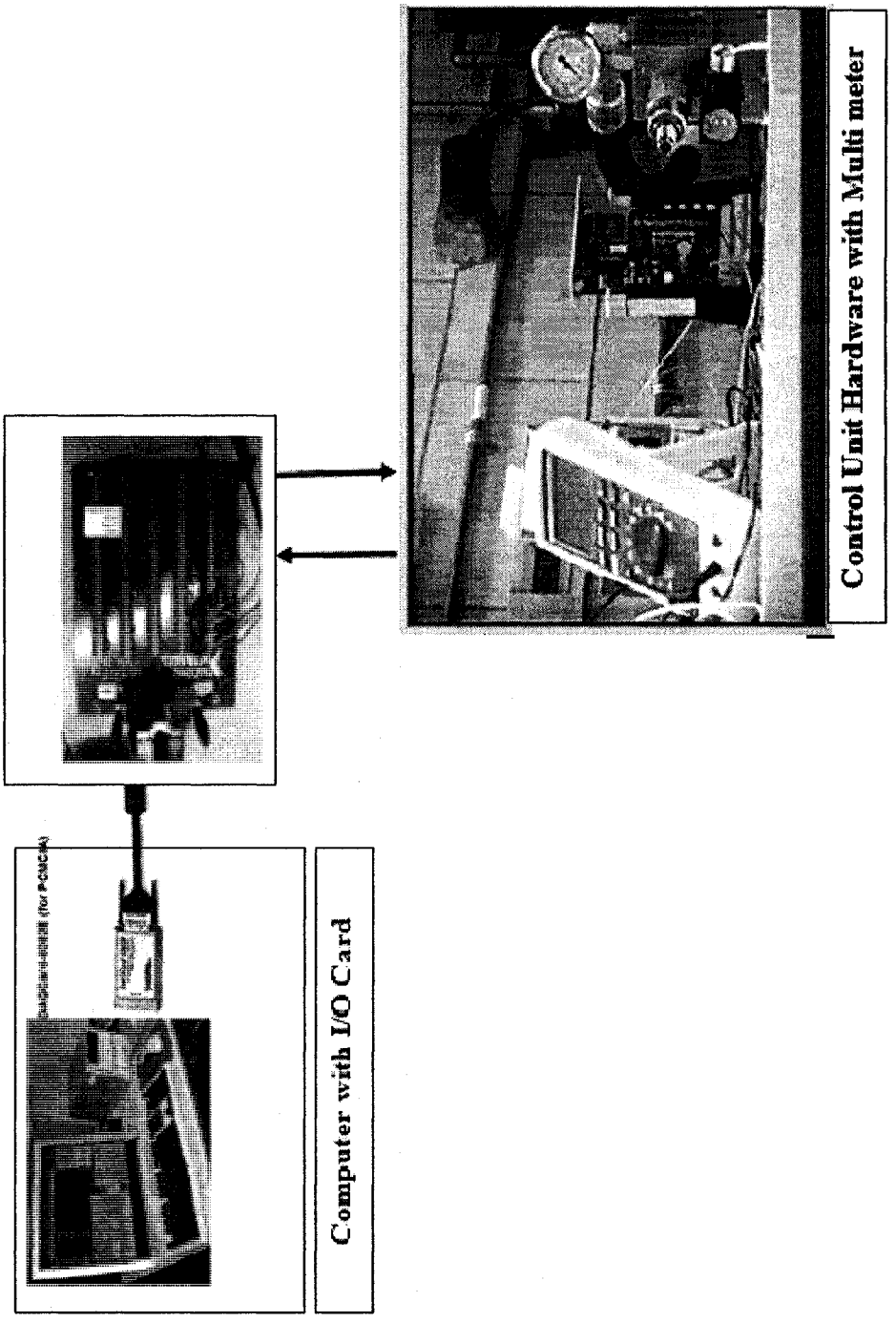

Figure 4.3: Control unit components

4.2.3 **The Test Instrument Unit**

The test instruments include two piezoelectric accelerometers, a flow meter, and a charge amplifier.

4.2.3.1 *Accelerometers*

In order to measure the acceleration of the pump and the pipes, two accelerometers are mounted, on the pipe in the X-direction and on the pump outlet. The different locations of the accelerometers are illustrated in Figure 4.4 and Figure 4.5.

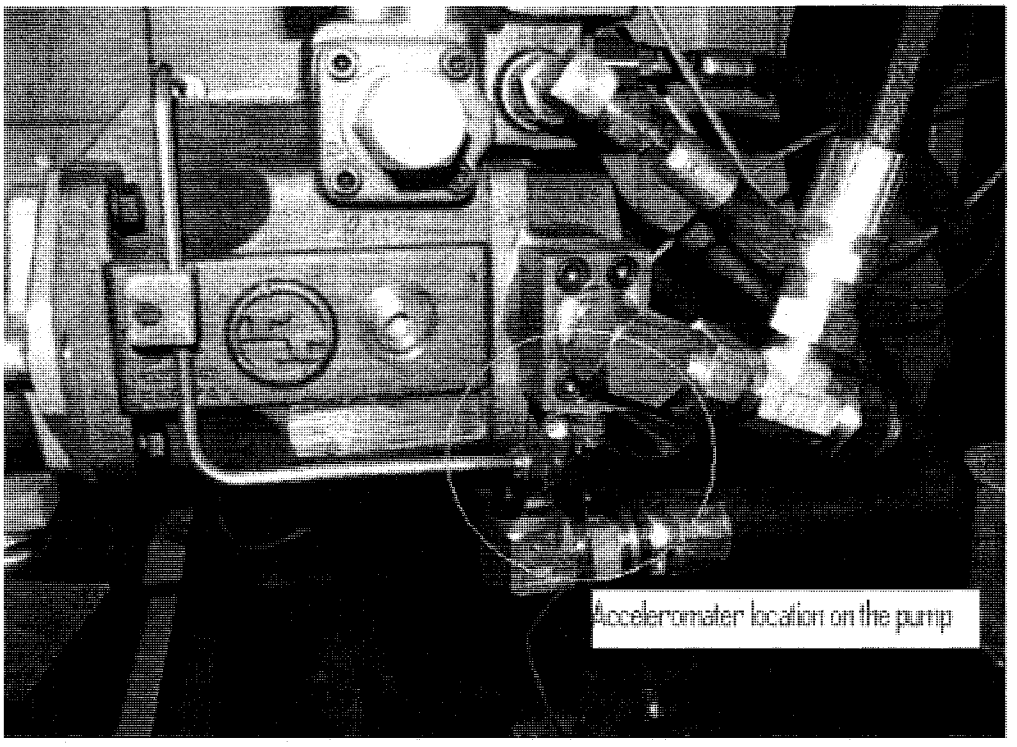

Figure 4.4: The location of the accelerometer on the pump outlet

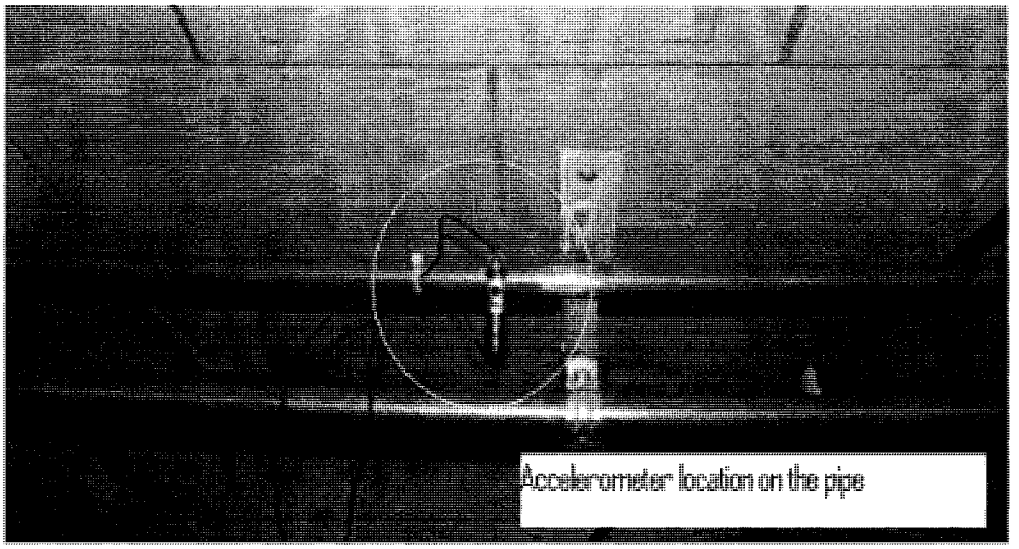

Figure 4.5: The location of the accelerometer on the pipe

4.2.3.2 *Flow Meter*

A flow meter is used to measure the volumetric flow rate of the pump. The flow meter is installed on the pipe outlet next to the pump's tank. The flow meter is designed to measure up to 0.00133 M^3/Sec, which is much more than the maximum flow rate of the pump studied (which is 0.001 M^3/Sec).

4.2.3.3 *Charge Amplifier*

The measured signals are relatively small. In order to process the signals and make them manageable, a charge amplifier is used. The output of the charge amplifier is an oscilloscope and a spectrum analyzer.

4.2.4 The Data Acquisition, Conditioning, and Recording Unit

After conditioning the signals, the data from the accelerometers are collected and recorded in the oscilloscope and the spectrum analyzer.

This unit contains the following equipment: a low-pass filter, an oscilloscope, and a spectrum analyzer.

The low-pass filter is used to obtain certain bands (up to 1000 Hz.), while the higher frequencies will be excluded. After passing the filter, the signals are displayed on the oscilloscope and the spectrum analyzer. The oscilloscope is used to record the time-series data, and the spectrum analyzer to calculate the Fast Fourier Transform (FFT). In order to analyze the signals, the collected data are entered in the computer by means of a floppy disc. The signals recorded in the computer are analyzed by MATLAB to obtain Wavelet Transform (WT), or by DADISP 2002 to indicate the Waterfall diagram. The schematic of this unit is illustrated in Figure 4.6.

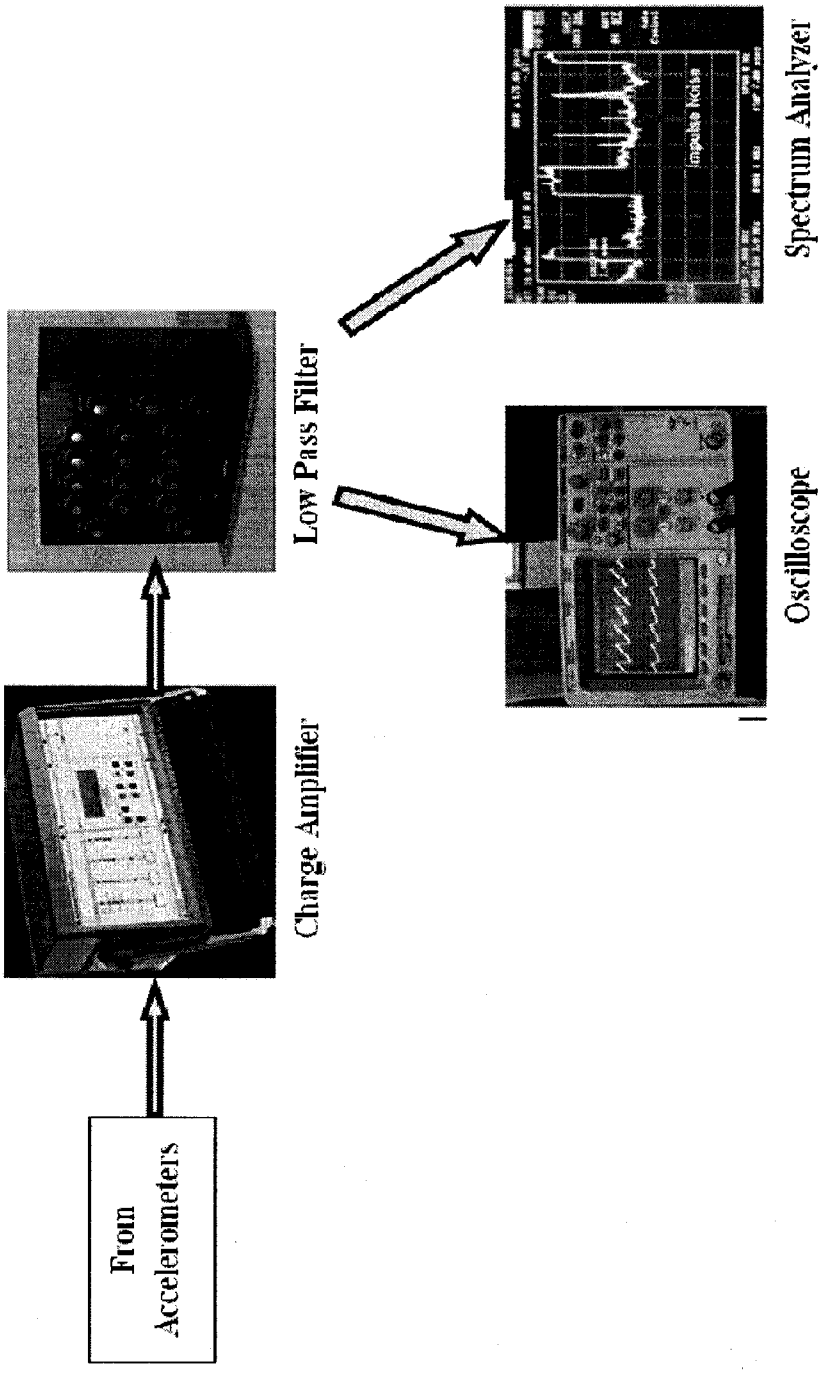

Figure 4.6: Data acquisition, conditioning, and recording

4.2.5 **Flow Loop**

The flow loop has the following parts:

1- The swash plate pump: explained as a part of the hydraulic facility.

2- The test section: contains a pair of simply supported steel pipes. Only one span is considered in the study. The specifications of the pipe are:

   1. Length: 3.5 m
   2. Outer diameter: 2.54 cm.
   3. Inner diameter: 2.33 cm.
   4. Young Modulus: 200 GPa.
   5. Material density: 8000 kg/m^3

3- A shut-down valve: used to separate the pipes from the rest of the hydraulic system.

4.3 **Test Methodology**

A series of tests were carried out to obtain the required signals of the pump and pipe under abnormal conditions. Another set of tests were performed to validate the proposed controller and the new control strategy. The major thrust of the experiments is to monitor the evolution of the signals under certain defects, such as electrical unbalance and excessive pump noise, and to determine the suitable parameters for the pump PID controller.

The procedure starts with tuning the PID controller and introducing the optimum parameters that ensure the smooth operation of the pump. The vibration levels are observed at different locations on the other hydraulic system components such as pipes,

the pump, and the supporting structure. The pump with the proposed PID controller is considered under normal operating conditions, and any deviation from this condition is considered an abnormal condition. The pump vibration signature and the pipe are recorded with two accelerometers. The sampling frequency is selected as 2000, and the test time is 1 sec. The time is long enough to characterize the signal. Every test is repeated 5 times for each operating condition. Then the vibration signals are plotted against time, and the FFT is taken from the spectrum analyzer.

4.4 Test Procedure

In order to reduce the effect of the vibrations transmitted through the supports, two rubber joints are installed between the pipe and the supports. Also, the experiments are carried out early in the mornings to remove the vibration disturbance from moving vehicles and from the machine shop. Generally, the test consists of monitoring the pump and pipe vibrations at the specific conditions.

- The PID pump controller is tuned to meet the desired specifications.
- The pipe and pump vibration signatures are obtained.
- The FFT and the raw signals are recorded.
- The pump is equipped with a PD controller (as introduced in reference [35]), and the experiments are carried out.
- The pipe and the pump signatures are recorded.
- The electric motor is put under an electric unbalance to simulate a potential defect in the motor-pump assembly. The pump with a PD controller leads to pipe flutter.

- The signals under the different conditions in the time domain are collected and then processed.
- Using the MATLAB toolbox, the Wavelet transform of the different signals is obtained.
- For a better comprehension for the signals, DADISP 2002 is used to represent the signals in 3D (Waterfall diagram).

The procedure of the two sets of experiments can be summarized as follows:

I. **Flutter**: The pump flow rate is 0.001 M^3/Sec, and the fluid velocity through the pipe is 2.94 M/Sec. The fluid velocity is too small to generate pipe flutter (the flutter velocity is 200 M/Sec). In order to create flutter in the pipe, a PD controller (proportional-derivative controller) is used to control the pump instead of a PID controller (proportional- integral- derivative controller). The derivative controller amplifies the noise (noise always has a small amplitude and high frequency), while the integral controller reduces the effect of the noise and suppresses it. The PD controller generates the flutter in this study case. The controller parameters are: the proportional gain is 1, and the derivative gain is 0.02, and this is sufficient to produce flutter in the pipe. The physical electrical control system is replaced by real time control software to help in the modeling of the control scheme. Two cases are considered for this setup:

- The normal case: the pump is equipped with a PID controller, and there is no flutter
- The PD case: the pipe shows flutter

II. Electrical Unbalance:

In order to create an unbalance in the motor voltage, a resistance is added to one of the three electrical lines. The selected resistance has two values: 0.5 Ω and 1 Ω.

The cases studied in this setup are:

- A healthy motor with voltage balance in the three phases.
- A motor with voltage unbalance in one line only due to an additional resistance of 0.5 Ω.
- A motor with 1 Ω resistance in that same line.

The components of the electric more are illustrated in Fig 4.7.

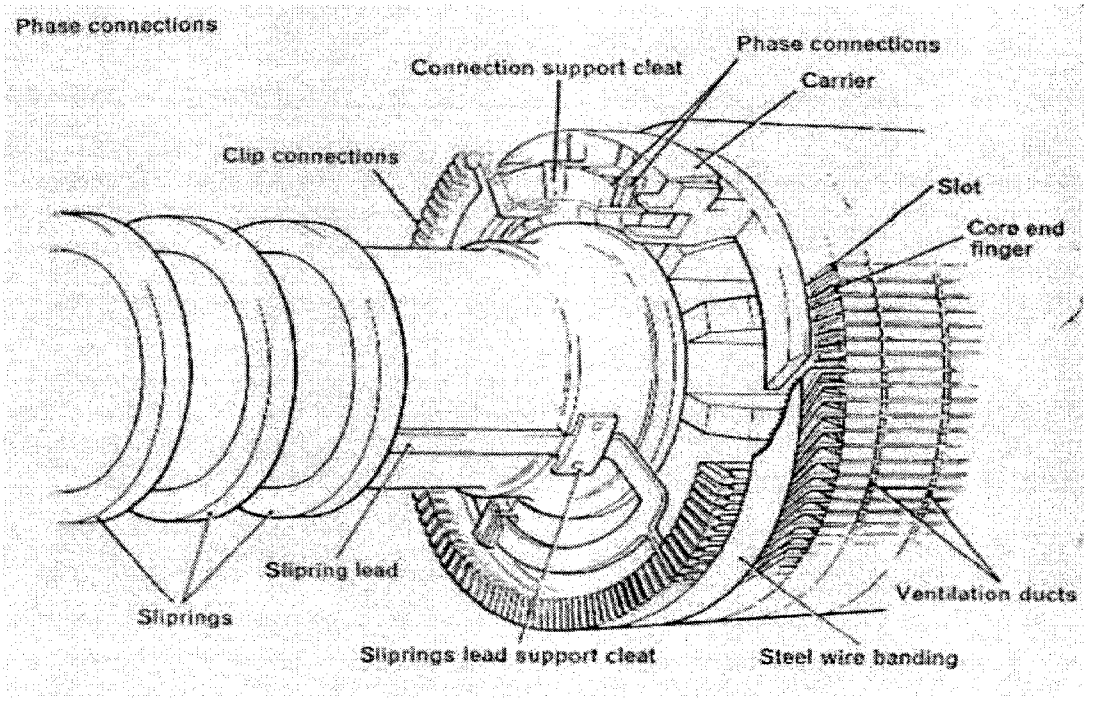

Figure 4.7: Schematic representation of the three-phase electric motor, [14]

4.5 Discussions and Summary

In this chapter we explained the components of the hydraulic unit setup, control unit, test instrument unit, and data acquisition. We started this chapter by explaining and describing the components of hydraulic test bed and the recommended specifications for the hydraulic system; then, we explained in detail the control pressure supply unit and the specifications of the secondary hydraulic pump used here. The control hardware was presented next. The data acquisition unit and test instruments were also described.

The chapter ended with the test methodology and the test procedure for the different experiments.

In the next chapter, experimental investigations will be carried out to validate and parameterize a strategy with a single-feedback PID controller. Also, the strategy will be extended to adjust the pump flow rate according to load demands and the pipe vibration levels. In order to evaluate the smoothness of the pump, the noise levels will be measured and compared with those of a single-feedback PD controller.

CHAPTER FIVE

5 OPTIMIZING PUMP PERFORMANCE BY IMPLEMENTING SUITABLE CONTROL STRATEGIES

5.1 Introduction

In chapter two, while discussing the dynamic characteristics of the pump for the current design, it was noted that the pump has pressure overshooting due to the design of the port plate. A new design for the port plate that replaces the shallow silencing grooves with two deep grooves was introduced, which improved the pump performance. The pump output was compared between two designs: a port plate with and without deep silencing grooves. The pump's output increased by 4% with the deep-grooved design. Also, the cylinder porting areas and pump kinematics were derived with new expressions. It was found that the pump flow rate increases with increasing swiveling angle, and there is a direct relationship between the pump flow rate (output) and load requirements. The pump output is adjusted by means of a control unit, where a pressure transducer senses the load and feeds this information to the arithmetic unit in the control device and accordingly, the control system generates the required output. The current pump design consists of double-negative feedback controls. The inner loop controls the position of the proportional hydraulic valve, while the outer loop controls the swash plate angle.

In this chapter, we will optimize the performance of the swash plate pump with conical arrangement by improving its response to the load requirements, while keeping the design simple, and with minimum levels of noise and vibrations. In order to achieve this goal, the pump is equipped with a single feedback PID controller (to suppress the noise in the system) which is parameterized for optimum performance. The results are obtained experimentally, and the new proposed control strategy shows promising results.

An active control strategy will also be introduced. The new control system adopts the same parameters of the PID and controls the pump output according to the load requirements and the vibration levels at the delivery pipe. The system will be able to suppress the unexpected and undesirable chaotic behaviour in the pipe that would appear at high fluid velocities (causing flutter or divergence) or under an external disturbance that excites the pipe.

A compensation factor is introduced to account for the negative impact of the pipe vibration. With this factor, the control unit considers another set value for the swash plate inclination angle. Different disturbances are introduced to simulate the actual situation, and the corresponding pump output is obtained. The results show the applicability and the advantages of the control strategy.

5.2 Importance of Control Unit for Swash Plate Pump

A swash plate pump is a variable displacement pump, and it can change its flow rates according to the load requirements. In earlier versions, this pump was used without a control unit, operating at a certain output (flow) regardless of the desired flow. In order to manage the excess flow, a relief valve was used. Although this valve solved the problem of the excessive flow; it introduced another problem, fluid overheating. Overheating of the hydraulic fluid changes the chemical and physical properties of the fluid. A fluid with poor chemical and physical properties leads to damages in the pump parts. The loss of pump power and overheating were major problems that challenged designers.

The solution of the above problems was to equip the pump with a control unit that controls the pump power according to the load requirements by controlling the swash plate swivelling angle (the cylinder stroke is determined by the angle). Hence, the pump power matches the load (regardless of whether it is a full or partial load), and the oil remains within the specifications.

The pump was equipped with its control unit to achieve two goals: to manage the pump power and to maintain the oil's properties within its specifications by reducing the accumulated heat.

5.3 Control Unit Components

The control unit has the following components: a secondary power pump, a hydraulic proportional valve, and an electronic control unit. A pressure transducer senses the load pressure and feeds it to the logic unit of the control unit. The logic unit calculates the required swash plate swivelling angle that matches the load demands without exceeding the pump manufacturer specifications such as: power, maximum flow, and maximum pressure. The components of the control unit are illustrated in Figure 5.1.

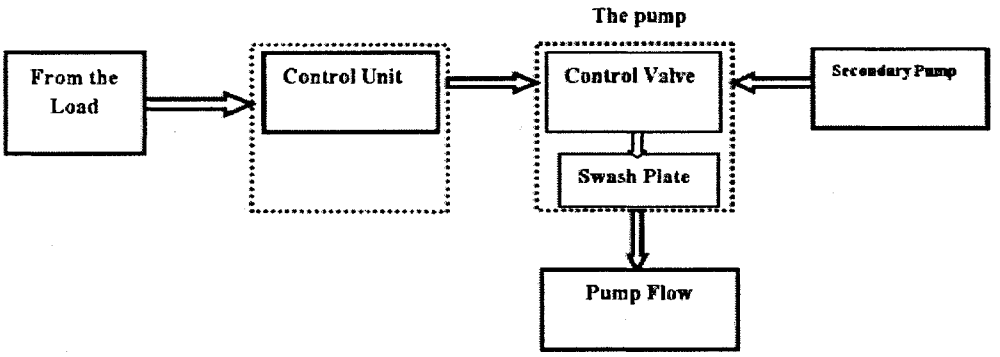

Figure 5.1: A schematic representation for the control unit/pumps, and the hydraulic and electrical flows

5.3.1 The Secondary Hydraulic Pump

In order to generate a hydraulic pressure (up to 15 MPa.) on the control cylinder to push the piston, a separate secondary hydraulic pump is used. This is part of a separate secondary hydraulic unit, operated by means of an electric motor. In order to reduce the

hydraulic lines, the pump is mounted next to the oil reservoir. The source of the pump oil is the main oil reservoir. Some precautions should be taken to keep the oil clean and within a specific range of temperature, such as

1- Installation of a 5 μm mesh size strainer on the return line.

2- Installation of an oil cooler on the return line after the mesh. The cooler is designed to keep the oil temperature below 60° C. The positioning of the cooler past the strainer is recommended for two reasons: the hot oil has lower viscosity at higher temperature and it will be easier to remove the impurities, and cooling efficiency increases with cleaner oil.

5.3.2 **Hydraulic Proportional Valve**

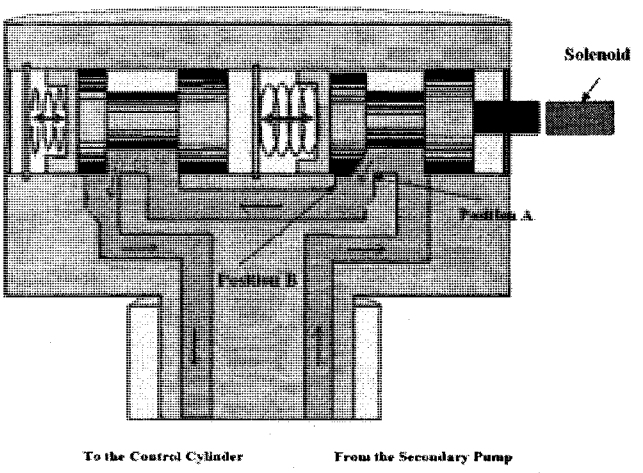

Figure 5.2: Hydraulic proportional valve

Figure 5.2 shows the hydraulic proportional valve, which consists of: a moving part (a spool), its case (a sleeve), and the returning springs. The sleeve inlet is connected to the power pump and the sleeve outlet is connected to the control cylinder. The control cylinder is rigidly linked to the swash plate, which is moved by the control cylinder to generate the swash plate swivelling angle.

The position of the spool is varied by a solenoid, which is activated by the control current. The position of the spool ranges between the maximum and the neutral positions. The springs are equipped to ensure that the flow is completely stopped when the solenoid is deactivated and the proportional valve is in its neutral position (referred as "A"). When the solenoid is operated by the control current, the spool is pushed against the springs granting the fluid a passage and pushing the control cylinder. The flow forces the control cylinder to move and the swash plate to swivel. When the spool is in its extreme position ("B"), the swash plate hits its maximum swivelling angle.

5.3.3 **The Electronic Control Unit:**

The control unit contains an electrical card and the control cylinder. The control card receives electrical signals from different transducers, computes the corresponding electrical current, and then generates the control signal to actuate the solenoid of the hydraulic proportional valve.

The control cylinder is mechanically connected to the swash plate through a linkage to enable the swash plate to change its swivelling angle; and hence, the pump flow rate. The

control cylinder is pushed by the control pressure that is generated by the secondary pump and passed through the proportional valve.

The structure of the control card varies according to the chosen control strategy. Two types of control are illustrated in Figure 5.3 and Figure 5.4, respectively.

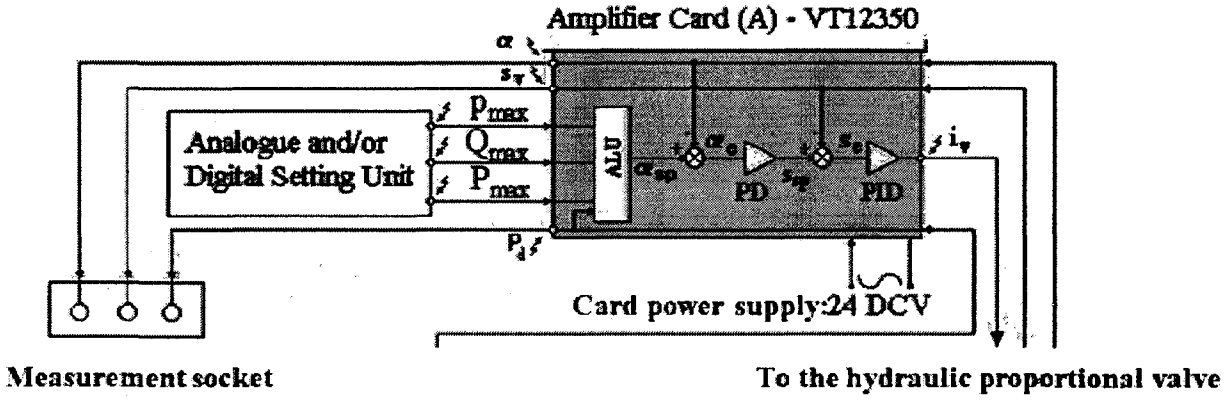

Figure 5.3: Control unit components for double negative feedback strategy

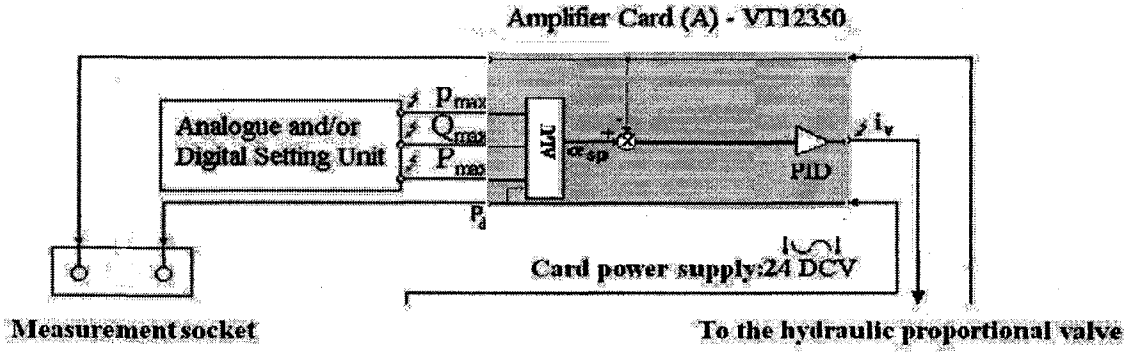

Figure 5.4: Control unit components for a single negative feedback strategy

Figure 5.3 shows the structure of the control card used with the current design of the swash plate pumps. There are three inputs for this design, which come from the:

1- Pressure transducer: senses the pressure on the pump delivery line next to the load, and feeds it to the logic unit to generate the required swivelling angle.
2- Spool position transducer: this LVDT-type transducer senses the position of the spool of the hydraulic proportional valve and then compares it with the set point of the spool.
3- Swash plate position transducer: an LVDT that is used to sense the swash plate position and compare it with the set point of the swash plate.

The outputs of the three transducers are in the form of electrical voltages, and are proportional to the measured values. For example, the generated voltage from the swash plate position transducer equals 10 volts at the maximum inclination angle (15^{o}), and it becomes zero when the angle is equal to zero.

The input of the pressure sensor is used by the arithmetic unit to determine the desired electric current (swivelling angle). However, the arithmetic unit is constrained with three limiting values, which are:

1- Maximum delivery pressure
2- Maximum pump flow rate
3- Maximum pump power

Hence, the current will be limited within a certain range. In addition to the arithmetic unit; there are two loops which are:

1- The inner loop: designed to control the spool position; and

2- The outer loop: used to control the piston stroke length by controlling the swash plate swivelling angle.

Figure 5.4 is a design modified from the general design illustrated in Figure 5.3. The inner loop is removed, and the card has only one feedback. It represents a control card that can be used with a single feedback. The controller can be a PD or a PID. There are two inputs for this simple strategy, which are:

1- Load pressure.

2- Swash plate position.

There is no change in the arithmetic unit.

The two or three different cards will be used for the specific control strategy in this work.

5.4 Swash Plate Pump Control Strategies

The previous section discussed the different designs of the control cards. In this section, we will discuss the possible control strategies for the swash plate; starting with the current design, we will then present a proposed single feedback with PD controller design, and finally, we will propose the optimum controller that is suited for the different applications of the swash plate pump. This control strategy has a single feedback with PID controller.

5.4.1 With a Double Negative Feedback Loop

Figure 5.5 illustrates the control strategy of a swash plate pump with a double negative feedback control loop. It consists of two loops, an inner loop and an outer loop. The inner loop controls the position of the moving part with an LVDT position sensor, which senses the position of the spool of the proportional valve, and with a PID controller. The outer loop controls the pump swivelling angle by using the LVDT position sensor, which senses the position of the swash plate, and the PD controller.

5.4.2 With a Single Negative Feedback Loop

5.4.2.1 *With the PD Controller*

Khalil et al [35] proposed a new control strategy to control the pump output by implementing a single feedback loop. They removed the electrical feedback line of the inner loop, and the controller controls only the pump swivelling angle (Figure 5.6). They first studied the linearity of the spool response with respect to the control signal and they concluded that the spool response exhibits very close to linear behaviour, as shown in Figure 5.7.

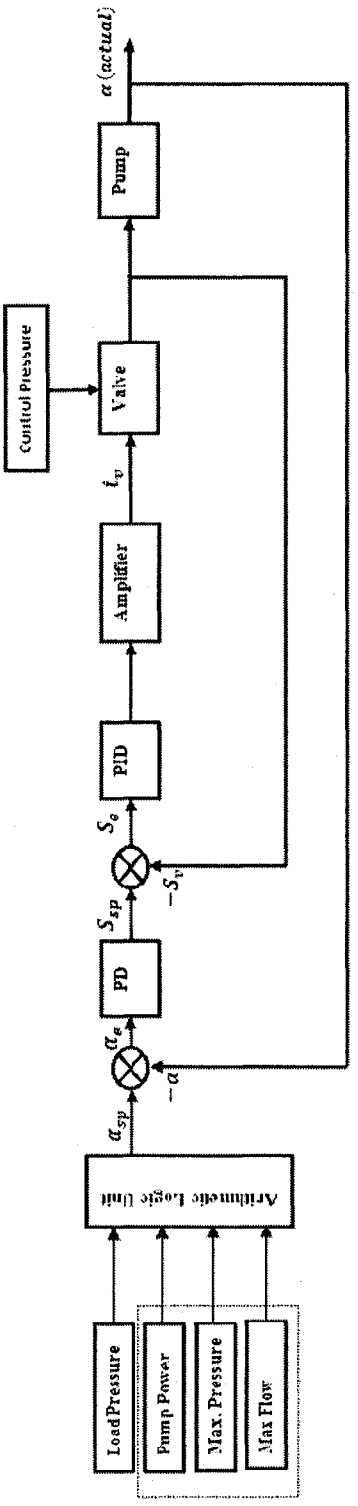

Figure 5.5: Swash plate pump with double feedback control loop representation

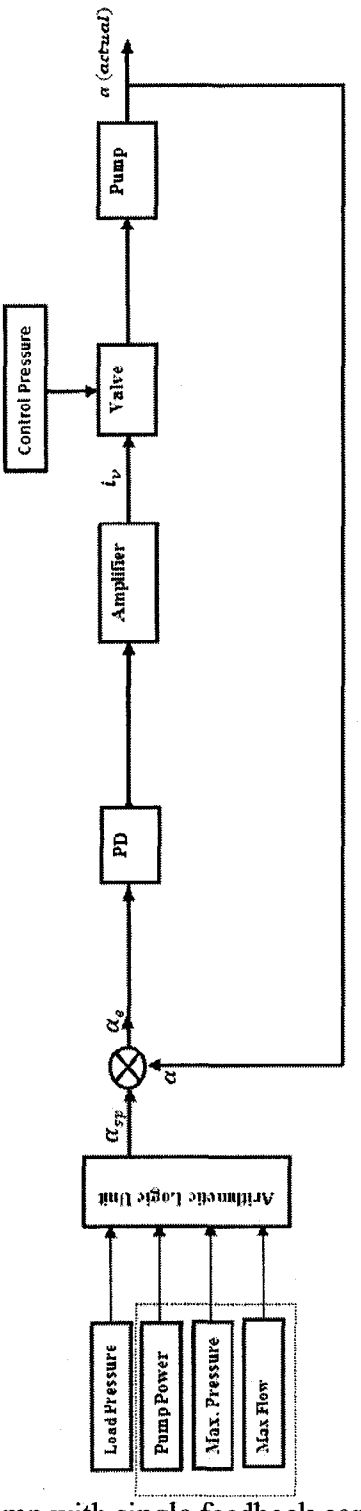

Figure 5.6: Swash plate pump with single feedback control loop representation (PD controller)

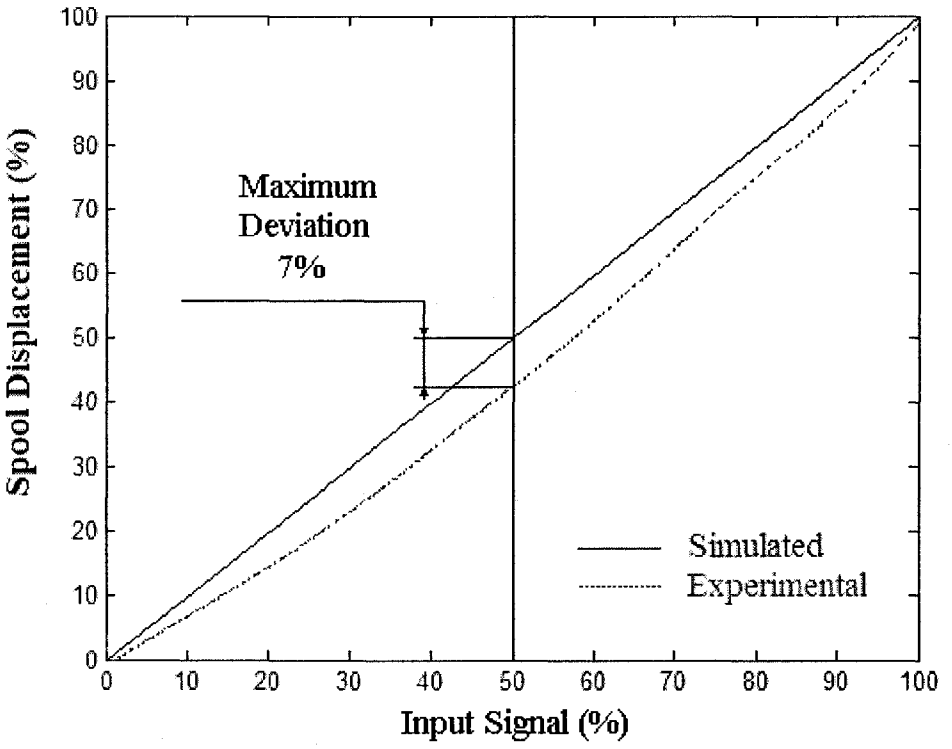

Figure 5.7: Measuring of open loop static characteristics of the proportional valve [35]

They then parameterized the PD controller by using the Ultimate Sensitivity method. The parameters of the PID controller were K_p=1, K_i=0, and K_d=0.02. The swash plate angle with its PD controller at a different percentage of the maximum value of the swash plate swivelling angle is given in [35].

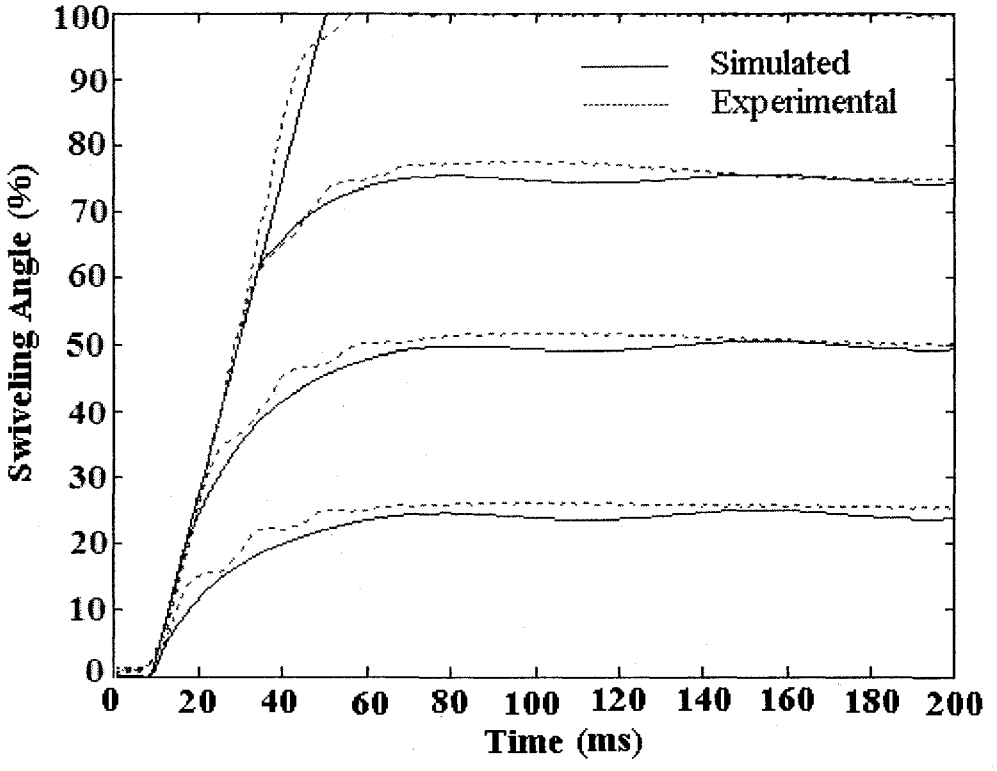

Figure 5.8: Simulated and experimental swivelling angle at different percentage of the maximum swivelling angle using a PD controller [35]

Figure 5.8 illustrates the transient response of the swash plate when the inclination angle changes from the zero position to different ratios of the maximum value using a double feedback control loop. It can be observed that the rise time is nearly 50 ms (for the maximum swivelling angle). In [35], they concluded that the rise time was reduced by implementing a single control strategy with a PD controller, whereas it was 120 ms when using the double negative feedback loops. In their study, they did not investigate the vibration levels.

5.4.2.2 *With PID Controller*

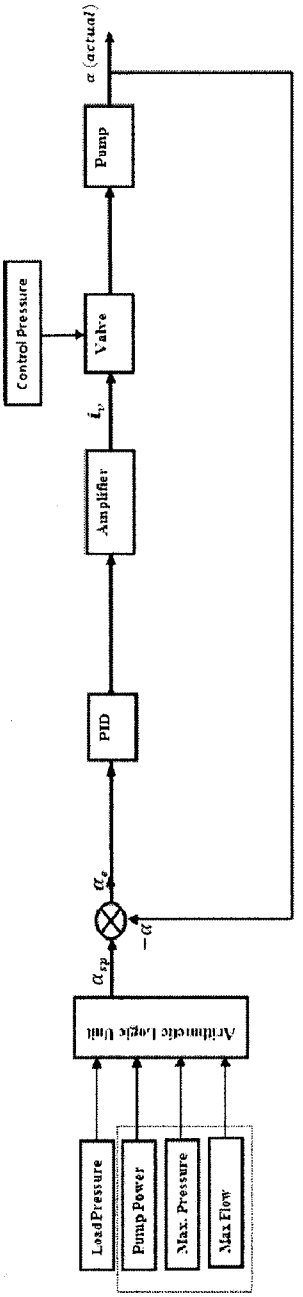

Figure 5.9: Swash plate pump with single feedback control loop representation (PID controller)

In the present work, a control strategy with a single feedback PID controller is proposed. This strategy has the same structure as the previous control strategy except that this design has a PID controller instead of the PD controller, and different gains.

Figure 5.9 illustrates the general structure of the new control strategy. The control variable is the swash plate swivelling angle, i.e. the pump flow rate. The logic unit receives an electrical signal from the pressure sensor, and it computes the specific swivelling angle. Some values must be considered by the logic unit such as the minimum inclination angle (for pump self-lubrication), the pump power, the maximum pressure and flow. The swivelling angle is compared with the actual swivelling angle, and a certain correction is achieved by the PID controller to achieve the required angle. In order to parameterize the controller gains, a set of experiments are carried out. Additional experiments are carried out to investigate the levels of the system vibration with each strategy (PD and PID).

5.4.2.2.1 Parameterizing the PID Controller:

An Ultimate Sensitivity approach is usually used to parameterize controllers. This method was proposed by Ziegler and Nichols in 1942. In this method, in the beginning the controller has only a proportional action (pure proportional controller) and the proportional gain increases gradually until the system loses its absolute stability and starts to oscillate. The period between two consecutive peaks defines the oscillation period and is called the ultimate period. The proponents of this theory suggested that there is a relationship between this ultimate period and its proportional gain and the PID parameters [35]. By denoting the critical period by P_{cr} and its proportional gain by K_{cr}, the PID parameters can be given as:

$K_p = 0.6K_{cr}$, $K_i = \frac{2K_p}{P_{cr}}$, and $K_d = 0.125p_{cr}K_p$.

The PID controller output is given as

$$u(t) = (k_p + \frac{k_i}{s} + sk_d)e(t) \tag{5.1}$$

where k_p is the controller proportional gain, k_i is the controller integral gain, k_d is the controller derivative gain, and $e(t)$ is the error between the desired and the actual input. In the PD controller, the controller integral gain equals 0, and the controller output is given as

$$u(t) = (k_p + sk_d)e(t) \tag{5.2}$$

The response of the swash plate is examined under two different operating conditions:

1- When the pump has different step loads (25%, 50%, 75%, and 100% of the maximum load) or the corresponding swash plate swivelling angle.
2- When the load increases gradually to reach the maximum value (which matches the maximum pump power).

When the pump is under step inputs: The optimum operation of the pump with the suggested single negative feedback control strategy is observed at $K_p = 1.9, K_i = 8.4$, and $K_d = 0.01$. The swash plate inclination angle step response with a PID controller is illustrated in Figure 5.10.

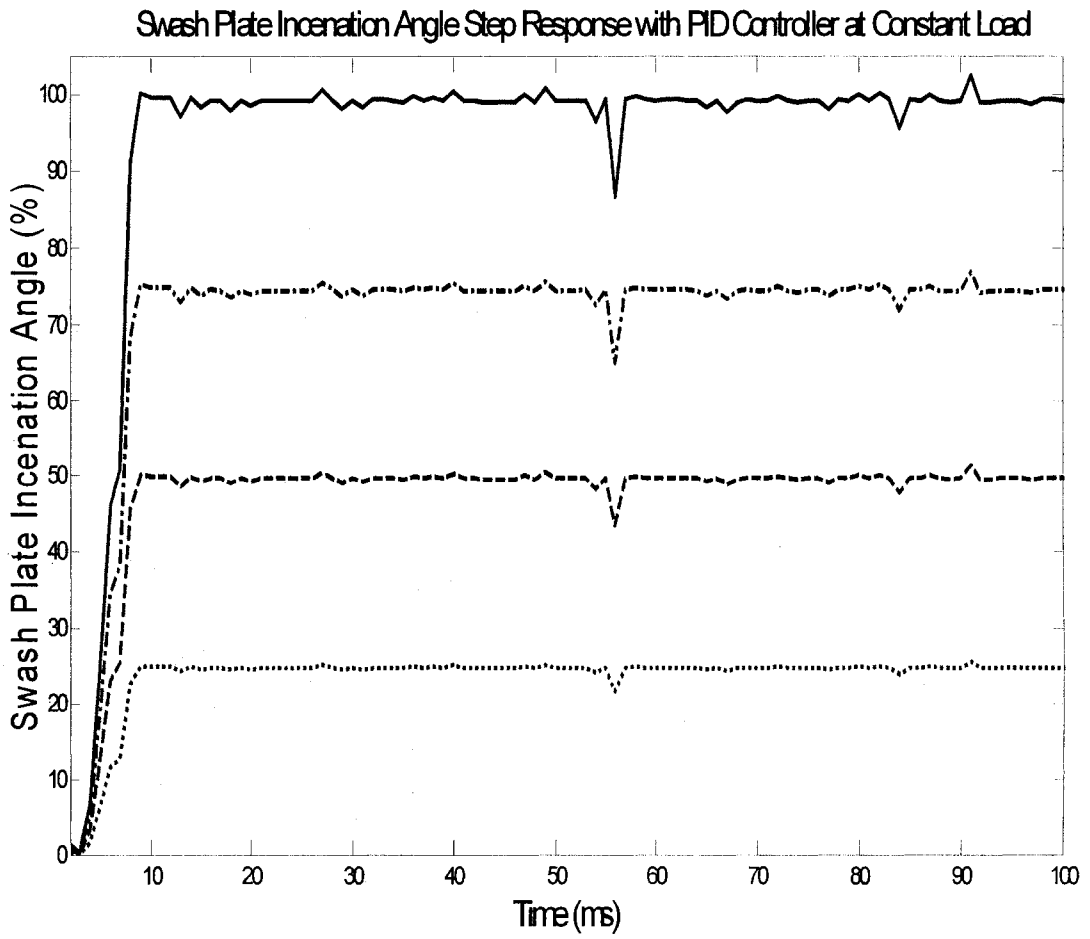

Figure 5.10: The transient periods of pump response when the swivelling angle increases from the zero position to different percentages of its maximum value

Figure 5.10 shows the response of the swash plate at different step inputs. It illustrates that the swash plate reaches its maximum swivelling angle in 15 ms, which decreases the shock of the pump power and makes the pump more responsive to the change in the load demands.

In order to investigate the suitability of the proposed controller for different types of loads (ramp input), additional experiments are performed with the proposed PID. The results are illustrated in Figure 5.11.

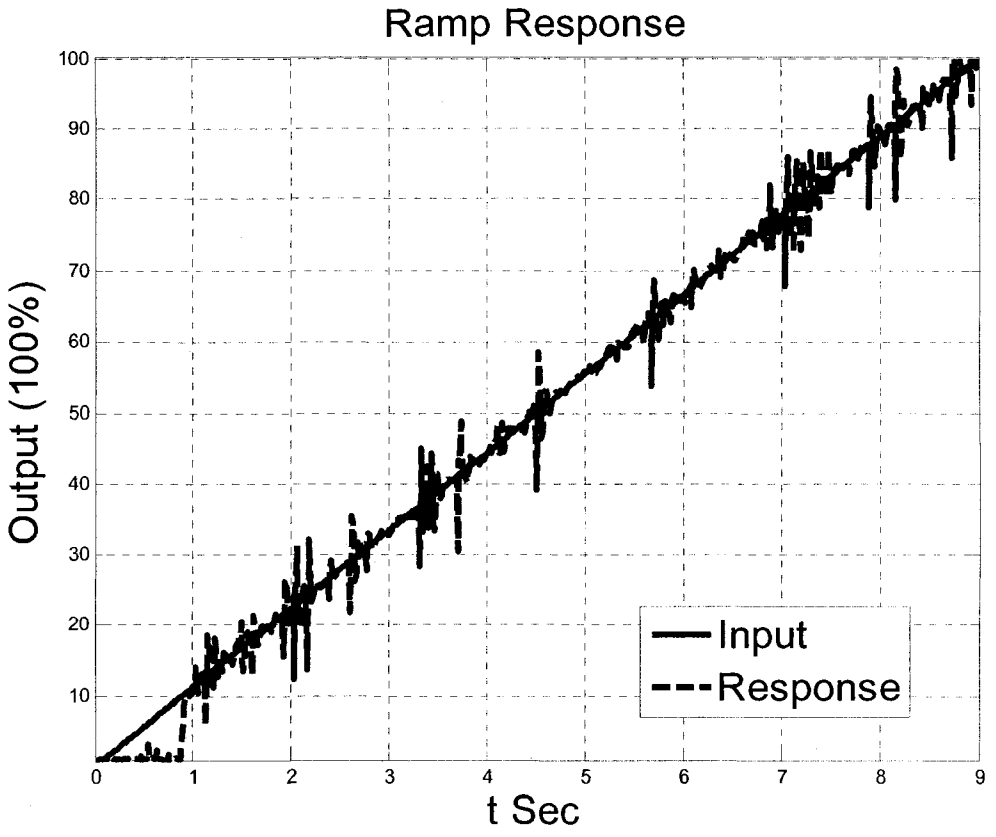

Figure 5.11: Pump response under a ramp input

Figure 5.11 shows the response of the swash plate to a ramp input. The results demonstrate an acceptable response, and the swash plate reaches its desired input in less than 1 sec.

5.4.2.3 *Evaluation of the Smoothness of the System Performance*

The overall performance of the hydraulic system includes the smoothness of the system's operation, without high levels of noise and vibration. In the previous sections, the responses of the pump with different control strategies were investigated. In this section, the vibration signatures of the pump and the pipe will be measured with the signal feedback control strategies using PD and PID controllers.

5.4.2.3.1 Pump Vibration Signatures

I- With a PD Controller: An accelerometer is placed at the pump outlet to measure the vibration levels. The vibration signature is illustrated in Figure 5.12.

II- With the proposed control strategy, with a PID controller: The vibration signature is recorded at the pump, where the accelerometer is placed at the same position. Figure 5.13 depicts the corresponding vibration signature.

From Figure 5.12 and Figure 5.13, it can be observed that the vibration amplitude drops from ± 0.2 mm to ± 0.02 mm, simply by replacing the PD controller with the PID controller. The pump performance exhibits smooth operation with a single feedback that has a PID controller.

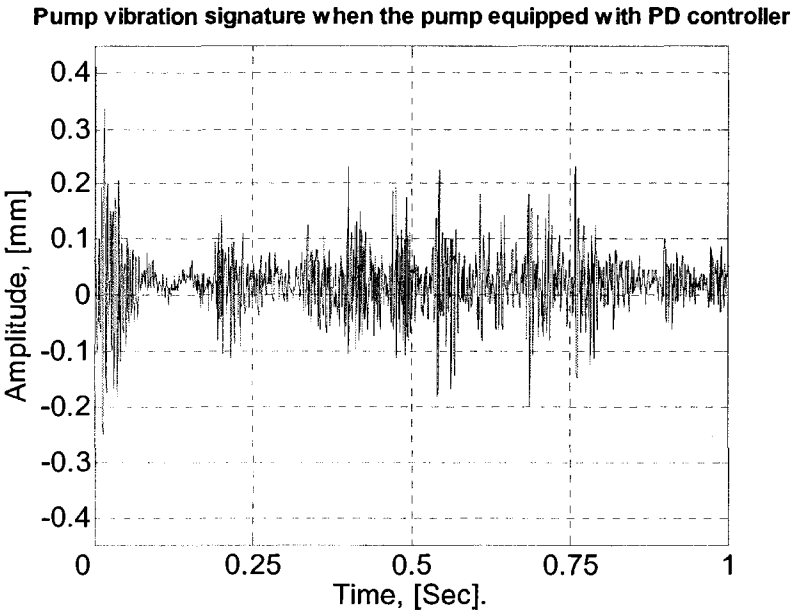

Figure 5.12: Pump vibration signature with the pump equipped with a PD controller

$(k_p = 1, k_d = 0.02)$

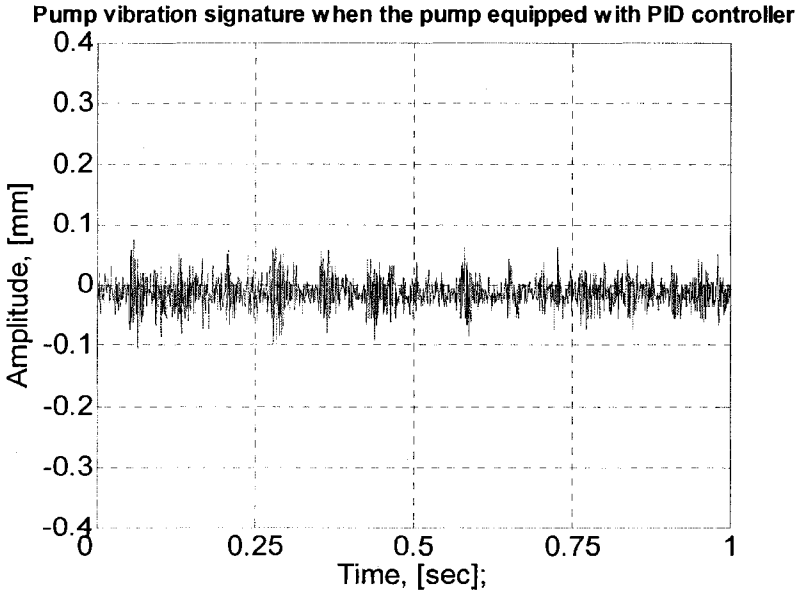

Figure 5.13: Pump vibration signature for a pump equipped with a PID controller

$(K_p = 1.9, K_i = 8.4, and\ K_d = 0.01)$

5.4.2.3.2 Pipe Vibration Signatures

In order to ensure the smooth operation of the pump, the vibration signatures of the pipe are measured. The pump's dynamic behaviour can be detected at all the components of the hydraulic system. First, and in order to ensure that the fluid is not the source of the excessive pipe vibration, the fluid velocity was calculated for the pipe dimensions, and it was 2.94 m/sec, which is much less than the fluid critical velocity. This velocity is far from the value of the critical velocity for buckling of the pipe, which is 200 m/sec.

I- With a PD Controller: To record the pipe vibration signature, a piezoelectric accelerometer is placed at the mid-point of the pipe. The measured signature is displayed in Figure 5.14.

II- With the proposed control strategy, with a PID controller: The pipe vibration signature is recorded for second case, where the pump is equipped with the PID controller. The measured signal is shown in Figure 5.15.

When the pump is equipped with the PD controller, the pipe vibration amplitude is high (± 0.5 mm), and it is noisy. This is predictable, because of the influence of the derivative action (the noise has high frequency and it comes with a small amplitude, and the derivative action amplifies it). The PID controller reduced the pipe vibration amplitude by 90%, to where it becomes equal to ± 0.05 mm.

Replacing the PD with a PID and tuning it with the proper parameters can optimize the overall performance by reducing the rise time and the vibration levels on the different system components.

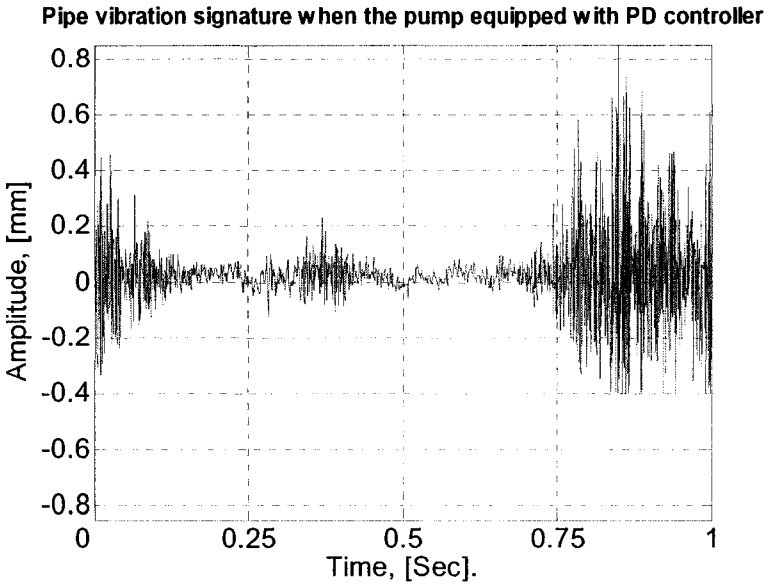

Figure 5.14: Pipe vibration signature with the pump equipped with a PD controller

$$(k_p = 1, k_d = 0.02)$$

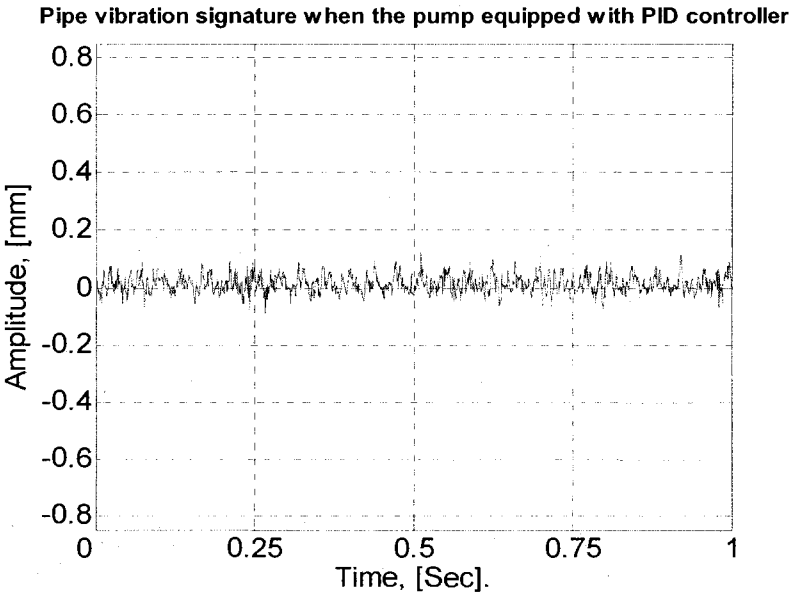

Figure 5.15: Pipe vibration signature for the pump equipped with a PID controller

$$(K_p = 1.9, K_i = 8.4, and\ K_d = 0.01)$$

5.4.2.4 *Qualitative Evaluation of the Pump Features with the Different Controllers*

Different experiments were carried out to ensure that the proposed control strategy of the swash plate pump with conical arrangement has the following features:

1- A simple electro-hydraulic system for controlling the pump output that:
   a) reduces the number of components,
   b) is compact, and
   c) is easy to maintain;
2- A fast response time: the pump reaches its required input with minimum time, and adapts to the changes in load without power shocks; and
3- A quiet and a smooth operation: the pump operates at very low levels of vibration. This improves the life of the pump and that of the entire system components.

These features are summarized in the following table, and they are also compared with those of the other control strategies.

Features of Interest in the Pump performance	Double Feedback	Single Feedback	
	PD/PID	PD	PID (Proposed)
1- Speed of response	120 ms	50 ms	15 ms
2- Convenience to constant power operation	✔	✔	✔
3- Vibration amplitude at the pump	N/A	±0.2 mm	±0.02 mm
4- Vibration amplitude at the pipe	N/A	±0.5 mm	±0.05 mm
5- Low production cost	x	✔	✔
6- compactness	x	✔	✔

Table 5-1: Qualitative evaluation of the pump features with double negative feedback controller and with single feedback PD and PID controllers

5.5 Controlling Swash Plate Pump Flow Rate According to Load Requirements and Pipe Dynamic Response

In practical applications, there are some conditions where pipes are excited with external sources such as surrounding machinery, shocks, the collapse of one of the pipe supports, and so on. Pipe designers usually design the pipes with dimensions that assure smooth operation and stability and with minimum installation cost. Hence, the excessive forces would cause a loss in their stability. As discussed in the previous section, a swash plate pump can change its flow rate according to the load requirements. In this section, a new control strategy that adopts the same parameters of the PID and controls the pump output according to the load requirements and also the vibration levels at the pipe is described. A compensation factor is introduced to account for the negative impact of the pipe vibration. With this factor, the control unit considers another set value for the swash plate inclination angle. Different disturbances are introduced to simulate the actual situations, and the corresponding pump output is obtained. The results show the applicability and the advantages of the control strategy.

5.5.1 The Proposed Control Strategy (Pipe-Pump)

In variable displacement pumps, the pump output is determined by the inclination angle of the swash plate, which determines the piston stroke length (the amount of the delivered flow). The inclination angle is set by the control arithmetic unit, according to the load value. The load is sensed by a pressure sensor and is conveyed to the arithmetic unit, which calculates the electrical current that should be given to the solenoid of the

proportional hydraulic valve. The solenoid pushes the valve's moving part (spool), and creates hydraulic pressure in the hydraulic line connected to the control cylinder. The control cylinder is rigidly connected to the swash plate, where the spherical end of each piston is connected to the swash plate by a ball-and-socket joint.

There is a linear relationship between the pump flow rate and the swash plate inclination angle. For example, the maximum flow rate for the pump studied is 0.001 M^3/Sec., and this occurs at the maximum inclination angle (15°). The pump flow rate is lower at lower angles. As mentioned earlier, in the current design the angle is determined only by the load requirement.

The relationship between the inclination angle, α, and the pump flow rate, Q, can be expressed as

$$Q = c_{t1}\alpha \qquad (5.3)$$

where C_{tl} is constant, and for the case studied, C_{tl}=4, where the pump flow rate is in M^3/Sec., and the inclination angle in degrees.

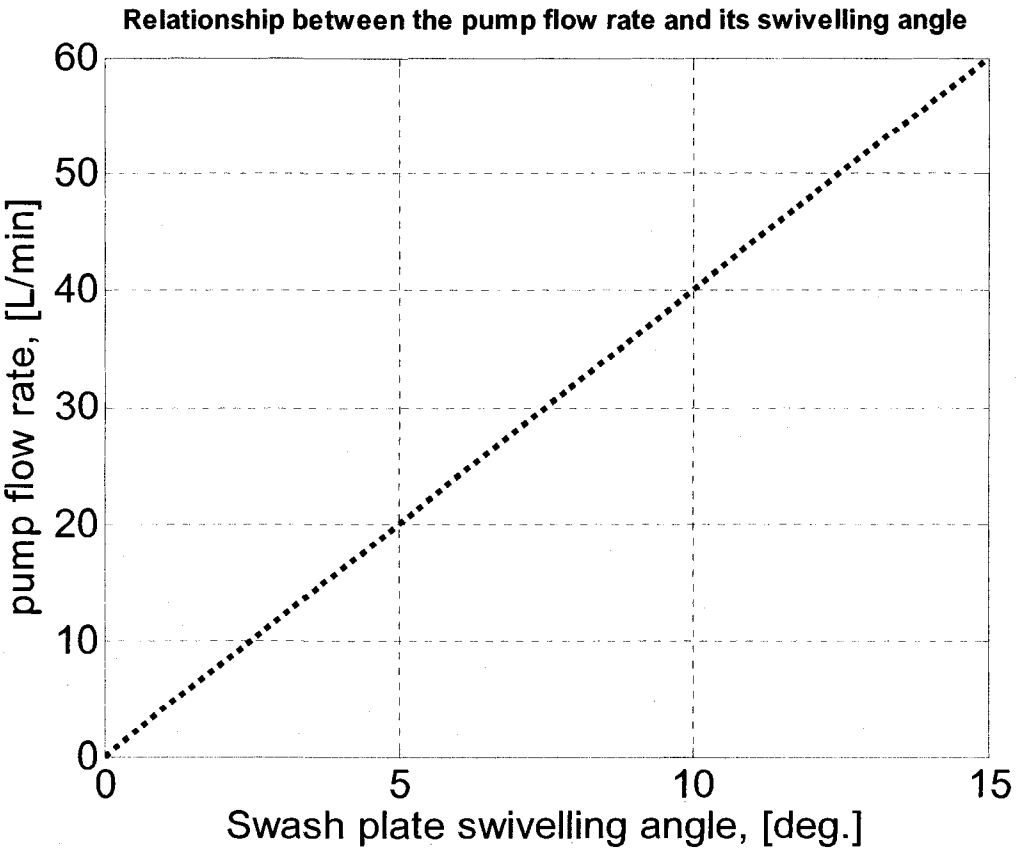

Figure 5.16: The relationship between the pump flow rate and the swash plate angle

In hydraulic systems, the pump should maintain a high degree of smoothness in operation and high reliability. If the fluid velocity in the pipe is excessively high it would lead to pipe flutter. Also, the fluid flow interacts with the pipe and causes it to vibrate. Fluid velocity and the pipe specifications are key parameters for pipe stability, and external disturbances affect stability as well. As illustrated in Figure 5.9, the only parameter that indicates the pump output is the load requirement. This would be insufficient from the safety point of view. The hydraulic system components are interconnected and work in series. Hence, the proposed strategy controls the pump output according to both the load requirements (the most important) and the pipe response. This important feature serves to

protect the system components to prevent the development of high levels of vibration and noise that lead to fatigue and component collapse. The strategy includes the following components:

- LVDT: used to sense the position of the swash plate
- Pressure transducer: installed to sense the accumulated pressure at the delivery side
- Accelerometer: measures the acceleration of the pipe vibration at strategic locations
- Arithmetic unit: computes the required flow rate according to the pressure value
- Compensation element: adjusts the swivelling angle according to the compensation factor
- PID controller: compares the new actual swivelling angle with the desired angle
- Amplifier: amplifies the control current and pushes the solenoid of the proportional valve to the desired position.

The structure of the strategy is illustrated in Figure 5.17.

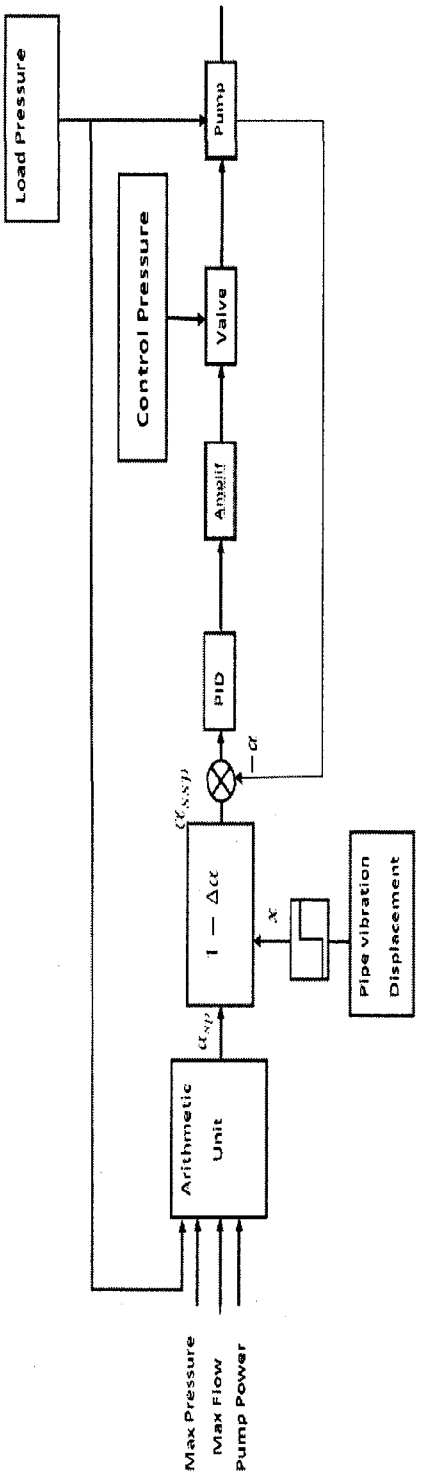

Figure 5.17: The block diagram of the new control strategy to control the pump output according to the load requirements and the pipe response.

Figure 5.17 shows the block diagram of the proposed model for the pump-pipe system. Like the pump model, the control variable remains the swash plate inclination angle, α. But here the set value of the inclination angle (α_{sp}) is affected by the output pressure and the pipe response x. Hence, a new value for the inclination (α_{ssp}) is considered. The value of α_{ssp} varies between 0 and α_{sp}.

α_{ssp} can be expressed mathematically as

$$\alpha_{ssp} = \alpha_{sp}(1 - \Delta\alpha) \tag{5.4}$$

where α_{sp} is the set value for the swash plate inclination angle according to the load requirement only, and $\Delta\alpha$ is the set point compensation factor, which is dependent on the levels of the pipe response, and on the maximum and minimum allowed values of the pipe amplitude. The compensation factor can be represented as in Figure 5.18.

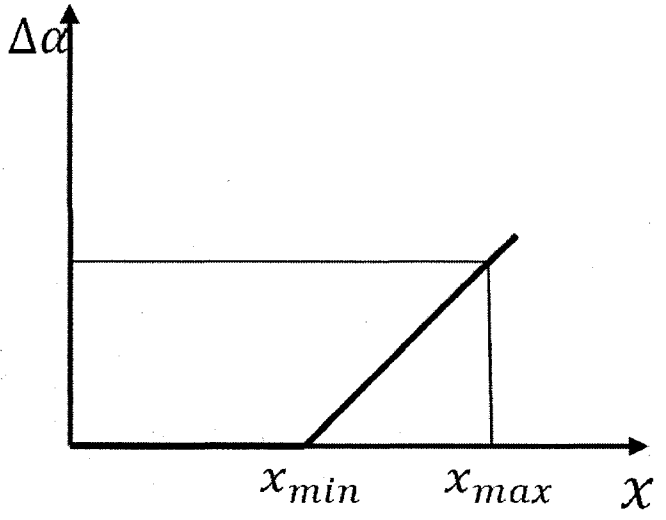

Figure 5.18: The relationship between the set point compensation factor and the pipe response

Figure 5.18 shows the relationship between the compensation factor and the pipe vibration values. The mathematical expression for Figure 5.18 can be given as

$$\Delta\alpha = \frac{(x - x_{min})}{(x_{max} - x_{min})} \tag{5.5}$$

where $\Delta\alpha$ is the compensation factor for the inclination angle, x is the amplitude of the pipe vibration, x_{max} is the maximum allowed vibration of the pipe, and x_{min} is the minimum allowed vibration of the pipe. Values of x_{min} and x_{max} are design parameters determined by the designer. According to Eq. (5.3), the pump delivers the pressurized fluid based on the new value for the inclination, and this value varies between α_{sp} (when the pipe response is less than the minimum allowed vibration) and zero (where the levels of the pipe vibrations exceed the maximum allowed value), i.e. no pump flow.

Figure 5.15 shows the pipe response under normal operating conditions. There is a small amplitude vibration superimposed over large amplitude due to the pump pressure overshooting.

It can be observed that the vibration amplitude is varying within the range of ± 0.05 mm. This value is to be considered as the minimum allowed vibration, and the maximum value is set at 0.2 mm (can be any value). A saturation function is used to limit the value of the vibration amplitude, i.e. the minimum allowed value of the vibration is +0.05 mm and any value greater than 0.2 equals 0.2.

5.6 Results

Different conditions are considered to investigate and evaluate the new proposed control strategy. In practical applications, the external disturbance could be constant (step), increase with time (ramp), or be a mixed case of ramp or step with a sinusoidal input. The pipe response is first measured at the maximum pump flow, where the fluid velocity is 2.94 m/sec. The fluid excites the pipe to certain limits without losing its static or dynamic stability, which is far above the fluid velocity (93.58m/sec.). The pipe response is recorded (to determine the minimum allowed pipe vibration amplitude, and which is measured under the normal operating condition for the pump).

5.6.1 Disturbance Generators

In order to introduce the external disturbances on the pipe, a function generator, which is denoted as the "*PIPE RESPONSE*", is connected to the model (As shown in Figures 5.19-5.22).

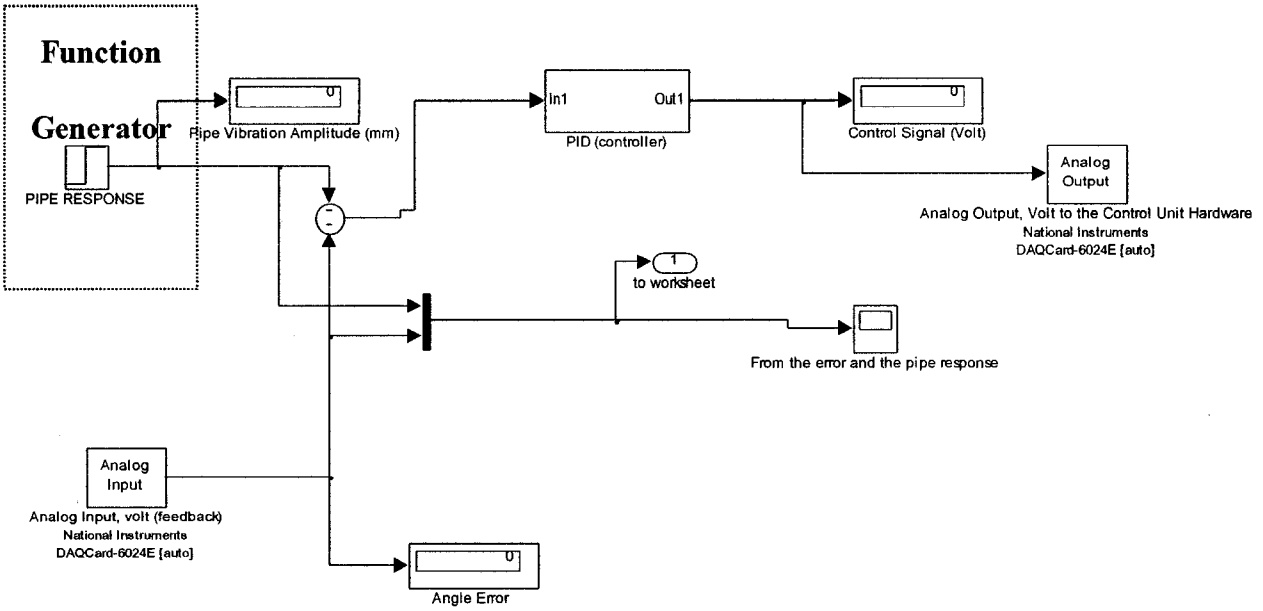

Figure 5.19: Control unit structure with a step disturbance

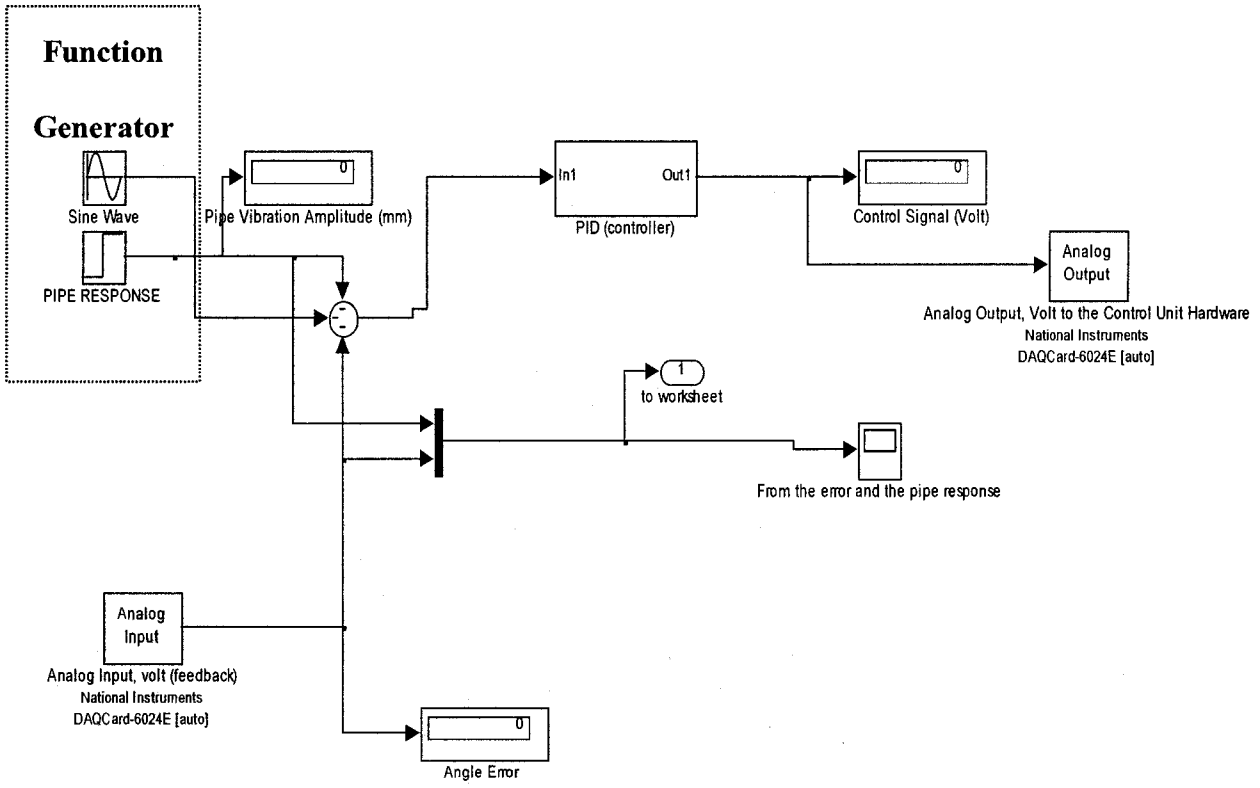

Figure 5.20: Control unit structure with a step and sinusoidal disturbance

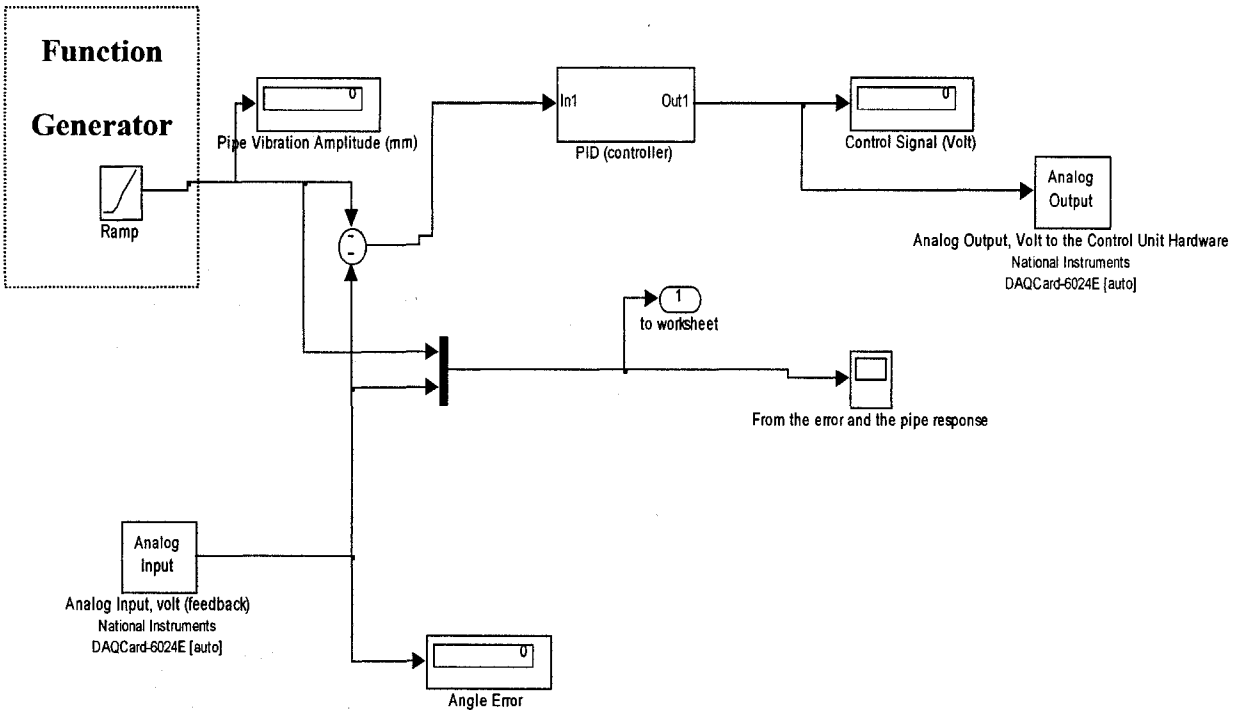

Figure 5.21: Control unit structure with a ramp disturbance

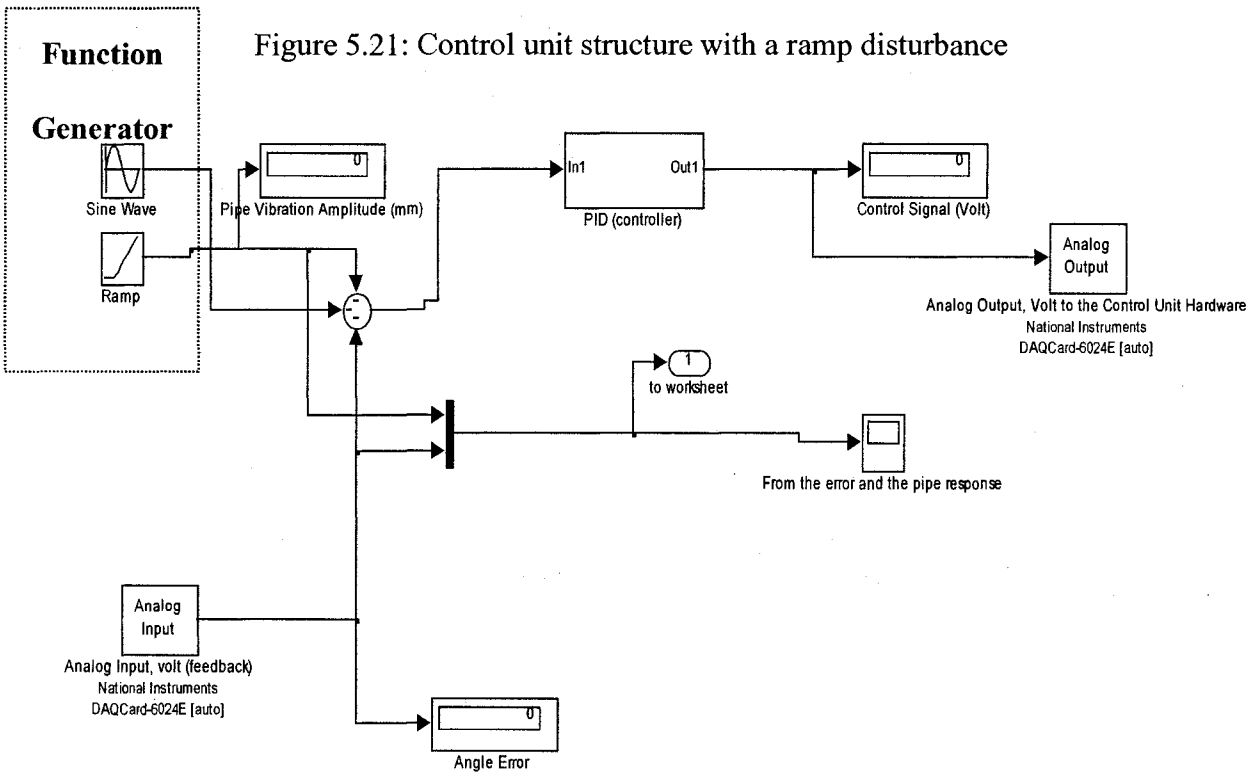

Figure 5.22: Control unit structure with a ramp and sinusoidal disturbance

Figures 5.19- 5.22 show the structure of the subsystem of the four major types of the external disturbances: step, step mixed with sinusoidal, ramp, and ramp mixed with sinusoidal. The sinusoidal functions have different amplitudes and frequencies (illustrated in the results).

5.6.2 Pump Flow Rate under External Disturbance

Different cases are considered to simulate the practical applications, and these cases are:

5.6.2.1 *Pump Flow Rate under an Extra Step Pipe Vibration (11%)*

The function generator is used to generate an extra step input (11%). It is assumed that the pipe response equals (0.0665 mm, 11% of 0.2 mm).

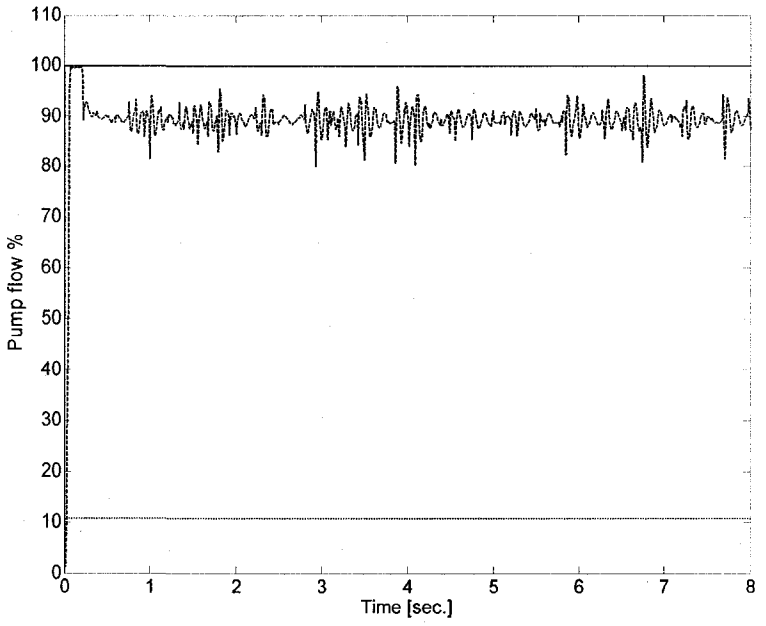

Figure 5.23: Pump flow under additional step pipe vibration (11%)

(____ desired pump flow (theoretical), -- external pipe vibration disturbance, ... actual pump flow rate)

5.6.2.2 *Pump Flow under Additional Mixed Step (11%) and Sinusoidal pipe vibration*

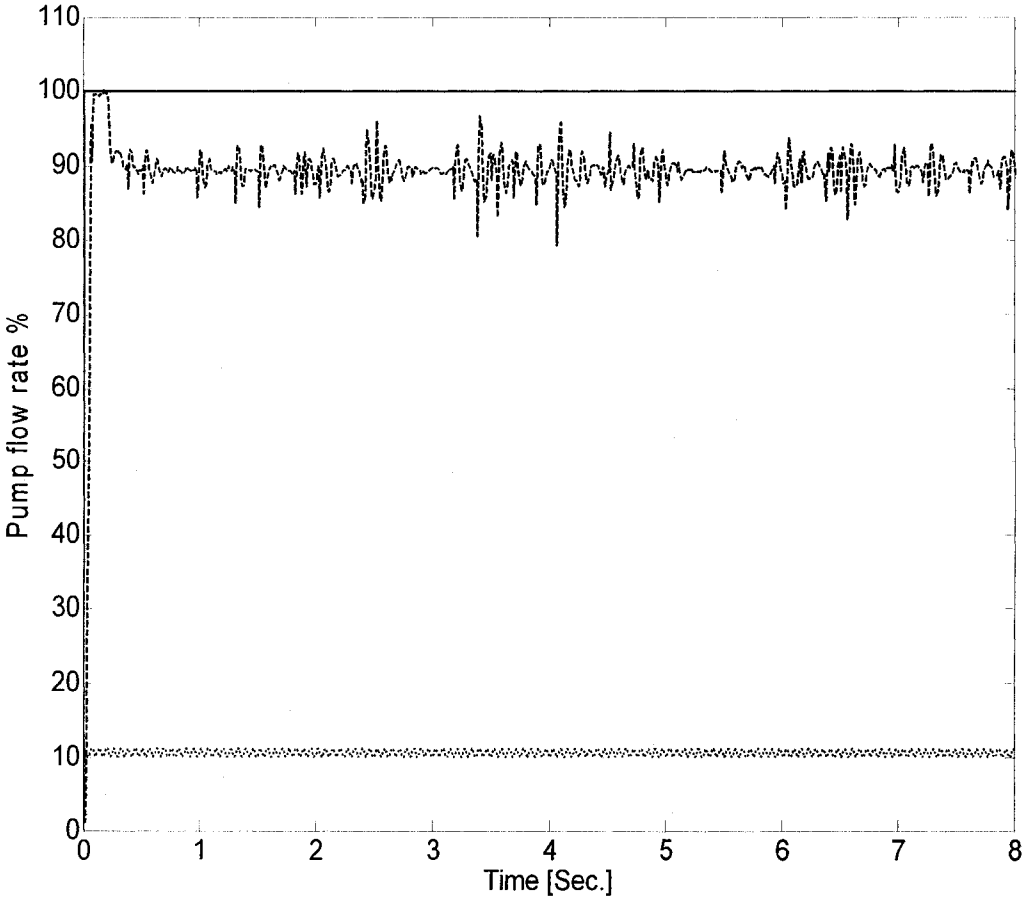

Figure 5.24: Pump flow under additional mixed step (11%) and sinusoidal pipe vibration (amplitude = 0.05, and frequency = 100 Hz.)

(____ desired pump flow (theoretical), -- external pipe vibration disturbance, ... actual pump flow rate)

5.6.2.3 *Pump Flow under Additional Mixed Step (11%) and Sinusoidal (Amplitude =0.2 and Frequency= 100 Hz) Pipe Vibration*

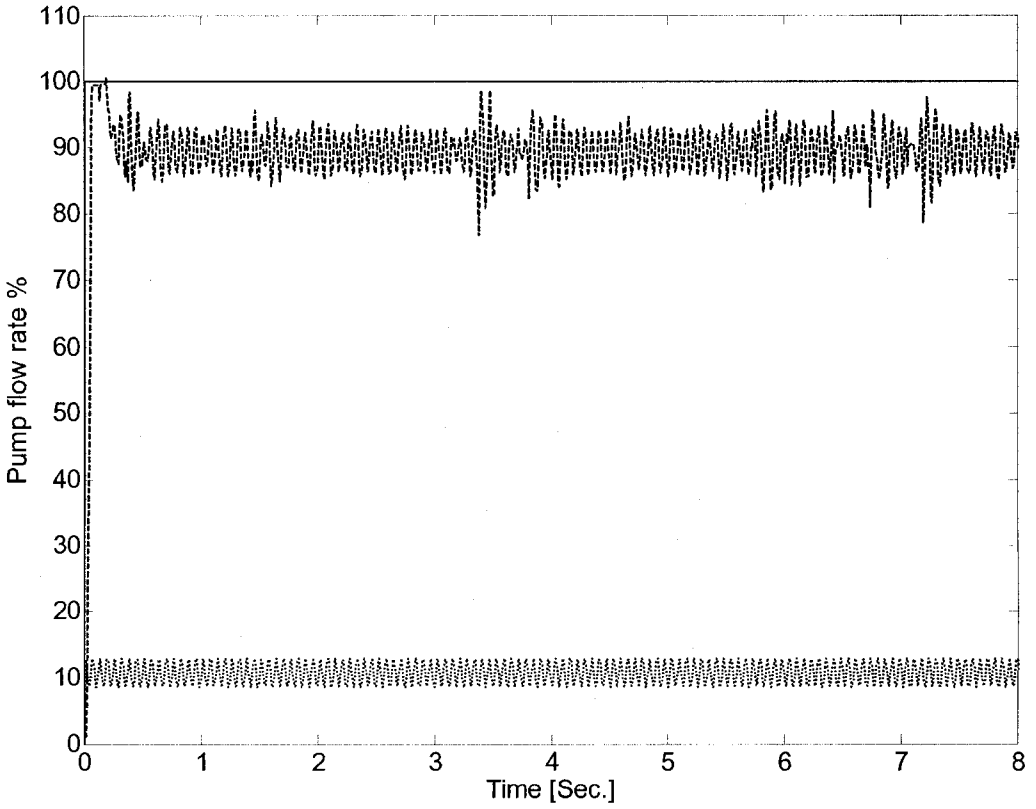

Figure 5.25: Pump flow under additional mixed step (11%) and sinusoidal pipe vibration (amplitude = 0.2, and frequency = 100 Hz.)

(____ desired pump flow (theoretical), -- external pipe vibration disturbance, ... actual pump flow rate)

5.6.2.4 *Pump Flow under Additional Ramp Pipe Vibration (Starts at 3 Sec)*

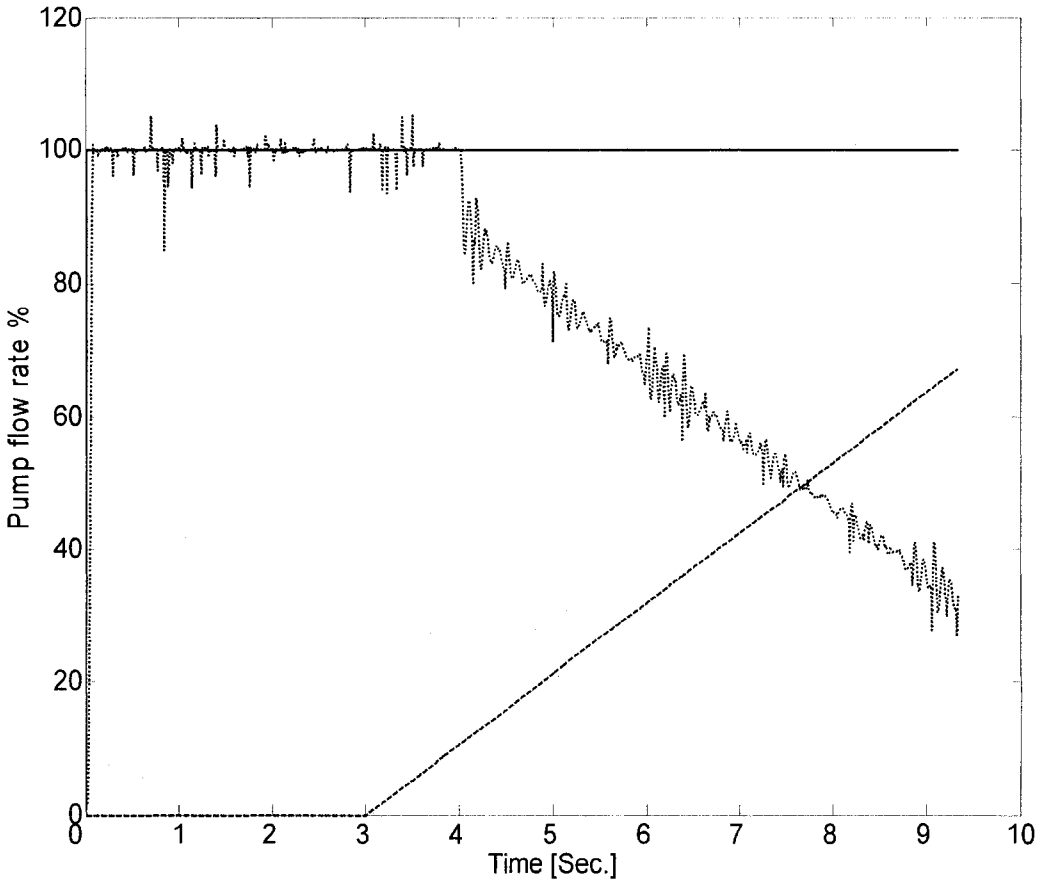

Figure 5.26: Pump flow under additional ramp pipe vibration (starts at 3 sec.)

(____ desired pump flow (theoretical), -- external pipe vibration disturbance, ..actual pump flow rate)

5.6.2.5 *Pump Flow under Additional Mixed Ramp and Sinusoidal (Amplitude = 0.05, Frequency = 100 Hz) Pipe Vibration*

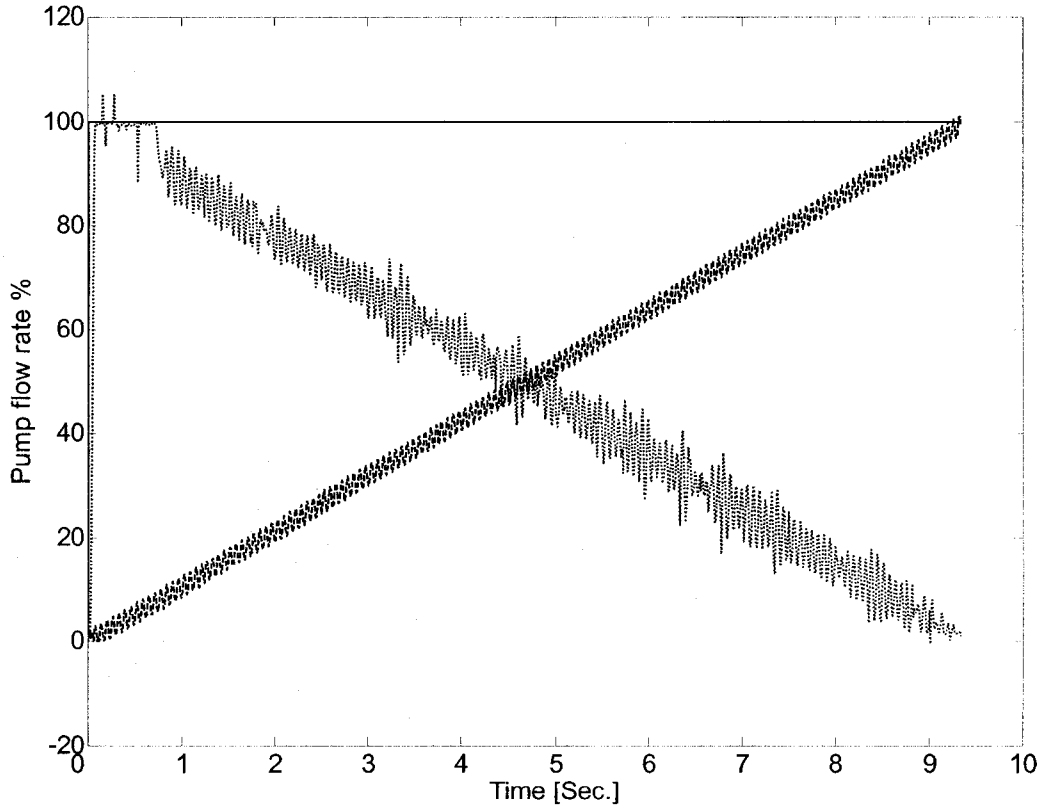

Figure 5.27: Pump flow under additional mixed ramp and sinusoidal pipe vibration (amplitude = 0.05, frequency = 100 Hz.)

(____ desired pump flow (theoretical), -- external pipe vibration disturbance, ... actual pump flow rate)

5.6.2.6 *Pump Flow under Additional Mixed Ramp and Sinusoidal (Amplitude = 0.2, Frequency = 100 Hz) Pipe Vibration*

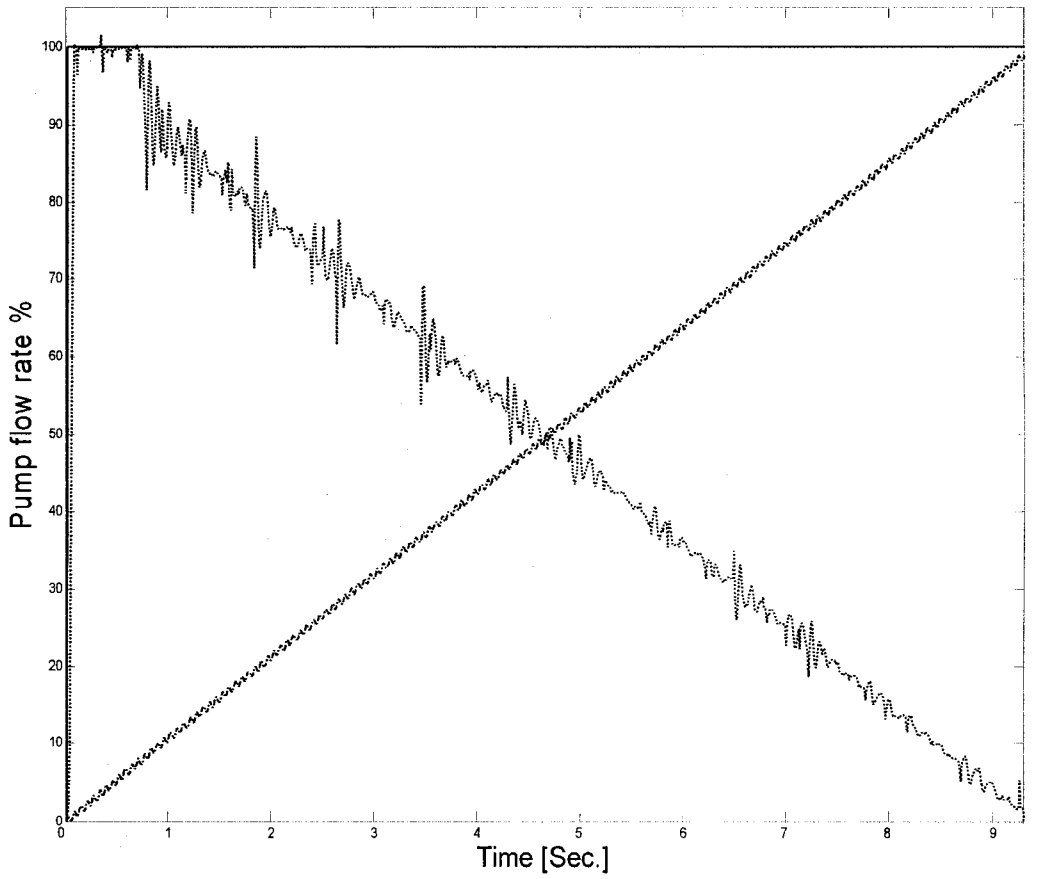

Figure 5.28: Pump flow under additional mixed ramp and sinusoidal pipe vibration (amplitude = 0.2, frequency = 100 Hz.)

(____ desired pump flow (theoretical), -- external pipe vibration disturbance, ... actual pump flow rate)

Figure 5.23 to Figure 5.28 show the pump flow behaviour under different external disturbances measured from the pipe. It can be observed in Figure 5.23 that the pump flow drops to 89% in the presence of the pipe vibration at 11% (the sum of the flow value and the extra pipe vibration value equal 100%). The same behaviour can be seen in the presence of the sinusoidal disturbances with respect to the value; and the flow fluctuates more at higher amplitudes of the sinusoidal disturbance. In the ramp disturbance, the pump flow decreases proportionally to the value of the disturbance, and the pump flow cuts off completely when the disturbance value reaches or exceeds the maximum allowed value (illustrated in Figure 5.28). These results show the applicability of the proposed control strategy for all conditions.

5.7 **Conclusions**

The current design of the swash plate pump is equipped with a double negative feedback control loop scheme. This design is complicated and entails extra cost. It also has a large rise time (about 120 ms.). It was proposed earlier that the pump can perform properly by implementing a single negative feedback control loop scheme by removing the return electrical line for the inner loop. That scheme was equipped with a PD controller and the results were good for certain applications but the levels of noise and vibration were not examined. In the present chapter, a control strategy that keeps the pump production cost low was achieved by implementing a single feedback control loop to control the swash plate swivelling angle. The experimental results show that the speed of the swash plate response was dramatically improved (dropped from 50 to 15 ms). Another experimental

investigation was conducted to compare the vibrations between the single feedback control scheme with PD and with PID controllers. The results with the PID controller decreased the vibrations to lower levels compared to with a PD controller. The proposed control strategy could be implemented in a pump that requires a high response and low vibration levels.

Also in the present chapter, the control strategy was extended by measuring the vibration levels at the pipe to ensure the smoothness of the pump control unit and to use it as an input for the pump-pipe control strategy. The pump-pipe control strategy was proposed to control the pump output according to the load requirements and the pipe vibration amplitude. The strategy worked to change the set point of the swash plate inclination by introducing the compensation factor that moderated the pipe vibration amplitude.

Experiments were carried out to examine the applicability of the strategy in the presence of different kinds of disturbances (similar to practical situations). It was found that the pump flow cut off completely when the pipe vibration amplitude reached the maximum allowed value, and decreased with different percentages depending on the vibration amplitude. The strategy is valid for all practical applications, and can be adapted to improve hydraulic system performance and improve safety levels and reliability.

The next chapter will deal with condition monitoring and fault diagnosis using vibration analysis. Different predetermined defects will be created, and the pump and the pipe vibration signatures will be transformed by using different transforms such as wavelet analysis (discrete and continuous transforms), waterfall diagram (3D representation for time, frequency and amplitude), and finally with fast Fourier transforms (FFTs).

CHAPTER SIX

6 HYDRAULIC SYSTEM FAULT MONITORING USING VIBRATION ANALYSIS

6.1 Introduction

In chapter five, a new control strategy for a pump with a single feedback and a PID controller was proposed, validated and parameterized experimentally. The control strategy was examined to verify that it could regulate the pump flow rate according to the pump load requirements and the pipe vibration levels, and the results showed the versatility of the strategy for this application.

Since the component vibration measurements are performed continuously in the new control strategy described in the last chapter, those measured signals can be conveniently exploited for condition monitoring and fault diagnosis in the hydraulic system. In this chapter, the different approaches in the analysis of the vibration signatures will be discussed. Condition Monitoring is a maintenance management approach that enables the current performance and the likely future performance of a specific machine to be evaluated. It is a perfect tool to detect defects of a progressive nature.

Hydraulic systems contain a finite amount of equipment. This equipment has moving parts, such as electric motors, pumps, and fans. The operating conditions of the

equipment vary, and any overloading condition will lead to the loss of the desired performance, and will increase the levels of vibration and noise. The vibration signature can be analyzed to monitor the condition of the components, the forces and their intensities. The vibration signature is a valuable tool in the comprehension of a system's performance, because the signature portrays the existing forces and their frequencies at any time.

6.2 Types of Vibration Signature Analysis

Vibration signatures are obtained by placing accelerometers at specific locations and measuring the acceleration levels in time. Different transforms are used to convert the signals into useful information, such as into frequency components and power spectrum density. Some of these transforms are: Fourier Transform, (FT), Fast Fourier Transform, (FFT), Short Term Fourier Transform, (STFT), and Wavelet Analysis, (WA). These tools are able to convert the raw signals in time to frequency-time, frequency-amplitude, or time-frequency-amplitude. Each type of transform serves a specific purpose, and it has its own application, as follows:

Fourier Transform (FT) is used to obtain the frequency components for a function which tends to zero when t tends to infinity and has a finite integral. FT transforms the time domain signal into a discrete spectrum of amplitude versus frequency values. When the time domain signal corresponds to a structured response, the first frequency is the largest in size and represents the fundamental frequency, and there are many different frequency components representing the higher natural frequencies.

Both FT and FFT represent the raw signals in a frequency domain. Sometimes, when the signal is non-stationary in nature, it is more convenient to represent the signal in time versus frequency. This can be achieved by the Short Term Fourier Transform (STFT) in time windows as the signal evolves over time.

Wavelet Transform is a time-scale representation, where the signal is filtered into different scales (inversely proportional to frequency) according to its frequency.

In addition to the previous transforms, there is another representation which includes frequency, time, and amplitude. It is known as the Waterfall diagram. This diagram gives a clear idea about the evolution of the signals using a 3D display.

6.3 The relationship between the type of the signature and the transform

The transforms are used to obtain more information from the raw signal (time domain) that is not generally available from the signal itself. For example, for a sinusoidal signal, it is possible to obtain the frequency by counting the number of cycles per unit time. Dealing with the sinusoidal signal, which is a periodic signal, is an easy task and is straightforward. However, in practical applications, rare periodic signals are rare.

The majority of signals in practical applications are random processes which may be stationary or non-stationary signals. Signals are called stationary when all frequency components exist at all times, and do not change with time. However, when the frequency components change with time, the signals are called non-stationary signals.

Two factors determine the sort of transform that is to be used: the type of the signal (periodic, stationary, or non-stationary) and the desired information. Hence, using FT or FFT will give only the frequency components, without any more information. This is suitable for periodic and stationary signals, where time does not have any effect (all frequency components are available at all times). However, for non-stationary signals, the two previous transforms are not satisfactory because they do not indicate when in time these frequency components take place. Therefore, another type of transform should be used to provide the complete information from the signals that indicates the frequency components and their intervals. In 1930, Gabor introduced the Linear Time Frequency Representation, which is also known as the Short Term Fourier Transform. The concept of this transform is to divide the non-stationary signal into small portions of sub-stationary signals. Every portion fits in a window, and is treated as a separate stationary signal, i.e. using FT (or FFT) for each window.

FT decomposes the signal with different frequencies as an exponential function, expressed as

$$\mathrm{X}(f) = \int_{-\infty}^{+\infty} x(t) e^{-i\omega t} \, . \, dt \qquad (6.1)$$

where $\mathrm{X}(f)$ is the FT of the raw signal, $x(t)$, t is time , and ω is the angular frequency.

In STFT, the same procedure is repeated, but by windowing signals. Every window includes a segment of the signal. The windows are uniform and identical, and this brings the time into the picture. Hence, in STFT, signals are represented in time versus frequency.

STFT can be expressed in the presence of the window as

$$STFT\{x(t)\}=X(\tau,f) = \int_{-\infty}^{+\infty} x(t)W(t-\tau)e^{-i\omega t}.dt \qquad (6.2)$$

STFT represents the Fourier Transform of the windowed raw translated signal, stands for the translation factor, and W (t) is the window function. There are two different types of windows. Each type has unique properties. For example, a Gaussian window has a bell shape, while a Hanning window has a similar shape with less height. A Hanning window is recommended more often because the window fits most of the practical signals.

Working with STFT brings the concept of the time and frequency resolution into the picture. In FT, there is no indication for time resolution, and the only available resolution is the frequency resolution. In STFT, because of the windows, there will be either time or frequency resolution. The width of the windows affects the resolution (time and frequency), and when the time resolution gets poorer, the frequency resolution improves. This explains the perfect frequency resolution in FT, where there is no time resolution. When the selected window is narrow, the time resolution is good, while the frequency resolution is poor. While the frequency resolution improves by increasing the width of the window, the time resolution gets poorer. Hence, resolution is a serious concern in STFT. The solution to this problem is to use a transform that changes its window width, or has a multi-resolution. This is the Wavelet Transform.

6.4 Wavelet Transform

Wavelet Transform is a time-frequency representation with good time and frequency resolution, and it is recommended for high-frequency signals and with many transients (discontinuities). WA (Wavelet Analysis) is defined as a mathematical function that is used to resolve a given function into different frequency components where each component can be situated in depth with a resolution that matches its scale [49].

6.4.1 Wavelet Properties

In order to consider a function as wavelet, there are two conditions that must be satisfied, which are:

- Regularity: Its mean value in the time domain should be zero, or if it has an oscillatory nature, the mean value over the entire time domain should be zero, which can be expressed as:

$$\int_{-\infty}^{+\infty} \psi(t)dt = 0 \tag{6.3}$$

- Admissibility: The wavelet has a band-pass filter, which means the wavelet has finite energy , and it may be mathematically expressed as

$$\int_{-\infty}^{+\infty} |\psi(t)|^2 \, dt < \infty \tag{6.4}$$

6.5 Types of Wavelet Transform

There are two types of wavelet transform:

6.5.1 Continuous Wavelet Transform (CWT):

The continuous wavelet transformation (CWT) of a function $f(t)$ with respect to a mother wavelet function $\psi(t)$ is defined as a convolution of the function $f(t)$ with the scaled and translated mother wavelet function $\psi(\frac{t-b}{a})$, [49].

The integral convolution is expressed as

$$w(a,b) = \frac{1}{\sqrt{a}}\int_{-\infty}^{+\infty} f(t)\ \psi\ \left(\frac{\mathrm{t-b}}{\mathrm{a}}\right)\mathrm{dt} \qquad (6.5)$$

where $\psi(\frac{t-b}{a})$ is the translated and scaled version of the mother wavelet $\psi(t)$. The $\frac{1}{\sqrt{a}}$ parameter is introduced to normalize the mother wavelet energy at every scale.

The scale parameter takes care of the dilation (a>1) and contraction (a<1). The translation parameter (b) localizes the wavelet with respect to time. The CWT is calculated by a continuously shifting and a continuous scalable function over the signal and then calculating the correlation between the signal and the mother wavelet. The signal is represented by the time function. The CWT takes time to calculate all details of the signal, and some of these details could be unimportant. To overcome this problem, the Discrete Wavelet Transform (DWT) is employed.

6.5.2 **Discrete Wavelet Transform (DWT)**

DWT is considered a powerful tool to detect the changes of a signal. DWT is translated and scaled in discrete steps. It is a piecewise continuous function and can be given as

$$W(a,b) = \frac{1}{\sqrt{a}} \sum_n \sum f(n)\, \varphi(\frac{n-b}{a}) \tag{6.6}$$

Eq. (6.6) represents a discrete wavelet transform, where "a" is a scale function, $\varphi(\frac{n-b}{a})$ is the mother wavelet or wavelet basis, n is an integer number, and "b" is a dilation indicating number. The parameter $\frac{1}{\sqrt{a}}$ is introduced in order to normalize the mother wavelet to have unit energy at every scale. To solve this equation, the parameters "a" and "b" should be determined.

For a dyadic discrete sampling, "a" can be expressed as

$$a = 2^j \tag{6.7}$$

where "j'' is the number of decompression levels, while "b" can be expressed as

$$b = 2^j . k \tag{6.8}$$

where k is an integer, t is time, $f(t)$ is the signal, and n is the number of samples. The scale, a, is inversely proportional to the frequency. W(a,b) can be represented as either frequency-time or scale-time representation. In most of the previous works, the W(a,b) representation is in scale-time representation. The reason is that there is no exact relationship between scale and the frequency.

In [49], Mallat suggested that multi-resolution analysis is needed to obtain the DWT of a discrete signal by implementing low and high pass filters, and then down sampling them by two as is illustrated in Figure 6.1 and described below.

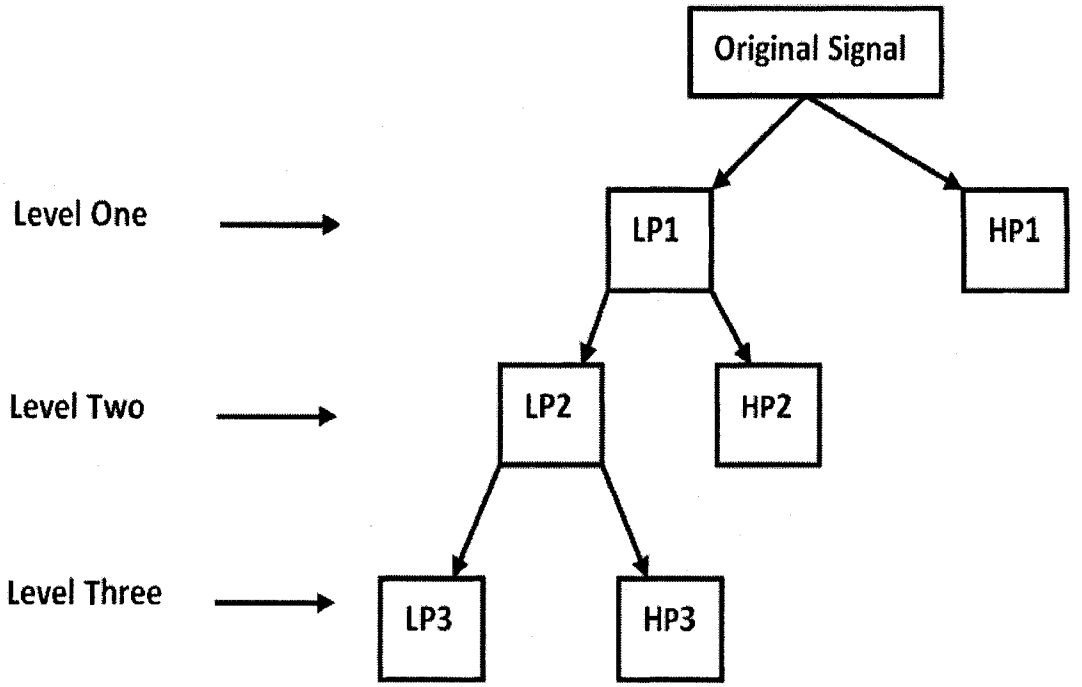

Figure 6.1: Computation of DWT by multi resolution analysis (Filters Bank)

Figure 6.1 shows the decompression of a signal at three levels. The signal passes through high and low pass filters to classify the signal according to the frequency range. The high pass filter in the first level allows the samples with high frequencies (f_{max}-$0.5f_{max}$) to pass

through, while the remaining samples pass through the low pass filter. The output of the high filter is halved to constitute the detail coefficient at the first level, while the output of the low pass filter ($0.5f_{max}$-0) is halved and prepared to be filtered in the second level. In the second level, the even samples of the first-level low pass filter are passed through low and high pass filters. The samples within a frequency range of ($0.5f_{max}$-$0.25f_{max}$) pass through the second-level high pass filter and then are halved to constitute the detail coefficient at the second level. The sub-band with a frequency range of ($0.25f_{max}$-0) is halved (subsampled by two) and the even samples are the input to the third-level high and low pass filters. The output of the second level passes through the third-level high and low pass filters. The output of the third-level high pass filter with a frequency range of ($0.25f_{max}$-$0.125f_{max}$) is halved and the even samples constitute the detail coefficient at the third level. The output of the third-level low pass filter, with a frequency range of ($0.125f_{max}$-0), is halved to form the approximate coefficient at the third level.

In order to understand these coefficients, it is vital to observe the location of the discontinuity in the signals, where it represents a joint between two frequencies. Also, the amplitude of the coefficients reflects a certain phenomena. By considering the level at which the coefficient has the discontinuity and its corresponding amplitude, it will be easy to determine the frequency band of the fault. Using this knowledge and with some experience, it will be an easy task to determine the defect accordingly.

6.6 Selection of the Mother Wavelet

In WT, selection of the mother wavelet is a very important step, where the selection of the mother wavelet depends on the type of the signal and allows us to predict the optimized solution. The function of the mother wavelet is to extract the discontinuities from the signal. Different types of mother wavelets are used. The most convenient type for hydraulic network applications are Daubechies wavelets. A Daubechies wavelet is mostly localized and compactly supported in time and it is appropriate for signals that have an impulsive nature. A hydraulic system has different interconnected components and one componen'st performance affects the entire system performance. These systems have impulsive vibration signals due to swash plate pump pressure overshooting.

6.7 Results

In the previous sections, Wavelet Transforms were discussed, including their properties, types, and the use of a mother wavelet. In this section, the typical shape of healthy pump/pipe vibration signatures will be experimentally obtained. Different known defects will be introduced. The signatures of every case will be analyzed. The deviation in the shape of the signature is considered a symptom of a "pathological" condition.

The results of the different cases will be analyzed with different approaches, which will help us to better understand the change that takes place in the presence of a certain defect. The transforms that will be used are: Wavelet Transform, FFT, and Waterfall diagram. The objective of this approach is to emphasize the strength of the Wavelet Transform as a powerful tool in transforming the signals, regardless of their nature; and also to illuminate

the overall signal evolution by using a Waterfall diagram. Finally, FFT is used to find the exact values for the signal.

6.7.1 **Pipe/Pump with Normal Operating Conditions**

By implementing the PID controller, the pump is tuned to have smooth operation. The vibration signatures for the pump and the pipe are recorded and labelled the standard cases. Then, these signatures are transformed with the different transforms.

6.7.1.1 ***Pump Standard Signature***

The vibration of the pump is recorded by placing a piezoelectric accelerometer on the pump outlet (The setup is presented in chapter 5). The pump vibration signature is shown in Figure 6.2.

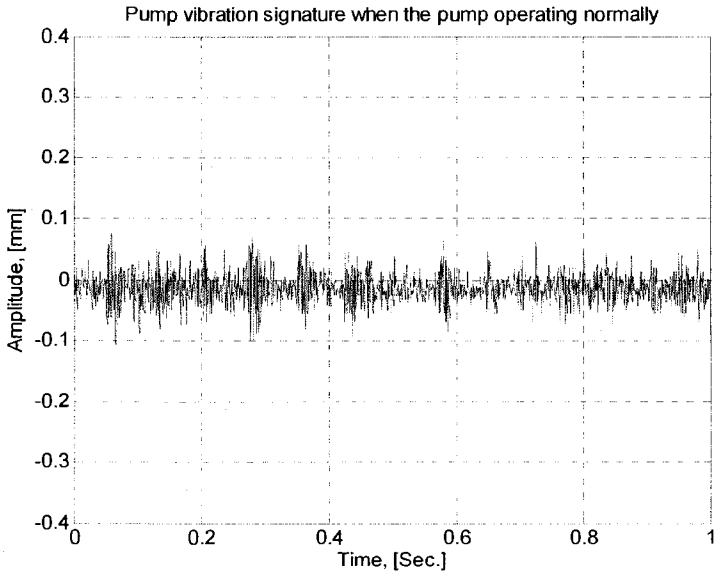

Figure 6.2: Pump vibration signature with normal operating conditions (standard)

6.7.1.1.1 CWT for Pump Vibration Signature (Normal Operating Conditions)

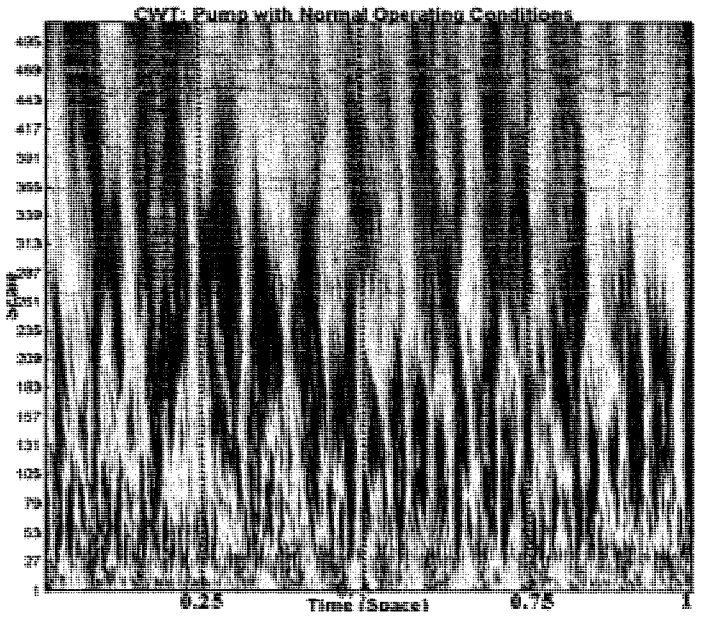

Figure 6.3: CWT for pump vibration signature with normal operating conditions (standard)

6.7.1.1.2 DWT for Pump Vibration Signature (Normal Operating Conditions)

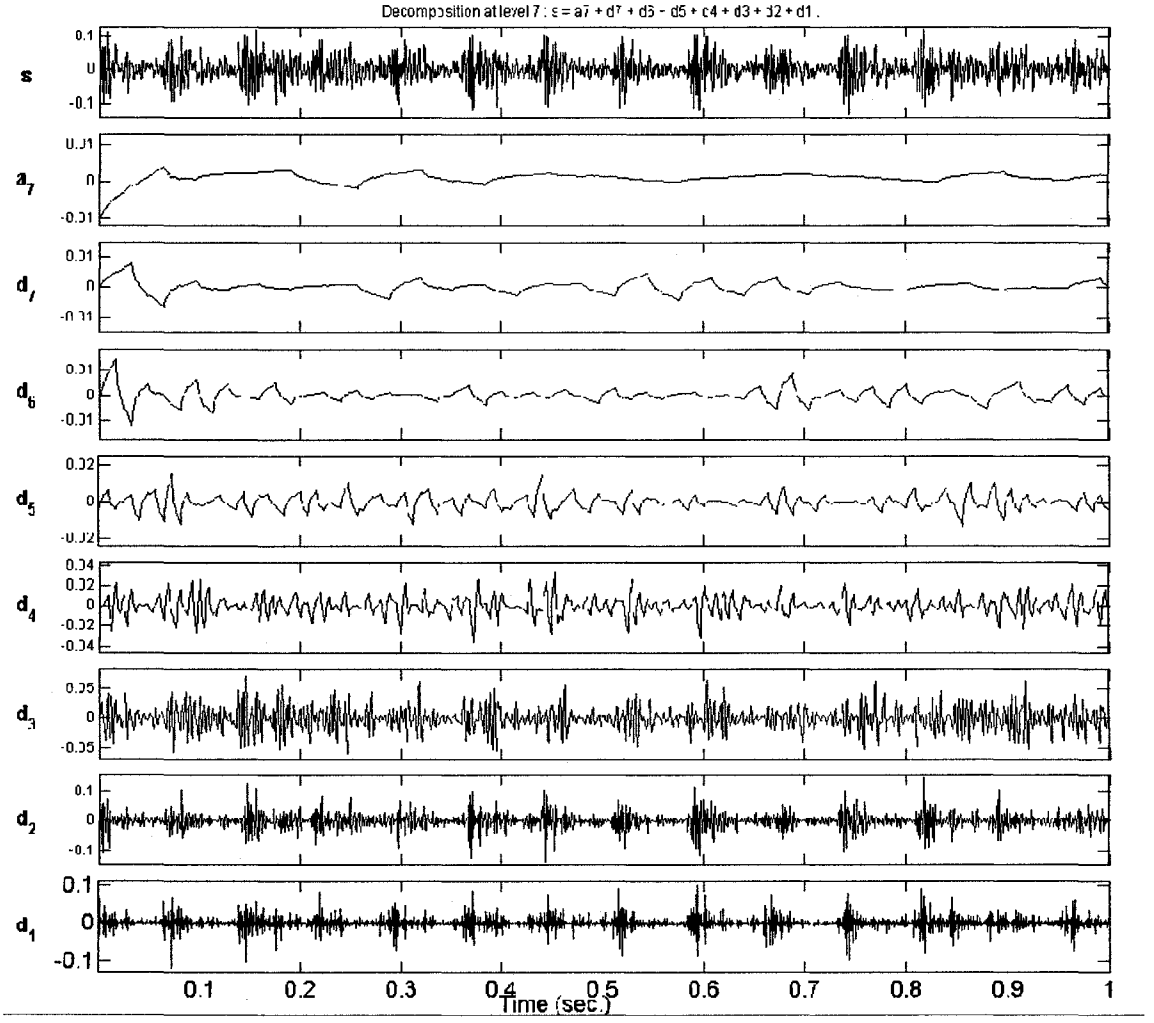

Figure 6.4: DWT for pump vibration signature with normal operating conditions

(standard)

6.7.1.1.3 Waterfall Diagram for Pump Vibration Signature (Normal Operating Conditions)

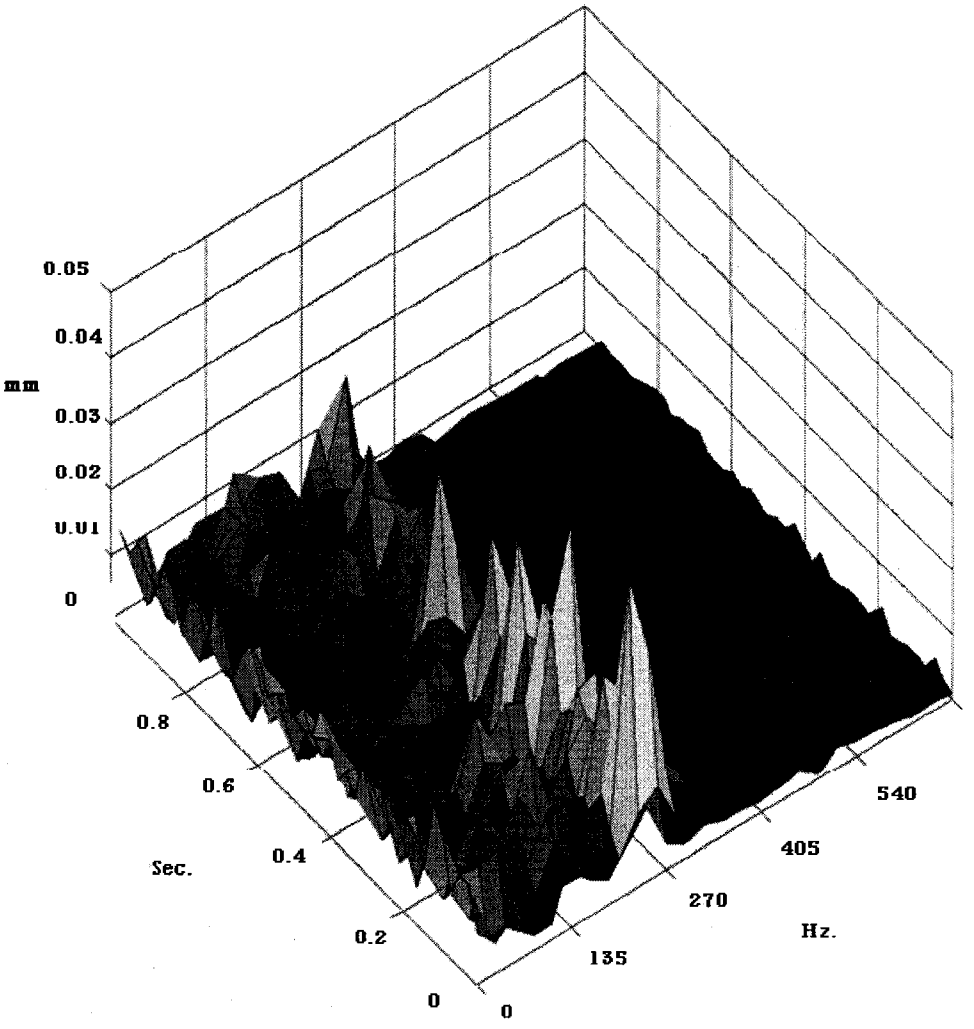

Figure 6.5: Waterfall diagram for the pump vibration signature

(Under normal operating conditions)

From Figure 6.2, is regularity in the pump vibration signature can be observed, where there are small amplitude vibrations superimposed with large amplitudes (13 large amplitudes). The small amplitude vibration varies in the range of ± 0.02 mm.

The signature transforms created by using WT are presented in Figure 6.3 and Figure 6.4.

CWT is calculated with respect to time in Figure 6.3. CWT representation has two linear axes, the horizontal axis is time, which matches the original signal with respect to time; the vertical axis is the scale axis, and the coefficients of the wavelet are classified on this axis according to the frequency contents of the signals. Hence, the highest frequencies can be seen at the lowest scales, but at the same time as the occurrence, and vice versa. Also, the colour represents the amplitude of the coefficients, for example, the blue spots represent the locations of the high amplitudes of the signals. In our case, we have a signal recorded over 1 second. Accordingly, the horizontal axis expands over 1 sec (1000 mSec.). The MATLAB toolbox does not display the time subdivision on the time axis.

It can be seen that the longest sub-band takes place when t= 250 mSec., and it spreads from scale 27 to 512. In other words, at t= 250 mSec, a wide sub-band with middle and low frequency is dominant. Moreover, in the first 250 ms, there are some periodicities at the lowest to middle scales (high and middle frequencies).

The DWT detail and approximate coefficients on the seventh level are calculated and illustrated in Figure 6.4. The signal was decomposed into 7 levels, and hence, we have 7 detail coefficients and one approximate coefficient. The approximate coefficient has the same trend as the original signals, and the locations of the frequency joints can be observed. There are different approaches to interpret the evolution of the signal, such as comparing the detail coefficients or the approximate coefficient. In this work, we will use the second approach, since it requires less explanation and the focus will be on only one coefficient for each case.

It can be seen here that the seventh approximate coefficient increases from -0.1 and then it fluctuates about zero. There are some periodic fluctuations with different intervals.

The 3D representation (waterfall diagram) for the signal is represented in Figure 6.5. The waterfall diagram represents the signal on the frequency-time-amplitude axes. The diagram shows the peaks of the frequency and the time of their occurrence. There are contents with high frequency (at 270 Hz) which have the highest amplitudes. They can be seen in different intervals such as 10, 250, 600, and 800. However, they have no tangible presence in the lower frequencies.

Hence, the characteristics of the normal operation for the pump can be summarized as follows:

1. The vibration signature fluctuates in the range ± 0.02 mm
2. CWT: sub-band frequency can be seen in the first 250 ms, and it spreads from scale 27 to 512
3. DWT: at first, the seventh approximate coefficient has amplitude -0.1, and afterwards, it slightly fluctuates about the zero value

4. Waterfall diagram: shows that the maximum frequency amplitudes take place in the first 250 mSec., and the frequency equals 270 Hz

6.7.1.2 *Normal Pipe Condition*

In a similar fashion, the pipe signature is recorded and then transformed with the same transforms. The experimental setup and details of the different predetermined defects were shown and discussed in chapter 4.

6.7.1.2.1 Pipe Vibration Signature with Normal Operating Conditions

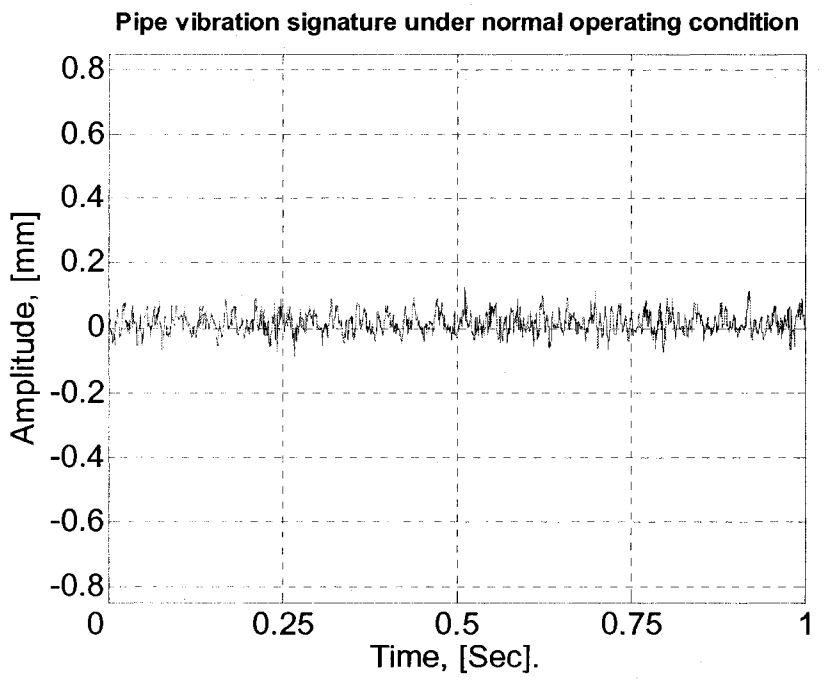

Figure 6.6: Pipe vibration signature with normal operating conditions

6.7.1.2.2 CWT for Pipe Vibration Signature with Normal Operating Conditions

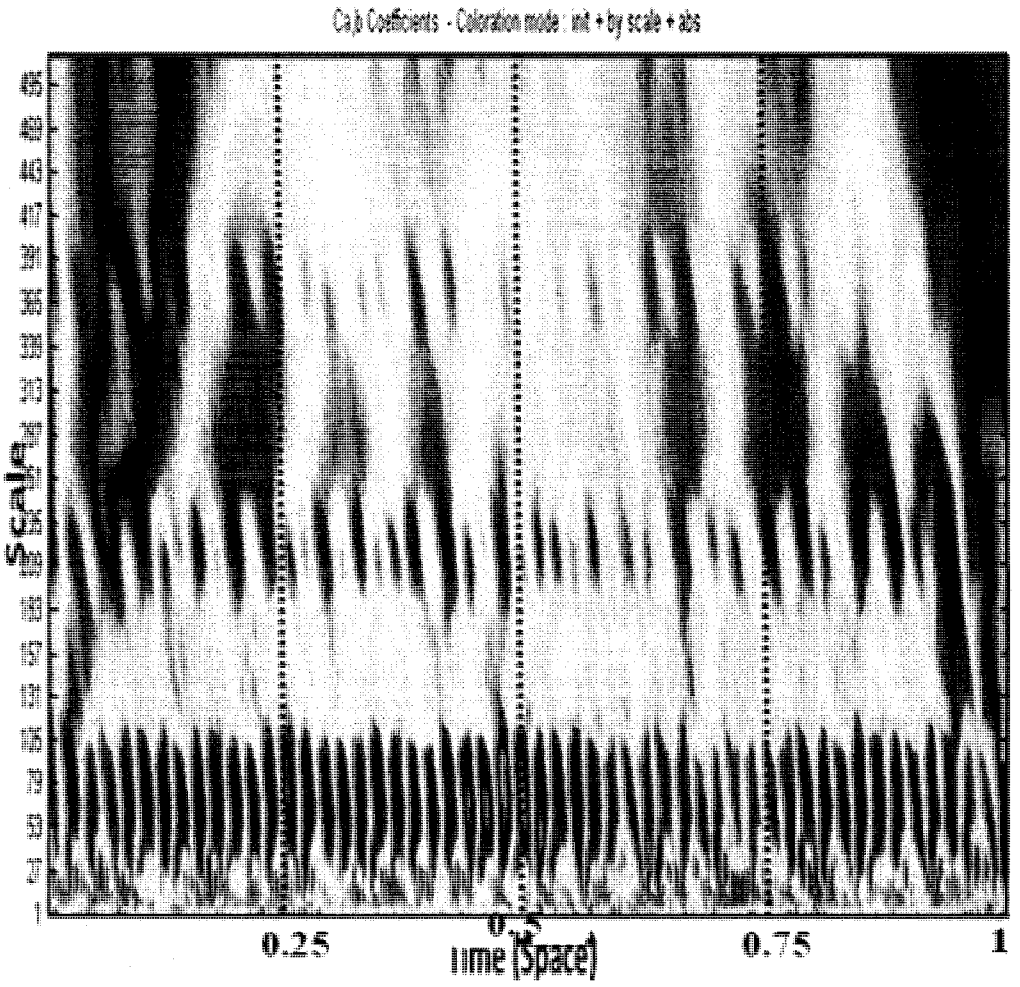

Figure 6.7: CWT for pipe vibration signature with normal operating conditions (standard)

6.7.1.2.3 DWT for Pipe Vibration Signature with Normal Operating Conditions

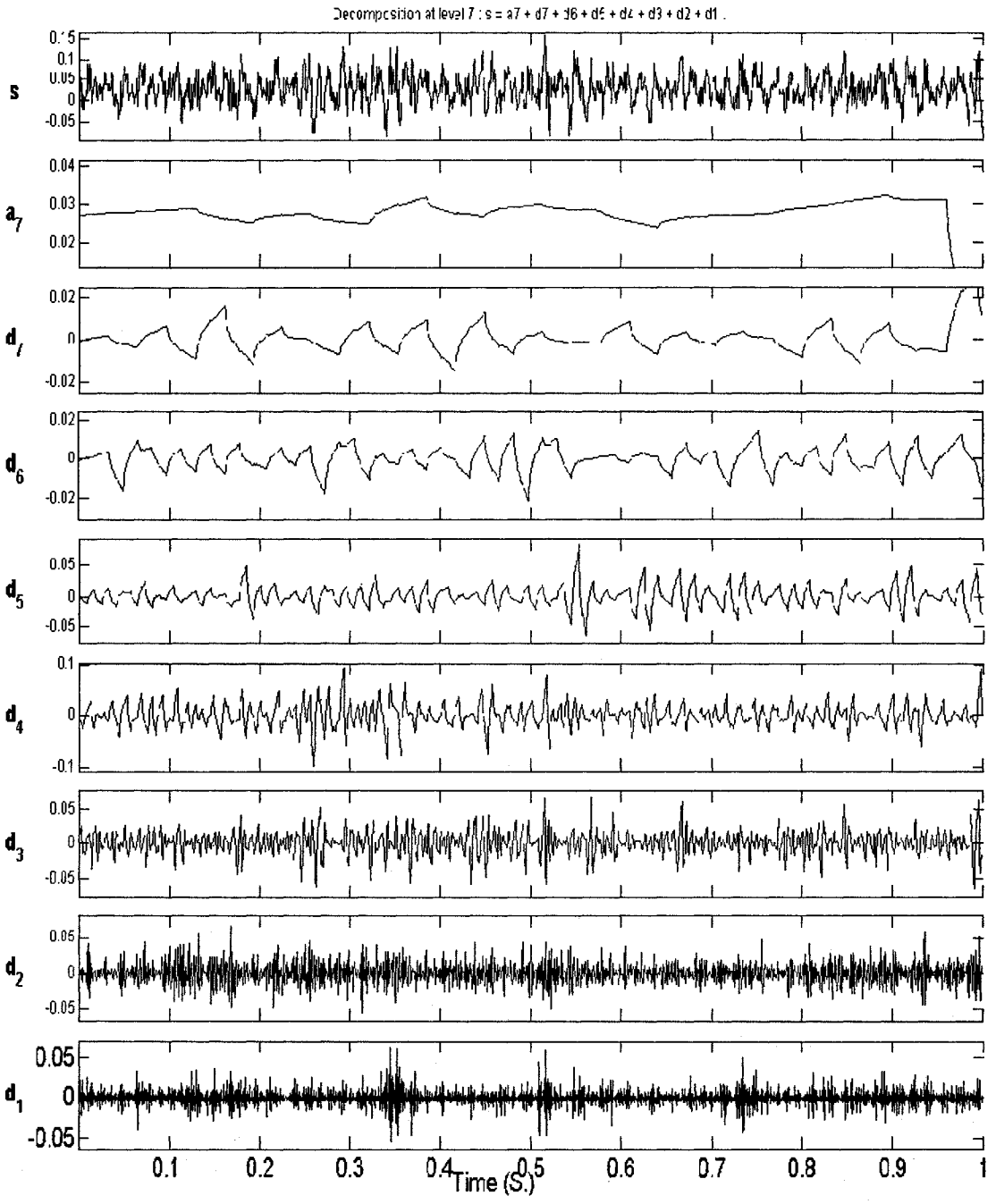

Figure 6.8: DWT for pipe vibration signature with normal operating conditions(standard)

6.7.1.2.4 Waterfall Diagram for Pipe Vibration Signature (Normal Operating Conditions)

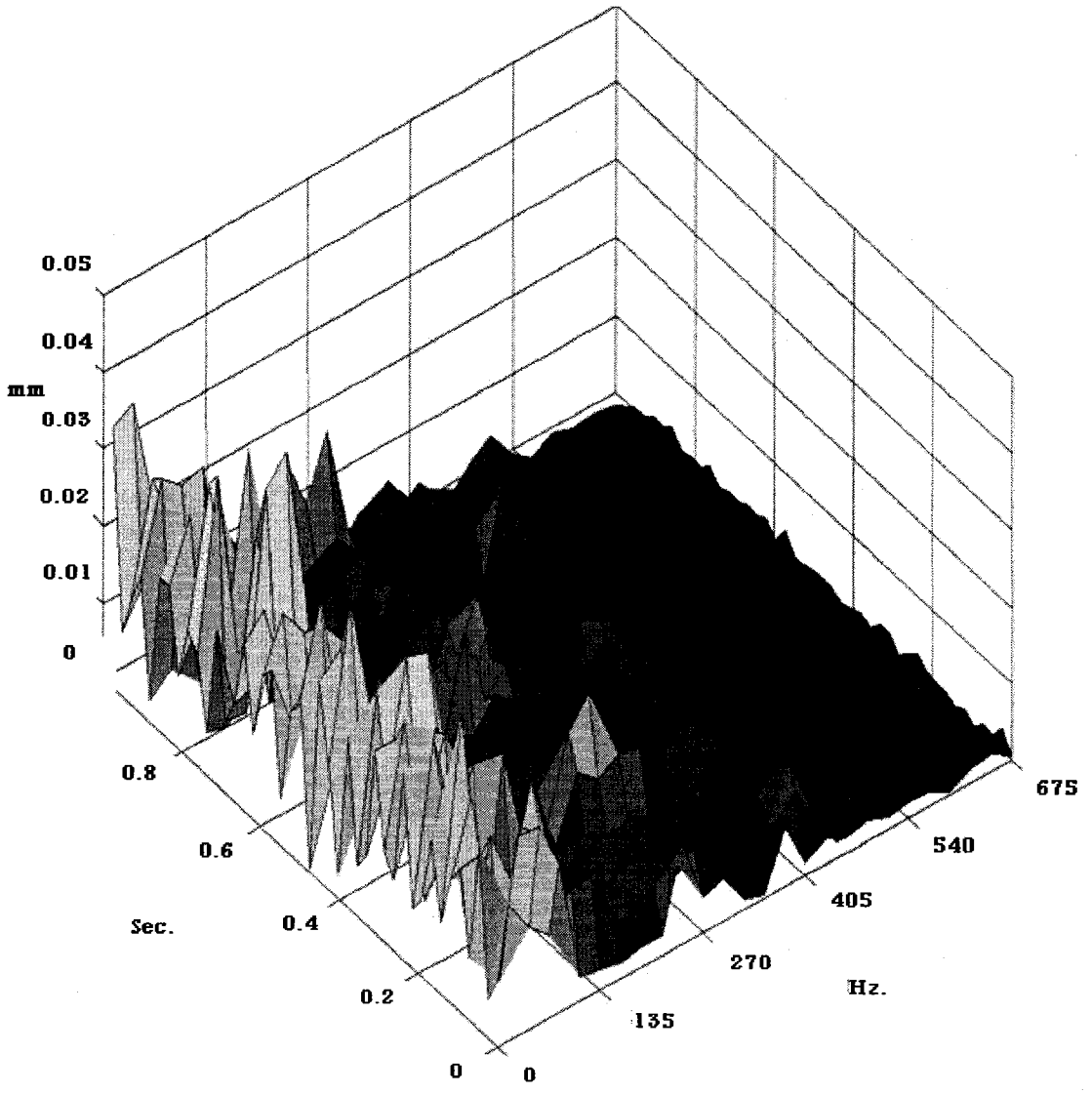

Figure 6.9: Waterfall diagram for the pipe vibration signature

(Under normal operating conditions)

Figure 6.6 shows the pipe vibration signatures under normal operating conditions. The vibration amplitude shows regularity and it vibrates in the range $\mp$ 0.075 mm.

In Figure 6.7, the time-scale representation (CWT) is shown for the normal case. It can be noticed that there are periodicities equally distributed within the (27-100) scale with two large periodicities at the high-scales sides at t=100 and 950 mSec.

The coefficients of DWT for the pipe signature when it is under normal operations are illustrated in Figure 6.8. The seventh approximate coefficient has a constant amplitude equal to 0.028 but and then sharply drops at t=950 mSec. For instance, when the pipe vibration signature has an approximate (the seventh) DWT equal to 0.028, the pipe has a normal operating condition.

Figure 6.9 gives more details about the signal in 3D representation. It shows that there is a series of low frequency (about 10 Hz, due to the fluid flow velocity) at the times with maximum amplitude equal to 0.033 mm at t=950 mSec.

The summarized characteristics are:

1- The vibration signature varies regularly within the range of $\mp$ 0.075 mm
2- The CWT contains most of the periodicities within the scale of (27-100)
3- The seventh approximate coefficient remains with a constant amplitude (0.028) at most times
4- A 10 Hz frequency band can be observed at most times, with amplitude of 0.033 mm.

6.7.1.3 *Pump under an Excessive Internal Noise*

6.7.1.3.1 Problem Description

In practical applications, there are different sources of undesired internal noise. The selection of the controller and its parameters can be a source of this noise. In this section, we will amplify the internal noise by selecting a PD controller for the pump. It is well known that the derivative action of the controller makes the system more dynamic and unstable [5].

Assuming that the noise has a sinusoidal nature, and can be expressed as

$$y(t) = ASin\ (\omega t) \tag{6.9}$$

where A is the amplitude of noise, t is time, and ω is the frequency of the noise signal.

Noise usually has a small amplitude and large frequency. In order to simulate the effect of the derivative controller, we have to differentiate Eq. (6.10), as follows

$$\frac{dy}{dt} = \omega\ A\ Cos\ (\omega t) \tag{6.10}$$

Eq. (6.10) represents the noise after passing though the PD controller. It has large value, because the noise will be multiplied by ω .

This approach is used to create internal dynamic instability for the pump.

6.7.1.3.2 Pump Vibration Signature with Internal Dynamic Instability

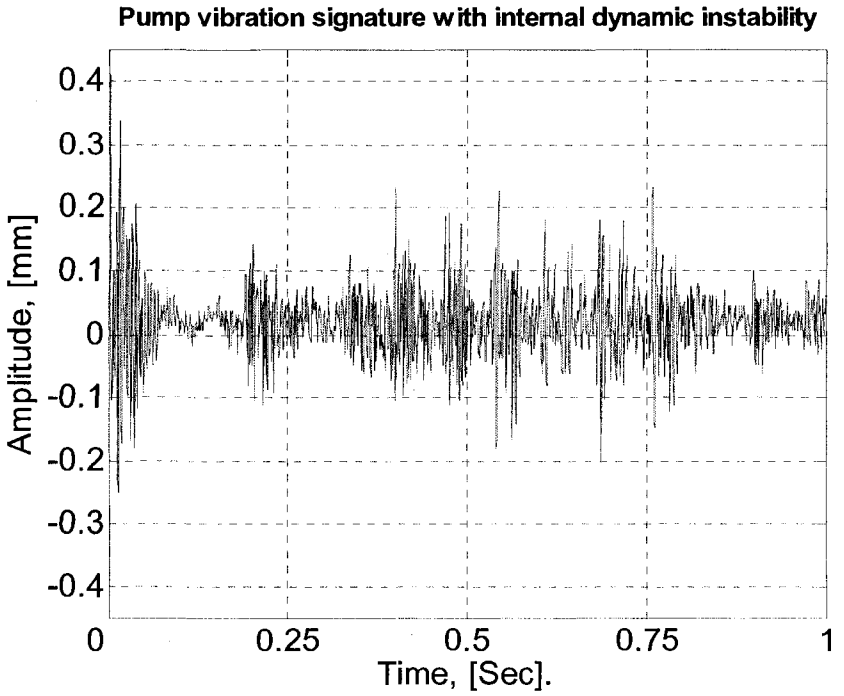

Figure 6.10: Pump vibration signature with internal dynamic instability

6.7.1.3.3 CWT for Pump Vibration Signature with Internal Dynamic Instability

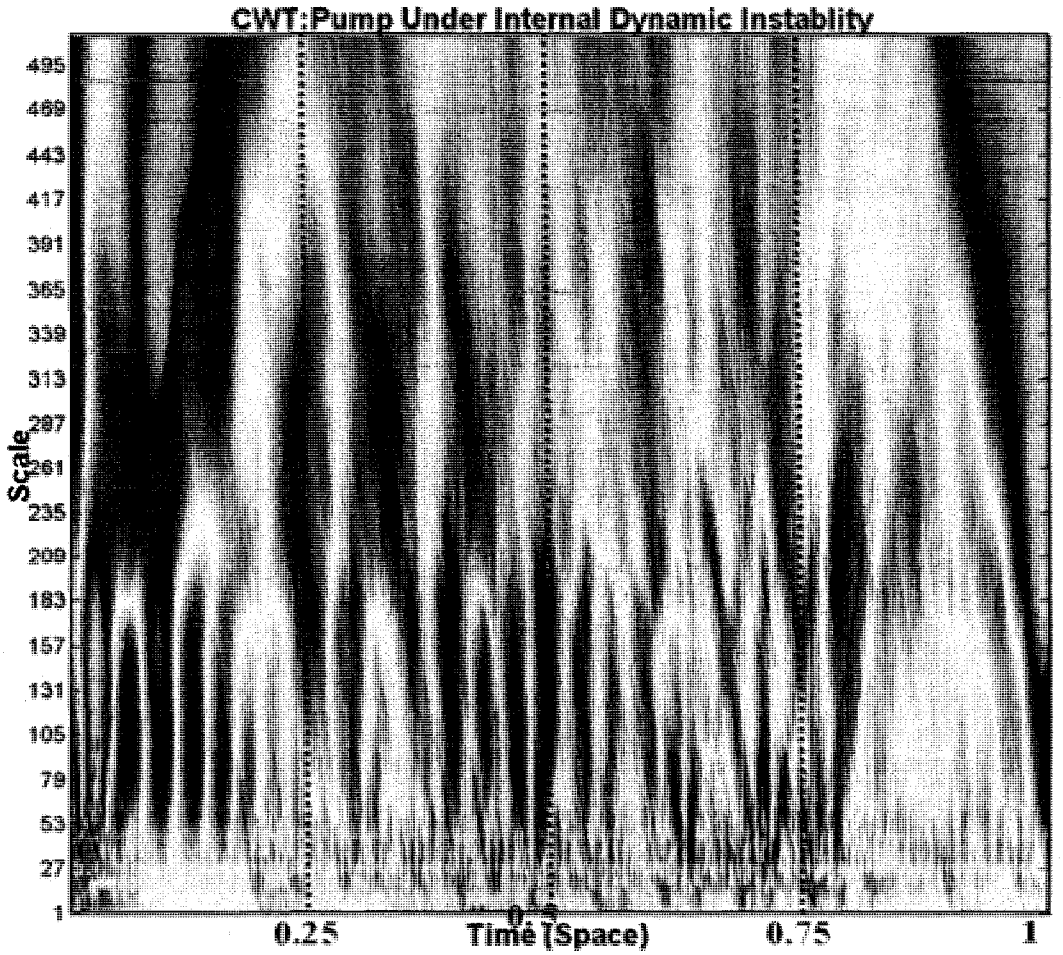

Figure 6.11: CWT for pump vibration signature with internal dynamic instability

6.7.1.3.4 DWT for Pump Vibration Signature with Internal Dynamic Instability

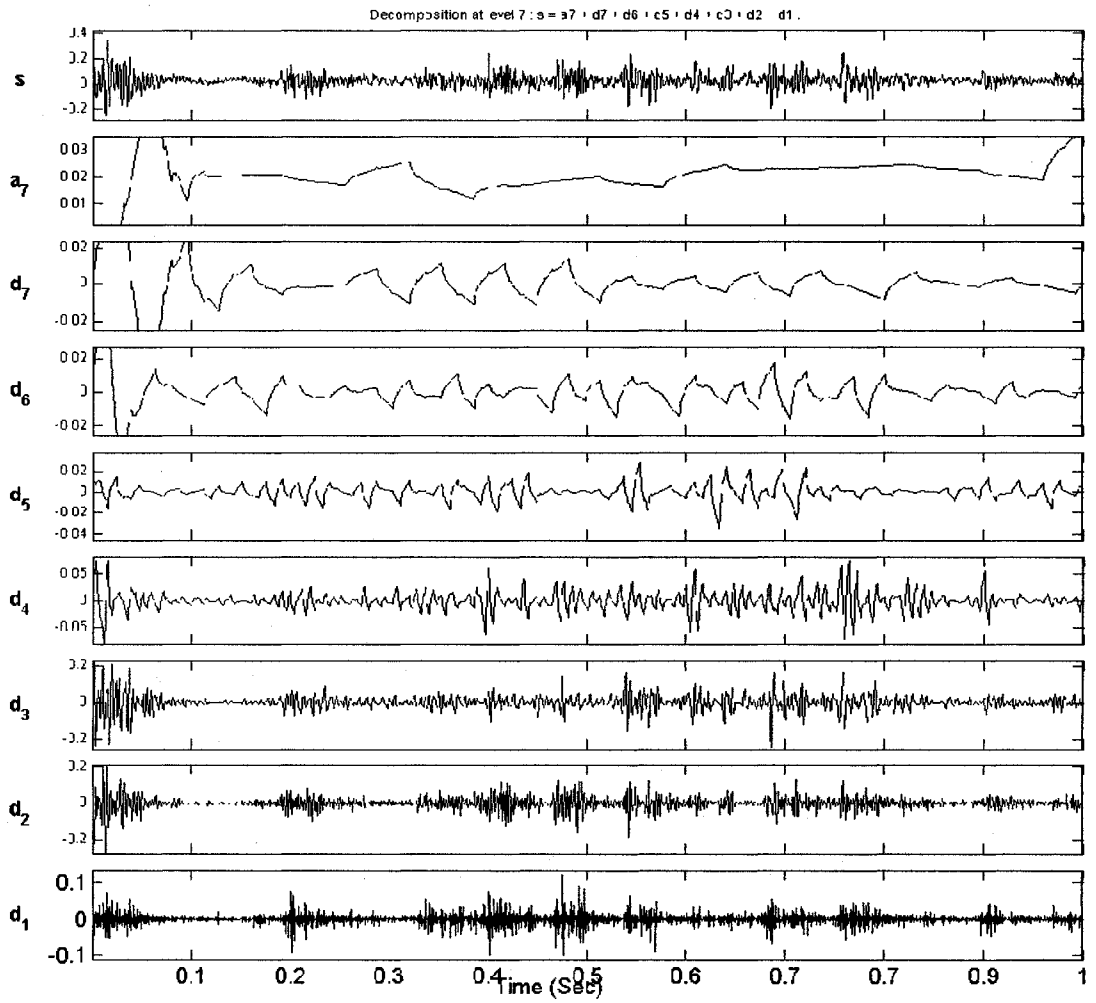

Figure 6.12: DWT for pump vibration signature with internal dynamic instability

6.7.1.3.5 Waterfall Diagram for Pump Vibration Signature with Internal Dynamic Instability

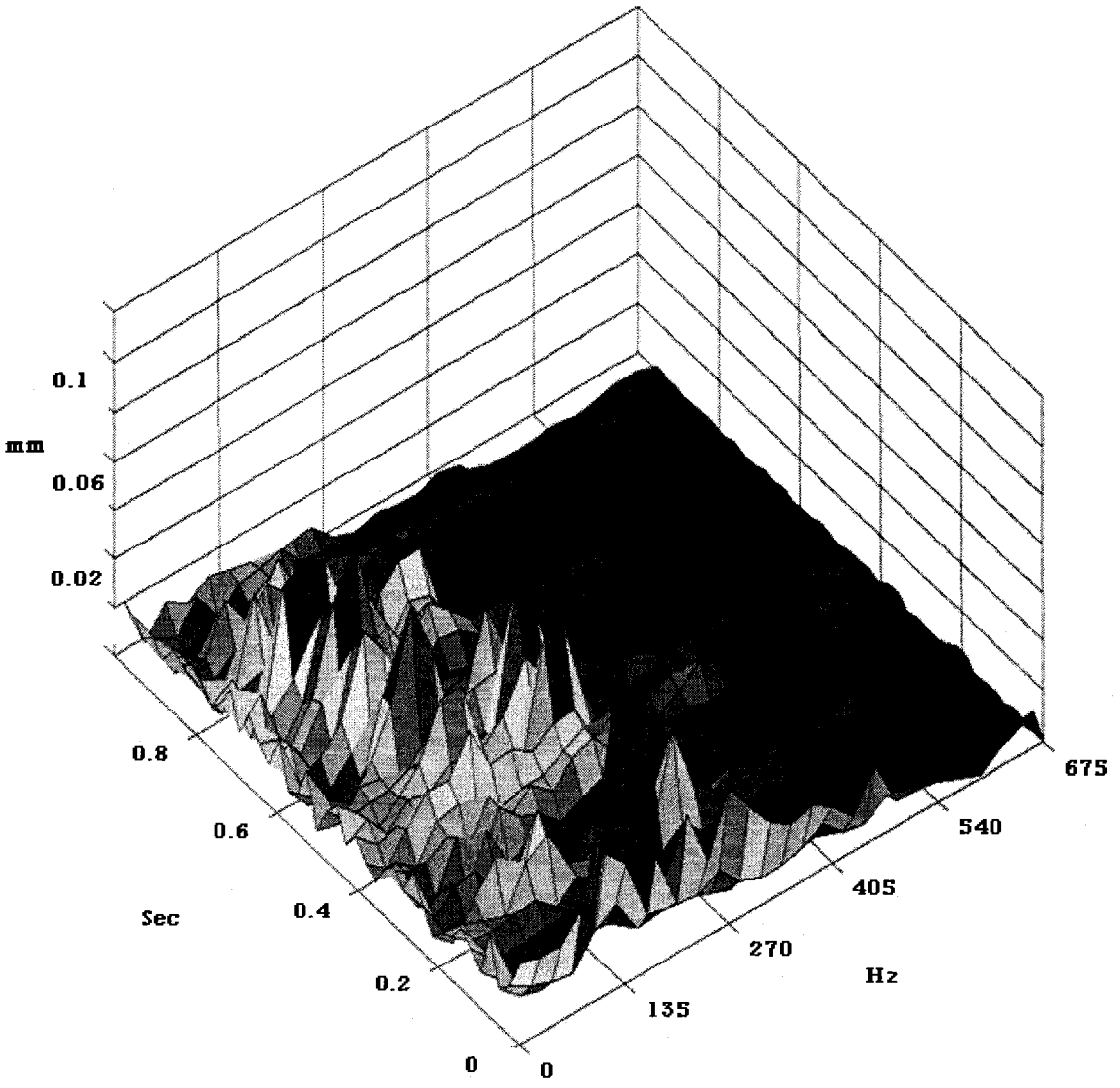

Figure 6.13: Waterfall diagram for the pump vibration signature

(Under internal instability operating conditions)

The pump has a different vibration signature when it is under internal dynamic instability. Figure 6.10 shows the pump vibration signatures with internal dynamic instability conditions. It can be seen that the vibration amplitude is high (± 0.3 mm), and exhibits an irregular behaviour.

In Figure 6.11, the time-scale representation (CWT) is shown for this case. The irregular behaviour can be observed in the time-scale representation, where the largest sub-band spreads within the (27-512) scale at t=990 mSec. Two other sub-bands with high energy can be seen at low-middle scales (1-209) at t=50 mSec, and at high scales (287-512) at t=200 mSec.

The coefficients of DWT for the unstable pump vibration signature are depicted in Figure 6.12. The seventh approximate coefficient amplitude rises at t= 50 mSec. and then it roughly settles at a constant value (0.02) to hike again at t=950 mSec.

The Waterfall diagram is represented in Figure 6.13. Two parallel series can be seen. The first series has the highest energy at t=50 mSec. and its frequency equals 180 Hz.

The characteristics can be summarized as follows:

1- The vibration signature varies irregularly within the range $\mp$ 0.3 mm
2- The CWT coefficients are scattered mainly in the middle scales.
3- The seventh approximate coefficient remains with a constant amplitude (0.028) at most times.
4- The high-energy frequency content can be seen in the waterfall diagram, and it occurs at t=50 mSec.

6.7.2 **Pipe under Flutter**

6.7.2.1 ***Problem Description***

Flutter is a common phenomenon in structure-fluid interaction. It happens when the fluid within the pipe delivers dynamic energy to the pipe instead of dissipating the energy through it, and the pipe damping is unable to dissipate that energy, forcing the pipe to vibrate excessively (the pipe loses its dynamic stability). The velocity at which the structure starts to flutter is named the flutter velocity. Flutter can be observed in different applications, such as in the ailerons and wings of aircraft and the pipe flutter in hydraulic systems. In every case, flutter has a negative impact on the structure, where it increases structural fatigue and reduces service life. Detecting flutter in fluid-structure systems is important in order to eliminate the cause of the flutter and improve a hydraulic system's performance. For a pipe with a single degree of freedom with mass M, damping C, and the stiffness K, the equation of motion is

$$M\ddot{y} + C\dot{y} + K\,y = 0 \tag{6.11}$$

When the pipe is filled with a fluid (the fluid in a stagnation state), the added fluid mass, M_1, will change the pipe's natural frequency, and the equation of motion is then

$$(M_1 + M)\ddot{y} + C\dot{y} + K\,y = 0 \tag{6.12}$$

The dynamic behaviour will be different when the fluid is in motion, and the new equation of motion can be written as

$$(M_1 + M)\ddot{y} + C\dot{y} + K\,y = F(t) \tag{6.13}$$

where $F(t)$ accounts for the force due to the moving fluid.

Naudascher and Rockwell (1994) proposed replacing the loading force F(t) by terms that account for the static and dynamic instabilities due to the fluid motion in the pipe. They suggest that the fluid motion introduces an added damping C_1 and an added stiffness K_1. Accordingly, Eq. (6.13) can be written as

$$(M_1 + M)\ddot{y} + C\dot{y} + K\,y = -(C_1\dot{y} + K_1 y) \tag{6.14}$$

and the final form of the equation of motion for a pipe conveying a fluid is

$$(M_1 + M)\ddot{y} + (C_1 + C)\dot{y} + (K_1 + K)y = 0 \tag{6.15}$$

or

$$M_{eq}\ddot{y} + C_{eq}\dot{y} + K_{eq}y = 0 \tag{6.16}$$

where

$M_{eq} = M_1 + M$ is the total mass of the pipe-fluid

$C_{eq} = C_1 + C$ is the total damping of the pipe-fluid

$K_{eq} = K_1 + K$ is the total stiffness of the pipe-fluid.

The system response is totally dependent upon the three terms (M_{eq}, C_{eq}, and K_{eq}). M_{eq}, C, and K are constant for the same pipe and fluid. There are no exact expressions for C_1 and K_1, however, Paidoussis [64] proposed two approximate expressions for $C_1, and\ K_1$ and related them to the fluid velocity and pipe geometry as follows

$$C_1 = c_d U \rho D L \tag{6.17}$$

$$K_1 = c_k \frac{U^2}{2} \rho D L \tag{6.18}$$

where ρ is the fluid density, U is the fluid velocity, D is the pipe diameter, L is the length of the pipe, c_d is the damping coefficient, c_k is the stiffness coefficient and is determined experimentally. c_d and c_k can take negative values depending on the fluid velocity and the boundary conditions.

From Eq. (6.16), the pipe-fluid natural angular frequency can be written as

$$\omega(u) = \sqrt{\frac{K_{eq}}{M_{eq}}} \tag{6.19}$$

and the damping ratio can be expressed as

$$\xi(u) = \frac{C_{eq}}{2\sqrt{K_{eq} M_{eq}}} \tag{6.20}$$

From the previous two equations, both the pipe-fluid natural frequency and the damping coefficient are dependent on the fluid velocity. This is because the fluid damping ratio and its stiffness decrease with increasing fluid velocity, and increase the fluid disturbance. The pipe starts to buckle at the values of fluid velocity that make, mathematically, the fluid stiffness negative, and then the pipe will be statically unstable, which is the condition for divergence. Next, the pipe starts to vibrate and its amplitude is amplified above a certain fluid velocity (flutter velocity) and then it vibrates faster with larger amplitude at higher velocity. In this case, the pipe is dynamically unstable, which

is known as flutter. This is another approach that can be implemented to identify the natural frequency and the damping coefficient for the pipe-conveying fluid (explained in chapter 3).

6.7.2.2 *Pipe Vibration Signature under Flutter Operating Conditions*

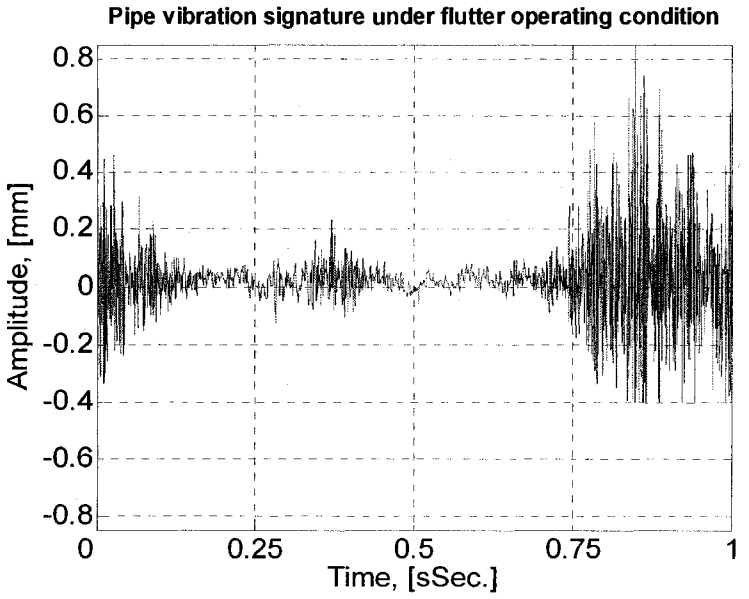

Figure 6.14: Pipe vibration signature

(Under flutter operating conditions)

6.7.2.3 *CWT for Pipe Vibration Signature under Flutter Operating Conditions*

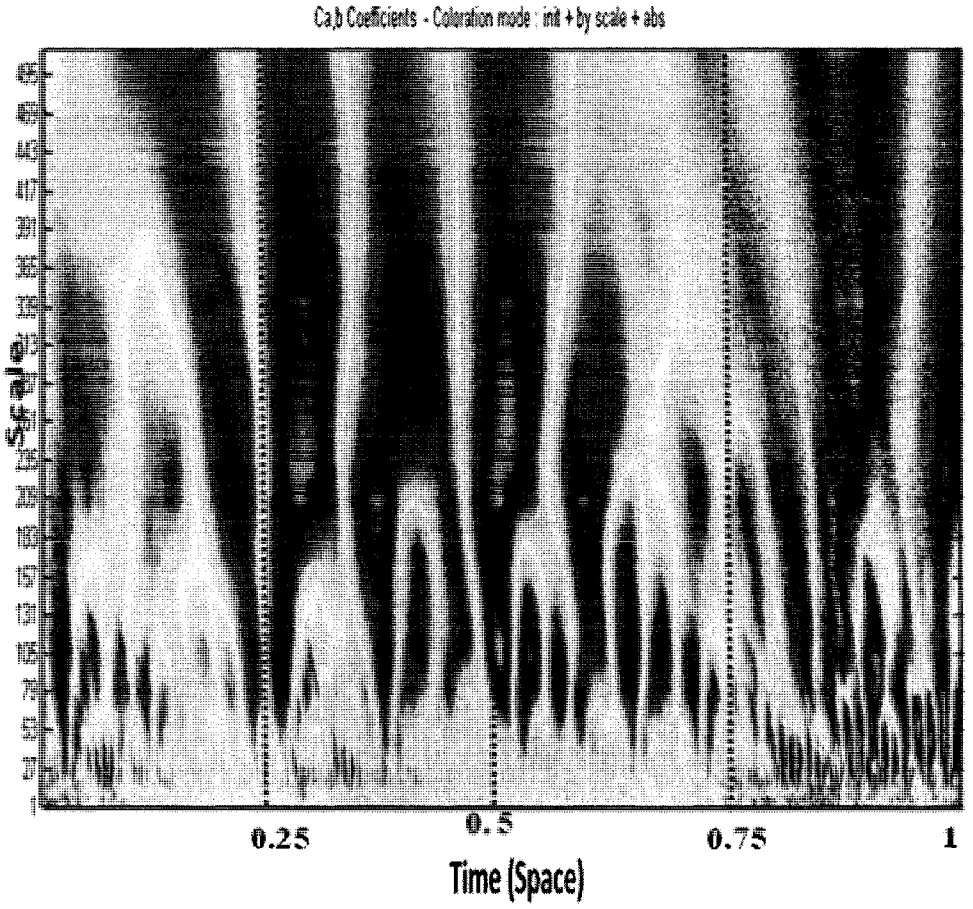

Figure 6.15: CWT for pipe vibration signature under flutter operating conditions

6.7.2.4 *DWT for Pipe Vibration Signature with Flutter Operating Conditions*

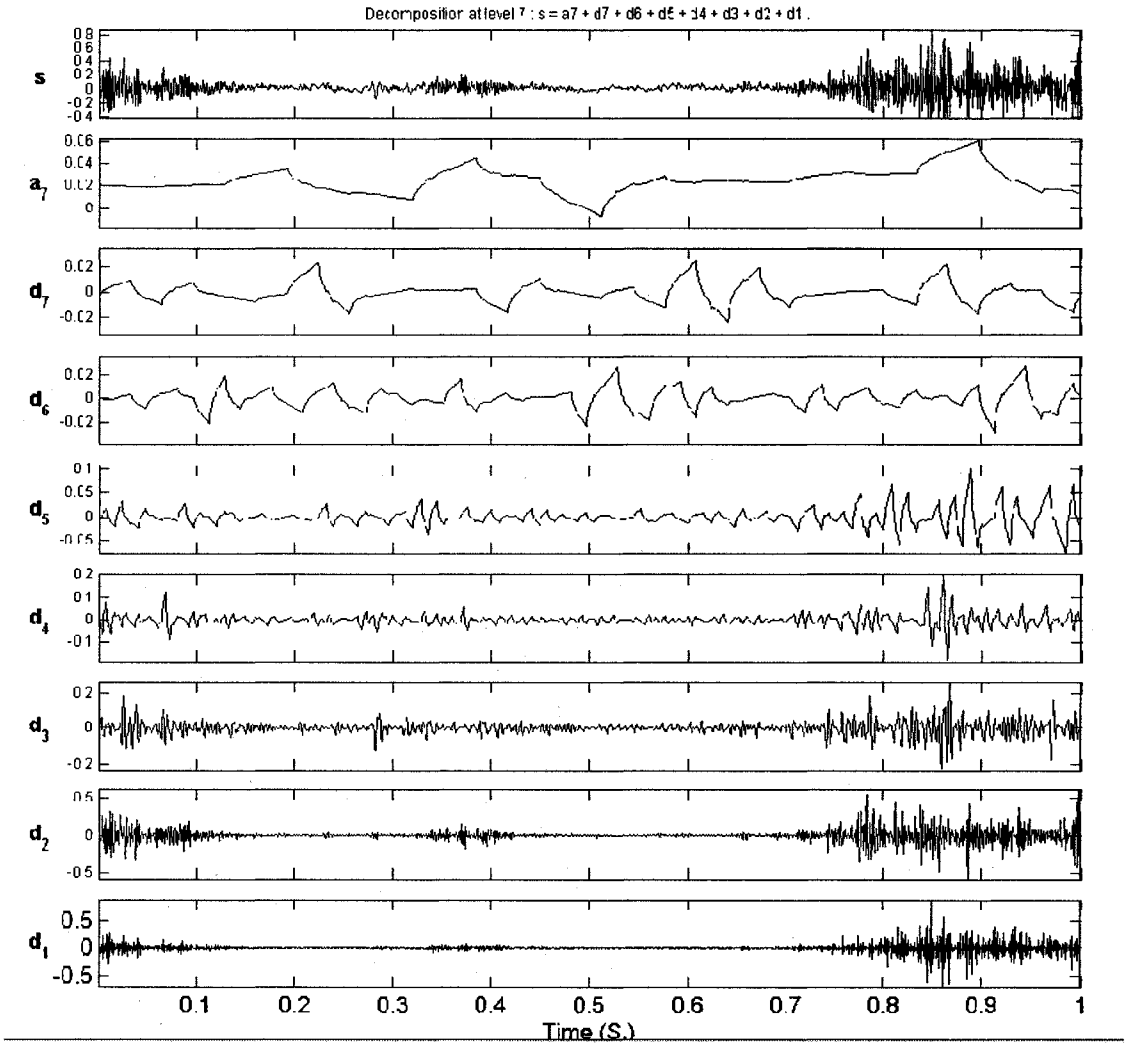

Figure 6.16: DWT for pipe vibration signature with flutter operating conditions

6.7.2.5 *Waterfall Diagram for Pipe Vibration Signature (Flutter Operating Conditions)*

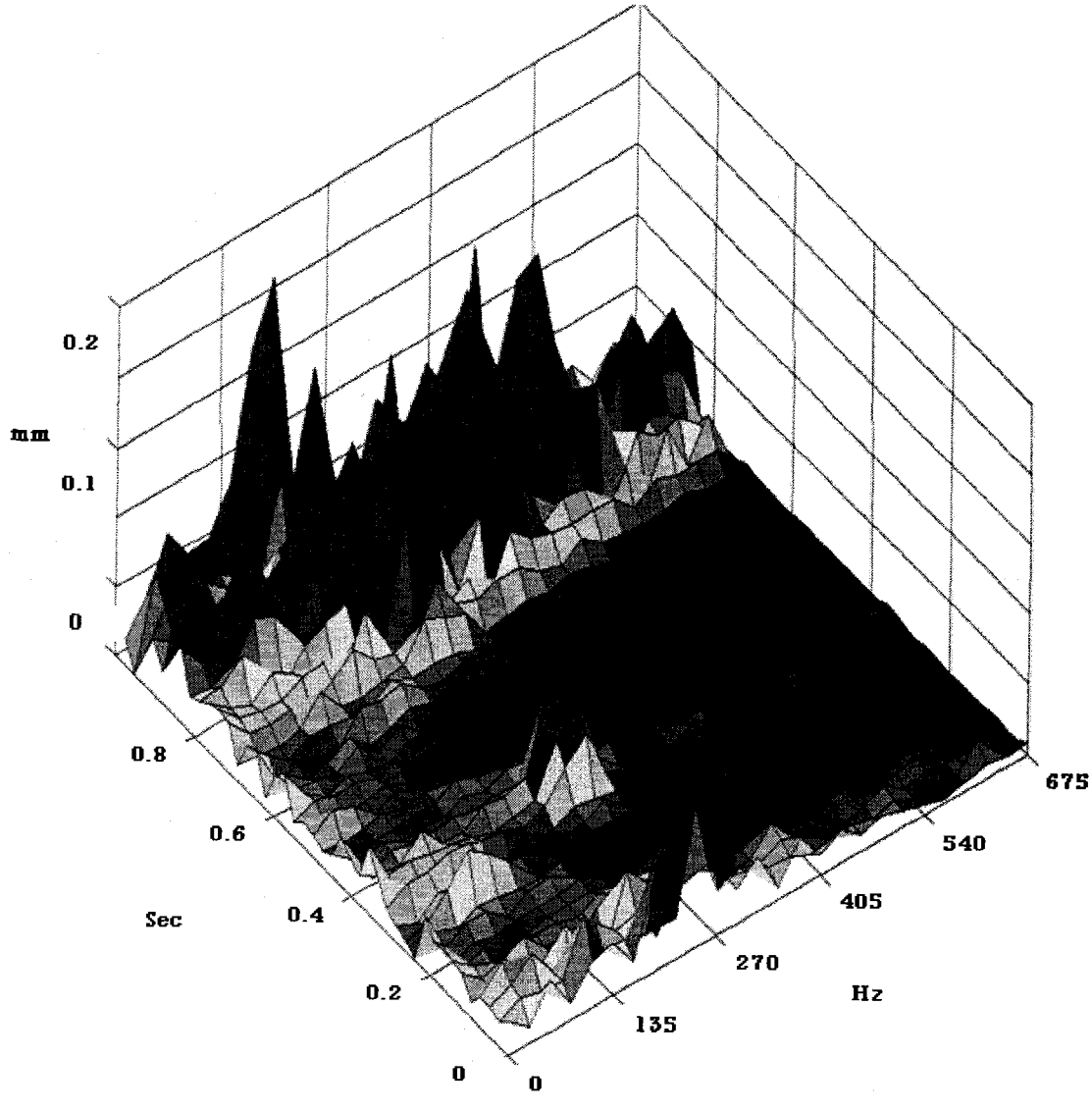

Figure 6.17: Waterfall diagram for the pipe vibration signature

(Under flutter operating conditions)

The pipe vibration signature (under flutter operating conditions) is illustrated in Figure 6.14. It can be noticed that the vibration amplitude is high (± 0.5 mm), and it is noisy.

Figure 6.15 represents the CWT of the flutter case, where different distributions for the frequency contents are shown. The contents are concentrated in the center of the Time-Scale representation and at higher scales (209-309). Other contents with wide bands start at low scales (27) and spread to the highest scales (512). These contents indicate the presence of flutter, where pipe amplitude is amplified.

The coefficients of DWT for the pipe signature under flutter operation are illustrated in Figure 6.16. The seventh approximate coefficient amplitude is 0.02; and it has a minima (equals zero) at t= 500 mSec., while its maxima is 0.06 at t= 900 mSec.

The Waterfall diagram for the pipe signature under flutter is shown in Figure 6.17. The vibration amplitude grows with time. This is a symptom of the flutter onset. The high amplitudes are developed starting from t=900 mSec.

<u>The summarized characteristics are:</u>

1. The vibration signature amplifies to reach (± 0.5 mm)
2. The CWT contains most of the coefficients within (209-309)
3. The seventh approximate coefficient has its minima (equals zero) at t=500 mSec., and its maxima is 0.06 at t=900 mSec.
4. High frequency contents, with the highest energy, can be seen at t= 900 mSec.

6.7.3 The Electric Motor under Electrical Unbalance in One of its Supply Lines

6.7.3.1 *Problem Description*

Hydraulic systems are used in different applications such as in civil and industrial systems and in energy distribution. They consist of: pumps, motors, pipes, valves and reservoirs. The heart of the system is the pump, which converts mechanical power to hydraulic power in the form of pressurized fluid. The pump is driven by a motor. There are two kinds of motors: electric motors for industrial applications, and internal combustion engines for mobile applications. About 95% of industrial applications use three-line motors to drive pumps. All lines of motors have the same value of voltage and are phase-shifted by 120^{o} in order to balance the lines. By definition, voltage balance occurs when the three voltage components have the same magnitude and are displaced at a phase angle of 120^{o}.

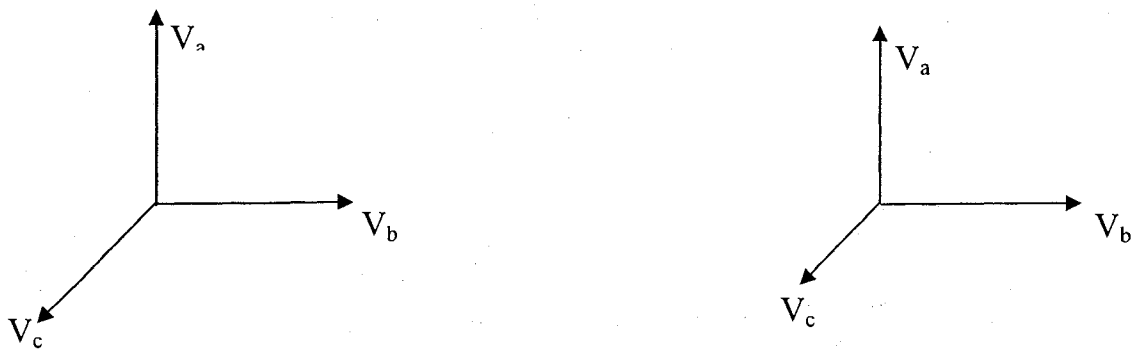

a: A balanced system b: An unbalanced system

Figure 6.18: Three-line voltage representation for an electric motor

Figure 6.18 shows a three-line motor representation, where Figure 6.18.a represents the voltage balance case and Figure 6.18.b illustrates the voltage unbalance case. The unbalance occurs due to uneven magnitudes of the three lines voltages.

One voltage cycle of a three-line AC motor has three sinusoidal waveforms, and in the case of voltage unbalance, there will be a change in one sinusoidal waveform. Figure 6.19 shows the voltage representation for a balanced and an unbalanced system.

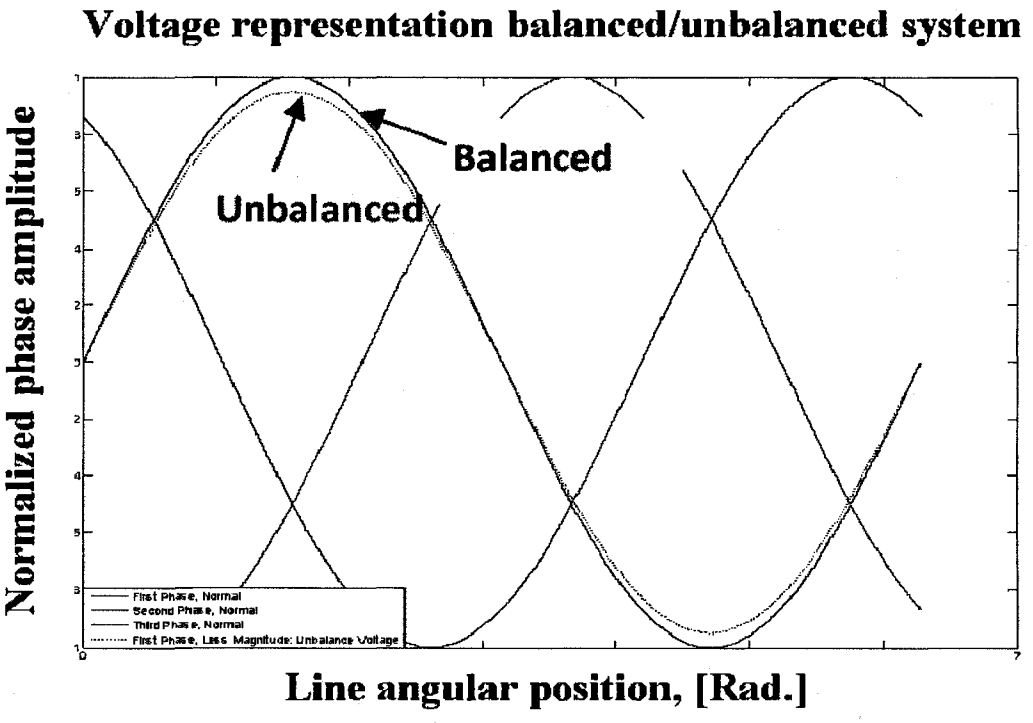

Figure 6.19: Voltage representation of a balanced and an unbalanced system

The seriousness of voltage unbalance is that it cannot be noticed visually nor does it produce noise. But, it has great impact on the motor's state, where voltage unbalance lowers the performance and reduces the life of the three-line motor. The amount of the unbalance will be amplified several times and this affects the induction current. For example, a three-line motor with a ratio of locked rotor current to running current of 6 will amplify a 5% voltage unbalance to 30% in unbalance for the motor line current (Von Jouanne and Banerja, [85]). Unbalanced current leads to torque pulsations, increased vibration and mechanical stresses, increased losses due to motor overheating, which shortens winding isolation.

The standard voltage of a three-line motor is 460 volts. Voltage unbalance is characterized as the percentage of maximum value of the absolute deviation of the line voltage from the average voltage on the three-line system, divided by the average voltage of the three lines. For example, if the measured line voltages are 464, 461, and 455, the average is 460 volts. The voltage unbalance, V.U, is

$$V.U = \frac{460 - 455}{460} 100 = 1.1\% \tag{6.21}$$

Voltage unbalance can occur for different reasons, such as unequal impedances in the three lines, or an unbalanced three-line load.

Hydraulic system components are in a state of continuous reaction among themselves. One component's performance will affect that of the other components. For example, damage in the motor, which drives the pump, will definitely affect the pump's performance. Knowledge of the ordinary signals of each component will enable us to identify the irregularity of the signal due to the abnormal behaviour of any component.

For this reason, it will be important to acquire signals of the different parts under normal operation and then detect changes in the signals to localize and isolate the reason for this irregularity. For example, a signal that is collected from a pump outlet or from a pipe can indicate the state of the motor and the pump; and by expanding this concept to include the entire hydraulic system, the vibration signals that are collected from the pipe can be used to obtain information about the entire system.

6.7.3.2 *Pump Vibration Signature with the Pump Driven by an Unbalanced Electric Motor: 0.5 Ω*

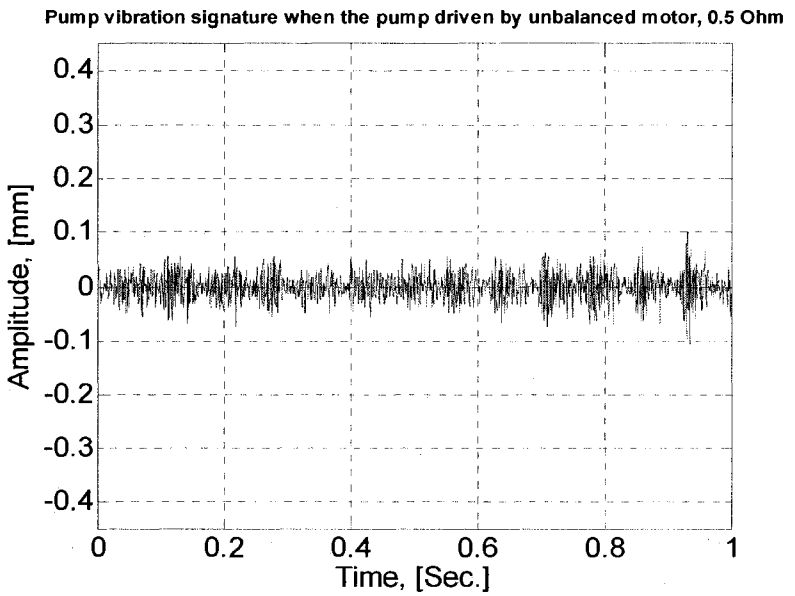

Figure 6.20: Pump vibration signature with the pump driven by an unbalanced electric motor, 0.5 Ω

6.7.3.3 *CWT for Pump Vibration Signature with the Pump Driven by an Unbalanced Electric Motor, 0.5 Ω*

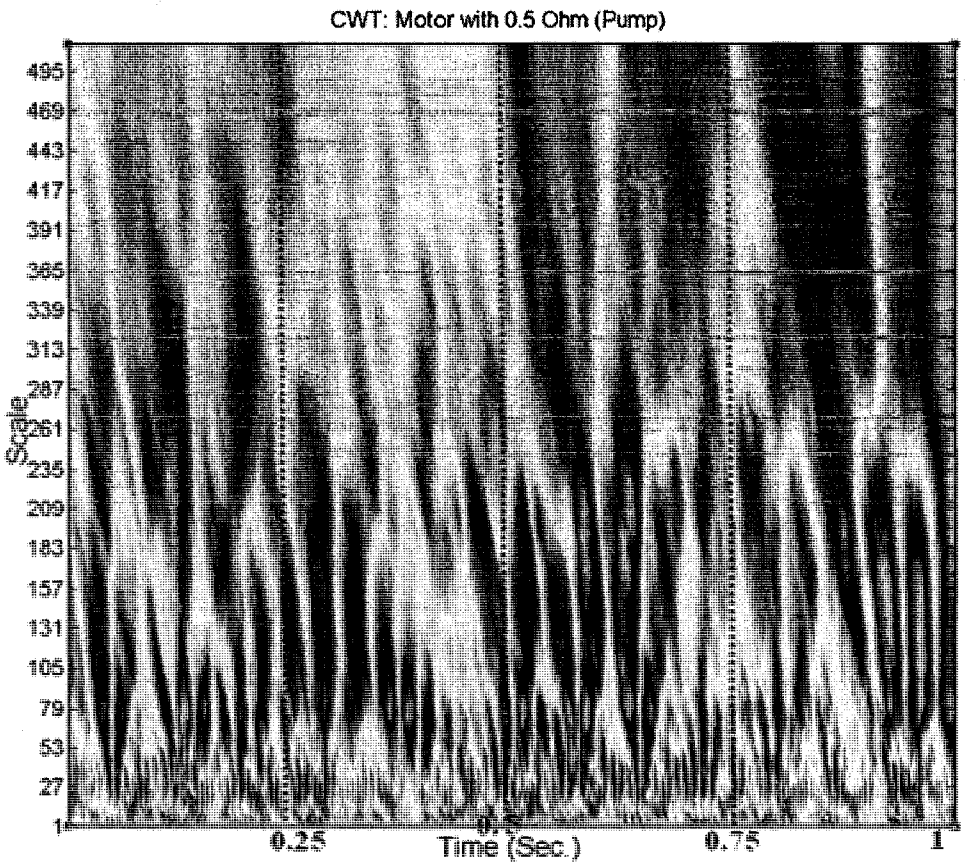

Figure 6.21: CWT for pump vibration signature with the pump driven by an unbalanced electric motor, 0.5 Ω

6.7.3.4 *DWT for Pump Vibration Signature with the Pump Driven by an Unbalanced Electric Motor, 0.5 Ω*

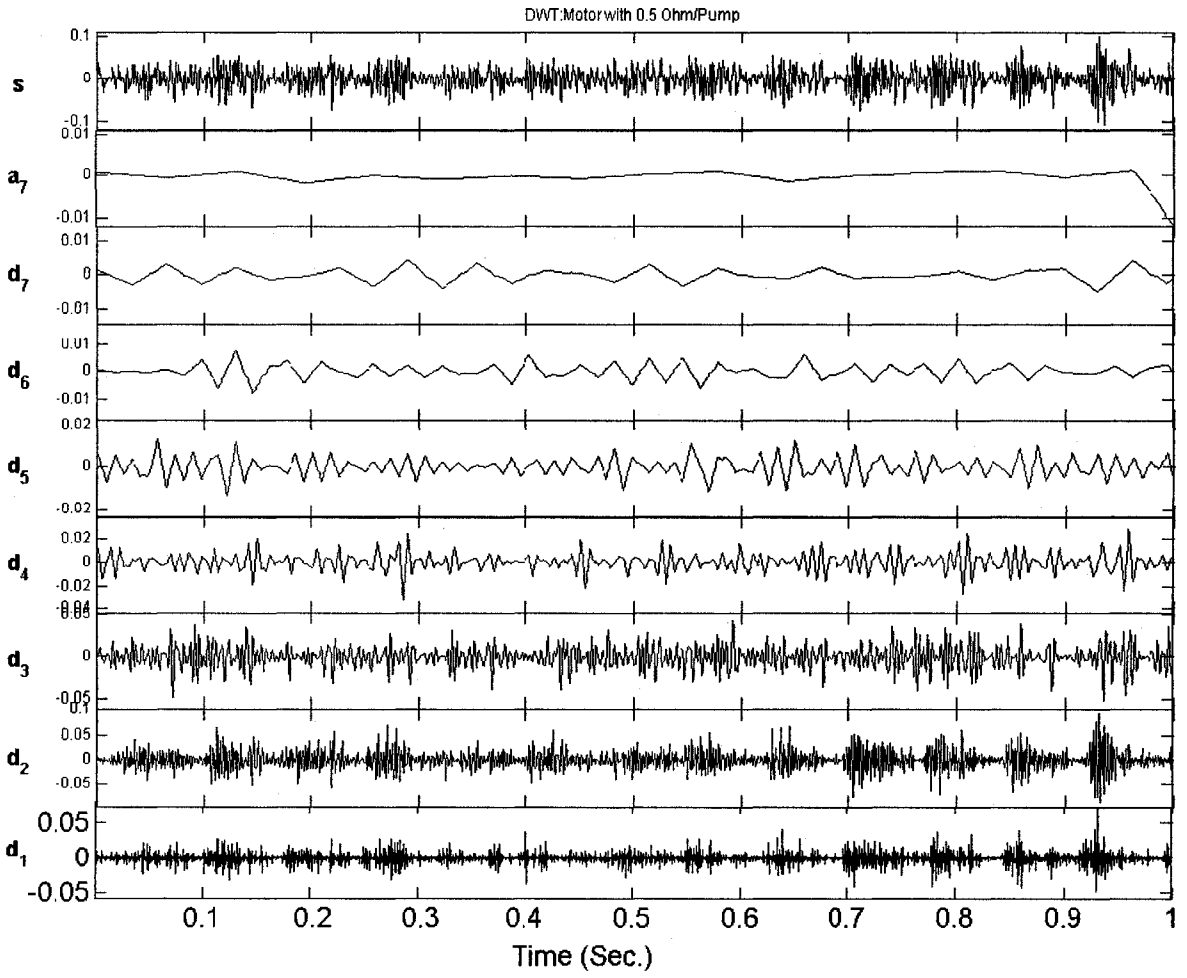

Figure 6.22: DWT for pump vibration signature with the pump driven by an unbalanced electric motor, 0.5 Ω

6.7.3.5 *Waterfall for Pump Vibration Signature with the Pump Driven by an Unbalanced Electric Motor, 0.5 Ω*

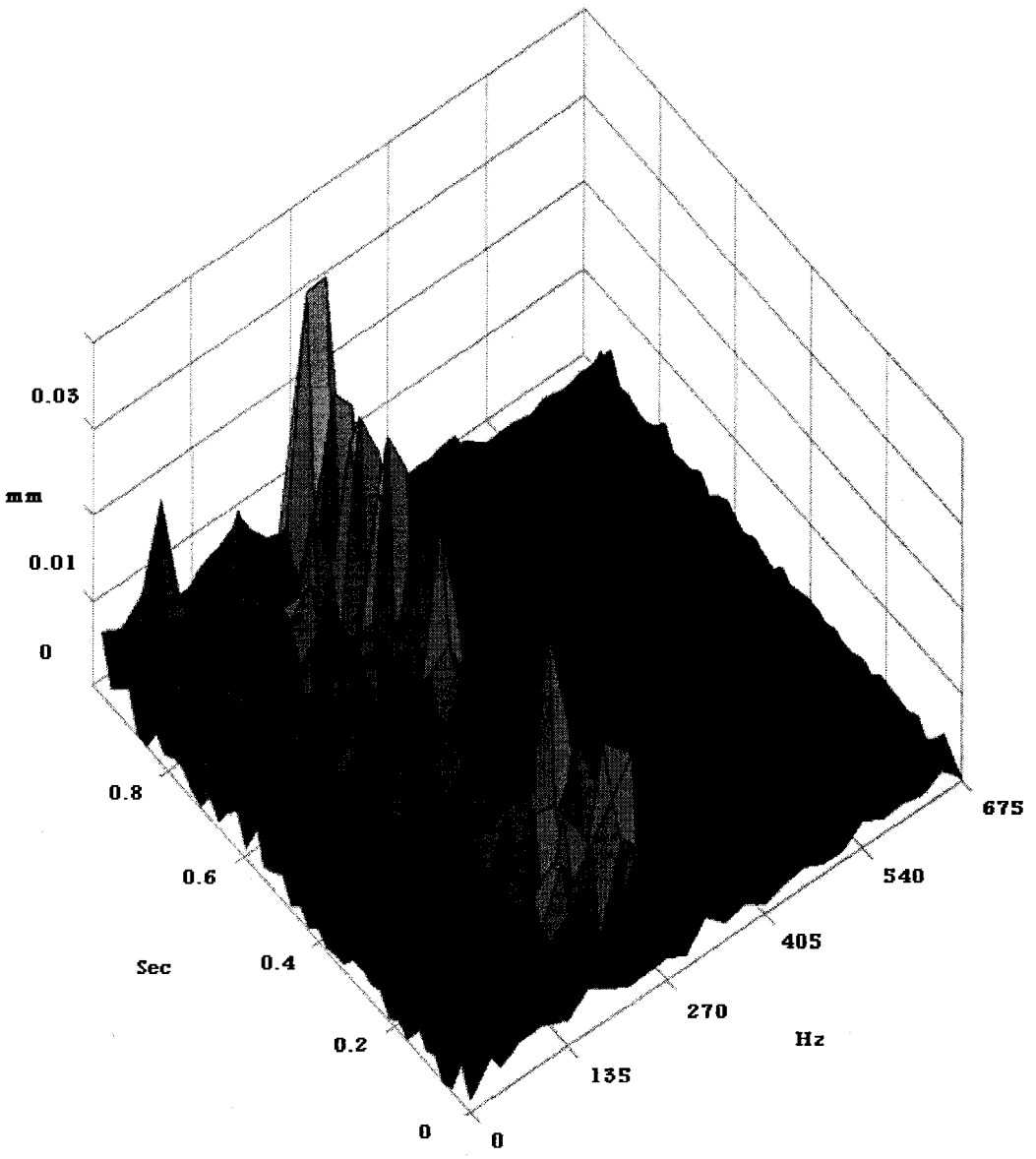

Figure 6.23: Waterfall diagram for pump vibration signature with the pump driven by an unbalanced electric motor, 0.5 Ω

The pump vibration signature (Pump Driven by an Unbalanced Electric Motor, 0.5 Ω) is illustrated in Figure 6.20. The amplitude varies in the range of (± 0.02 mm) most of the time. However, there is a spike with amplitude of ± 0.1 mm at t=950 mSec. This is due to the electrical unbalance.

The CWT for this case (Pump Driven by an Unbalanced Electric Motor, 0.5 Ω) is shown in Figure 6.21. The largest coefficient with the highest energy can be seen at the scale (79-512), and this occurs at t= 950 mSec.

The DWT coefficients are seen in Figure 6.22. The seventh approximate coefficient has zero amplitude most of the time, dropping to -0.01 at t= 950 mSec.

Similar results can be seen in the 3D representation (waterfall diagram), which is illustrated in Figure 6.23. The largest amplitude occurs at t=950 mSec.

The summarized characteristics are:

1. The vibration signature varies regularly within the range of ∓ 0.02 mm, with one spike (∓ 0.1) at t=950 mSec.
2. The CWT contains the largest coefficient, which is located within (79-512) at t=950 mSec.
3. The seventh approximate coefficient starts to change its amplitude (from zero to -0.01) at t=950 mSec.
4. The waterfall diagram shows the maximum amplitude 0.028 at t=950 mSec.

6.7.3.6 *Pipe Vibration Signature when the Pump is Driven by an Unbalanced Electric Motor, 0.5 Ω*

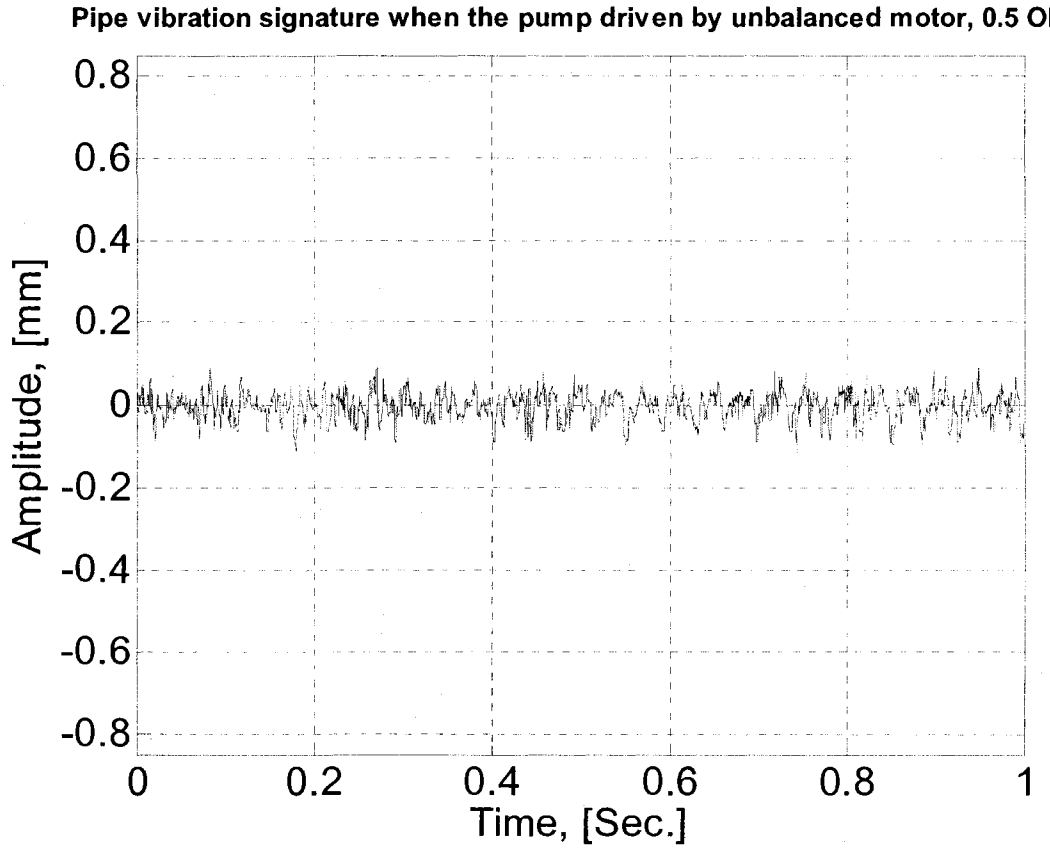

Figure 6.24: Pipe vibration signature when the pump is driven by an unbalanced electric motor: 0.5 Ω

6.7.3.7 *CWT of the Pipe Vibration Signature when the Pump is Driven by an Unbalanced Electric Motor: 0.5 Ω*

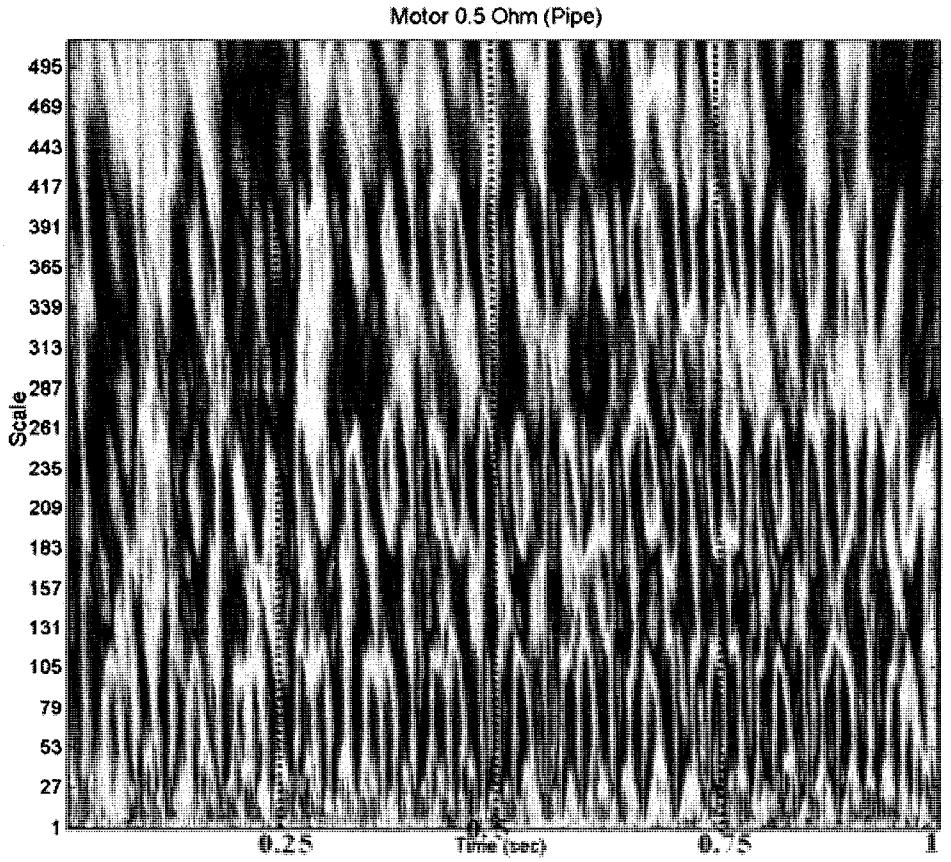

Figure 6.25: CWT of the pipe vibration signature when the pump is driven by an unbalanced electric motor, 0.5 Ω

6.7.3.8 *DWT of the Pipe Vibration Signature when the Pump is Driven by an Unbalanced Electric Motor: 0.5 Ω*

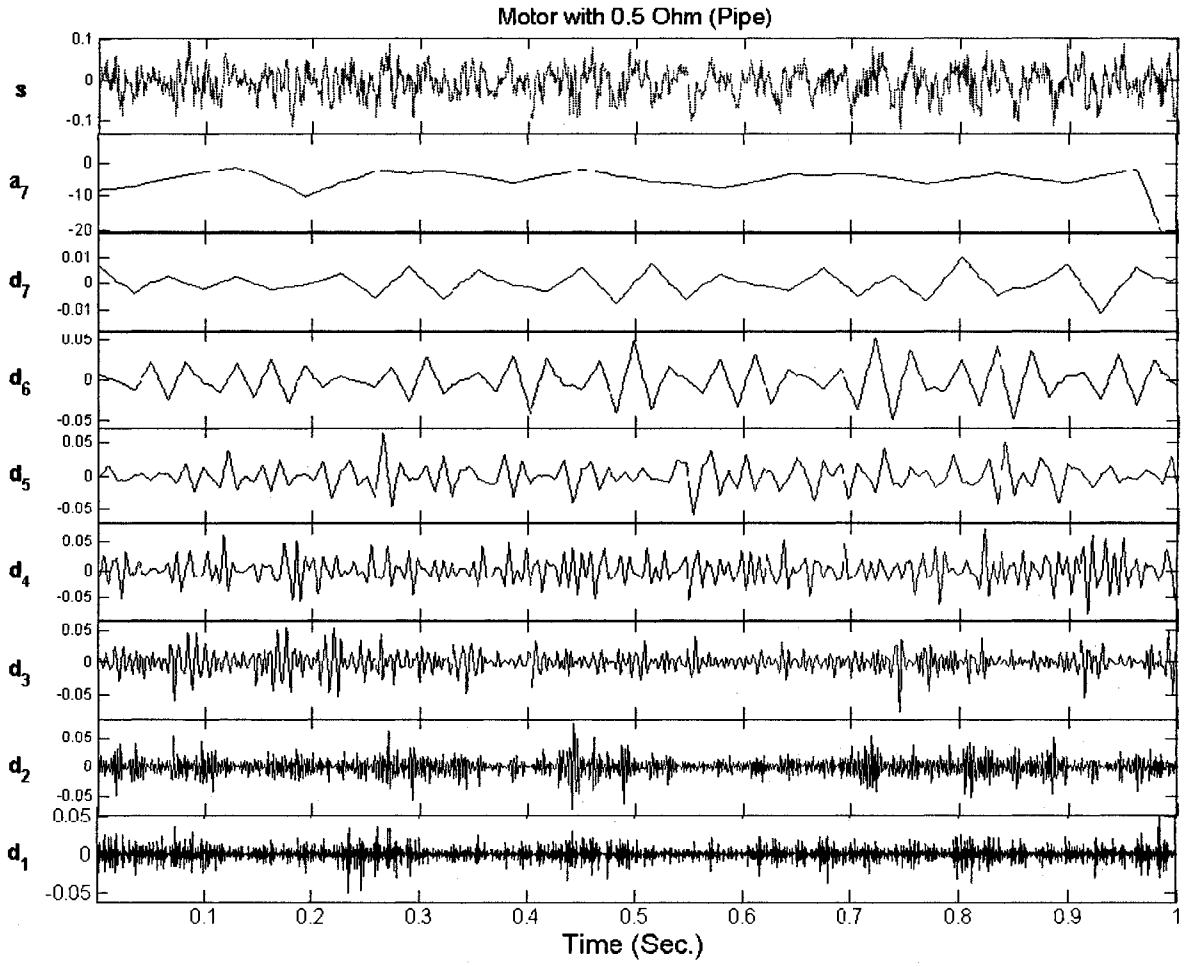

Figure 6.26: DWT of the pipe vibration signature when the pump is driven by an unbalanced electric motor, 0.5 Ω

6.7.3.9 *Waterfall for the Pipe Vibration Signature when the Pump is Driven by an Unbalanced Electric Motor: 0.5 Ω*

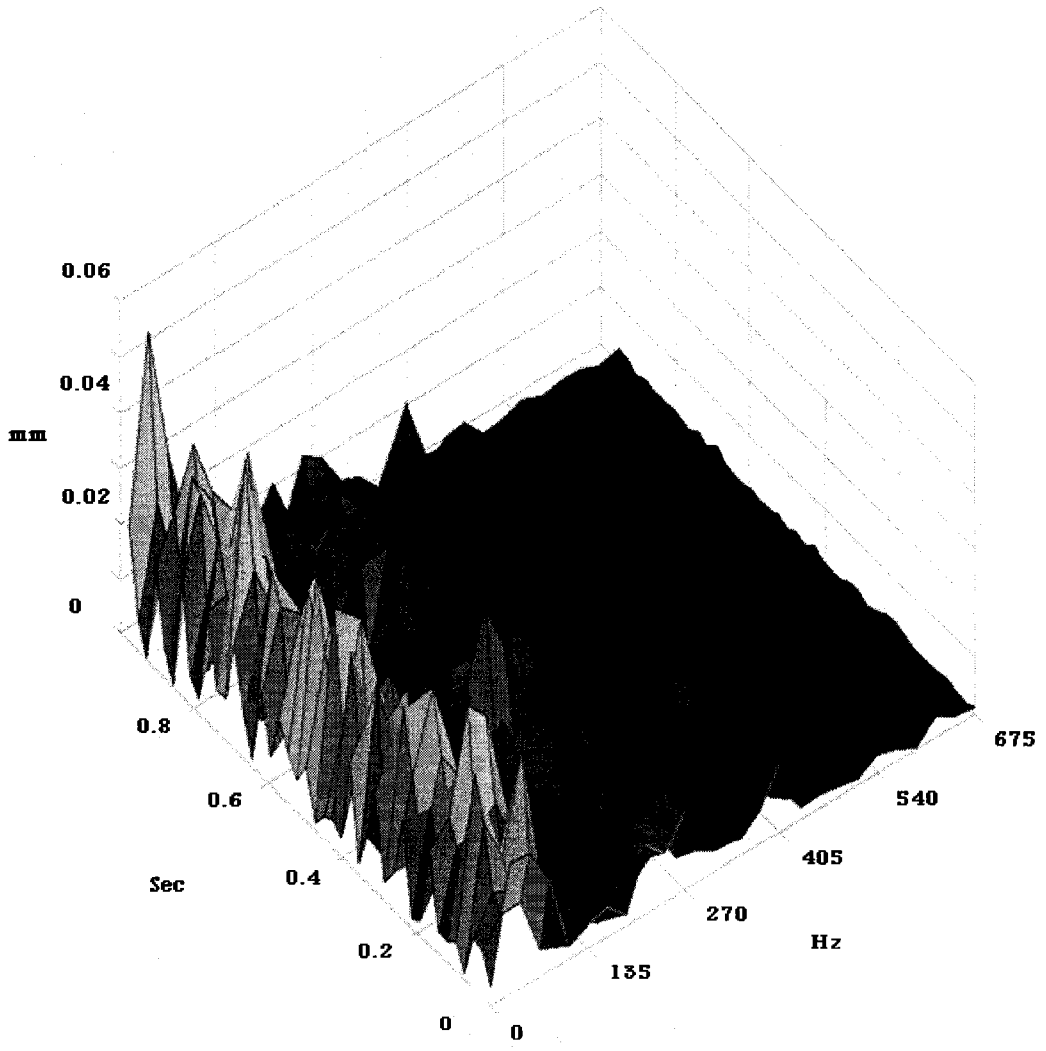

Figure 6.27: Waterfall diagram of the pipe vibration signature when the pump is driven by an unbalanced electric motor (0.5 Ω)

The signature of the pipe (when the pump is driven by an unbalanced electric motor, 0.5 Ω) response is shown in Figure 6.24. This signature does not give the required

information. Hence, WT and Waterfall diagrams are illustrated in Figure 6.25, Figure 6.26, and Figure 6.27.

In Figure 6.25, the CWT reveals that the two largest coefficients can be seen at middle to large scales (200-512), and that they occur at t=250 and 950 mSec.

The DWT coefficients of this case are represented in Figure 6.26. The seventh approximate coefficient has a constant value (-10) at almost all times, dropping at t=950 mSec.

The waterfall diagram of this case is illustrated in Figure 6.27. There is a series of low frequencies at almost all times. However, the maximum amplitude (0.06 mm) is seen at t=950 mSec.

We can briefly classify the characteristics of this case, as follows:

1. The vibration signature varies regularly within a range $\mp$ 0.02 mm. However, there a set of a periodic pair spikes with amplitude ($\mp$ 0.1 *and* $\mp$ 0.08 mm, respectively)
2. The CWT contains two large coefficients at (200-512)
3. The seventh approximate coefficient remains with a constant amplitude (-10) at most times, except for the last 50 mSec.
4. A 10 Hz frequency band can be seen at most times, and the maximum amplitude equals 0.06 mm at t=950 mSec.

6.7.3.10 *Pump Vibration Signature when the Pump is Driven by an Unbalanced Electric Motor, 1 Ω*

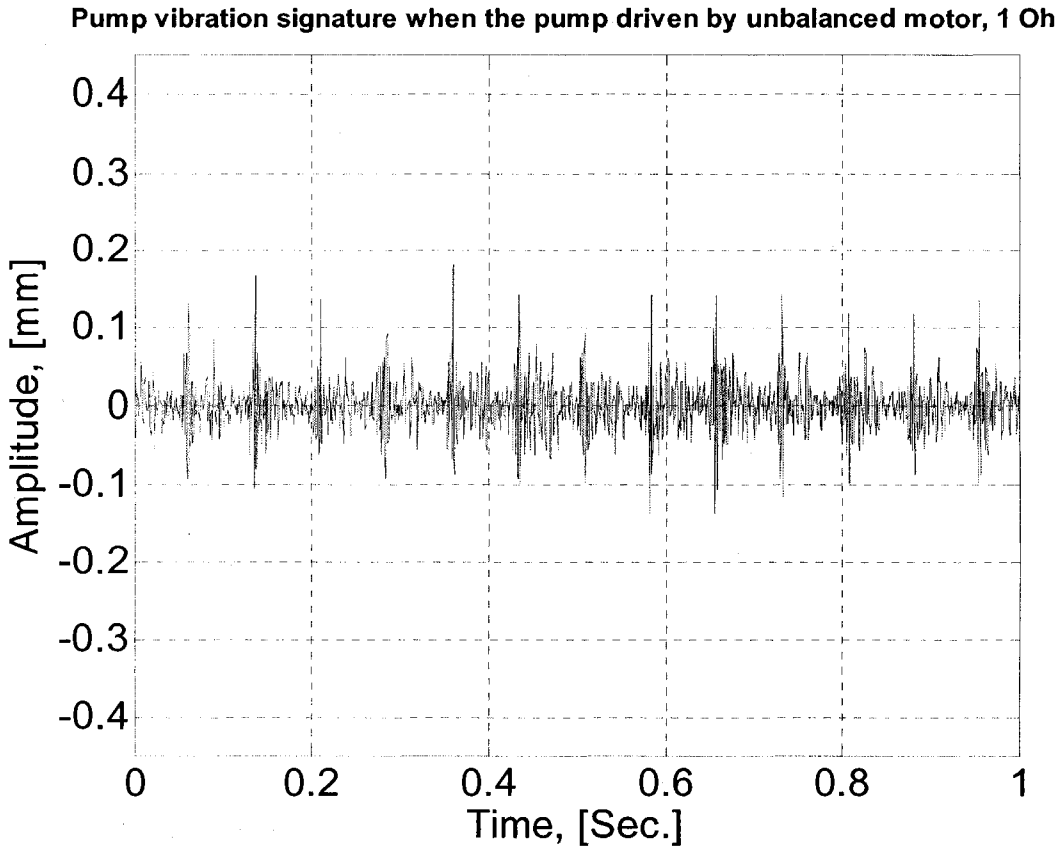

Figure 6.28: Pump vibration signature when the pump is driven by an unbalanced electric motor (1 Ω)

6.7.3.11 *CWT for the Pump Vibration Signature when the Pump is Driven by an Unbalanced Electric Motor, 1 Ω*

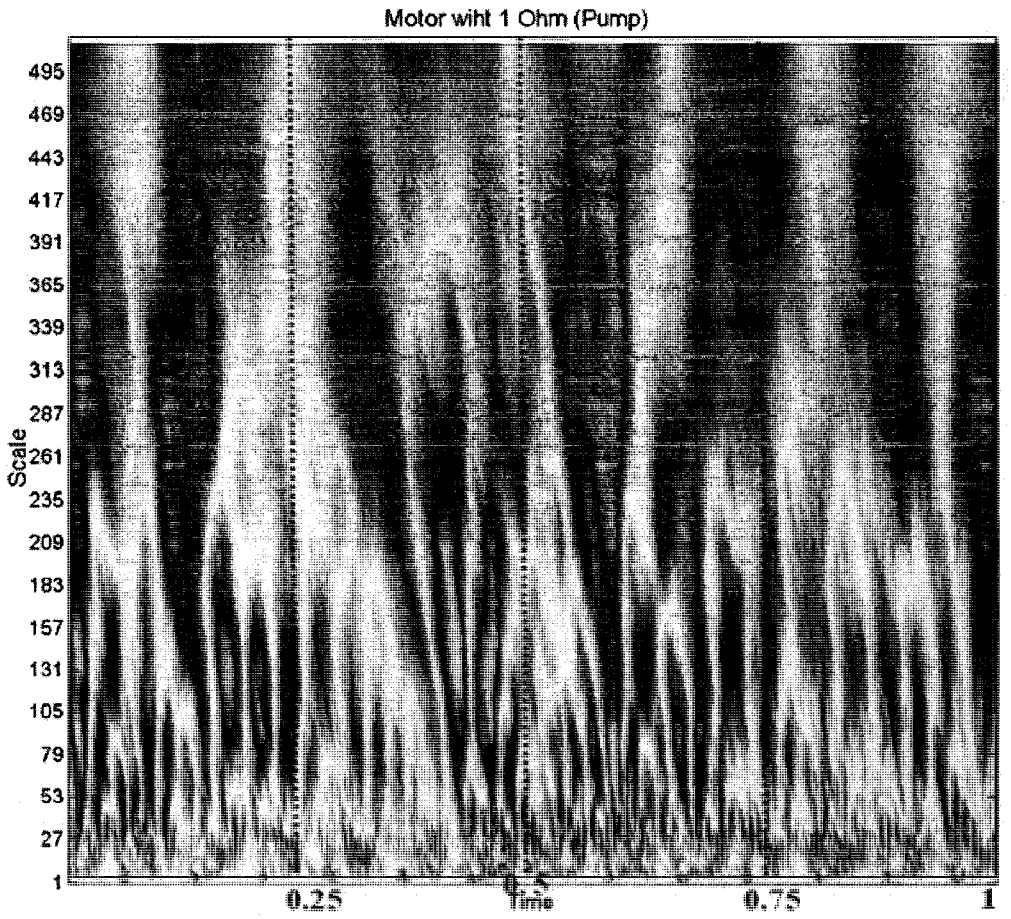

Figure 6.29: CWT for the pump vibration signature when the pump is driven by an unbalanced electric motor (1 Ω)

6.7.3.12 *DWT for the Pump Vibration Signature when the Pump is Driven by an Unbalanced Electric Motor, 1 Ω*

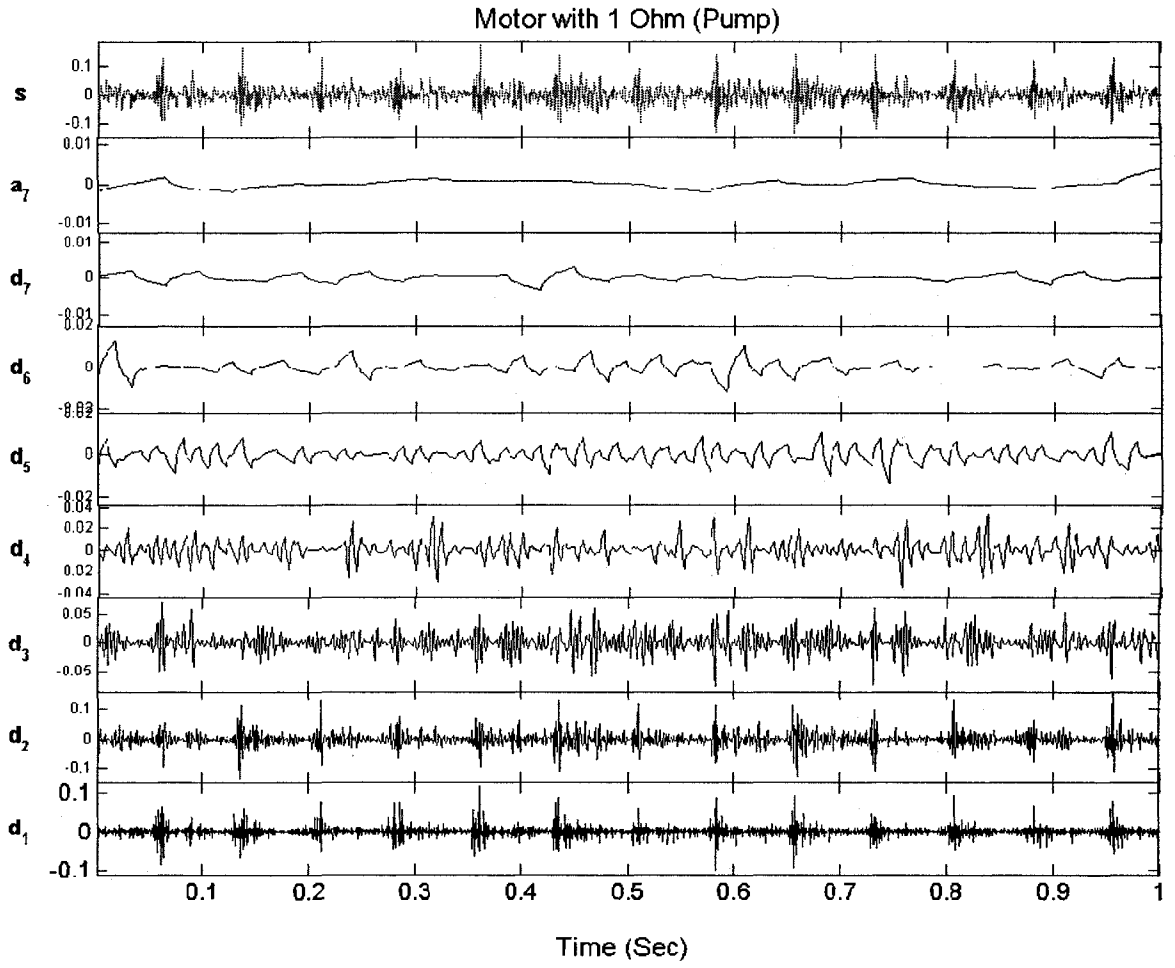

Figure 6.30: DWT for the pump vibration signature when the pump is driven by an unbalanced electric motor (1 Ω)

6.7.3.13 *Waterfall Diagram for the Pump Vibration Signature when the Pump is Driven by an Unbalanced Electric Motor, 1 Ω*

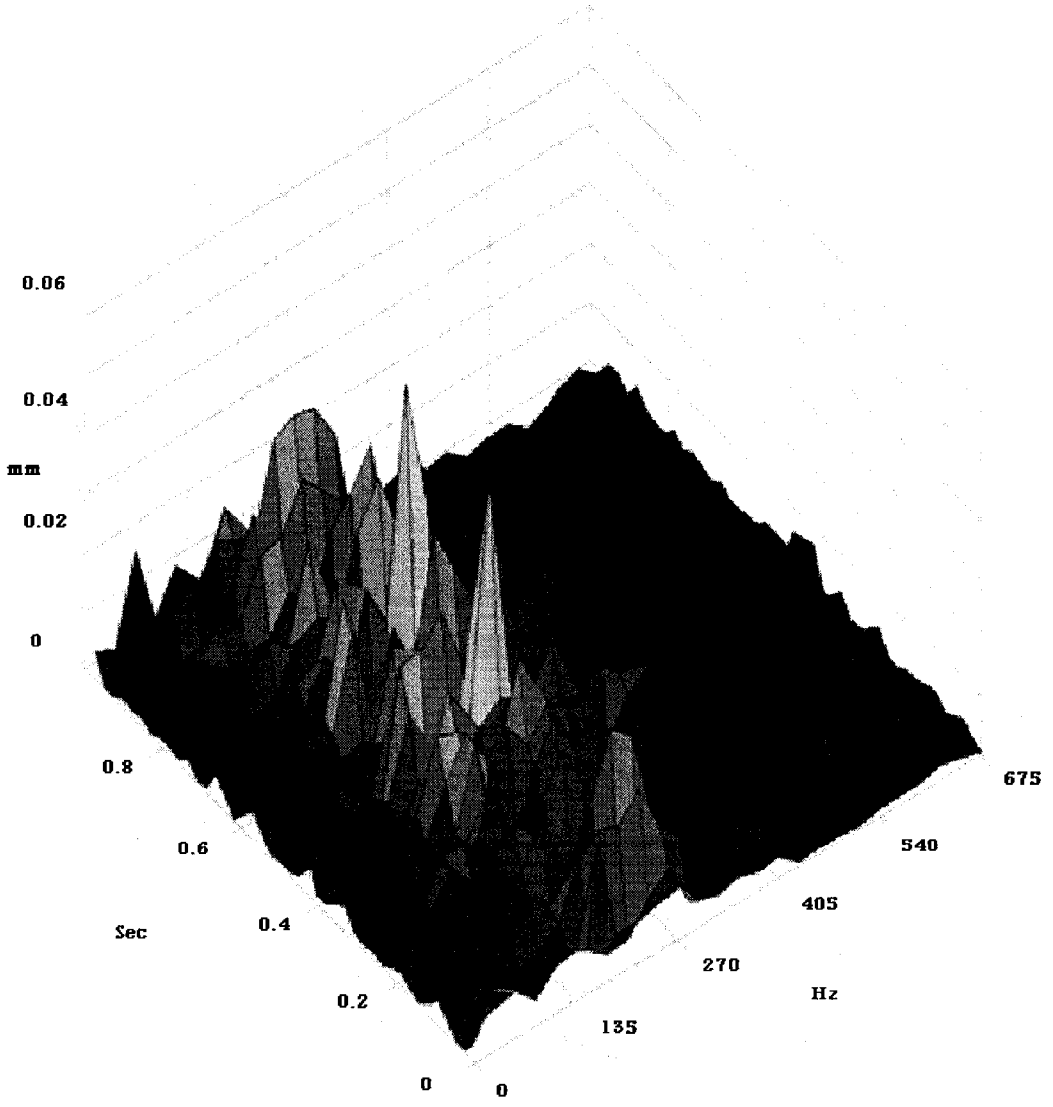

Figure 6.31: Waterfall diagram for the pump vibration signature when the pump is driven by an unbalanced electric motor (1 Ω)

The pump vibration signature when it is driven by an unbalanced electric motor (1 Ω) is shown in Figure 6.28. The vibration signature vibrates regularly within a range of $\mp$ 0.05 mm. However, there is a set of periodic pair of spikes with amplitude ($\mp$ 0.12 *and* $\mp$ 0.1 mm).

The CWT of this case is illustrated in Figure 6.29. We can see that more coefficients spread at the middle and high scales (79-512), and they can also be seen at the edges and at the center of the figure.

The DWT of the pump under this case is shown in Figure 6.30. The seventh approximate coefficient equals almost zero at all times.

The waterfall representation (Figure 6.31) indicates the presence of two maximum frequency values with amplitudes of 0.025 and 0.03mm; and they occur at t=0.400 and 600 mSec.

The characteristics of this case are:

1- The vibration signature has a pair of spikes with amplitudes of $\mp$ 0.12 and $\mp$ 0.1 mm, respectively.
2- Most of the CWT coefficients can be seen in the middle and high scales (79-512).
3- The seventh approximate coefficient does not change its amplitude (zero at all times).
4- The waterfall diagram shows two frequencies with the highest amplitude of 0.025 and 0.03mm.

6.7.3.14 *Pipe Vibration Signature when the Pump is Driven by an Unbalanced Electric Motor: 1 Ω*

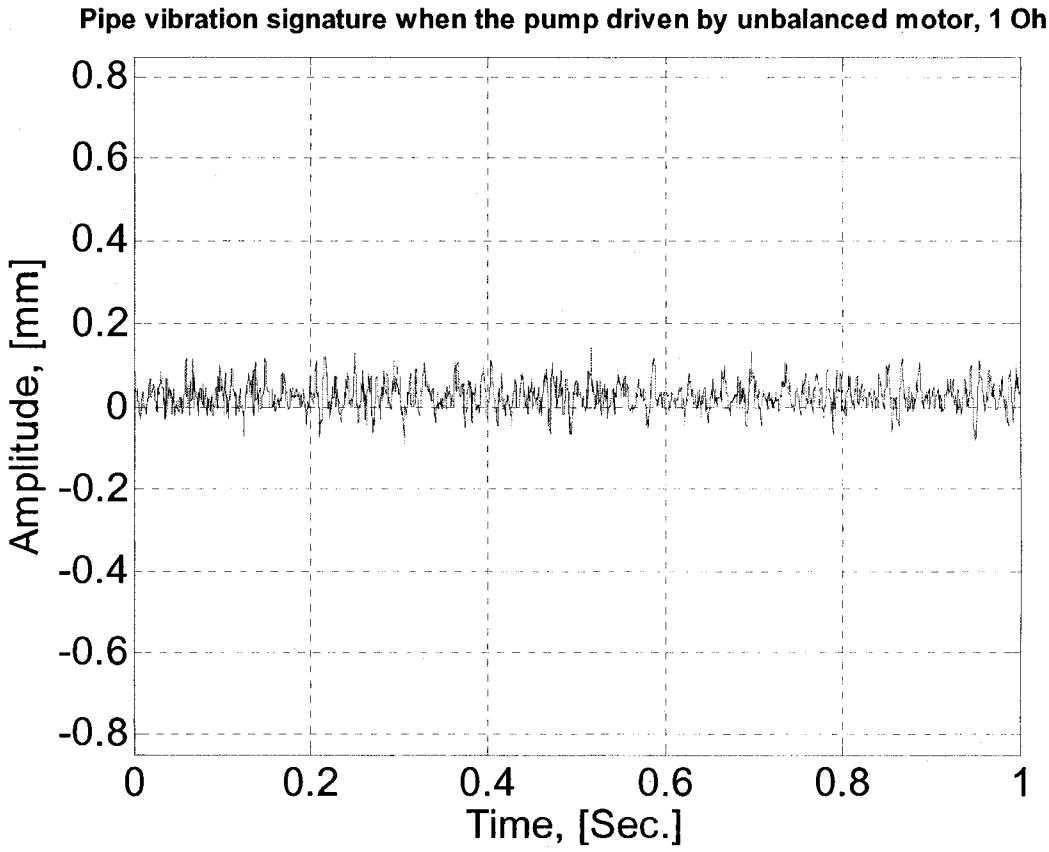

Figure 6.32: Pipe vibration signature when the pump is driven by an unbalanced electric motor (1 Ω)

6.7.3.15 *CWT for the Pipe Vibration Signature when the Pump is Driven by an Unbalanced Electric Motor, 1 Ω*

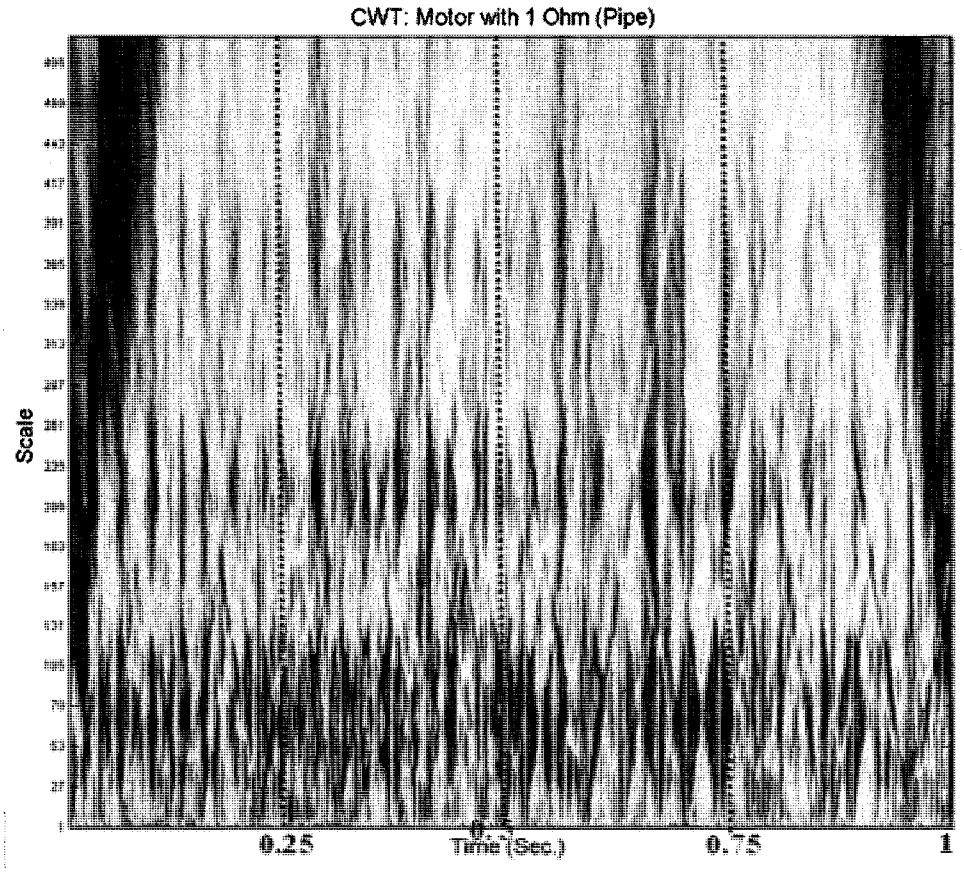

Figure 6.33: CWT for the pipe vibration signature when the pump is driven by an unbalanced electric motor 1 Ω

6.7.3.16 *DWT Pipe Vibration Signature when the Pump is Driven by an Unbalanced Electric Motor, 1 Ω*

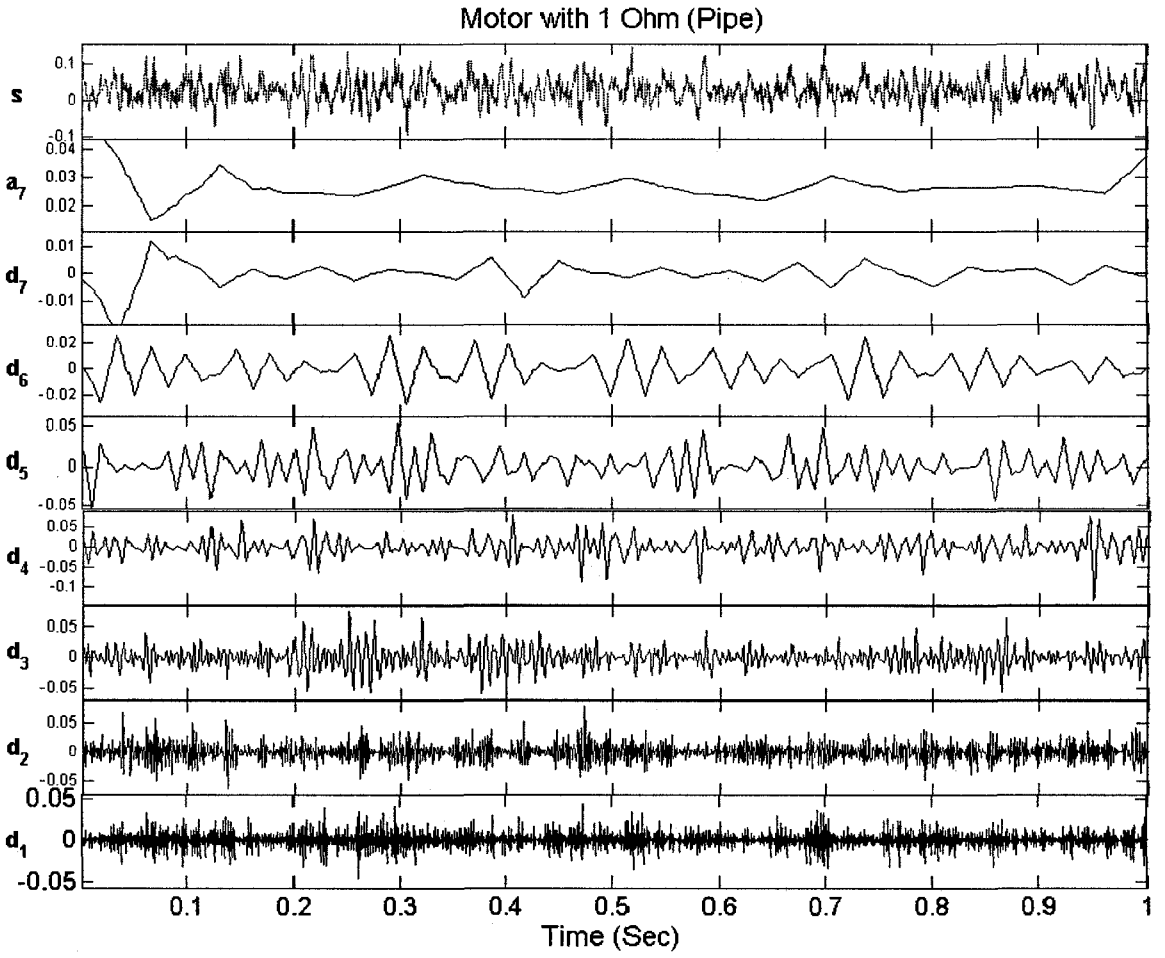

Figure 6.34: DWT for the pipe vibration signature when the pump is driven by an unbalanced electric motor (1 Ω)

6.7.3.17 *Waterfall Diagram for the Pipe Vibration Signature when the Pump is Driven by an Unbalanced Electric Motor, 1 Ω*

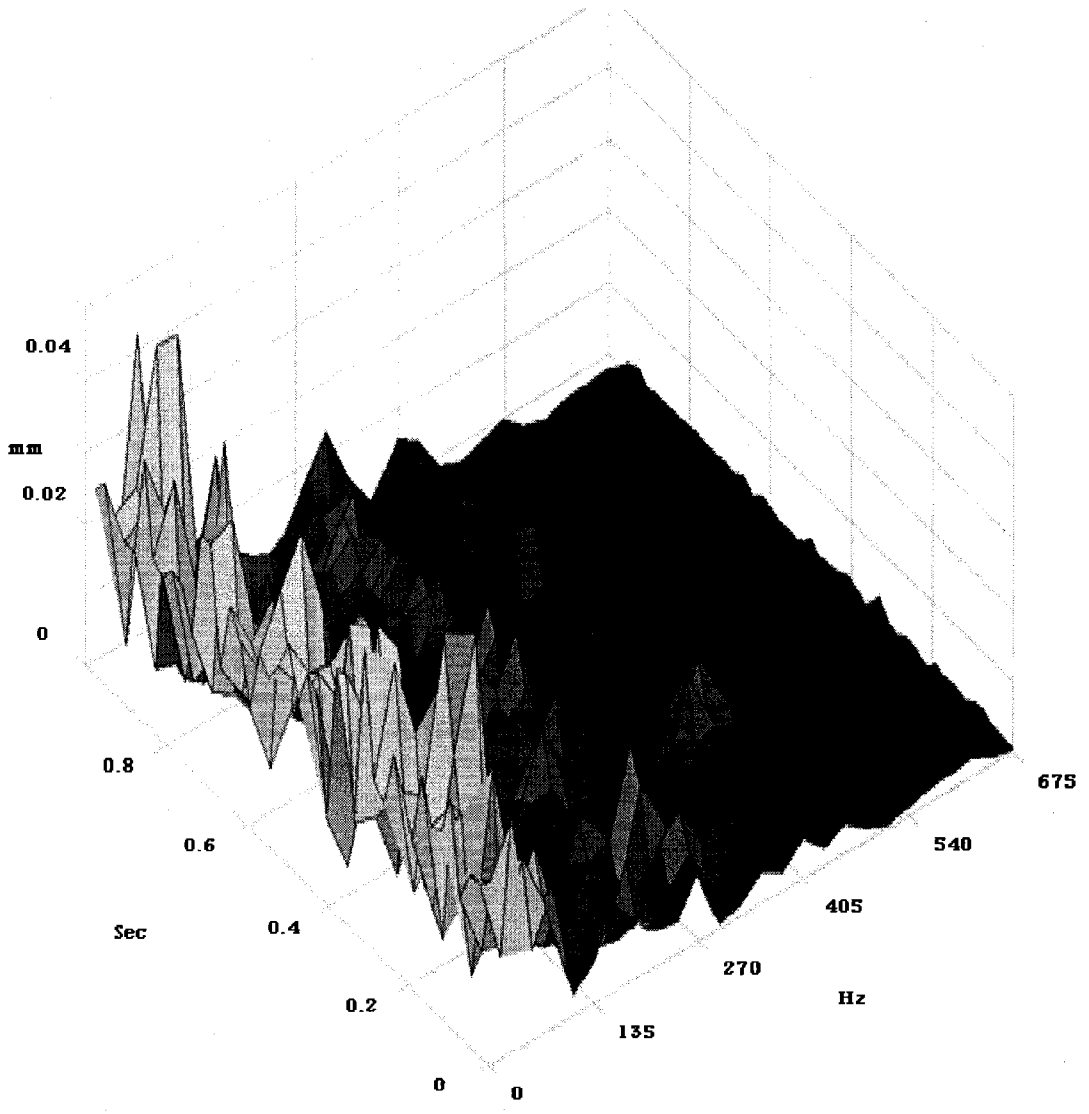

Figure 6.35: Waterfall diagram for the pipe vibration signature when the pump is driven by an unbalanced electric motor (1 Ω)

The pipe vibration signature (with the ump riven by an unbalanced electric motor 1 Ω) is illustrated in Figure 6.32. There is a kind of regularity in the pipe response, and the pipe vibrates mainly within the range of ∓ 0.1 mm.

Figure 6.33 shows the CWT for the pipe vibration signature when the pump is driven by an unbalanced electric motor 1 Ω. The regularity that was observed in the pipe response can be seen in the middle scales (27-105). However, two large sub-bands can be seen at the edges of the figure at t = 20 and t = 980 mSec., respectively.

The DWT coefficients are shown in Figure 6.34. The maxima (0.045) of the seventh approximate coefficient occur at t= 20 mSec., and then it drops to have its minima (0.018) at t=50 mSec. Afterwards, the coefficient settles at 0.02 mm.

Figure 6.35 represents the waterfall diagram for this case. A set of low frequencies can be seen at almost times. The maximum amplitude (0.04 mm) occurs at t=980 mSec.

The characteristics of this case are:

1- The vibration amplitude is regular and it varies within the range ∓ 0.1 mm.
2- At t=20 and t=980 mSec., two large sub-bands are extended from small to large scales (80-512)
3- The maxima of the seventh approximate coefficient takes place at t= 20 mSec., and its amplitude equals 0.045 mm
4- The waterfall diagram shows that the largest amplitude (0.04 mm) occurs at t=980 mSec.

6.8 Fast Fourier Transform (FFT)

In the previous sections, clear ideas about the signals evolution were carried out by transforming those using WT and Waterfall diagrams. The exact frequencies can be obtained from FFT. In the following section, the FFTs for the different cases will be displayed.

6.8.1 FFT for Pump Instability vs. Normal Pump

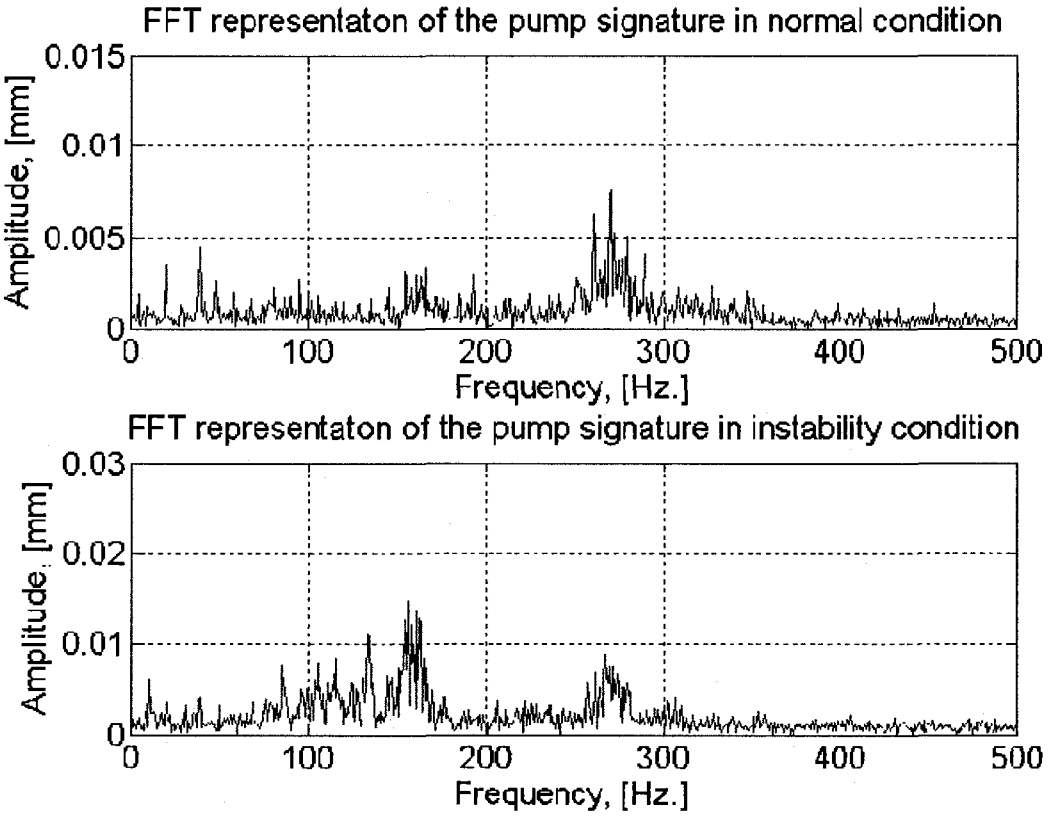

Figure 6.36: FFT representation of the pump signatures under normal and instability conditions

From Figure 6.36, it can be noticed that the frequency amplitudes increase dramatically when the pump is equipped with a PD controller (creating dynamic instability). For example, the dominant frequency amplitude equals 0.0075 mm; however, for the unstable pump, the maximum amplitude of the frequency jumps to 0.015 mm.

6.8.2 FFT for Pump Driven by an Unbalanced Electric Motor vs. Normal Pump

With normal operating conditions, the dominant frequency is equal to 270 Hz, and its amplitude is 0.0075 mm. There are two different dominant frequencies with different amplitudes, and they are 0.0085 mm and 0.009 mm for the electrical unbalance (0.5 Ω and 1 Ω) cases, respectively. These results are shown in Figure 6.37.

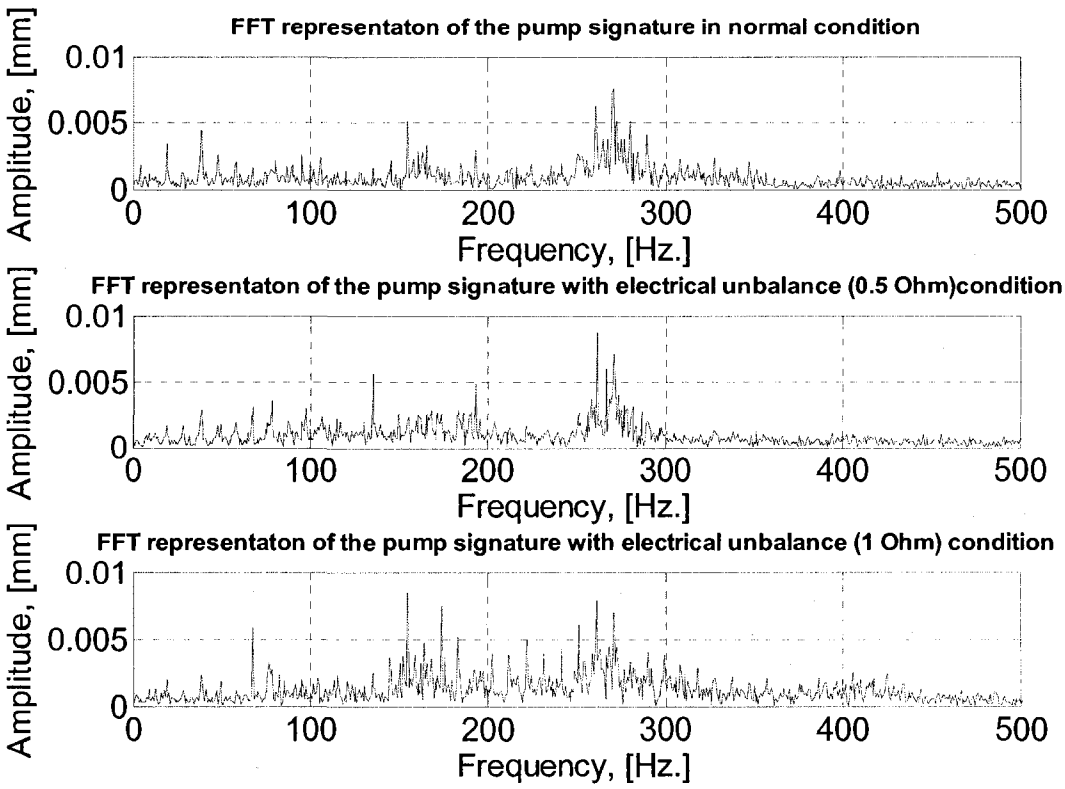

Figure 6.37: FFT representation of the pump signatures under normal and electrical unbalance conditions (0.5 Ω and 1 Ω)

6.8.3 **FFT for Pipe Flutter vs. Normal Pipe**

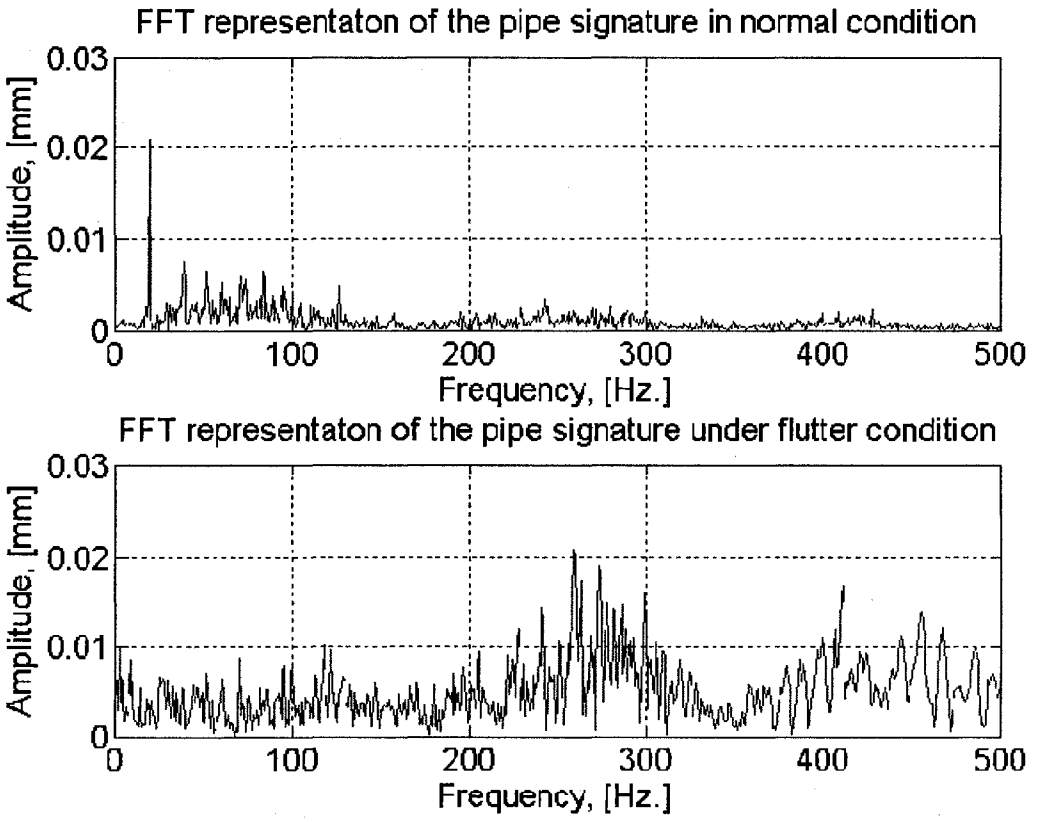

Figure 6.38: FFT representation of the pipe response in both normal and flutter cases

Figure 6.38 shows the exact value of the frequencies for the two cases, where the maximum frequency of the normal operation is 10 Hz (the pipe fundamental frequency due to the fluid flow); while the maximum frequency can be seen at 270 Hz under flutter condition.

6.8.4 FFT for Pipe Response when the Pump is Driven by an Unbalanced Electric Motor vs. Normal Pipe

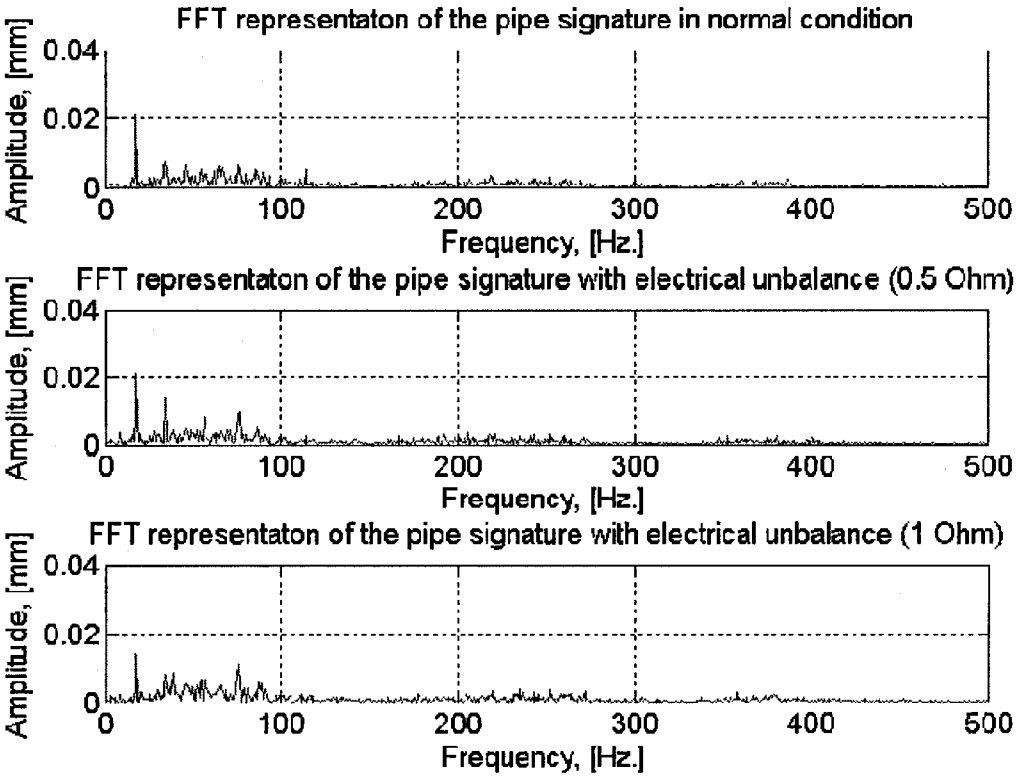

Figure 6.39: FFT representation of the pipe response in normal and electrical unbalance (0.5 Ω and 1 Ω) cases

The dominant frequency for the pipe equals 10 Hz. In the presence of the electrical unbalance defects, other frequencies can be noticed. For example, at 10 Hz, the frequency amplitude increases from 0.1 (normal condition) to 0.22 (with electrical unbalance, 0.5 Ω). Also, frequencies at 60 and120 Hz are found with the electrical unbalance conditions.

From the previous section, it can be seen that FFT gives us the values of the frequencies and their amplitudes for the different cases. It is a complementary tool to indicate the frequency contents and all the information about the frequency, with high frequency resolution.

6.9 Using Vibration Signatures as Safe-Mode Strategy (SMS)

In the previous sections, we discussed some defects that can be discovered in hydraulic systems components, and some of those can lead to catastrophic results. In order to avoid the undesired performance, it is recommended to shut down the entire hydraulic system at specific conditions. The shut down can be done by stopping the mechanical driving source of the hydraulic system, in our case the electric motor. Different resources can be used as an input for the SMS, such as:

- Accelerometer readings
- CWT and DWT statistical data

The SMS is trained to work within a certain range of vibration levels or within certain values for the CWT and DWT, with a specified tolerance. If these readings exceed the specification, the SMS shuts down the electric motor and prevents the pump from delivering fluid. The operator of the hydraulic system can notice the stall of the system, and the vibration signatures are analyzed to determine the defect.

The following flow chart illustrates the principle of the SMS.

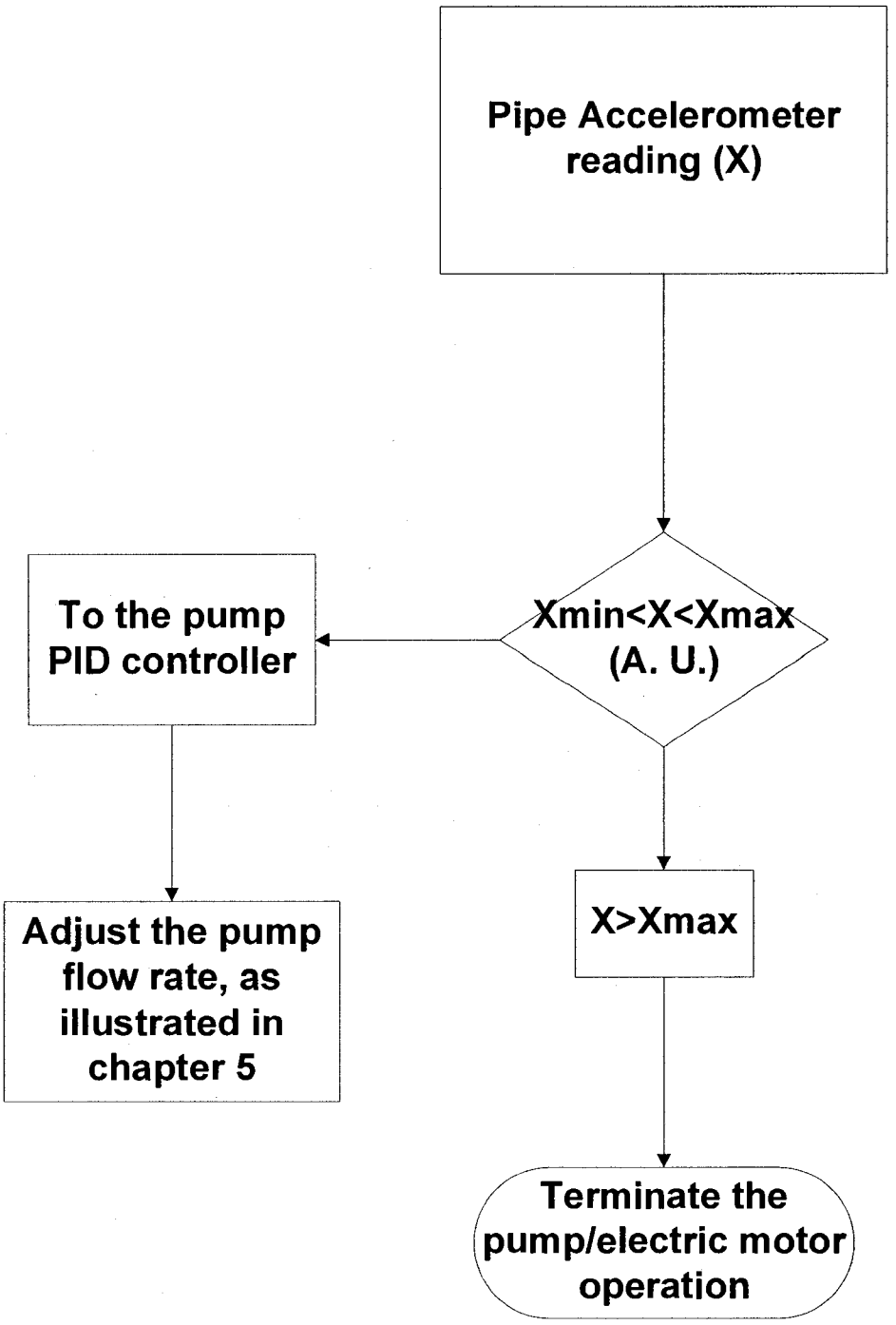

Figure 6.40: SMS flow chart

Figure 6.40 illustrates how the fault tree diagram for a pipeline can be controlled by SMS. The diagram shows the input from the pipe accelerometer. However, this can be extended to include the DWT and CWT. The SMS helps to protect the hydraulic system by a combination of the pump PID controller and the electric motor relay (which can be equipped to the motor). Normal operation is considered and evaluated under values of pipe vibration levels that are less than the minimum allowed level, or when the CWT and DWT have the same values as determined in the previous sections. Operation is considered abnormal when the pipe vibration level exceeds the minimum allowed level, and the arithmetic unit (A.U.) makes its decision according to the pipe vibration levels. If the vibration level is still less than the maximum allowed value, the pump PID controller reduces proportionally to the vibration value and the pump flow rate. However, if the vibration level exceeds the maximum allowed value, the A.U. will activate the electric motor relay terminating the operation of the hydraulic system.

6.10 Conclusions

In this chapter, a general introduction and the importance of implementing condition monitoring to improve system performance is given. Also, we explained the different techniques used in condition monitoring, which include using the vibration signature as a rich source for information about the health of systems.

Then, the different types of transforms used to obtain the information from the signals are listed; and we also showed the applicability of these transforms. The limitations of each transform were presented, and we showed that the transform can be selected according to two factors: the nature of the signal, and what we want to know from the signal.

Only wavelet analysis is capable of analyzing the signals recorded from a hydraulic system with impulsive nature. The other transforms cannot be used for this kind of system, and they have limitations in monitoring hydraulic system conditions.

We presented the properties of both continuous and discrete wavelet analysis. The advantages of both kinds of wavelet analysis were introduced. The theory of wavelet analysis was explained along with the multi-resolution technique and the filters bank. The expressions of the continuous and discrete wavelet transforms were explained and we showed the importance of selecting the mother wavelet to obtain meaningful results.

A set of experiments was carried out to examine the applicability of wavelet analysis in detecting the changes of the signals and the time at which these changes started and ended; and the duration of every frequency sub-band and the density of the sub-bands were also examined.

We started our investigations by recording the vibration signatures for the pump and pipe under normal operating conditions, and then we created two defects: pump dynamic instability (by using a PD controller) and voltage unbalance for the electric motor, which drives the swash plate pump. The pump instability created flutter in the pipe. The different signatures were analyzed with continuous and discrete wavelet transform, waterfall diagram, and FFT. The changes in the signatures were identified and parameterized for the different cases.

It was found that some defects can be recognized from their signatures, such as the flutter and instability cases, while other defects, like the voltage unbalance, cannot.

The results showed the applicability of wavelet transforms in detecting the changes in the signals with full details, such as the start and the end of any frequency sub-band and the range of the frequencies.

The objective in using waterfall diagrams and FFT was to obtain certain information that was not included in the signals, and was implied in the wavelet transforms.

The results can be fed to other computer programs (for example, a neural network).

In the seventh chapter, the conclusions and recommendations that can be obtained from the present research will be provided.

CHAPTER SEVEN

7 CONCLUSIONS AND RECOMMENDATIONS FOR FUTURE WORK

7.1 Summary

In the sixth chapter, we dealt with fault diagnosis in hydraulic systems and how the control system could respond in such situations. Different approaches were used to transform the signals and obtain the required information that reflects the condition of the hydraulic system components. This chapter summarizes the research, presents conclusions and outlines.

The research objectives, as stated in 1.4, are:

1. Evaluate the effect of port plate configurations on pump performance
2. Improve control strategies
3. Study the vibration phenomena in hydraulic networks driven by a swash plate pump
4. Hydraulic system component fault diagnosis and investigation of the use of wavelet analysis to detect system defects

In the first chapter, we introduced hydraulic system components in general, and the different types of pumps were discussed. The different controllers used with variable displacement pumps were also presented, and the pipe dynamics and flow induced

vibrations were briefly introduced. Moreover, the current maintenance philosophies were presented and the different signals transformations were introduced.

In the second chapter, the pump description, structure, dynamics, and control volume were explained in detail. Afterwards, the pump performance was studied with different approaches and assumptions, and the pump output was investigated. The pump performance was investigated with different designs for the pump port plate (without silencing grooves and with shallow triangular silencing grooves), and a new port plate was proposed. The new design utilizes a pair of silencing grooves. New expressions for the porting area, piston kinematics, cylinder pressure, pump flow rate, and pump output were derived, and the results were obtained numerically.

The third chapter dealt with the pipe dynamics and flow induced vibrations. It started by explaining the relationship between the fluid flow and pipe vibration. The equation of motion of a pipe conveying fluid was derived, and different solution approaches were examined. Complex Argand planes of the different cases were presented showing the values of fluid velocities at which the fluid loses its static or dynamic instabilities.

The experimental setup(s) and their specifications were described in the fourth chapter. Also, the test methodology was explained and the individual setup of every experiment was introduced.

In chapter five, the concept of fault diagnosis of hydraulic systems was discussed in detail, and the importance of the vibration signature as a source of the information about the health of the system components was made clear. Then, the different types of the transforms used to obtain information from the signals were discussed.

Different predetermined faults (pump with dynamic instability, pipe flutter, and an electric motor with unbalanced voltage) were formulated, explained and investigated by wavelet analysis, waterfall, and FFT. These results were compared with the standard signature representations in wavelet analysis.

In chapter six, we explained the need for a control unit in variable displacement pump, and the relationship between the pump flow rate and the swivelling angle, which is created by the control cylinder. The current pump models that implement a double negative feedback and one with a single PD controller were investigated. The two different strategies were evaluated and their characteristics were determined. A new single PID controller was proposed, investigated, and was validated experimentally.

The same controller was modified to control the pump flow according to two inputs: the load requirements and pipe vibration levels. The mathematical background of this strategy was discussed and presented, and this arrangement was examined under different external disturbances.

7.2 Conclusions

In order to parameterize the PID controller of the swash plate pump and investigate its response with the accordance of the entire hydraulic system operation; the pump should be redesigned to improve its performance and the pipe response should be free of external disturbances, or under the minimum levels of vibration. The new proposed control strategy requires two inputs, which are the load pressure and the pipe response, to achieve its tasks. Moreover, it is more comprehensive to analyze the pipe vibration signature,

which is an important input in our control strategy, to detect changes in the health of the components of the hydraulic system. The conclusions are listed as follows:

1. To optimize the performance and response of the swash plate controller, the pump performance should be satisfactory; and this objective was achieved by redesigning the port plate, which determines the characteristics of the pump flow. A pair of deep silencing grooves on the entry and exit ends of the delivery slot were added, and the pump's performance was then modeled and simulated. In order to obtain reliable results, there was a need to consider the overlapping areas between the cylinder mouth and the port plate and the pump performance was investigated. The silencing grooves eliminated the overshooting of the cylinder pressure and reduced the flow fluctuations. Also, the new port plate was observed to increase the pump output up to 4%. This improvement is due to the pump porting area with the new design that incorporates two end grooves.
2. The pipe loses its stability according to the boundary conditions. Comparing the three different boundary conditions of the pipe filled-fluid, the cantilever pipe loses its dynamic stability (at flutter) at low nondimensional velocity of 4.8; while for the simply supported and fixed-fixed pipes, flutter develops at fluid velocity equal to 6.7 and 8, respectively.
3. The swash plate pump can be equipped with a single PID controller instead of the current design, which is with a double negative feedback, or with a single PD controller. Certain improvements in the implementation of a single PID controller can be listed as follows:

- With the PID controller, the rise time drops from 120 mSec. (double negative feedback) or 50 mSec. (with the single PD controller) to 15 mSec. (with the single PID controller). The decrease in the rise time reduces the power shocks.
- The vibration levels decrease dramatically with the PID controller, where they drop from ± 0.2 mm (with a PD controller) to ± 0.02 mm (with a PID controller) on the pump side. The smoothness of the pump can also be observed on the pipe, where the levels of the vibrations on the pipe side decrease from ± 0.5 mm to ± 0.05 mm.

4. The extended control strategy (with the PID controller) fits with all pipe disturbances (step, sinusoidal, ramp, or mixed inputs), where the PID controller was able to reduce the pump flow rate with the same percentage of pipe disturbance. This is possible because the compensation factor of the control strategy modified the set point of the swash plate swiveling angle, and the control unit has another set point, smaller swiveling angle proportional to the levels of the pipe vibrations. For example, the pump flow rate was shut off completely at the highest allowed vibration levels of the pipe, and the pump discharges less fluid when the pipe vibration level is above the minimum allowed level.
5. The vibration signature of the pipe is used as a control input to adjust the pump flow rate. When a fault is initiated in the system and deteriorates over time, the vibration signatures are non-stationary signals. It is useful to transform these signals by a suitable transform, such as wavelet analysis. It, was found that with wavelet analysis, the predetermined defects can be identified, where the analysis

maps the signal in both time and scale representation in the DWT and CWT. Two predetermined defects were created in the hydraulic system; the first defect was an electrical unbalance in the electric motor driving the pump, and the second defect was pump dynamic instability, which was created using a PD controller. The vibration signatures of the pump and the pipe were recorded and transformed by wavelet analysis. According to wavelet transform and by comparison between the wavelet coefficients of the normal condition and the defective condition, the following observations can be listed:

- The CWT: for the pump standard operation it was noticed that the longest sub-band takes place when t = 250 mSec., and it spreads from scale 27 to 512. This trend changed in the abnormal operation (internal dynamic instability), and we found that the largest sub-band spreads were within (27-512) scale at t = 990 mSec. Two other sub-bands with high energy can be seen at low- middle scales (1-209) at t = 50 mSec., and at t = 200 mSec. at high scales (287-512).
- DWT: the seventh approximate coefficient of the pump under normal operating condition has amplitude of -0.1; afterwards, it slightly fluctuates about the zero value. This coefficient has a different behavior when the pump is under internal dynamic instability, where it remains with constant amplitude (0.028) for most of the time.

7.3 Main Contributions

In order to control the pump flow rate according to the load demands and the pipe response and to improve the performance of the pump, there was a need to study the pipe dynamics and to reconsider some design aspects of the hydraulic system components. The contributions in this thesis are summarized as follows:

1. New mathematical expressions for the piston kinematics.
2. New and exact expressions for the porting area, where the overlapping areas were considered and evaluated.
3. A new port plate design with two deep triangular silencing grooves, which can improve the pump performance and increase the pump output.
4. A novel PID controller with a smooth operation, minimum levels of noise and vibration, and the shortest rise time (15 mSec.). The new controller was constructed and validated experimentally, and the pump performance was investigated.
5. A Pump-pipe controller (the same PID controller), which enable us to control the pump according to the pump requirements and the pipe vibration.
6. A comprehensive, accurate, and simple study of the stability of a pipe conveying fluid.
7. Investigation of the applicability and accuracy of using wavelet analysis in condition monitoring and fault detection of hydraulic systems.

7.4 Recommendations for Future Work

Some suggestions for the future work that would extend the present research are given as follows:

1. The pump performance was modeled and validated numerically. Hence, the proposed port plate should be machined and installed in the pump, and experiments should be carried out on the pump equipped with the proposed port plate. This would enable us to experimentally validate our theoretical results, and evaluate the pump performance and its output with the new port plate.
2. Due to certain experimental limitations with the current setup, we were not able to operate the hydraulic system at flutter speeds. Hence, a set of experiments that enables us to reach the critical fluid flow velocity (flutter) should be carried out. This would help to map the evolution of the pipe response.
3. In addition to mapping the evolution of the pipe stability with the different flow values, and instead of generating the external disturbance by the function generator; we need to reach the chaotic performance of the pipe, and will then be able to examine the behavior and response of the PID controller under chaotic conditions.
4. More defects should be studied and analyzed to create a comprehensive database for hydraulic systems, which will enable us to understand the nature of each defect.
5. The collected data from the different defects should be used in other applications that analyze the uniqueness of every defect and then take the suitable action to

protect the hydraulic system. Neural network is a promising application that can be used to analyze this data.

REFERENCES

[1] Adewusi, S.A., and Al-Bedoor, B.O., 2001."Wavelet Analysis of Vibration Signals of an Overhang Rotor with a Propagating Transverse Crack". Journal of Sound and Vibration, Vol. 246, Issue 5, pp. 777–793

[2] Akay, M., 1997. "Time-Frequency and Wavelets in Biomedical Signals Processing". John Wiley & Sons, New York

[3] Akers, A., and Lin, S. J., 1987."The Control of an Axial Piston Pump Using Single-Stage Electro Hydraulic Servo Valve". Proceedings of the American Control Conference 3, pp. 1865–1187

[4] Atsushi, Y., 1992. "Cavitation in an Axial Piston Pump". JSME, Vol. 26, No. 211, pp. 72-78

[5] Bishop, R., and Dorf, R., 2005." Modern Control Systems". ISBN 0-13-145733-0, Pearson Education Ltd., London

[6] Blake, W., 1986" Mechanics of Flow-Induced Sound and Vibration", Vol. 1, Academic Press Inc., Harcort Brace Jovanovich publisher, Orland

[7] Blevins, R., 1990. "Flow-induced vibration". Van Nostrand Reinhold, New York

[8] Chainais, P., Abry, P., and Pinton, J., 1999. "Intermittency and Coherent Structures in Swirling Flow: A Wavelet Analysis of Pressure and Velocity Measurements". Journal Physics of Fluids, Vol. 11, Issue 11, pp. 3524-353

[9] Chen, H. X., Chua, P.S. K, and Lin G. H., 2006. "Vibration Analysis with Lifting Scheme and Generalized Cross Validation in Fault Diagnosis of Water Hydraulic System". Journal of Sound and Vibration, Vol. 301, pp. 458-480

[10] Chen, Z., and Zhang, W., 1998. "Stability Analysis of Simple Pipe System Conveying Fluid". Journal of Vibration Engineering, Vol. 11, pp. 38–45

[11] Chikhalsouk, M., and Bhat, R. B., 2007. ''Reduction Noise Generating Flow Fluctuation in Hydraulic System Driven by Swash Plate Pumps by Improved Port Plate Design". Proceedings of the 2007 Annual Canadian Acoustical Association Conference, Montreal

[12] Chikhalsouk, M. H., and Bhat, R. B., 2008." Optimizing the Performance of the Swash Plate Pump with Conical Arrangement by Implementing Single Loop Feedback Controller". Proceedings of CSME, Ottawa, Canada

[13] Corcos, G., 1964. "The Structure of the Turbulent Pressure Field in Boundary-Layer Flows". Journal of Fluid Mechanics, Vol. 23, pp. 353-378

[14] Daif, M., 2005. "Electric Motors I". Technical Note, pp. 1-54

[15] Dobchuk, J.W., Nikiforuk, P.N., Ukrainetz, P.R., and Burton, R.T., 2002. "Effect of Internal Pump Dynamics on Control Piston Pressure Ripple". Master's thesis, University of Saskatchewan, Saskatchewan, Canada

[16] Doki, H., Aso, K. and Kanno, A., 1995. "Simplified Active Control of Cantilever Pipes Conveying Fluid Using a PID Controller" .Transactions of the Japan Society of Mechanical Engineers, Vol. 61, pp. 1816–1821

[17] Edge, K., 1989. "Reduction of Piston Pump Pressure Ripple". Proceedings, 2nd Int. Conference on Fluid Power Transmission and Control, Hangzhou, China, pp. 250–256

[18] Ehsan, Md., 2000. "Modeling of Digital-Displacement Pump-Motors and Their Application as Hydraulic Drives for Non Uniform Loads". Journal of Dynamic Systems, Measurement, and Control, Vol. 122, pp. 135-142

[19] Evans, R., and Stephens, G., 1998.'' Geothermal Mass Flow Measurement Feasibility Report''. Idaho State University, Collage of Engineering Internal Report

[20] Gencay, R., and Whitcher, B., 2001. "An Introduction to Wavelets and Other Filtering Methods in Finance and Economics". Academic Press, London

[21] Goa, Y., Zhang, Q., and Kong, X., 2003." Wavelet-Based Pressure Analysis for Hydraulic Pump Health Diagnosis". Transactions of the ASAE, Vol. 46, No. 4, pp. 969–976

[22] Hadj-Sadok, C., Payen, T., and de Langre, E., 1997. "Nonlinear Vibrations of Loosely Supported Tubes Excited by Fluid Elastic and Turbulence Forces". Proceedings of ASME International Mechanical Engineering Congress and Exposition, Dallas, pp. 193–199

[23] Hassan, M.A., D.S. Weaver, M.A. Dokainish, 2003. "The Effects of Support Geometry on the Turbulence Response of Loosely Supported Heat Exchanger Tubes". Journal of Fluids and Structures, Vol. 18, pp.529–554

[24] Housner, G., 1952. "Bending Vibrations of a Pipe Line Containing Flowing Fluid". Journal of Applied Mechanics, pp.205-208

[25] Hsue, C.Y., and Hullender, D.A, 1983. "Model Approximation for the Fluid Dynamics of Hydraulic and Pneumatic Transmission Lines". Proceeding of the Winter Annual Meeting of the ASME, Boston, MA

[26] Jerry, R. Dunn, P.E., 2003. "Fluid Mechanics". Chapter 2,, John Wiley & Sons Inc., pp. 171-178, New York

[27] Jubran, B. A., Hamdan, M. N., and Shabaneh N. H., 1998. "Wavelet and Chaos Analysis of Flow Induced Vibration of a Single Cylinder in Cross-Flow," International Journal of Engineering Science, Vol. 36, pp. 843–864

[28] Jun, Z., and Yi W., 1989. "Research for Pressure and Flow Pulsating Characteristic of Swash Plate Axial Piston Pump with Even Pistons". Proceedings, 2nd Int. Conference on Fluid Power Transmission and Control, Hangzhou, China, pp. 325–330

[29] Kaliafetis, P., and Costopoulos, T., 1995. "Modeling and Simulation of an Axial Piston Variable Displacement Pump with Pressure Control". Mechanical Machinery Theory, Vol. 30, No. 4, pp. 599-612

[30] Kamar, P., and Georgiou, E., 1997. "Wavelet Analysis for Geophysical Applications". Reviews of Geophys, Vol. 35, Issue 4, pp. 385-412

[31] Kang, H.S., Song, K.N. , Kim, H.K., Yoon, K.H., 2003. "Axial-Flow-Induced Vibration for a Rod Supported by Translational Springs at Both Ends". Nuclear Engineering and Design, Vol. 220, pp. 83-90

[32] Katsuhisa, F., 2003." Axial Leakage Flow-Induced Vibration of a Thin Cylindrical Shell with Respect to Axisymmetric Vibration". Journal of Pressure Vessel Technology, Vol. 125, pp.149- 156

[33] Khalil, M. K., and Kassem, S.A, 2002. "On the Dynamics of Swash Plate Axial Piston Pumps with Conical Cylinder Blocks''. Sixth Triennial International Symposium on Fluid Control and Visualization". pp. 13-17, Sherbrooke University, Sherbrooke, Canada

[34] Khalil, M. K. B., Yurkevich, V., Svoboda, J., and Bhat, R. B., 2002."Implementation of Single Feedback Control Loop for Constant Power Regulated Swash Plate Axial Piston Pumps". International Journal of Fluid Power, Vol. 3, No. 3, pp. 27-36

[35] Khalil, M., 2003. "Performance Investigation of the Swash Plate Axial Piston Pumps with Conical Cylinder Blocks", PhD thesis, Concordia University, Montreal, Canada

[36] Khalil, M., Svoboda, J. and Bhat, R. B., 2002. "Response Of Constant Power Regulated Swash Plate Axial Piston Pumps to Harmonic and Random Inputs". Proceedings of the International Conference on Multidisciplinary Design in Engineering, CSME-MDE2001, Concordia University, Montreal, Canada

[37] Khalil, M., Svoboda, J., and Bhat, R. B., 2003. "Vibration Analysis of Constant Power Regulated Swash Plate Axial Pumps". Journal of Sound and Vibration, Vol. 259(5), pp. 1225-1236

[38] Kojima, E., and Shinada, M., 1986." Characteristics of Fluid Borne Noise Generated by a Fluid Power pump". Bulletin of JSME, Vol.29, pp. 4147-4155

[39] Kollek, W., and, Mazur, M. K., 1989. "Cylinder Pressure Transient in Oil Hydraulic Pumps with Sliding Plate Valves". Proceedings, 2nd Int. Conference on Fluid Power Transmission And Control, Hangzhou, China, pp. 281–288

[40] Kondo, M., and Anoda, Y., 1998. "Wavelet Analysis of in-Line Oscillation". Proceedings of ASME/JSME Pressure Vessel and Piping Conference, pp. 95–101, San Diego

[41] Koo, G. H., and Park, Y. S., 1998. "Vibration Reduction by Using Periodic Supports in a Piping System". Journal of Sound and Vibration, Vol. 210, pp. 53–68

[42] Kopparapu, C., and Chandrasekaren, A., 1998.'' A Study on Application of Wavelet Analysis to Power Quality". the Thirtieth Symposium on System Theory, pp. 350-353, Morgantown, West V.A., USA

[43] Lee U. and Kim J., 1999. "Dynamics of Branched Pipeline Systems Conveying Internal Unsteady Flow". Journal of Vibration and Acoustics, Vol. 121, pp. 114–122

[44] Lin, C. W., 1996. "Design Guide to Reduce Potential for Vibration Caused by Fluid flow Inside Pipes – review and survey". Welding Research Council Bulletin, no. 417, pp. 1–28

[45] Lin J. and Zeiger G., 1985. ''the Effect of Oil Entrapment in an Axial Piston Pump''. ASME, Journal Dynamic Systems Measurements and Control, Vol. 107, pp. 246–251

[46] Lin, Y. H., and Tsai, Y. K., 1997. "Nonlinear Vibration of Timoshenko Pipes Conveying Fluid". International Journal of Solids and Structures, Vol. 34, pp. 2945–2956

[47] Lin, Y., Huang, R. and Chu, C., 2004. "Optimal Modal Vibration Suppression of A Fluid-Conveying Pipe with A Divergent Mode". Journal of Sound and Vibration, Vol. 271, pp. 577–597

[48] Luenberger, G., 2003. "Linear and Nonlinear Programming", Kluwer Academic Publishers, Boston

[49] Mallat, S., 1999. "A Wavelet Tour of Signal Processing". Academic Press, Boston

[50] Manring, N. D., and. Damtew, F. A., 2001. "The Control Torque on The Swash Plate of an Axial-Piston Pump Utilizing Piston-Bore Springs". ASME Journal of Dynamic Systems, Measurement, and Control. Vol.123, pp. 471-78

[51] Manring, N. D., and Zhang, Y., 2001. "The Improved Volumetric-Efficiency of an Axial-Piston Pump Utilizing A Trapped-Volume Design". ASME Journal of Dynamic Systems, Measurement, and Control. Vol. 123, pp. 479-487

[52] Manring, N. D., 2000." The Discharge Flow Ripples of an Axial-Piston Swash-Plate Type Hydrostatic Pump". ASME Journal of Dynamic Systems, Measurement, and Control. Vol. 122, pp. 263-268

[53] Manring, N. D., 2003. "Valve-Plate Design for an Axial Piston Pumps Operating at Low Displacements". ASME Journal of Mechanical Design. Technical Brief. Vol. 125, pp. 200-205

[54] Manring, N.D. and Johnson, 1996."Modeling and Designing a Variable-Displacement Open-Loop Pump". Journal of Dynamic Systems, Measurement, and Control, Vol. 116, pp. 267-272

[55] Martin, B., Lind, R., and Voracek, D.: NASA, 1997. "Overview of Recent Flight Flutter Testing Research at NASA Dryden". Technical Memorandum 4792, California, USA

[56] Metrovitch, L., 2001 "Fundamental of Vibrations". McGraw Hill Higher Education

[57] Misra, A.K., Paidussis, M.P., and Van, K.S., 1988."Dynamics and Stability of Fluid- Conveying Curved Pipes". The American Society of Mechanical Engineers, International Symposium on Flow-Induced Vibration and Noise, Vol. 4, Presented in the Winter Annual Meeting, pp. 1-24, Chicago

[58] Moussou, P., 2005." A kinematics Method for the Computation of the Natural Modes of Fluid–Structure Interaction Systems". Journal of Fluids and Structures Vol. 20, 643–658

[59] Naudascher, E., and Rockwell, D., 1994. "Flow-Induced Vibrations: An Engineering Guide". Cambridge University Press, pp.413

[60] Omari, T., and, Takaya, K., 2004."Acquisition of Dynamic Characteristics of a Pump-Pipe System by Neural-Network, and Application to the System Control". Journal of Optimization Symposium, Vol. 6, pp109-114

[61] Osama, G., 2000." Prediction and Improvement of Steady-State Performance of a Power Controlled Axial Piston". Journal of Dynamic Systems, Measurement, and Control, Vol. 124, 443-451

[62] Otani, A., Kobayashi, H., Kobayashi, N. and Tadaishi, Y., 1994. "Performance of a Viscous Damper Using Electrorheological Fluid" .Proceedings of ASME Pressure Vessel and Piping Conference, Minneapolis, pp. 93–97

[63] Ozguc, A., Atac, T., and Rybak, J., 2003. "Temporal Variability of The Flare Index (1966-2001), solar Physics". Vol. 214, pp. 406-409

[64] Paidoussis, M. P., 1998. "Fluid-Structure Interactions: Slender Structures and Axial flow". ISBN 0-12-544360-9, Volume 1, Academic Press, London

[65] Pettigrew, M. J., Taylor, C. E., Fisher, N. J., Yetsir, M. and Smith, B. A., 1998. "Flow-Induced Vibration: Recent Findings and Open Questions". Nuclear Engineering and Design, Vol. 185, pp. 249–276

[66] Prasuhn, A., 1980. "Fundamentals of Fluid Mechanics". Prentice-Hall, Englewood Cliffs, New Jersey

[67] Reference for wavelet. "http:\\ mathwork.com"

[68] Reference for signal processing. "http:\\ dadisp.com"

[69] Rexroth Corporation, 1997." Electronic Control Systems for Closed Loop Control of Variable Displacement Axial Piston Pumps Type A4VS with HS3 Control". RE 30021, 6/20

[70] Rocard, Y., 1960. "General Dynamics of Vibration". Frederick Ungar Publishing Co., New York

[71] Roseau, M., 1998."Vibrations in Mechanical Systems". Springer, New York

[72] Rougier, J., 2003. "Probabilistic Leak Detection in Pipelines Using the Mass Imbalance Approach", University of Durham, U.K

[73] Saito, N., Hagiwara, T., and Miyano, H., 1998 "Flow-Induced Vibration Characteristics of ABWR Reactor Internal Components". Proceedings of the 1998 ASME/JSME Pressure and Piping Conference, San Diego

[74] Schlichting, H., 1997. "Boundary-Layer Theory", McGraw-Hill Book Company, New York

[75] Semercigil, C. E., Turan, O. F., and Lu, S., 1997. "Employing Fluid Flow in a Cantilever Pipe for the Vibration Control," Journal of Sound and Vibration, Vol. 205, pp. 103–111

[76] Seto, W., 1964. "Theory and Problems of Mechanical Vibrations", Schaum Publishing Co., New York

[77] Stack, C. P., Garnett, R. B., and Pawlas, G. E., 1993. "Finite Element For the Vibration Analysis of a Fluid-Conveying Timoshenko Beam". Proceedings of the 34th AIAA/ASME Conference on Structures, Structural Dynamics and Materials, La Jolla, pp. 2120–2129

[78] Staszewski, W.J., and Cooper, J.E., 1995."Flutter Data Analysis Using the Wavelet Transform''. Proceedings of the International Seminar on New Advances in Modal Synthesis of Large Structures: Nonlinear, Damped and Non-deterministic Cases", Lyon, France, pp. 203–214

[79] Steve, P.S., Keith, J. M., Paul A. C., and William J. H., 2003." Response of the Above-Ground Trans-Alaska Pipeline to the Magnitude 7.9 Denali Fault Earthquake". the conference Proceedings at the Sixth U.S. Conference and Workshop on Lifeline Earthquake Engineering, ASCE Technical Council on Lifeline Earthquake Engineering, Long Beach, CA, USA

[80] Taylor, C. E., Pettigrew, M. J., Dickinson, T. J., Currie, I. G. and Vidalou, P., 1997. "Vibration Damping in Multi-span Heat Exchanger Tubes". Proceedings of ASME International Mechanical Engineering Congress and Exposition, pp. 201–208

[81] Thompson, W., 1998. "Theory of Vibration with Applications". Prentice Hall, Upper Saddle River, 5th Ed , New Jersey

[82] Tucker, R.W., Kercel, S.W., and Varma, V.K, 2003." Characterization of Gas Pipeline Flaws Using Wavelet Analysis". Proceeding of SPIE6th International Conference on Quality Control by Artificial Vision, Vol. 5132, pp. 485-493

[83] Tullis, J., 1998. "Hydraulics of Pipelines". John Wiley & sons, New York

[84] University of Wollongong, 2002. "Voltage Unbalance". Technical Note, No. 06, pp. 1-20

[85] Von Jouanne, A., and Banerja, B., 2001. "Assessment of Voltage Unbalance". IEEE Transaction on Power Delivery, Vol. 16, No. 04, pp. 782-790

[86] Wang, Y.J., 2001. "Analysis of Effect of Three-Phase Voltage Unbalance on Induction Motors with Emphasis on the Angle of the Complex Voltage Unbalance Factor". IEEE Transaction on Energy Conversion, vol. 16, No. 3, pp. 270-275

[87] Yamaguchi A., 1966. ''Studies on the Characteristics of Axial Plunger Pumps and Motors". Bull. JSME, Vol. 9, No. 34, pp. 305–313

[88] Yau, C. H., Bajaj, A. K., and Newokah, O. D., 1992. "Active Control of Chaotic Vibration in a Constrained Flexible Pipe Conveying Fluid" .Proceedings of the Winter Annual Meeting of the American Society of Mechanical Engineers, pp. 93–108

[89] Yoshizawa, M., Watanabe, M., Hashimoto, K., and Takayamanagi, M., 1997. "Nonlinear Lateral Vibration of a Vertical Fluid-Conveying Pipe with End-Mass". Proceedings of the ASME International Mechanical Engineering Congress and Exposition, Dallas, pp. 281–288